# $^{230}$Th and $^{231}$Pa

# –

# Tracers for Particle Fluxes and Deep Water Circulation in the Central Arctic Ocean

Dissertation zur Erlangung des akademischen Doktorgrades
der Naturwissenschaften

Dr. rer. nat.
im Fachbereich Geowissenschaften
der Universität Bremen

1. Gutachter: Prof. Dr. Sabine Kasten
2. Gutachter: Prof Dr. Martin Frank

Dissertationskolloquium: 14.06.2021

vorgelegt von
Ole Christian Valk
Bremen, im Januar 2021

Universität Bremen

# PREFACE

This PhD project was conducted in the framework of GEOTRACES, a global program to investigate the biogeochemical cycles of trace elements and their isotopes (TEIs) in the ocean, and was funded by the *Alfred Wegener Institute Helmholtz Centre for Polar and Marine Research (AWI),* in Bremerhaven, Germany. The PhD project was supervised by Dr. Michiel M. Rutgers van der Loeff (AWI), Dr. Walter Geibert (AWI) and Prof. Dr. Sabine Kasten (AWI). The outcome is submitted as a cumulative doctoral thesis.

Each individual chapter in this dissertation is designed to stand alone. Therefore each chapter is given an abstract and introduction of its own in greater detail and more specific on the individual topic than the initial one. Specific references and acknowledgements are also presented at the end of each chapter.

The dissertation starts with a general introduction about the working area and scientific aims, giving broad scientific background information, as well as the motivation and aims of the thesis (Chapter 1).

First-author manuscripts published in (ISI) peer-reviewed journals (Chapters 2+3) and a first-author manuscript in preparation (Chapter 4) are presented before selected published co-author manuscripts (Chapters 5 + 6). (Co-) Author contributions for each manuscript are stated at the end of the Introduction in section *1.6.1 Declaration of Co-Author Contributions*. The dissertation ends with the conclusion of the key findings and perspectives on open research questions, which might require further investigation (Chapter 7).

# TABLE OF CONTENTS

# THESIS SUMMARY

The currently ongoing climate change can be ascribed without exaggerating as one the most important topics and threats for humanity. Understanding its mechanisms and consequences is an important step to target and manage arising problems, which accompany a rapidly warming climate.

The oceans play a crucial role in the Earth's climate controlling and response mechanism. Its physical and biological carbon pump systems are crucial regulators for the atmospheric $CO_2$ content. Biological primary production is an important part of the Oceans $CO_2$ uptake capability. Some trace elements are important (micro-) nutrients in oceanic primary production. Therefore it is important to investigate and understand the reaction of those elements to changing environmental conditions.

Particle fluxes and ocean circulation contribute to their distribution in the water column. $^{230}$Th and $^{231}$Pa are suitable tracers for both particle fluxes and deep water circulation. Their well-known sources and production ratio, as well as their fractionation by particle fluxes and deep water circulation, enables their use as tracers. Their water column distribution serves as an indicator for recent environmental changes, while their sedimentary $^{231}$Pa/$^{230}$Th activity ratio is used as a paleoceanographic tool. Therefore $^{230}$Th and $^{231}$Pa are standard parameters of GEOTRACES, an international programme with the goal to improve understanding of the cycling of trace elements and their isotopes in the Ocean.

Different areas of the World's Ocean react in different velocities and intensities to climate change. The Arctic Ocean is the most sensitive one to climate change. Climate change related consequences are already visible, e.g. the retreat and thinning of sea ice. Other consequences, like increasing particle fluxes and changing particle composition, as well as potentially changing circulation patterns and ventilation times are less obvious. It is expected that climate change will cause significant changes on the Arctic Oceans' primary production and particle input. The consequences of these changes are not well understood and known. Therefore it is important to investigate changes in particle fluxes and composition, already in an initial stage of these changes. $^{230}$Th and $^{231}$Pa are valuable tools to gain insights into changes, which will potentially influence the global climate in the near future.

In order to derive information about trace element cycling from $^{230}$Th and $^{231}$Pa in a changing Arctic Ocean, it is therefore crucial to investigate and understand the processes that control the distribution and concentrations of $^{230}$Th and $^{231}$Pa in the Arctic Ocean. To achieve this, a time series of this tracer pair, consisting of data from 1991, 2007 and 2015, was created to investigate

the temporal development of $^{230}$Th and $^{231}$Pa over the past three decades. This new time series revealed quite variable $^{230}$Th and $^{231}$Pa inventories, indicating changing removal processes, caused by changing environmental conditions.

This thesis consists of three first author manuscripts that are either published or in preparation for submission to international peer-reviewed journals. Additionally, two co-author manuscripts, published in international peer-reviewed journals, are part of this thesis. This section assigns the role of each manuscript, presented in this thesis, in the context of the general introduction.

Changes in scavenging behaviour of $^{230}$Th need not necessarily have to be related to a changing climate. Hydrothermal activity and submarine volcanic eruptions at the ultra-slow spreading Gakkel Ridge caused a significant reduction of dissolved $^{230}$Th in only eight years in the deep Nansen Basin, contributing to sporadically increased removal and sedimentation rates of $^{230}$Th. The role of hydrothermal activity in the variation of scavenging behaviour of $^{230}$Th in the Eurasian Basin is described in CHAPTER 2 (Valk *et al.*, 2018).

Changing environmental conditions caused a significant decrease of dissolved $^{230}$Th concentrations in the entire Eurasian Basin between 2007 and 2015. Those changes include elevated particle fluxes at the shelves and margins of the deep basins, specifically the Barents Sea shelf and the Nansen Basin margin. Those increased particle fluxes caused increased scavenging removal of $^{230}$Th and to a minor degree of $^{231}$Pa, indicating an increasing sink for particle reactive trace elements. Increased scavenging removal of $^{230}$Th at the Barents Sea shelf and at the margins of the Nansen Basin caused a drastic decrease of dissolved $^{230}$Th in the central Amundsen Basin (CHAPTER 3, Valk *et al.*, 2020). This highlights the increasing importance of shelf-basin interactions in the Arctic Ocean, due to rapidly increasing particle fluxes at the shelves and margins. Even before particle fluxes within the central basins increase, climate change already causes notable changes in trace element distributions and probably in their export to the North Atlantic. This is important for the nutrient availability in the North Atlantic as well as the paleoceanographic application of the $^{231}$Pa/$^{230}$Th sedimentary activity ratio.

Distribution and concentrations of dissolved $^{230}$Th and $^{231}$Pa can change significantly within less than ten years in the central Arctic Ocean. In CHAPTER 4 (Valk *et al*., in preparation) new budgets for dissolved $^{230}$Th and $^{231}$Pa, based on a water column data from 1991 over 2007 to 2015, as well as box models, are presented to illustrate scavenging removal and sedimentation patterns for these tracers. The model results are discussed in the context of boundary scavenging

of $^{230}$Th and $^{231}$Pa in the Eurasian Basin and their export to the GIN Seas (Greenland, Iceland and Norwegian Seas). Consequences of the identified removal processes of $^{230}$Th and $^{231}$Pa from CHAPTER 1 and CHAPTER 2 on the sedimentary $^{231}$Pa/$^{230}$Th activity ratios in the Eurasian Basin, its margins and the GIN Seas are discussed in the context of the paleoceanographic use of these tracers.

It is an open question whether $^{230}$Th and $^{231}$Pa are subject to boundary scavenging in the Arctic Ocean. The study presented in CHAPTER 5 (Gdaniec *et al.*, 2020) investigates the influence of boundary scavenging and shelf-basin interactions on the observed distribution of $^{230}$Th and $^{231}$Pa in the Arctic Ocean. A modelling approach adapted from Roy-Barman (2009) is used to constrain the scavenging behaviour of $^{230}$Th and $^{231}$Pa between the Arctic margin and the inner ocean. This study links very well to CHAPTER 3 and CHAPTER 4, giving detailed insight in particulate and dissolved radionuclide data from 2015.

The study presented in CHAPTER 6 (Grenier *et al.*, 2019) investigates the temporal $^{230}$Th and $^{231}$Pa developments in the Amerasian Basin of the Arctic Ocean, based on $^{230}$Th and $^{231}$Pa time series and therefore links well to CHAPTER 2, CHAPTER 3 and CHAPTER 4 which focus on the Eurasian Basin. The Amerasian Basin time series reveal a large scale decrease in dissolved $^{230}$Th and $^{231}$Pa concentrations, indicating intensification of scavenging removal, especially in coastal areas. This study illustrates how dissolved $^{230}$Th and $^{231}$Pa combined with εNd, can give insights into changes in particle fluxes, as well as into the evolution of ocean circulation and mixing.

Thus the research presented in this thesis contributes to the understanding of trace element cycling and the tracer application of $^{230}$Th and $^{231}$Pa in the Arctic Ocean under changing environmental conditions.

# ZUSAMMENFASSUNG DER THESIS

Der derzeitige Klimawandel kann ohne Übertreibung als eines der wichtigsten Themen und eine der größten Bedrohungen für die Menschheit bezeichnet werden. Das Verständnis seiner Mechanismen und Konsequenzen ist ein wichtiger Schritt, um auftretende Probleme, die mit einem sich schnell erwärmenden Klima einhergehen, anzugehen und zu bewältigen.

Die Ozeane spielen eine entscheidende Rolle im Klimakontroll- und Reaktionsmechanismus der Erde. Ihre physikalischen und biologischen Kohlenstoffpumpensysteme sind entscheidende Regulatoren für den atmosphärischen $CO_2$-Gehalt. Die biologische Primärproduktion ist ein wichtiger Bestandteil der $CO_2$-Aufnahmefähigkeit der Ozeane. Einige Spurenelemente sind wichtige (Mikro-) Nährstoffe in der marinen Primärproduktion. Es ist daher wichtig, die Reaktion dieser Elemente auf sich ändernde Umweltbedingungen zu erforschen und diese zu verstehen.

Partikelflüsse und Ozeanzirkulation steuern ihre Verteilung in der Wassersäule. $^{230}$Th und $^{231}$Pa sind geeignete Tracer für beide Prozesse. Ihre Wassersäulenverteilung dient als Indikator für rezente Veränderungen, während das $^{231}$Pa/$^{230}$Th Verhältnis in Sedimenten als paläoozeanographisches Werkzeug verwendet wird. Aufgrund der Bekanntheit ihrer Quellen- und ihres bekannten Produktionsverhältnisses, sowie ihrer Fraktionierung durch Prozesse, die direkt mit Partikelflüssen und der Tiefenwasserzirkulation verbunden sind, also wichtige Prozesse für die Primärproduktion und die Verteilung von Spurenelementen, eigenen sich $^{230}$Th und $^{231}$Pa als Tracer. Daher sind $^{230}$Th und $^{231}$Pa Standardparameter des internationalen Programms GEOTRACES, das das Ziel hat, die Zyklen von Spurenelementen im Ozean besser zu verstehen.

Verschiedene Gebiete des Weltozeans reagieren mit unterschiedlichen Geschwindigkeiten auf den Klimawandel. Der Arktische Ozean ist am empfindlichsten für den Klimawandel. Konsequenzen im Zusammenhang mit dem Klimawandel sind bereits sichtbar, z.B. der Rückzug des Meereises. Andere Konsequenzen wie erhöhte Partikelflüsse und Änderungen in der Partikelzusammensetzung, sowie möglicherweise Zirkulations- und Ventilationsänderungen sind weniger offensichtlich. Es ist zu erwarten, dass der Klimawandel die Primärproduktion und den Partikeleintrag in den Arktischen Ozean erheblich beeinflussen wird. Die Folgen dieser Änderungen sind noch nicht ausreichend bekannt und verstanden. Es ist daher wichtig, Änderungen in Partikelflüssen und –Zusammensetzung bereits in einem Anfangsstadium zu untersuchen. $^{230}$Th und $^{231}$Pa sind daher wertvolle Indikatoren, um Einblicke in Veränderungen

zu gewinnen, die in naher Zukunft Auswirkungen auf das Klima auf globaler Ebene haben werden.

Um Informationen über Spurenelementzyklen aus $^{230}$Th und $^{231}$Pa in einem sich verändernden Arktischen Ozean abzuleiten, ist es daher wichtig, die Prozesse, die die Verteilung und Konzentration von $^{230}$Th und $^{231}$Pa im Arktischen Ozean steuern, zu untersuchen und zu verstehen. Um dieses Ziel zu erreichen, wurde eine Zeitreihe dieses Tracer-Paares, basierend auf Daten von 1991, 2007 und 2015, erstellt, um die zeitliche Entwicklung von $^{230}$Th und $^{231}$Pa in den letzten drei Jahrzehnten zu untersuchen. Diese Zeitreihe ergab recht variable Inventare von $^{230}$Th und $^{231}$Pa, was auf, durch verändernde Umweltbedingungen verursachte, Änderungen in Entfernungsprozessen hinweist. Diese Prozesse sind eine verstärkte Entfernung durch Scavenging an den Rändern des Eurasischen Beckens, was auf eine zunehmende Senke für partikelreaktive Spurenelemente hinweist. Dies führte zu einer Verringerung von gelösten $^{230}$Th im zentralen Amundsen-Becken. Diese Erkenntnis unterstreicht die zunehmende Bedeutung von Schelf-Becken-Wechselwirkungen im Arktischen Ozean, aufgrund der schnell zunehmenden Partikelflüsse auf den Schelfen und an den Rändern der zentralen Becken. Dies deutet darauf hin, dass der Klimawandel bereits vor dem Anstieg der Partikelflüsse in den zentralen Becken zu erheblichen Veränderungen der Spurenelementverteilung und wahrscheinlich auch zu Veränderungen in deren Export in den Nordatlantik, führt.

Diese Arbeit besteht aus drei Erstautor-Manuskripten, die entweder veröffentlicht wurden, oder sich in der Vorbereitung für die Einreichung in internationale Fachzeitschriften befinden. Darüber hinaus sind auch zwei Co-Autor-Manuskripte, die in internationalen Fachzeitschriften veröffentlicht wurden, Teil dieser Arbeit. In diesem Abschnitt wird die Rolle der einzelnen Artikel im Kontext der allgemeinen Einleitung beschrieben.

Änderungen des Scavenging-Verhaltens von $^{230}$Th müssen nicht unbedingt mit klimatischen Veränderungen zusammenhängen. Hydrothermale Aktivität und submarine Vulkanausbrüche am sich extrem langsam spreizenden Gakkel Rücken führten in nur acht Jahren zu einer signifikanten Verringerung von gelösten $^{230}$Th Konzentrationen im tiefen Nansen Becken, was zu sporadisch erhöhten Entfernungssraten von $^{230}$Th beitrug. Beide Prozesse beeinflussen den Spurenelementkreislauf im Arktischen Ozean. Die Rolle der hydrothermalen Aktivität für die Variation des Scavenging-Verhaltens von $^{230}$Th im Eurasischen Becken wird in KAPITEL 2 beschrieben.

Veränderte Umweltbedingungen führten zwischen 2007 und 2015 zu einer signifikanten Reduzierung von gelösten $^{230}$Th Konzentrationen im gesamten Eurasischen Becken. Diese Veränderungen umfassen erhöhte Partikelflüsse auf den Schelfen und an den Rändern der tiefen Becken, genauer gesagt am Barentssee Schelf und am Rand des Nansen Beckens. Diese erhöhten Partikelflüsse verursachten eine erhöhte Entfernung von $^{230}$Th und in geringerem Maße von $^{231}$Pa, was auf eine zunehmende Senke für partikelreaktive Spurenelemente hinweist. Eine erhöhte Entfernung von $^{230}$Th an den Rändern des Nansen Beckens führte zu einer drastischen Abnahme von gelösten $^{230}$Th Konzentrationen im zentralen Amundsen Becken (KAPITEL 3). Dies unterstreicht die zunehmende Bedeutung von Schelf-Becken-Wechselwirkungen im Arktischen Ozean aufgrund der schnell zunehmenden Partikelflüsse auf den Schelfen und an den Rändern der zentralen Becken. Noch bevor die Partikelflüsse in den zentralen Becken zunehmen, führt der Klimawandel bereits zu erheblichen Veränderungen der Spurenelementverteilung und wahrscheinlich zu einem veränderten Export in den Nordatlantik. Dies ist wichtig für die Nährstoffverfügbarkeit im Nordatlantik sowie für die paläozeanographische Anwendung des Sedimentaktivitätsverhältnisses $^{231}$Pa/$^{230}$Th.

Verteilung und Konzentrationen von gelöstem $^{230}$Th und $^{231}$Pa können sich im zentralen Arktischen Ozean innerhalb von weniger als zehn Jahren erheblich ändern. In KAPITEL 4 werden neue Budgets für gelöstes $^{230}$Th und $^{231}$Pa sowie Box-Modelle, die auf Wassersäulendaten von 1991, 2007 und 2015 basieren, zur Veranschaulichung der Scavenging Situation und Sedimentationsmustern für diese Tracer vorgestellt.. Die Modellergebnisse werden im Zusammenhang mit Boundary Scavenging von $^{230}$Th und $^{231}$Pa im Eurasischen Becken und deren Export in die GIN-Meere (Grönland, Island und Norwegische Meere) diskutiert. Die Konsequenzen der identifizierten Entfernungsprozesse von $^{230}$Th und $^{231}$Pa aus KAPITEL 1 und KAPITEL 2 auf die Sedimentaktivitätsverhältnisse $^{231}$Pa/$^{230}$Th im Eurasischen Becken, seinen Rändern und in den GIN-Meeren werden im Zusammenhang mit der paläozeanografischen Verwendung dieser Tracer diskutiert.

Es ist eine offene Frage, ob $^{230}$Th und $^{231}$Pa im Arktischen Ozean Boundary Scavenging unterliegen. Die in KAPITEL 5 vorgestellte Studie untersucht den Einfluss von Boundary Scavenging und Wechselwirkungen zwischen Schelfbecken und Becken auf die beobachtete Verteilung von $^{230}$Th und $^{231}$Pa im Arktischen Ozean. Ein von Roy-Barman (2009) adaptierter Modellierungsansatz wird verwendet, um das Scavenging-Verhalten von $^{231}$Pa und $^{230}$Th an den Rändern des Arktischen Ozeans und dem inneren Arktischen Ozean zu ermitteln. Diese Studie

ist sehr gut mit KAPITEL 3 und KAPITEL 4 verknüpft und bietet detaillierte Einblicke in Daten zu Partikeln und gelösten Radionukliden aus dem Jahr 2015.

Die in KAPITEL 6 vorgestellte Studie untersucht die zeitlichen Entwicklungen von $^{230}$Th und $^{231}$Pa im Amerasischem Becken des Arktischen Ozeans auf der Grundlage von $^{230}$Th- und $^{231}$Pa-Zeitreihen und ist daher gut mit KAPITEL 2, KAPITEL 3 und KAPITEL 4, die sich auf das Eurasische Becken konzentrieren, verknüpft, . Die Zeitreihen des Amerasischen Beckens zeigen eine starke Abnahme der gelösten $^{230}$Th- und $^{231}$Pa Konzentrationen in großem Maßstab, was auf eine Intensivierung der Entfernung durch Scavenging hinweist, insbesondere in Küstennähe. Diese Studie zeigt, wie gelöste $^{230}$Th und $^{231}$Pa, in Kombination mit εNd, Einblicke in Änderungen der Partikelflüsse sowie in die Entwicklung der Zirkulation und Vermischung der Ozeane geben können.

Die in dieser Arbeit vorgestellten Forschungsergebnisse tragen somit zum Verständnis des Spurenelementzyklus und der Tracer-Anwendung von $^{230}$Th und $^{231}$Pa im Arktischen Ozean, unter sich aufgrund des modernen Klimawandels ändernden Umweltbedingungen, bei.

# LIST OF FIGURES

## CHAPTER 1: Introduction

LIST OF FIGURES

**CHAPTER 6: Changes in Circulation and Particle Scavenging in the Amerasian Basin of the Arctic Ocean over the Last Three Decades Inferred from the Water Column Distribution of Geochemical Tracers**

# LIST OF TABLES

# CHAPTER 1: Introduction

## 1.1 The changing Arctic Ocean

The Arctic Ocean experiences changes with ongoing climate warming. Due to a phenomenon called Arctic amplification the Arctic Ocean is especially vulnerable to climate change. Arctic amplification causes warming rates up to twice as high as the global average (Serreze *et al.*, 2009; Serreze and Francis, 2006; Serreze *et al.*, 2007). Air temperature in the Arctic increased by 10%, averaged over 30 years (Proshutinsky *et al.*, 2015). Probably the most visual and prominent change in the Arctic Ocean is the decline of sea ice extent and thickness in recent decades (Perovich *et al.*, 2019). The decadal perennial loss is about 11% of the sea ice extent (Comiso *et al.*, 2017). This trend is expected to continue and will eventually lead to an ice free Arctic summer and thinner sea ice in winter (Haine and Martin, 2017). This might already be the case in 2050 (Collins *et al.*, 2014) or even earlier (Liu *et al.*, 2013). Even an only seasonally (in summer) ice free Arctic Ocean will have an impact on the Arctic Ocean's oceanography and its marine ecosystems, but will also affect the climate on a global scale (Timmermans and Marshall, 2020), e.g. due to reduction of the Earth's planetary albedo (Pistone *et al.*, 2014). Thinning and retreat of Arctic sea ice (Perovich, 2011; Perovich *et al.*, 2019; Rothrock *et al.*, 1999) causes changes in particle fluxes and concentrations (Boetius *et al.*, 2013). Especially at the margins of the Arctic Ocean, such as the Barents Sea, long term observations show prolonged growing seasons and increased annual NPP (Net Primary Production) since the late 1990s, due to decreasing sea ice cover (Dalpadado *et al.*, 2020). Additionally global warming causes increased particle fluxes by permafrost thawing (Günther *et al.*, 2013), which leads to an increasing input of terrestrial matter to the Arctic Ocean (Schuur *et al.*, 2013; Schuur *et al.*, 2015). The large riverine discharge to the Arctic Ocean (McClelland *et al.*, 2012) is also increasing since the last decades (Peterson *et al.*, 2002), e.g. by approximately 14% averaged over 30 years in the Eurasian Arctic (Proshutinsky *et al.*, 2015). Release of Fe and Mn from Arctic shelves causes increased scavenging of trace metals throughout the water column, due to the mobilization of these redox-sensitive metals (Jensen *et al.*, 2020). This can be linked to the increasing presence of Fe-rich particles or aggregates at the Nansen Basin margin, compared to the central basins, indicated by relatively high dissolved iron (dFe) values (Rijkenberg *et al.*, 2018). Furthermore beam attenuation data from PS94 show increased particle freight along the Nansen Basin margin, relative to the central Nansen Basin (Gardner *et al.*, 2020).

These developments can have an impact on the (re)distribution of particle reactive elements within the Arctic Ocean and changes in their export to the Atlantic Ocean with potential

consequences for lower latitude areas. This implies e.g. changes in the export of micronutrient elements like Fe. Changes in circulation or ventilation can affect the export non scavenging prone waste materials, like artificial radionuclides, such as $^{129}$I and $^{236}$U, which can be used as a circulation tracer (Smith *et al.*, 2011) and whose ratio is used as a circulation age tracer (Casacuberta *et al.*, 2016), may affect the interpretation of the distribution of elements and isotopes that are used as tracers for a variety of processes occurring in the Atlantic Ocean.

The tracer pair of the particle reactive isotopes $^{230}$Th and $^{231}$Pa has been used extensively to study particle fluxes and circulation changes in the ocean (Anderson *et al.*, 1983a, b; Hayes *et al.*, 2015b; Marchal *et al.*, 2000). As a result of their high particle reactivity they can be used as indicators of changing particle fluxes in the Arctic Ocean, already in an early stage of these changes.

### 1.1.1 Data Origin and Reliability

This section briefly describes the 2015 GEOTRACES Arctic Ocean sampling campaign and gives information on data quality and availability. In summer 2015 three simultaneous GEOTRACES cruises to the Arctic Ocean took place. A wide array of particulate and dissolved GEOTRACES parameters was sampled over the entire water column, covering the entire central Arctic Ocean. The US operated *USCGC Healy* focused on the Amerasian Basin (GEOTRACES section GN01), the Canadian *CCGS Amundsen* covered the Arctic Archipelago and the southern Canada Basin (GN02), while German *RV Polarstern* focused on the Eurasian- and the Makarov Basin (GN04). Two cruises respectively conducted cross-over stations, in order to intercalibrate data, granting reliable and comparable results. This unprecedented sampling campaign of the Arctic Ocean water column and the resulting international collaborations are the basis of the studies presented in this thesis. Cruise tracks of the 2015 GEOTRACES expeditions, including locations of cross-over stations, are shown in figure 1.

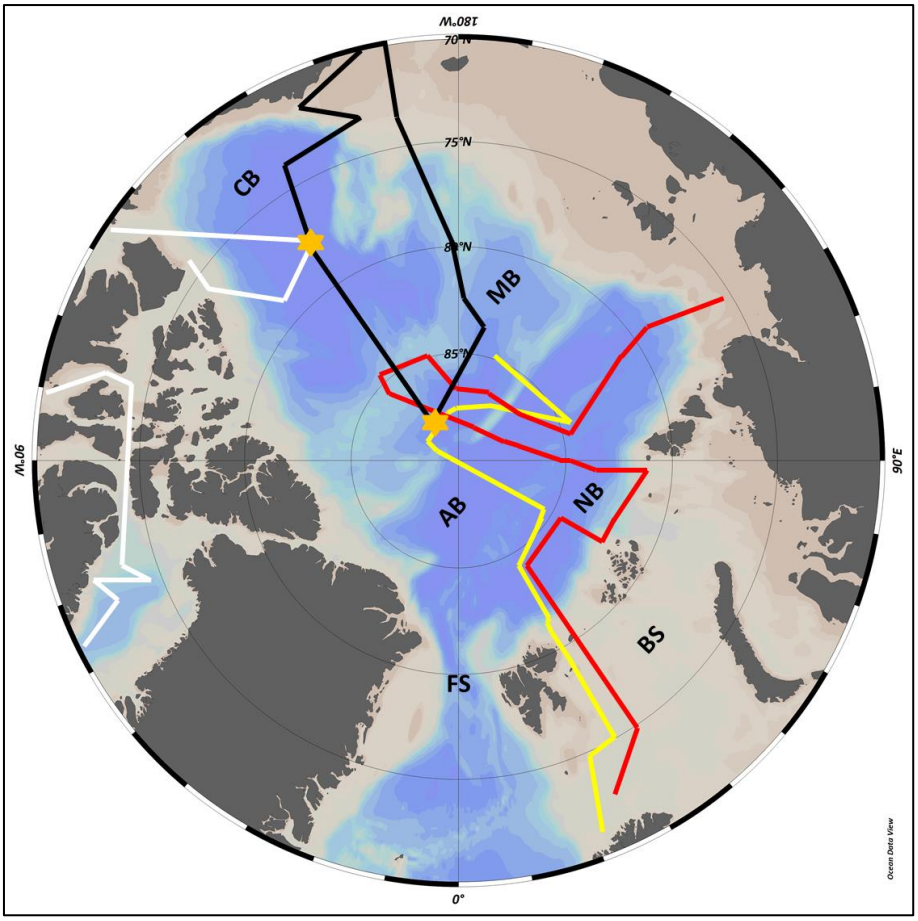


**Figure 1: Cruise tracks of the 2015 GEOTRACES Arctic Ocean expeditions: GN04 (yellow), GN01 (black), GN03 (white). And the GEOTRACES 2007 expedition: GIPY11 (red). Orange stars indicate locations of cross-over stations. AB = Amundsen Basin, BS = Barents Sea, CB = Canada Basin, FS = Fram Strait, MB = Makarov Basin, NB = Nansen Basin. Map was created using Ocean Data View® (Schlitzer, 2016).**

Naturally occurring radionuclide samples (dissolved and particulate $^{230}$Th, $^{231}$Pa and $^{232}$Th) from GN04 were additionally divided, in a close cooperation, between the *AWI* and a combined group of *Stockholm University* and the *Laboratoire des Sciences du Climat et de l'Environnement (LSCE)* in Gif-sur-Yvette, France. This collaboration allowed focussing on individual tasks and research questions. The *AWI* part focused on the central Eurasian Basins, while the *LSCE* analysed the samples from the Barents Sea and the margin of the Nansen Basin.

To allow comparison with data analysed from the partner laboratories, all samples were sampled and analysed according to standardized GEOTRACES methods (Anderson *et al.*, 2012). Additionally an intercalibration exercise between the *RV Polarstern* and the *USCGC Healy* cruises was conducted. Intercalibration sampling took place at the same location and approximately same time, with an offset of ca. two weeks between *USCGC Healy* and *RV Polarstern* sampling. A station in the central Makarov Basin (figure 1) was chosen as the cross-over station (*RV Polarstern* station 101, *USCGC Healy* station 30). The whole water column was sampled by participants from both the *RV Polarstern* and the *USCGC Healy* cruises. *AWI* and

*LSCE* samples were taken at the same time on board *RV Polarstern*. This was done in order to compare results and to evaluate the agreement between the participating parties, in order to ensure reliability of the data. Figure 2 shows the results of this intercalibration exercise for dissolved $^{230}$Th, $^{231}$Pa and $^{232}$Th.

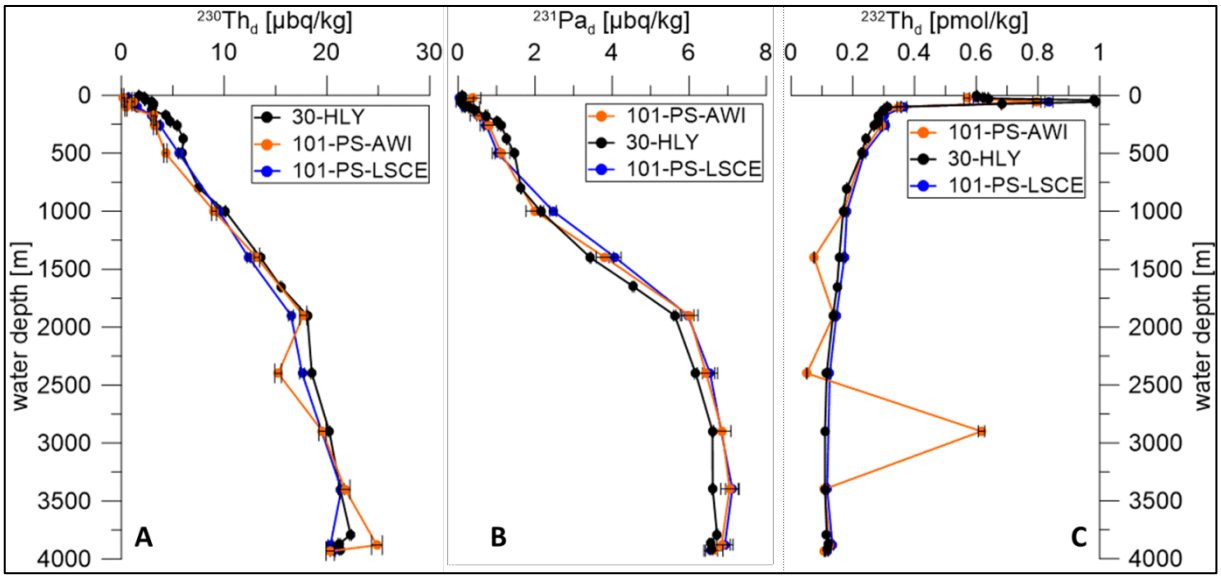


**Figure 2: Cross-over station depth profiles for dissolved $^{230}$Th (A), dissolved $^{231}$Pa (B) dissolved $^{232}$Th (C).**

There is a generally good agreement between the three participating laboratories, especially below 500 m. Data obtained in 2007 from GEOTRACES section GIPY11 on *RV Polarstern*, combined with published data from Scholten *et al.* (1995) from 1991 enables creating a time series of dissolved $^{230}$Th and $^{231}$Pa over the last three decades. All *AWI* data from first and co-author manuscripts are available at the online data publisher PANGAEA® (www.pangaea.de) and are shown in the Appendix. Individual data links are given in the respective sections. *AWI* data of dissolved $^{230}$Th, $^{231}$Pa and $^{232}$Th was also submitted for the GEOTRACES intermediate data product 2021.

## 1.2 The Arctic Ocean: Hydrography and Particle Fluxes

### 1.2.1 General Setting

The Arctic Ocean, the world's northern most ocean, is almost landlocked, comparable to the Mediterranean Sea. It is surrounded by North America, Asia and Europe, as well as Greenland. The only deep water passage from the Atlantic and Pacific Oceans to the Arctic Ocean is the Fram Strait, located between Svalbard and Greenland and with a maximum sill depth of ca. 2500 m connecting the Atlantic and the Arctic Ocean. The Arctic Ocean is, compared to other ocean basins, relatively small and consists of a large proportion of shallow shelves (<300 m), approximately 53% (Jakobsson *et al.*, 2003). The Arctic Ocean can be divided into two major basins, the Amerasian- and Eurasian Basin, separated by the ca. 1600 m deep Lomonosov Ridge, which builds a topographic barrier. This barrier is only passable below 1600 m through the intra Basin with a sill depth of ca. 1800 m, where an exchange flow between the two major basins is possible (Björk *et al.*, 2010; Björk *et al.*, 2007). The exchange flow through the Intra-Basin from the Eurasian Basin into the Amerasian Basin is estimated to be 0.25 Sv (Sverdrup, 1 Sv = $10^6$ $m^3/s$) (Timmermans *et al.*, 2005). A flow in the reverse direction through this pathway (Björk *et al.*, 2007) and above 1600 m (Middag *et al.*, 2009) is possible.

Both the Eurasian Basin and the Amerasian Basin are divided into two basins. The Amerasian basin is separated by the Alpha-Mendeleev Ridge into the Makarov- and the Canada Basin, while the mid-ocean Gakkel Ridge geographically divides the Eurasian Basin into the Nansen- and the Amundsen Basin, with the latter one being the deepest of all Arctic Ocean basins. A geographic overview is given in figure 3.

Water masses of the Arctic Ocean have mainly an Atlantic origin, about 90% of the total inflow of waters to the Arctic Ocean are derived from the Atlantic Ocean, the remaining proportions consist of ~9% of Pacific Waters entering through Bering Strait and ~1% freshwater from continental discharge and precipitation (Woodgate, 2013). Atlantic waters enter from the Nordic Seas through the Fram Strait and the shallow Barents Sea (ca. 200 m deep). The Pacific water component enters through the only 45 m deep and 50 km wide Bering Strait. Nevertheless the Bering Strait is an important fresh water and heat source of the Arctic Ocean (Haine *et al.*, 2015; Woodgate *et al.*, 2010). Outflow occurs primarily through the Fram Strait (Woodgate *et al.*, 1999) and to a small degree through the Canadian Archipelago (Leblond, 1980; Münchow *et al.*, 2006).

The Arctic Ocean receives a significant freshwater input from riverine discharge (~1 Sv) and net precipitation (~0.07 Sv) (Rudels, 2009). More than 10% of the world's total river discharge

reaches the Arctic Ocean, which comprises only 1% of the world's ocean volume (McClelland *et al.*, 2012). Therefore the Arctic Ocean is strongly stratified by salinity depth gradients with the low-salinity surface layer being able to form sea ice in winter and (Rudels, 2009), although sea ice extent and thickness are decreasing in recent decades (Perovich and Richter-Menge, 2009). The fresh water content of the central Arctic Ocean varies with time, currently it is at the highest level since the early 1980s, and is expected to further increase in the future (Rabe *et al.*, 2014). An increase in fresh water content would lead to a stronger stratification of the water column.
The strong stratification of the Arctic Ocean water column allows dividing the water column into five distinct depth layers. Due to the topographic division between the Amerasian- and the Eurasian Basin it is possible to distinguish between Eurasian- and Amerasian deep and intermediate waters, according to Rudels (2009):

1. The uppermost low salinity Polar Mixed Layer (PML) varies in its thickness between winter and summer, due to melting and freezing of sea ice. Salinity ranges from 30-32.5 PSU (Practical Salinity Unit) (Amerasian Basin) to 32-34 PSU (Eurasian Basin). The upper 10-20 m of the PML are diluted by sea ice meltwater in summer and homogenized in winter by haline convection and freezing.
2. Below the PML is the 100–250 m-thick halocline in which salinity increases sharply with depth from approximately 32.5PSU to 34.5 PSU. Water temperatures are close to the freezing.
3. The underlying Atlantic Layer is characterized in salinity and temperature by waters of Atlantic origin and is usually found between 400 m and 700 m water depth, salinity is 34.5-35 PSU and water temperatures are around 0°C.
4. Intermediate waters, under the Atlantic layer, down to 1500 m, have a salinity of 34.87-34.92 PSU and are still able to exchange over the Lomonosov Ridge. Water temperatures are -0.5-0°C.
5. Deep and bottom waters vary in the Eurasian Basin (salinity: 34.92-34.945 PSU) and the Amerasian Basin (34.92-34.96 PSU), while temperatures range from -0.55°C to 0.5°C PSU in the Canadian Basin and from -0.97°C to -0.5°C in the deep Eurasian Basin.

These layers are affected by lateral circulation and mixing processes changing their characteristics regionally (Rudels, 2009; Timmermans and Marshall, 2020).

### 1.2.2 Surface Circulation and Sea Ice Motion

The strongly stratified surface waters of the Arctic Ocean follow wind driven ice motion (Aagaard *et al.*, 1980). This is expected to be influenced by climate change since geostrophic wind speeds over the Arctic Ocean increased by about 15% as a 30 years average (Proshutinsky *et al.*, 2015).

Atlantic water moves cyclonically around the deep basins (Rudels, 2012). Sea-ice motion and surface geostrophic flow in the Arctic Ocean is generally wind driven and follows the anticyclonic flow of the Beaufort Gyre and the Transpolar Drift Stream in the Amerasian Basin and is cyclonical in the Eurasian Basin. The Beaufort Gyre is the most important upper-ocean circulation feature in the Canadian Basin (Timmermans and Marshall, 2020).

Among many other environmental parameters, the Arctic Oceans' wind driven surface circulation is controlled by atmospheric pressure and temperature gradients between the cold Arctic and the more temperate North Atlantic, a system called the Arctic Ocean Oscillation (AOO). The AOO is closely coupled to the North Atlantic Oscillation (NAO) (Dukhovskoy *et al.*, 2004; Proshutinsky and Johnson, 1997; Proshutinsky *et al.*, 1999) and is described by the Arctic Ocean Oscillation Index (AOOI) (Proshutinsky and Johnson, 1997). Figure 3 shows major surface currents of the Arctic Ocean for the early twenty first century.

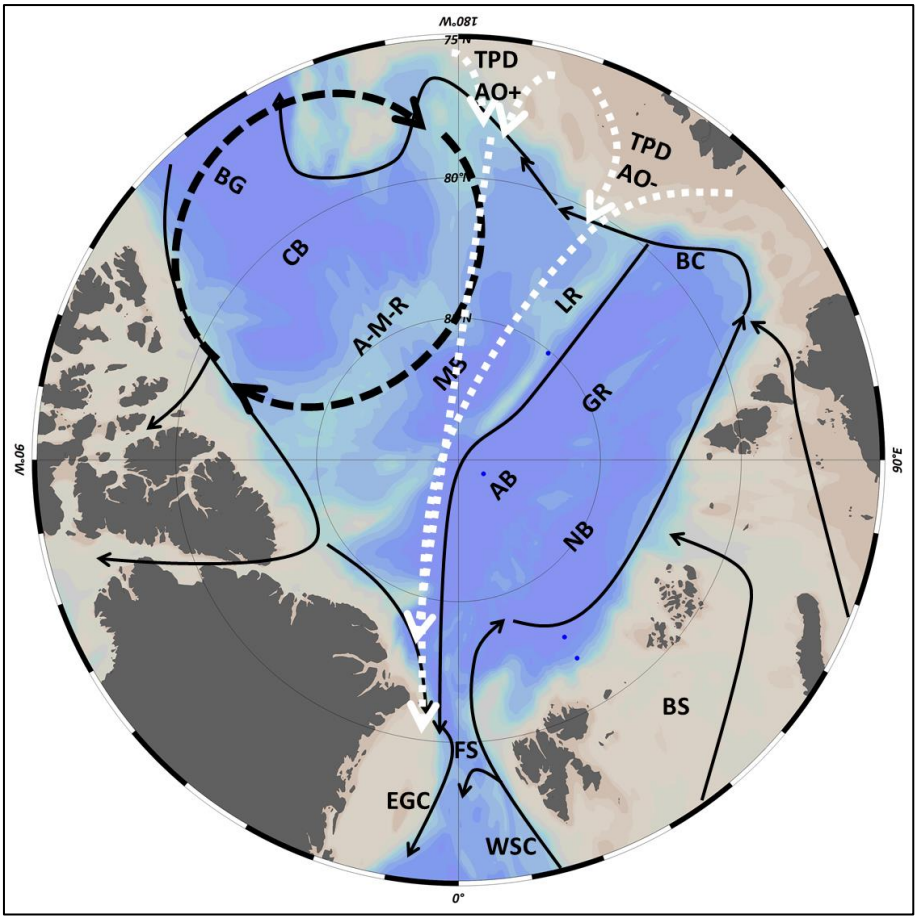


**Figure 3: Circulation pattern of major surface currents (Beszczynska-Moeller *et al.*, 2011) and the locations of the TPD (Trans Polar Drift) according to AO stages (white dashed lines), AO- represents the 2015 situation (Charette *et al.*, 2020). AB = Amundsen Basin, A-M-R = Alpha-Mendeleev-Ridge, BC= Boundary Current, BG = Beaufort Gyre, BS = Barents Sea, CB = Canada Basin, EGC = East Greenland Current, FS = Fram Strait, GR = Gakkel Ridge, LR = Lomonosov Ridge, MB = Makarov Basin, NB = Nansen Basin, WSC = West Spitzbergen Current. Map was created using Ocean Data View® (Schlitzer, 2016).**

The AOOI determines whether the Arctic Ocean surface layer is dominated by Cyclonic- (CCR) or Anti-Cyclonic (ACCR) circulation regimes. In times of a positive AOOI circulation regimes are in a clockwise ACCR stage and in a counter clockwise CCR mode during periods of negative AOOI (Proshutinsky and Johnson, 1997; Proshutinsky *et al.*, 1999). During ACCR stages ice drift and surface currents in the Eurasian Basin are expected to flow towards the Fram Strait along the shelf-break, while during CCR stages they are shifted northwards more to the centre of the Eurasian Basin (Proshutinsky *et al.*, 2015). Additionally, upwelling can occur during ACCR stages, causing a flow of deeper waters (from down to ca. 500 m) from the interior basins to the shelves, (Proshutinsky and Johnson, 1997; Randelhoff and Sundfjord, 2017). ACCR and CCR stages change in a rhythm of approximately 5- to 7-year intervals (Proshutinsky *et al.*, 2015). Since 1997, the AOOI is in a permanently positive stage. It is expected that the AOOI remains positive over longer periods with short phases of negative (CCR) stages in the future, contrasting the twentieth century conditions (Proshutinsky *et al.*, 2015). In addition, the environmental

consequences of AOOI stages seem to differ in recent times, especially surface circulation at the shelves and shelf-breaks might change their reaction to differing AOOI stages in the future (Armitage *et al.*, 2018).

A major surface current in the Arctic Ocean is the Trans Polar Drift (TPD). It is the most important transport mechanism for shelf water and sea ice from the Laptev and East Siberian Seas toward the central basin and subsequently to the Fram Strait (Ekwurzel *et al.*, 2001; Rigor *et al.*, 2002; Rudels, 2015; Schlosser *et al.*, 1994). This Trans-Arctic current crosses the Arctic Ocean in 1-3 years (Pfirman *et al.*, 1997).

The Arctic Oscillation (AO) controls the location of the TPD (Mysak, 2001), shown in figure 3. Low or negative AOOI stages lead to an expansion of the anticyclonic Beaufort Gyre and in these phases the TPD flows from the Laptev- and East Siberian Seas over the Lomonosov Ridge (Morison *et al.*, 2006; Woodgate *et al.*, 2005). Positive AO phases scale down the Beaufort Gyre and the TPD shifts eastward towards the Alpha-Mendeleev Ridge (Mysak, 2001). Like the entire Arctic Ocean the TPD system is expected to change, however it is unclear whether it might intensify in the next decades, due to wind forcing by thinned ice cover (Newton *et al.*, 2017) or slow down due to decreasing sea ice cover (Krumpen *et al.*, 2019).

### 1.2.3 Intermediate- and Deep Water Circulation

Before entering the Arctic Ocean, Atlantic Waters flow across the Scotland-Greenland Ridge and through the Nordic Seas in the North Atlantic Current extension of the Gulf Stream. Their northward propagation in the Norwegian Sea consists of a western and an eastern branch of the Norwegian Atlantic Current, which are topographically determined (Orvik and Niiler, 2002). Atlantic waters from the Norwegian Atlantic Current enter the Arctic Ocean via the Fram Strait and the Barents Sea Opening. The Fram Strait Branch Water (FSBW) is supplied through the northward directed West Spitsbergen Current (WSC) (Rudels, 2012). It brings relatively salty and warm Atlantic Water into the Arctic Ocean (~7 Sv) and recirculation within the Fram Strait can occur (Beszczynska-Möller *et al.*, 2012; Schauer *et al.*, 2004). Outflow of Arctic waters in the Fram Strait is transported by the southward flowing East Greenland Current (EGC) (~9 Sv) (de Steur *et al.*, 2014) contributing to a southward net flow through the Fram Strait of several Sv, with a huge monthly variability (Schauer and Beszczynska-Moeller, 2009). The Barents Sea Branch Water (BSBW) enters through the Barents Sea (~2 Sv) (Ingvaldsen *et al.*, 2002) and consists of Atlantic water that undergoes strong modifications in Barents- and Kara Seas by cooling and mixing with continental runoff and meltwater (Rudels *et al.*, 2015). Heat flow to the Arctic Ocean is expected to be higher in the BSBW than in the FSBW (Schauer and

Beszczynska-Moeller, 2009). The BSBW enters the Nansen Basin through the St. Anna Trough, where limited mixing with the FSBW occurs (Rudels *et al.*, 2015). Atlantic Water entering the Arctic Ocean causes sea ice melt and its surface experiences modifications, such as cooling and freshening. Therefore the distinct temperature maximum of Atlantic waters within the Arctic Ocean consists only in deeper parts of the water column (Rudels *et al.*, 1996). BSBW and FSBW flow to the east forming a cyclonic boundary current along the continental slopes of the Nansen and Amundsen Basin (Rudels, 2009; Woodgate *et al.*, 2001). Transient tracer studies indicate circulation times of Atlantic waters from the Barents Sea opening through the Arctic Ocean and back to the Fram Strait of 15-30 years (Karcher *et al.*, 2011; Smith *et al.*, 2011).

Atlantic inflow into the Arctic Ocean is likely to gain more importance, as warming of these waters is partly responsible for warming of Arctic Waters since the 1990s (Karcher *et al.*, 2003). This increasing importance also holds beyond hydrographic features as accelerating Atlantic currents are expected to cause an expansion of Atlantic phytoplankton polewards (Oziel *et al.*, 2020). Together with sea ice melt caused by warm Atlantic Waters (Årthun *et al.*, 2019; Polyakov *et al.*, 2005; Polyakov *et al.*, 2017) an increased accumulation of anthropogenic $CO_2$ in the central Arctic Ocean is observed (Terhaar *et al.*, 2020; Ulfsbo *et al.*, 2018). These developments of stronger Atlantic influence on the Arctic Ocean are usually referred to as "Atlantification", which is especially relevant for the Eurasian Basin of the Arctic Ocean.The BSBW and the FSBW return in the Atlantic- and intermediate water layers along the Lomonosov Ridge at depths of ~1025 m and ~425 m, respectively (Tanhua *et al.*, 2009), towards the Fram Strait (Rudels *et al.*, 2013). Recirculation within the Eurasian Basin is possible (Rudels *et al.*, 1994). One branch of the BSBW crosses the Lomonosov Ridge entering the Canada Basin following the Arctic Ocean Boundary Current (AOBC) (Rudels, 2009) and circulates cyclonically along the basin margins following isobaths (Woodgate *et al.*, 2001). Figure 4 shows circulation patterns of intermediate waters of Atlantic origin in the Arctic Ocean after Rudels (2009). Observations and modelling of anthropogenic $^{129}I$ (129-Iodine) indicate a flow direction reversal of intermediate Atlantic Waters in the Canada Basin, linked to AOOI controlled circulation (Karcher *et al.*, 2012). This can imply a potential decoupling of flow regimes in the Canada- and Eurasian Basins, reducing exchange times between the two major basins of the Arctic Ocean (Karcher *et al.*, 2012).

Deep and bottom water circulation, below the Atlantic Water layer, is cyclonic in the Eurasian- and Canadian Basin, similar to the intermediate water circulation, yet deep and bottom water circulation is much less understood (Aagaard, 1981; Rudels, 2015). Renewal rates of Arctic deep waters are slow, which is also evident from recent CFCs and $SF_6$ data (Smethie, 2017). Eurasian

and Canadian basin bottom waters are topographically isolated and therefore show mean ages based on $^{14}C$ measurements, of 250 and 450 years, respectively (Schlosser *et al.*, 1997). It seems still to be an open question to which degree deep water renewal in the Eurasian Basin is a continuous process or controlled by sporadic and relatively short-lived events (Björk and Winsor, 2006). Parts of the Eurasian Basin Bottom Waters (EBBW) originate from sinking high-density waters from the neighbouring shelves of the Barents- and Kara Seas (Aagaard *et al.*, 1985; Årthun *et al.*, 2011). Deep water masses in the Eurasian Basin are also influenced by the inflow of Atlantic Water via the Fram Strait, indicated by CFC distributions (Smethie *et al.*, 1988). Deep waters of the Amerasian Basin consist partly of brine rejection induced density flows of waters from the continental slopes (Jones *et al.*, 1995; Rudels, 2012).

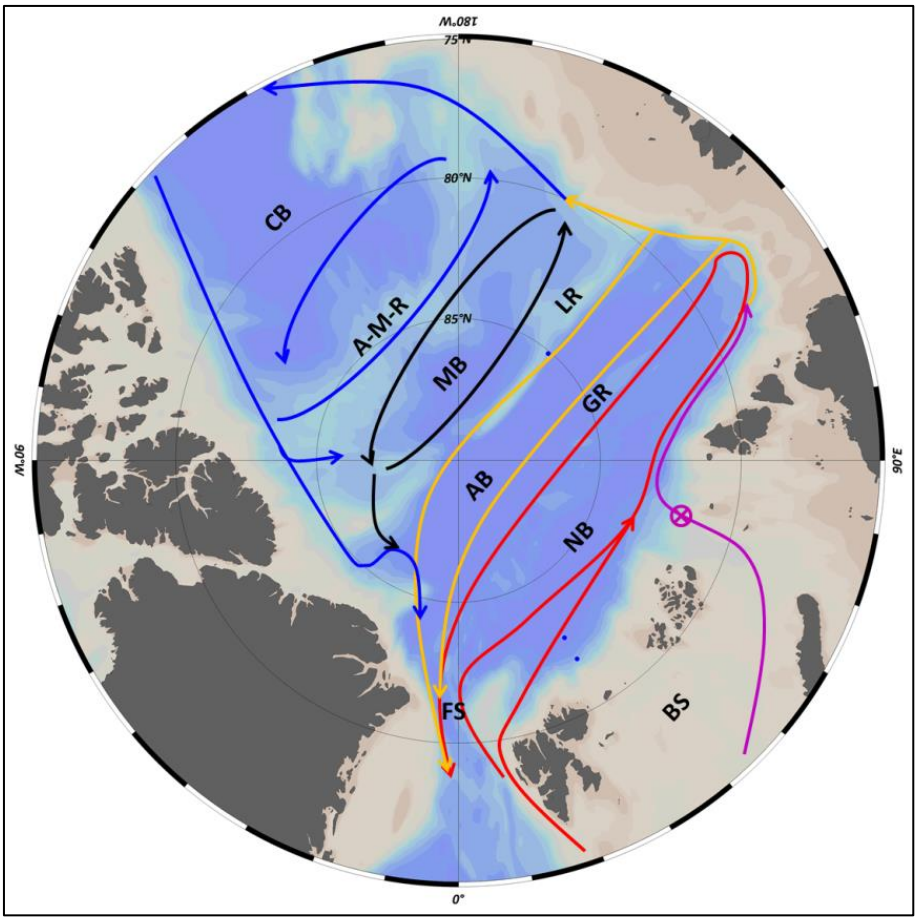


**Figure 4: Circulation pattern of intermediate waters (~500-1500 m) and inflow of Atlantic waters through the Barents Sea (BS) (Rudels, 2009). Crossed circle indicates subsidence and mixing with ambient waters of BSBW (~500m) at the St. Anna Through. AB = Amundsen Basin, A-M-R = Alpha-Mendeleev-Ridge, CB = Canada Basin, FS = Fram Strait, GR = Gakkel Ridge, LR = Lomonosov Ridge, MB = Makarov Basin, NB = Nansen Basin. Map was created using Ocean Data View® (Schlitzer, 2016).**

### 1.2.4 Particle Fluxes, Composition and Transport

Particle inputs into the Arctic Ocean have a variety of sources. First of all continental sources such as riverine discharge (Klunder *et al.*, 2012a) and coastal erosion, due to permafrost thawing (Schuur *et al.*, 2013; Schuur *et al.*, 2015), are important components of particles transported to the central Arctic Ocean. Resuspension of slope and shelf sediments add to this source (Klunder *et al.*, 2012a). Additionally, biological production within the central basins plays a role in Arctic Ocean particle fluxes (Arrigo *et al.*, 2008). A particle source, exclusive to the Eurasian Basin, are hydrothermal vents at the Gakkel Ridge (Edmonds *et al.*, 2003). Sea ice melt induced release of particulate matter, both biogenic and lithogenic, adds to these sources as a transport mechanism of particles to the central basins (Boetius *et al.*, 2013).

Particle concentration, fluxes, and composition in the Arctic Ocean are very different at the margins compared to the ice-covered central deep basins and also differ between the Amerasian- and the Eurasian Basin (Xiang and Lam, 2020), and to a lesser degree also between the Nansen- and Amundsen Basin (Nöthig *et al.*, 2020). Generally, vertical particle fluxes in the sea ice–covered central Arctic Ocean are low, with the Canada Basin showing the lowest biogenic fluxes reported for any region of the world's ocean (Honjo *et al.*, 2010).

In the central Arctic Ocean close to the Eurasian continental margin above the southern Lomonosov Ridge ice cover used to be about 95% throughout most of the year and even in summer above 90% (Haas and Eicken, 2001), although it is declining by about 6-10% per decade (Jansen *et al.*, 2020) and is locally only covered by 35-55% in recent summers (Piontek *et al.*, 2020). In this nearly permanently ice-covered region reduced light penetration restricts biological primary production to about only three summer months (Sakshaug, 2004). Therefore, lithogenic material dominates the particle composition there due to the relatively high input of terrigenous matter by the Eurasian and Amerasian rivers combined with the relatively low primary production. This is also reflected in most sediments of the central Arctic Ocean (Fahl and Nöthig, 2007). Low primary production in the central basins is also reported from $^{234}$Th-derived POC exports (Cai *et al.*, 2010).

In contrast to lithogenic material, carbonate is of minor importance in suspended particles and sediments of the central Arctic Ocean (Stein *et al.*, 1994), leading Fahl and Nöthig (2007) to conclude that the central Arctic Ocean seems to be a ''terrigenous, low-productivity ocean''. This is in contrast to the Arctic shelves and margins like the Kara- (Gaye *et al.*, 2007) and Beaufort Seas (O'Brien *et al.*, 2006), where organic carbon fluxes are up to nine times higher than at the Lomonosov Ridge, due to river discharge (Fahl and Nöthig, 2007).

Net Primary Production (NPP) is changing in the Arctic Ocean, especially at the shelves and in waters around the shelf break, e.g. the Barents Sea and the Nansen Basin margin (Arrigo and van Dijken, 2015). Large under-ice phytoplankton blooms have been observed under less solid sea ice (Arrigo *et al.*, 2012; Arrigo *et al.*, 2014; Assmy *et al.*, 2017). The reasons are reduced ice cover and therefore prolonged growing seasons due to increased light transmission (Dalpadado *et al.*, 2020) as well as an increasing availability of nutrients (Tremblay and Gagnon, 2009). Nevertheless, it is still unknown whether these changes will directly lead to enhanced primary productivity in the central Arctic Ocean. Lund-Hansen *et al.* (2020) suggest, based on model results, that primary production rates in the Amundsen Basin will increase 10- to 14-fold under ice free summer conditions in the future. While Slagstad *et al.* (2015) predicted that productivity in Arctic waters will remain low until approximately 2100. According to the latter authors, only some margins and shelves where surface water column stratification is weak, such as the northern Barents Sea and the Kara Sea shelf break, will experience significant NPP increases in the near future (Slagstad *et al.*, 2015). A freshening of Arctic surface waters due to enhanced ice melt (Morison *et al.*, 2012) and larger riverine input (Peterson *et al.*, 2002) as well as warming by warmer Atlantic inflow (Beszczynska-Möller *et al.*, 2012; Polyakov *et al.*, 2017), will stabilize the upper water column by stratification (Ardyna *et al.*, 2013; Tremblay and Gagnon, 2009). Intensified stratification of the water columns can prevent nutrient transport into the sunlit surface layers, if no nutrient-rich waters are brought to the surface by regional upwelling (Codispoti *et al.*, 2005; Tremblay and Gagnon, 2009). Hence under the presence of low vertical particle fluxes from the surface, lateral particle transport processes play an important role in the particle transport of the Arctic Ocean *(Fahl and Nöthig, 2007; Honjo et al., 2010; Hwang et al., 2008).*

One important and rapid lateral transport mechanism for shelf-derived particulate matter in the central Arctic Ocean is the TPD (Kipp *et al.*, 2018; Letscher *et al.*, 2011). As discussed in more detail in section *1.1.2 Surface circulation and sea ice* this drift system is expected to undergo changes with changing climate conditions. Any change, acceleration or slowing down of the TPD will have an impact on particle transports to the central basins and therefore the ecosystem dynamics of the central Arctic Ocean. The TPD is responsible for higher amounts of both lithogenic material and diatoms in the Amundsen Basin compared to the Nansen Basin (Nöthig *et al.*, 2020), which is less influenced by the TPD than the Amundsen Basin (Rutgers van der Loeff *et al.*, 2018). Still particle fluxes are low compared to the margins and shelves (Cai *et al.*, 2010). Approximate location of the TPD in 2015 following Charette *et al.* (2020) is shown in figure 3. Sea-ice transport of particles to the central basins will increase with increasing summer

ice melt (Charette *et al.*, 2020). Particles that used to be transported to Fram Strait and released at lower latitudes (Granskog *et al.*, 2012) are going to be released within the central basins (Charette *et al.*, 2020).

Recent GEOTRACES studies based on Radium isotopes have shown that the TPD is already changing. For example, changes of its chemical composition indicate potentially significant changes in nutrients and carbon fluxes from the Siberian shelves (Kadko *et al.*, 2019; Kipp *et al.*, 2018; Rutgers van der Loeff *et al.*, 2018). An increase of dissolved iron (dFe) at TPD influenced stations (Rijkenberg *et al.*, 2018) additionally indicates stronger release and mobilization of trace elements such as Fe or Mn (Manganese), as observed for Amerasian Basin shelves (Jensen *et al.*, 2020).

Additionally, Benthic Nepheloid Layers (BNLs) can add lithogenic material by sediment resuspension to the deep water column, as observed in the Canada Basin (Hwang *et al.*, 2015) and suggested to occur at least sporadically at the Nansen Basin slope and margin (Scholten *et al.*, 1995). Increased particle fluxes at the Eurasian Basin margins are already indicated by locally elevated particulate $^{230}$Th and $^{232}$Th values close to Svalbard (Gdaniec *et al.*, 2020), pointing at resuspension or at particles transported by glacier and/or coastal erosion leading to increased $^{230}$Th scavenging. These particles are reflected in transmission data as shown in figure 5 (Gardner *et al.,* 2020). The distribution of these particles along the margins of the Nansen Basin is probably affected by eddies causing exchange between the boundary current and the more central parts of the Nansen Basin (Våge *et al.*, 2016).

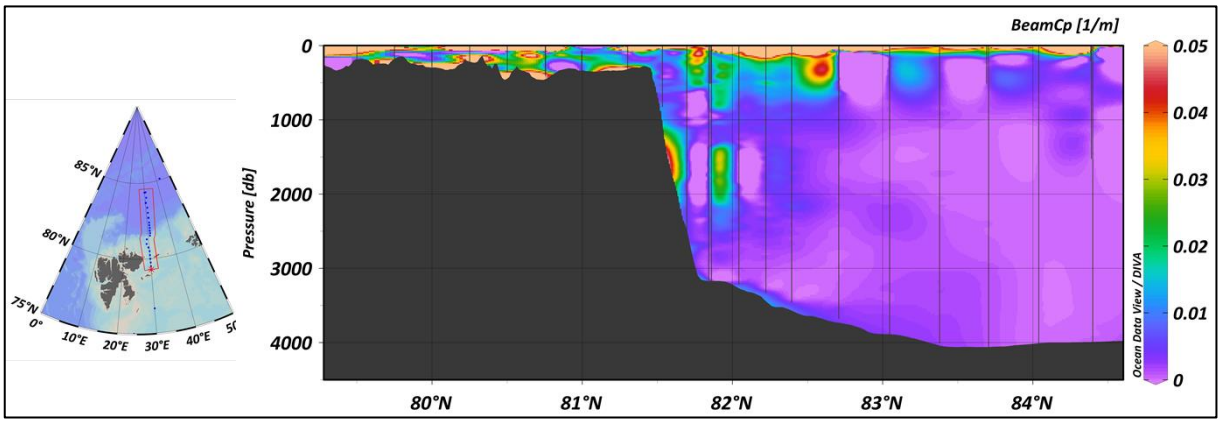


**Figure 5: Transmission data section from the Barents Sea shelf to the central Nansen Basin (Gardner *et al.*, 2020)). The figure was created using Ocean Data View® (Schlitzer, 2016).**

Similar processes are expected for intermediate waters, Intermediate Nepheloid Layers (INLs) originate from the continental slopes, carrying lithogenic material to the interior Arctic Ocean (Xiang and Lam, 2020). In the Nansen Basin deep water particles can also have a significant admixture of hydrothermal particles, containing trace elements such as Fe and Mn (Klunder *et*

*al.*, 2012b; Middag *et al.*, 2011), due to hydrothermal venting at the Gakkel Ridge (Baker *et al.*, 2004; Edmonds *et al.*, 2003). Large explosive volcanic eruptions occur sporadically in addition to the constant hydrothermal venting (Sohn *et al.*, 2008). The importance of these hydrothermal features is explained in section *1.4.3 Role of Hydrothermal vents for $^{230}$Th and $^{231}$Pa scavenging in the Arctic*.

## 1.3 $^{230}$Th and $^{231}$Pa in the Ocean and their Application as Tracers

### 1.3.1. U-Series and $^{230}$Th, $^{231}$Pa.

Uranium isotopes $^{238}$U and $^{235}$U, as well as the thorium isotope $^{232}$Th, are long-lived radioactive isotopes occurring in all rocks of the Earth. Long lived radioactive isotopes, like some naturally occurring radionuclides from the uranium and thorium decay-series are important for understanding the Earth system on geological timescales (>millions of years) (Moore and Sackett, 1964). Daughter isotopes have activities equal to the activity of their parent isotope at secular equilibrium. If parent and daughter isotopes have different chemical behaviour, this creates differences between their activities, hence radioactive disequilibrium. This disequilibrium reflects the removal or addition of a daughter isotope by a geochemical process and in many cases allows quantifying the rate of this process (Roy-Barman and Jeandel, 2016; Rutgers van der Loeff and Geibert, 2008). The chemical behaviour of the parent isotope determines the daughter isotopes' oceanographic input function. Soluble elements, such as uranium, produced by radioactive decay of insoluble parent isotopes have a continental source and are released to the ocean from continents or sediments (Rutgers van der Loeff and Geibert, 2008). Isotopes from the U- and Th-decay series are distributed in the ocean according to their parent isotopes distribution and their chemical behaviour, half-lives ($t_{1/2}$). Therefore, different isotopes of the same element differ in their oceanographic distribution, allowing the use of isotope ratios as tracers for materials with the same origin as the parent isotopes (Roy-Barman and Jeandel, 2016).

230-thorium, ($^{230}$Th, $t_{1/2}$: 75.69 kyrs (Cheng *et al.*, 2000)) and 231-protactinium ($^{231}$Pa, $t_{1/2}$: 32.57 kyrs (Jerome *et al.*, 2020)) are two of these isotopes. They are produced by the radioactive decay of their dissolved parent isotopes $^{234}$U and $^{235}$U, respectively, which are homogeneously distributed in sea-water, at a constant rate and at a well-known $^{231}$Pa/$^{230}$Th activity ratio of 0.093 (Andersen *et al.*, 2010; Delanghe *et al.*, 2002; Robinson *et al.*, 2004). Their production depends on the uranium concentration in seawater, which varies with salinity (Chen *et al.*, 1986). Thus there is a uniform and steady source of $^{230}$Th and $^{231}$Pa everywhere in the ocean.

### 1.3.2 $^{230}$Th, $^{231}$Pa Fractionation in the Ocean

Particles in the ocean can be produced in the water column by biological production or authigenic mineral precipitation or are derived externally from terrigenous material released from the continents and added to the ocean by atmospheric transport, rivers or coastal erosion (Jeandel *et al.*, 2015). Removal of particle reactive elements from the dissolved phase by adsorption to settling particles and the subsequent transport to the seafloor is a process called scavenging (Goldberg, 1954). Scavenging of particle reactive elements onto constantly settling suspended particulate matter and subsequent removal from the water column is a key component of biogeochemical cycles in the ocean (Rutgers van der Loeff and Geibert, 2008). Residence times of many elements in the ocean are controlled by particle formation, remineralization and transport (Geibert, 2018; Jeandel *et al.*, 2015; Lal, 1977). $^{230}$Th is about 10 times more particle reactive than $^{231}$Pa and therefore the residence time of $^{230}$Th in the ocean is shorter compared to $^{231}$Pa (<40 yrs and <200 yrs, respectively) (Anderson *et al.*, 1983b). $^{230}$Th and $^{231}$Pa are both particle reactive and insoluble in sea water, in contrast to their soluble uranium parent isotopes. In fact, Th is one of the elements with the lowest solubility in seawater (Turner *et al.*, 1981). Their insolubility causes their removal to sediments by adsorption onto settling particles. Their scavenging removal is much faster than removal by their radioactive decay (Bacon and Anderson, 1982; Nozaki *et al.*, 1987). The scavenging intensity of $^{230}$Th relative to $^{231}$Pa can be described using their fractionation factor $F_{(Th/Pa)}$ (Anderson *et al.*, 1983b), which is described as:

$$F_{(Th/Pa)} = (^{230}Th/^{231}Pa)_{particulate}/(^{230}Th/^{231}Pa)_{dissolved}$$

If $^{231}$Pa and $^{230}$Th had the same scavenging behaviour, the dissolved and particulate $^{231}$Pa/$^{230}$Th ratio would be equal, resulting in a fractionation factor of 1, and there would be no scavenging removal intensity information in the $^{231}$Pa/$^{230}$Th ratio.

$^{230}$Th is quickly removed from the water column and transported to the seafloor, due to its high particle reactivity (Henderson *et al.*, 1999). Therefore, one might expect an increase of particulate $^{230}$Th with depth and uniformly low dissolved $^{230}$Th, due to quick removal of the $^{230}$Th produced homogeneously throughout the water column from the dissolved phase. However, many reported $^{230}$Th depth profiles show an increase of both particulate and dissolved $^{230}$Th with depth (Gdaniec *et al.*, 2017; Hayes *et al.*, 2015a; Moore and Sackett, 1964; Venchiarutti *et al.*, 2011). This can best be explained by reversible scavenging (Bacon and Anderson, 1982; Nozaki *et al.*, 1981). Reversible scavenging is a process of adsorption onto particles of an element with following desorption, hence an exchange between the dissolved and the particulate phase as the particles sink through the water column. The reversible scavenging

process leads to a general increase of dissolved and particulate $^{230}$Th and $^{231}$Pa concentrations with depth (Bacon and Anderson, 1982; Roy-Barman *et al.*, 1996). Hence in the absence of lateral input or removal fluxes it is expected that concentrations of $^{230}$Th and $^{231}$Pa are controlled by an adsorption-desorption equilibrium with sinking particles, leading to a linear increase with depth (Bacon and Anderson, 1982; Krishnaswami *et al.*, 1976; Nozaki *et al.*, 1981). Figure 6 shows idealized water column distributions of natural long-lived uranium isotopes $^{238}$U, $^{235}$U, $^{234}$U, as well as $^{230}$Th and $^{231}$Pa.

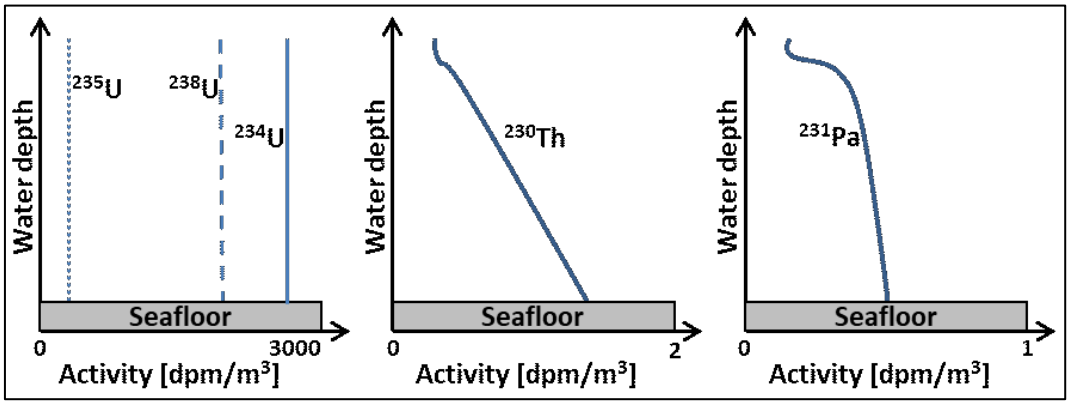


**Figure 6: Schematic water column distribution profiles and range of activities in dpm/m$^3$ of natural uranium isotopes (left), $^{230}$Th (middle) and $^{231}$Pa (right) in seawater. The figure was modified after Rutgers van der Loeff and Geibert (2008).**

All deviations from such a linear radionuclide profile (like the nonlinear behaviour of $^{231}$Pa in Fig. 6) therefore can give information about changing scavenging intensities or the influence of lateral transport by ocean circulation. Therefore, the sediment $^{231}$Pa/$^{230}$Th activity ratio can be used as a tracer for ocean circulation (Marchal *et al.*, 2000; Yu *et al.*, 1996), as well as marine particle fluxes (Moore and Sackett, 1964; Roy-Barman, 2009). Relatively linear depth profiles of $^{230}$Th and $^{231}$Pa do not necessarily exclude lateral fluxes entirely (Roy-Barman, 2009; Venchiarutti *et al.*, 2008). The distribution of $^{230}$Th and $^{231}$Pa in the water column, as well as their sedimentary ratio can be used as proxies for biological production, scavenging processes and past ocean circulation (Chase *et al.*, 2002; McManus *et al.*, 2004).

### 1.3.3 $^{230}$Th, $^{231}$Pa Fractionation in the Ocean: Boundary Scavenging

Due to their different particle reactivity and subsequent fractionation, the removal of $^{230}$Th and $^{231}$Pa from the water column is controlled by different transport processes, representing two model types of trace metal removal. $^{230}$Th is primarily removed from the water column in the open ocean by the uptake onto settling particles, while $^{231}$Pa is mainly transported to environments with higher particle fluxes (Anderson *et al.*, 1983b) and removed there enabled by the longer residence time of $^{231}$Pa compared to $^{230}$Th (Anderson *et al.*, 1983a). Continental

margins and ocean boundaries in general are among the areas where high biological production and high input of terrestrial inputs (Roy-Barman and Jeandel, 2016) causes much higher particle fluxes than in the open ocean (Nittrouer and Wright, 1994). This process of $^{230}$Th, $^{231}$Pa fractionation is called boundary scavenging (Bacon *et al.*, 1988). Boundary scavenging fractionates $^{230}$Th and $^{231}$Pa on a basin-wide scale (Anderson *et al.*, 1983b; Bacon *et al.*, 1988). This fractionation causes different $^{231}$Pa /$^{230}$Th activity ratios in open ocean and ocean margin sediments. The boundary scavenging process and the sedimentary consequences of it are illustrated schematically in figure 7. Open ocean sedimentary $^{231}$Pa/$^{230}$Th ratios are below the $^{231}$Pa/$^{230}$Th production ratio of 0.093 and are above their production ratio in ocean margin sediments or sediments in other high particle flux areas (Anderson *et al.*, 1983a; Luo *et al.*, 2010).

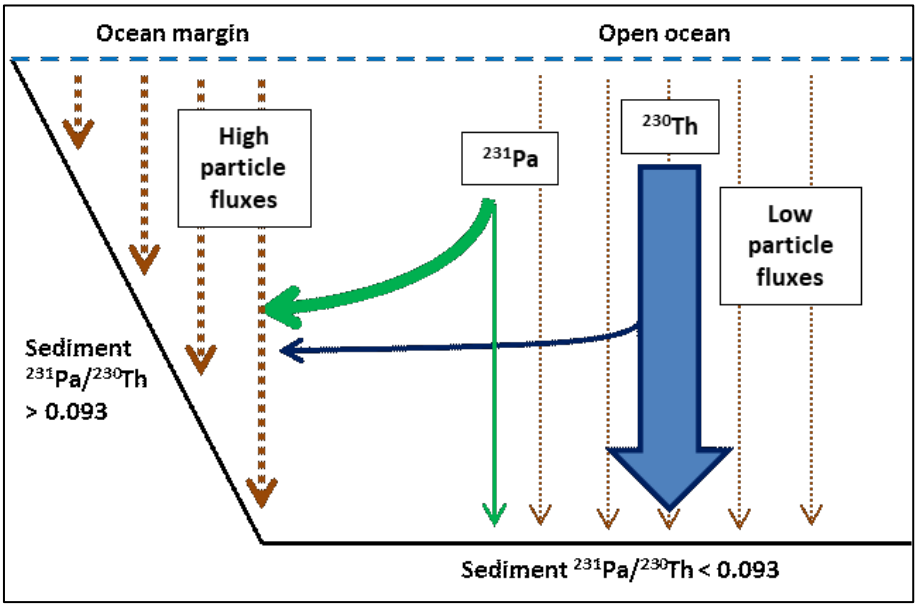


**Figure 7: Schematic illustration of the boundary scavenging process between the high productivity ocean margins and the low productive open ocean, showing the different sedimentary activity ratios of $^{231}$Pa/$^{230}$Th at the margins and in the open ocean, due to scavenging removal of $^{230}$Th in the open ocean and lateral transport of $^{231}$Pa to the margins, in relation to their production ratio of 0.093.**

### 1.3.4 $^{230}$Th, $^{231}$Pa Fractionation in the Ocean: Particle Composition

In addition to the aforementioned specific particle reactivities and importance of particle fluxes, particle composition controls trace element scavenging from seawater (Chase *et al.*, 2002). Scavenging intensities of $^{230}$Th and $^{231}$Pa in the ocean depend highly on particle composition, because not all marine particle types scavenge $^{230}$Th and $^{231}$Pa equally. $^{230}$Th and $^{231}$Pa have distinct affinities for adsorption onto different specific particle types (Chase *et al.*, 2002; Geibert and Usbeck, 2004; Hayes *et al.*, 2015; Kretschmer *et al.*, 2011). $^{230}$Th tends to be removed by lithogenic material and $CaCO_3$ primarily, while $^{231}$Pa prefers biogenic opal rich particles, both of

them show a strong adsorption affinity for Fe and Mn oxides (Chase *et al.*, 2002; Geibert and Usbeck, 2004; Pavia *et al.*, 2018). For example a deviation from a linear depth profile can result from changing F factors with depth, due to changing particle composition, e.g. a change in opal content of settling particles (Scholten *et al.*, 2008). Due to their different particle reactivity and preferred scavenging types of particles, fractionation of $^{231}$Pa and $^{230}$Th by chemical particle composition is important to interpret scavenging intensities and sedimentary $^{231}$Pa/$^{230}$Th ratios (Lippold *et al.*, 2012; Rutgers van der Loeff and Geibert, 2008).

### 1.3.5 $^{230}$Th, $^{231}$Pa Fractionation in the Ocean: Deep Water Circulation

As mentioned earlier $^{231}$Pa is more prone to be advected by ocean currents compared to $^{230}$Th. Mean scavenging residence times in deep waters of $^{231}$Pa (~200 years) are much longer compared to $^{230}$Th (~30 years) (Yu *et al.*, 1996). If the scavenging residence time of an element or isotope exceeds or is in the order of water mass ventilation times, it can be exported from an ocean basin or area by circulation currents. For example Marchal *et al.* (2000) report that in the deep Atlantic Ocean the mean ventilation time is similar to the mean scavenging residence time of $^{231}$Pa. This enables a quite big proportion of the $^{231}$Pa, produced within the Atlantic Ocean, to be exported to the Southern Ocean by the southward directed flow of the North Atlantic Deep Water (Marchal *et al.*, 2000). This substantial southward net export of $^{231}$Pa from the Atlantic Ocean is represented in sedimentary $^{231}$Pa/$^{230}$Th activity ratios below their water column production ratio, in Atlantic Holocene sediments (Walter *et al.*, 1999; Yu *et al.*, 1996). Due to deep water circulation, about 45% of the dissolved $^{231}$Pa, produced in the Atlantic Ocean are exported to the Southern Ocean, in contrast to only around 15% of the Atlantic $^{230}$Th (Yu *et al.*, 1996). This deep water fractionation of $^{231}$Pa and $^{230}$Th is reflected in sediments from the Southern Ocean, where the $^{231}$Pa/$^{230}$Th activity ratio is above their production ratio (Walter *et al.*, 1999). Hence the $^{231}$Pa exported from the Atlantic Ocean is partly deposited there (Marchal *et al.*, 2000; Rutgers van der Loeff *et al.*, 2016). This example shows the importance of deep and intermediate water circulation on $^{231}$Pa, $^{230}$Th fractionation in addition to particle fluxes, particle composition and lateral gradients in particle fluxes.

## 1.4 $^{230}$Th and $^{231}$Pa in the Arctic Ocean

### 1.4.1 Water Column

Several studies have investigated the water column distribution of dissolved $^{230}$Th and $^{231}$Pa in the Arctic Ocean in relation to particle fluxes and water mass residence time over the past decades. Still, some key points in removal processes of dissolved $^{230}$Th and $^{231}$Pa are not entirely understood and the sensitivity of dissolved $^{230}$Th and $^{231}$Pa especially to environmental changes in the Arctic Ocean is still not explained sufficiently. Bacon *et al.* (1989) observed high $^{230}$Th and $^{231}$Pa concentrations at the perennially sea ice-covered Alpha Ridge and the northern Makarov Basin and concluded that scavenging of particle reactive elements in the central Arctic Ocean was significantly lower than in other parts of the world's ocean. Edmonds *et al.* (1998), later confirmed by Trimble *et al.* (2004), showed that $^{230}$Th and $^{231}$Pa activities in the deep southern Canada Basin were much lower, and residence times correspondingly shorter, than at the Alpha Ridge (Bacon *et al.*, 1989). Dissolved $^{230}$Th depth profiles in the central Arctic Ocean show higher surface concentrations under permanent sea ice cover and less steep profiles in general, due to low particle fluxes and conseqently reduced scavenging. Figure 8 shows a simplified theoretical comparison between sea ice covered dissolved $^{230}$Th profiles and dissolved $^{230}$Th profiles under sea ice free conditions. Both are shown in absence of lateral transport. The perennial ice covered situation would represent the location of the Alpha Ridge, with high dissolved $^{230}$Th concentrations, while the ice free situation would explain lower concentrations in areas with less sea ice cover, like the southern Canada Basin with lower dissolved $^{230}$Th concentrations (Edmonds *et al.*, 1998).

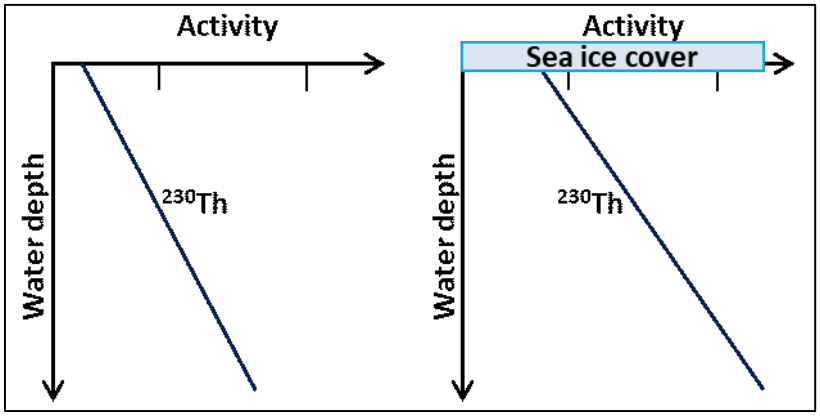


**Figure 8: Schematic representation of dissolved $^{230}$Th concentration profiles under perennial sea ice cover (right) and under sea ice free conditions (left). The figure was modified after Grenier *et al.* (2019).**

Cochran *et al.* (1995) found residence times of dissolved $^{230}$Th of 18–19 years in the central Nansen Basin and of 10–12 years on the Barents Sea slope. $^{230}$Th concentrations in the Nansen Basin were lower than those from the Alpha Ridge reported by Bacon *et al.* (1989), and deep

waters in the central Nansen Basin showed higher dissolved $^{230}$Th concentrations and lower particulate concentrations than near the slopes (Cochran *et al.*, 1995). Scholten *et al.* (1995) reported that the shallower Eurasian Basin Deep Water (EBDW) is rather more influenced by ventilation than the deeper Eurasian Basin Bottom Water (EBBW) and suggested resuspension of slope sediments as the cause for the increased scavenging rates in the EBBW.

Gdaniec *et al.* (2020) showed that elevated particle fluxes at the margins of the Eurasian Basin cause increased scavenging of $^{230}$Th and $^{231}$Pa. Recent investigations on time series of water column $^{230}$Th and $^{231}$Pa show that concentrations have changed significantly on decadal timescales in the Amerasian Basin, attributed to increased particle fluxes by sea ice retreat and increased transport of shelf particles to the central basins in the Amerasian Basin (Grenier *et al.*, 2019; Yu *et al.*, 2020).

### 1.4.2 Sediments

The sedimentary $^{231}$Pa/$^{230}$Th activity ratio is a well-known and frequently applied paleoceanographic tool applied as a proxy for particle fluxes and composition, biological productivity or overturning advective circulation (Chase *et al.*, 2002; Walter *et al.*, 1999; Yu *et al.*, 1996). In the Arctic Ocean, the $^{231}$Pa/$^{230}$Th sedimentary activity ratio was used to identify basin wide fractionation (Moran *et al.*, 2005), boundary scavenging (Edmonds *et al.*, 2004), production of $^{230}$Th and $^{231}$Pa related advective export (Moran *et al.*, 2005), scavenging rates (Edmonds *et al.*, 2004) or past advective export (Hoffmann *et al.*, 2013). Some questions remain unanswered, for example if boundary scavenging occurs in the Arctic Ocean, and were evaluated differently over time by Huh *et al.* (1997), Moran *et al.* (2005) and Hoffmann and McManus (2007). More information on the boundary scavenging discussion in the Arctic Ocean is provided in section *1.5 (Motivation and objectives - Why studying $^{230}$Th and $^{231}$Pa in the Arctic Ocean?).* Additionally, it still remains unknown why there is a $^{231}$Pa deficit in Arctic sediments. Gdaniec *et al.* (2020) found high $^{231}$Pa/$^{230}$Th activity ratios in sediments of the Nansen Basin margin, which might be a so far overlooked sink of $^{231}$Pa in the Arctic Ocean.

### 1.4.3 Role of Hydrothermal Vents for $^{230}$Th and $^{231}$Pa Scavenging in the Arctic Ocean

Hydrothermal plumes are sources of many trace elements, for example, Fe and Mn (Klinkhammer *et al.*, 1977; Resing *et al.*, 2015; Saito *et al.*, 2013) and sinks for others due to scavenging onto particles or mineral co-precipitation (German *et al.*, 2002; German *et al.*, 1991), including $^{230}$Th and $^{231}$Pa, as observed by $^{230}$Th and $^{231}$Pa removal in the South East Pacific even several thousand kilometres off axis (Pavia *et al.*, 2018). Especially hydrothermal particulate Fe

is an effective $^{230}$Th scavenger (Hayes *et al.*, 2015b; Pavia *et al.*, 2018). These hydrothermal plumes can travel over large distances affecting an entire ocean basin over time (Fitzsimmons *et al.*, 2014).

In the Arctic Ocean, the ultra-slow spreading Gakkel Ridge, dividing the Amundsen- and Nansen Basin, is the only hydrothermally active ridge. Along the Gakkel Ridge constant hydrothermal venting (Baker *et al.*, 2004) as well as huge explosive eruptions in conjunction with earthquakes can occur, which release huge amounts of dissolved and particulate trace elements (Schlindwein and Riedel, 2010; Sohn *et al.*, 2008). Among these trace element particles are Fe rich particles, which are effective $^{230}$Th scavengers (Geibert and Usbeck, 2003; Pavia *et al.*, 2018). Frequencies of explosive eruptions might increase in the future, due to a potential opening of a volcanic conduit (Riedel and Schlindwein, 2010). It is possible that those events trigger significant scavenging removal of $^{230}$Th.

## 1.5 Motivation and Objectives - Why studying $^{230}$Th and $^{231}$Pa in the Arctic Ocean?

This section describes and explains the overall motives and aims of this thesis and briefly states how the research questions are targeted and why it is important to investigate them. Even though the Arctic Ocean undergoes vast and partly obvious changes, as stated in the previous sections, yet the consequences of environmental changes are still not fully understood. $^{230}$Th and $^{231}$Pa are sensitive indicators of particle fluxes and composition as well as of changes in circulation and ventilation of water masses. The main aims of this thesis can be broken down to the following questions:

**I)** What are the natural background processes affecting $^{231}$Pa and $^{230}$Th in the Arctic Ocean?

**II)** Do ongoing environmental changes in the Arctic Ocean already result in measurable changes in $^{230}$Th and $^{231}$Pa concentrations and distributions and what are the implications?

**III)** To which extent can the budgets of $^{231}$Pa and $^{230}$Th in the Arctic Ocean be used to trace important environmental processes in time?

These guiding questions determine the structure of our study. They require a new understanding, based on new and historical data, of the impact of changes in Arctic Ocean circulation, its outflow to the Atlantic Ocean, as well as changes in particle flux characteristics on the use of these isotopes as tracers for other fundamental processes like paleoproductivity or ocean circulation.

Therefore, it is needed to constrain changes in $^{230}$Th and $^{231}$Pa concentrations and distribution in the water column, both particulate and dissolved, as well as their distribution within the different basins. In order to determine whether climate change is influencing $^{230}$Th, $^{231}$Pa and their activity ratio, it is crucial to identify and understand removal processes of $^{230}$Th and $^{231}$Pa in the Arctic Ocean and to identify changes over time. The dissolved $^{230}$Th and $^{231}$Pa time series from 1991 over 2007 to 2015 was established in order to investigate temporal changes. Investigating distributions of particulate and dissolved $^{230}$Th and $^{231}$Pa in high spatial resolution is crucial to understand how their removal processes work in detail and whether those removal processes are controlled by changing particle fluxes and composition or by ventilation or circulation changes. Therefore, a first step of investigation and an important aspect of this understanding is to identify time scales of changes in $^{230}$Th and $^{231}$Pa distribution and concentrations.

After identifying spatial and temporal patterns of changes in $^{230}$Th and $^{231}$Pa distribution and concentration, it is necessary to investigate if those changes are accompanied by changes in water mass properties, in order to identify the influence of potential circulation or ventilation changes on $^{230}$Th and $^{231}$Pa developments. A change in circulation and ventilation time scales of Atlantic derived intermediate waters would affect $^{230}$Th and moreover $^{231}$Pa in the Arctic Ocean, as well as general export of waters from the Arctic Ocean. Therefore, other parameters obtained from the 2015 GEOTRACES Arctic Ocean campaign are included. To identify if a circulation and/or ventilation change controls temporal developments of $^{230}$Th and $^{231}$Pa in the central Arctic Ocean, the ratio of anthropogenic $^{129}$I/$^{236}$U, a circulation tracer (Casacuberta *et al.*, 2016), is included in combination with water mass properties, such as salinity and potential temperature. Furthermore, water mass ages evident from ventilation tracers such as CFCs (Chlorofluorocarbons) and $SF_6$ (Sulfur Hexafluoride) are compared with temporal developments of $^{230}$Th and $^{231}$Pa.

Identifying changes in water mass ventilation and circulation in the Arctic Ocean is an important topic. Export of water masses from the Arctic Ocean to the Atlantic Ocean is crucial for ecosystems in both the North Atlantic and the Arctic Ocean. If ventilation times exceed or are in the order of scavenging residence times of any given element, its distribution is likely to be affected by advection. Hence, the time scales of Arctic intermediate water circulation have an influence on the export of $^{230}$Th and $^{231}$Pa to the Atlantic Ocean and therefore influence the paleoceanographic use of $^{230}$Th and $^{231}$Pa in the Arctic Ocean and the North Atlantic.

In addition to the question if environmental changes in the Arctic Ocean have influence on $^{230}$Th and $^{231}$Pa as paleoceanographic tools, the development of their spatial distribution in the Arctic Ocean over the past two decades can give insights in trace element cycling in the Arctic Ocean and potential changes of it.

Trace elements, such as Fe, are essential nutrients in the ocean controlling biological production (Bruland *et al.*, 1991) and are affected by scavenging (Boyd and Ellwood, 2010). In order to understand effects of climate change on sources and sinks, hence cycling of trace elements it is important to investigate how particle reactive isotopes change over time to estimate how e.g. Fe in the Arctic Ocean might change its distribution and removal mechanisms. Therefore, it is helpful to include investigations on how scavenging of $^{230}$Th and the controlling processes change in the Arctic Ocean. That means looking at particle fluxes at the time of sampling, which would be reflected in any particle reactive element investigated in suspended matter.

In order to investigate changing scavenging intensities in the Arctic Ocean the inclusion of other thorium isotopes, such as long lived $^{232}$Th ($t_{1/2}$: 1.405*$10^{10}$ yrs (Holden, 1990)) and short lived $^{234}$Th ($t_{1/2:}$ 24.1 d (Knight and Macklin, 1948)) widens the information that can be gained from a single sample. $^{232}$Th, the way most abundant thorium isotope has, in contrast to $^{230}$Th and $^{231}$Pa, a continental source and thus can be used as a tracer for lithogenic material (Hsieh *et al.*, 2011). As described in section *1.1.4 Particle fluxes, composition and transport*, lithogenic material plays an important role in the Arctic Ocean. Therefore $^{232}$Th is a suitable tracer for identifying terrestrial material from the shelves and continents and has the same source in the Arctic Ocean as some nutrients and trace elements such as Fe (Klunder *et al.*, 2012a; Rijkenberg *et al.*, 2018). $^{234}$Th, which is highly particle reactive often serves as tracer for the removal rate of particles, especially for Particulate Organic Carbon (Buesseler, 1998) from the surface ocean. To this end the total concentration is expressed as fraction of the parent $^{238}$U activity (Owens *et al.*, 2011). But because of the reversible nature of Th adsorption, the fraction of $^{234}$Th associated with particles can also be used as a measure for particle concentrations, particularly in deep water.

GEOTRACES expeditions are a valuable source of comparable parameters, since most of these were sampled at the same time and at the same locations. Hence it is possible to compare temporal developments of $^{230}$Th and $^{231}$Pa with developments of e.g. Fe. For example the comparison of Fe data obtained from PS70 (2007) and PS94 (2015) can indicate presence of hydrothermal plumes, which are sources of many trace elements (German *et al.*, 2016) and sinks for $^{230}$Th and $^{231}$Pa (Pavia *et al.*, 2018). The importance of hydrothermal vents in the Arctic Ocean for trace element cycling is not well understood. It is a source of Fe and Mn in the Eurasian Basin (Klunder *et al.*, 2012b; Middag *et al.*, 2011), but there is little knowledge of the ineraction between hydrothermal plume particles and scavenging of particle reactive elments. The semi enclosed nature of the Arctic Ocean, especially its deep basins, as well as the small size of the deep basins point at maybe unique conditions, different to other ocean basins. Hence the influence of hydrothermal vents on $^{230}$Th and $^{231}$Pa in the Arctic Ocean is important to understand the variability of deep water $^{230}$Th and $^{231}$Pa inventories, which in turn can give information about cycling of trace elements in the deep Arctic Ocean. Furthermore scavenging removal of $^{230}$Th, due to hydrothermal activity or explosive eruptions, can impact the sedimentary $^{231}$Pa/$^{230}$Th activity ratio on decadal timescales.

Findings about the scavenging behaviour of e.g. $^{230}$Th help understanding and identifying the impact of changing particles fluxes on other, more biologically important trace elements, e.g. Fe. An important process in terms of trace element cycling is boundary scavenging (Boyd and

Ellwood, 2010). It is still an open question if boundary scavenging occurs in the Arctic Ocean or not. It used to be assumed that boundary scavenging plays a role as reported by Huh *et al.* (1997) on basis of sedimentary Plutonium isotopes combined with $^{210}$Pb and $^{230}$Th. This assumption was also supported by Moran *et al.* (2005) who investigated budgets of $^{230}$Th and $^{231}$Pa based on their sedimentary activities in relation to their in-situ production. Hoffmann and McManus (2007) later falsified this assumption, as they found no evidence for boundary scavenging in sedimentary $^{230}$Th inventories. Nevertheless there is evidence for increasing boundary scavenging along the margins of the Amerasian Basin of the Arctic Ocean based on margin sedimentary $^{210}$Pb and $^{137}$Cs (Kuzyk *et al.*, 2013). Smith *et al.* (2003) reported relatively high scavenging efficiencies of $^{210}$Pb based on the comparison between water column $^{210}$Pb and $^{210}$Pb sediment inventories. They concluded that an observed $^{210}$Pb deficit in the Arctic Ocean is probably due to the contribution of boundary scavenging to the removal of $^{210}$Pb along the inflow pathways of Atlantic waters in the Barents Sea and along the Nansen Basin margin, leading to a net export of $^{210}$Pb from the central Eurasian Basin. Additionally Gdaniec *et al.* (2020) and Costa *et al.* (2020) suggested that boundary scavenging of $^{230}$Th does occur at the margins of the Eurasian Basin.

Boundary scavenging or its intensity in the Eurasian Basin might be changing, due to the aforementioned changes in particle fluxes in the Barents Sea and the Nansen Basin margins. The evaluation of this question might depend on the timescales of observations. Sediment core $^{231}$Pa/$^{230}$Th data does not show evidence for boundary scavenging in the past (Hoffmann and McManus, 2007), but might be developing under the influence of climate change. Furthermore phases of more pronounced boundary scavenging, as recently indicated for the Eurasian Basin (Gdaniec *et al.*, 2020), could potentially be hidden under background situations in bulk sediment records, given the low sedimentation rates of 1 cm/kyrs (Backman *et al.*, 2004) to 5 cm/kyrs (Gard, 1993) and a bioturbation depth of 2-10 cm (Clough *et al.*, 1997) in the Eurasian Basin. Therefore, in order to investigate changes over time, time series are a crucial instrument to identify changes on time scales of years and decades.

The different preferences of $^{230}$Th and $^{231}$Pa to react with certain particles, as well as their general particle reactivity, leading to a fractionation of $^{230}$Th and $^{231}$Pa, can give information about removal processes, such as boundary scavenging, of these isotopes, which in turn can be related to environmental changes. Boundary scavenging in the Arctic Ocean would have significant impact not only on scavenging removal and distributions of particle reactive trace elements, but also on the export of those to the Atlantic Ocean. Boundary scavenging would affect the ratio of $^{231}$Pa and $^{230}$Th in waters leaving the Arctic Ocean if boundary scavenging

would lead to a basin wide fractionation of $^{230}$Th and $^{231}$Pa. This would again have impact on the interpretation of their paleoceanographic use, depending on the time scale of this process.

In order to identify basin wide changes and fractionation of $^{230}$Th and $^{231}$Pa it helps to calculate basin inventories of $^{230}$Th and $^{231}$Pa to constrain time scales and the importance of these changes in addition to changes of individual profiles, which can be influenced locally. Due to its almost enclosed nature, with only one deep opening at the Fram Strait, the Arctic Ocean also seems to be suitable to investigate and constrain budgets of $^{230}$Th and $^{231}$Pa in a semi closed system. Any evidence of relatively fast occurring changes of $^{230}$Th and $^{231}$Pa inventories might imply a complication of the interpretation of $^{230}$Th, $^{231}$Pa as well as the $^{231}$Pa/$^{230}$Th activity ratios in sediments. These consequences depend on the timescales of processes controlling the removal of these isotopes. Figure 9 shows a simplified overview of processes potentially controlling distribution and concentration changes of $^{230}$Th (and $^{231}$Pa) in the Eurasian Basin of the Arctic Ocean, which will be investigated in the following chapters of this thesis.

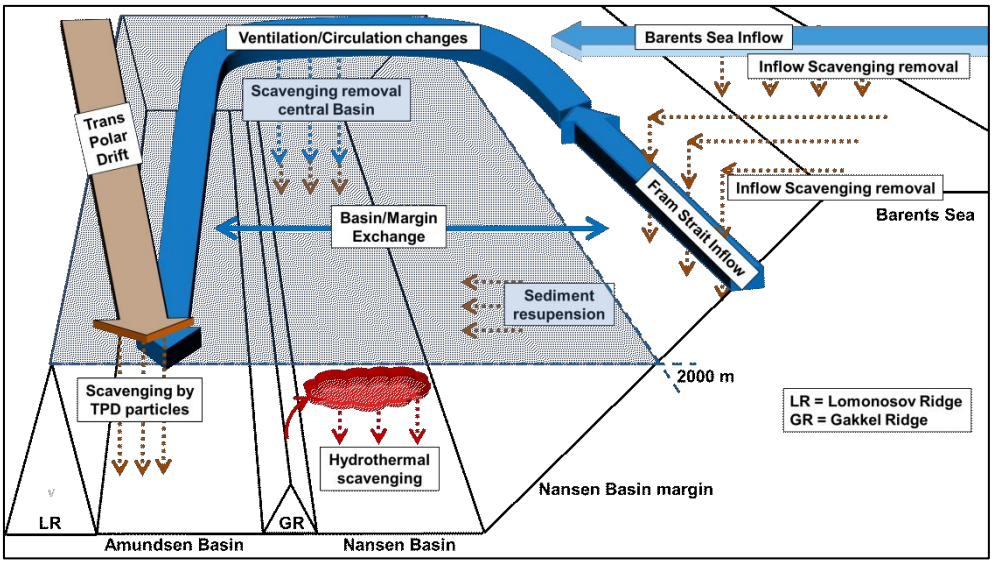


**Figure 9: Simplified illustration of the Eurasian Basin and processes with a potential for controlling removal of $^{230}$Th and $^{231}$Pa. Blue shaded layer indicates 2000 m depth and distinguishes between deeper and shallower processes.**

Summarized, the main objective of this thesis is identifying the temporal and spatial developments of $^{230}$Th and $^{231}$Pa in order to link them to environmental changes and climate change. These findings serve reaching the overlying goal of linking radionuclide-based conclusions to broader scale processes such as scavenging removal and advective export of other trace elements and to determine to what extent the identified removal processes of $^{230}$Th and $^{231}$Pa influence their application as paleoceanographic tracers.

## 1.6 Manuscripts presented in the Thesis

### 1.6.1 Declaration of (Co-) Author Contributions

The individual (co-) author contributions to the published articles and the manuscript statuses are reported in this section.

**Chapter 2: Importance of Hydrothermal Vents in Scavenging Removal of $^{230}$Th in the Nansen Basin**

Ole Valk, Michiel M. Rutgers van der Loeff, Walter Geibert, Sandra Gdaniec, Micha J. A. Rijkenberg, S. Bradley Moran, Kate Lepore, Richard Lawrence Edwards, Yanbin Lu, and Viena Puigcorbé

Status: Published in *Geophysical Research Letters*, doi.org/10.1029/2018GL079829, published online September, 19th 2018

The study was conceived by Ole Valk, Michiel M. Rutgers van der Loeff and Walter Geibert.

Ole Valk and Sandra Gdaniec carried out the sampling on board during *RV Polarstern* cruise PS94 ($^{230}$Th, $^{232}$Th, and $^{234}$Th). Ole Valk performed analyses of $^{230}$Th and $^{232}$Th, Viena Puigcorbé analysed $^{234}$Th. S. Bradley Moran, Kate Lepore sampled data from 2007 during *RV Polarstern* cruise PS70. Richard Lawrence Edwards and Yanbin Lu analysed $^{230}$Th and $^{232}$Th from PS70. Micha J. A. Rijkenberg provided and helped interpreting dissolved Fe data from PS94. Ole Valk wrote the manuscript with substantial contributions from Michiel M. Rutgers van der Loeff and Walter Geibert. The personal contribution is estimated to 80%.

**Chapter 3: Decrease in $^{230}$Th in the Amundsen Basin since 2007: far-field effect of increased scavenging on the shelf?**

Ole Valk, Michiel M. Rutgers van der Loeff, Walter Geibert, Sandra Gdaniec, S. Bradley Moran, Kate Lepore, Richard Lawrence Edwards, Yanbin Lu, Viena Puigcorbé, Nuria Casacuberta, Ronja Paffrath, William Smethie and Matthieu Roy-Barman

Status: Published in *Ocean Science*, doi.org/10.5194/os-16-221-2020, published online February, 14th 2020

This study was designed and planned by Ole Valk, Michiel M. Rutgers van der Loeff and Walter Geibert. Ole Valk, Sandra Gdaniec and Ronja Paffrath carried out the sampling on board during *RV Polarstern* cruise PS94 ($^{230}$Th, $^{232}$Th, and $^{234}$Th). Ole Valk performed analyses of $^{230}$Th and $^{232}$Th. Viena Puigcorbé analysed $^{234}$Th. S. Bradley Moran and Kate Lepore sampled data from 2007 during *RV Polarstern* cruise PS70. Richard Lawrence Edwards and Yanbin Lu analysed

$^{230}$Th and $^{232}$Th from PS70. William Smethie provided interpreted $SF_6$ and CFC-11 data from PS94. Nuria Casacuberta provided and helped interpreting $^{129}I/^{236}U$ data from PS94. Ole Valk wrote the manuscript with substantial contributions from Michiel M. Rutgers van der Loeff, Walter Geibert and S. Bradley Moran. The personal contribution is estimated to 80%.

**Chapter 4: Short-term vs. long-term removal processes of dissolved $^{230}$Th and $^{231}$Pa in the Eurasian Basin**

Ole Valk, Michiel M. Rutgers van der Loeff, Walter Geibert, Sandra Gdaniec, S. Bradley Moran, Kate Lepore, Richard Lawrence Edwards, Ronja Paffrath and Yanbin Lu

Status: In preparation (24.11.2020), planned to submit to *Geochemistry, Geophysics, Geosystems*.

This study was designed and planned by Ole Valk, Michiel M. Rutgers van der Loeff and Walter Geibert. Ole Valk and, partly, Sandra Gdaniec conducted sampling during PS94 and performed analyses of $^{230}$Th, $^{231}$Pa and $^{232}$Th. S. Bradley Moran, Kate Lepore sampled data from 2007 during *RV Polarstern* cruise PS70. Richard Lawrence Edwards and Yanbin Lu analysed $^{230}$Th and $^{232}$Th from PS70. Ole Valk wrote the manuscript with substantial contributions from Michiel M. Rutgers van der Loeff and Walter Geibert. The personal contribution is estimated to 80%.

**Chapter 5: $^{231}$Pa and $^{230}$Th in the Arctic Ocean: Implications for boundary scavenging and $^{231}$Pa-$^{230}$Th fractionation in the Eurasian Basin**

Sandra Gdaniec, Matthieu Roy-Barman, Martin Levier, Ole Valk, Michiel M. Rutgers van der Loeff, Lorna Foliot, Arnaud Dapoigny, Lise Missiaen, Carl-Magnus Mörth and Per S. Andersson

Status: Published in *Chemical Geology*, doi.org/10.1016/j.chemgeo.2019.119380, published online November, 09th 2020.

The study was conceived by Sandra Gdaniec and Matthieu Roy-Barman. Ole Valk conducted parts of the sampling at sea and the analytical work and contributed to the writing of the manuscript, performed by Sandra Gdaniec. The personal contribution is estimated to 10%.

**Chapter 6: Changes in Circulation and Particle Scavenging in the Amerasian Basin of the Arctic Ocean over the Last Three Decades Inferred from the Water Column Distribution of Geochemical Tracers**

Melanie Grenier, Roger François, Maureen Soon, Michiel Rutgers van der Loeff, Xiaoxin Yu, Ole Valk, Christelle Not, S. Bradley Moran, Richard Lawrence Edwards, Yanbin Lu, Kate Lepore, and Susan E. Allen

Status: Published in J*ournal of Geophysical Research: Oceans*, doi.org/10.1029/2019JC0152650, published online December, 18th 2019.

The study was designed by Melanie Grenier and Roger François. Ole Valk conducted parts of the sampling at sea and the analytical work providing $^{230}$Th, $^{231}$Pa and $^{232}$Th data for the Makarov Basin and contributed to the writing of the manuscript, performed by Melanie Grenier. The personal contribution is estimated to 10%.

### 1.6.2 Additional Co-Author Contributions (not presented in the Thesis):

Michiel M. Rutgers van der Loeff, Lauren E. Kipp, Matthew A. Charette, Willard S. Moore, Erin E. Black, Ingrid Stimac, Alexander Charkin, Dorothea Bauch, **Ole Valk**, Michael J. Karcher, Thomas Krumpen, Nuria Casacuberta, William M. Smethie, Robert D. Rember. 2018. Radium Isotopes Across the Arctic Ocean Show Time Scales of Water Mass Ventilation and Increasing Shelf Inputs. *Journal of Geophysical Research*: Oceans, 123, 4853– 4873. https://doi.org/10.1029/2018JC013888.

Matthew A. Charette, Lauren E. Kipp, Laramie T. Jensen, Jessica S. Dabrowski, Laura M. Whitmore, Jessica N. Fitzsimmons, Tatiana Williford, Adam Ulfsbo, Elizabeth Jones, Randelle M. Bundy, Sebastian M. Vivancos, Katharina Pahnke, Seth G. John, Yang Xiang, Mariko Hatta, Mariia V. Petrova, Lars-Eric Heimbürger-Boavida, Dorothea Bauch, Robet Newton, Angelica Pasqualini, Alison M. Agather, Rainer M. W. Amon, Robert F. Arnderson, Per S. Andersson, Ronald Benner, Katlin L. Bowman, R. Lawrence Edwards, Sandra Gdaniec, Loes J. A. Gerringa, Aridane G. González, Mats Granskog, Brian Haley, Chad R. Hammerschmidt, Dennis A. Hansell, Paul B. Henderson, David C. Kadko, Karl Kaiser, Patrick Laan, Phoebe J. Lam, Carl H. Lamborg, Martin Levier, Xianglei Li, Andrew R. Margolin, Chis Measures, Rob Middag, Frank J. Millero, Willard S Moore, Ronja Paffrath, Hélène Planquette, Benjamin Rabe, Heather Reader, Robert D. Rember, Micha. J. A. Rijkenberg, Matthieu Roy-Barman, Michiel M Rutgers van der Loeff, Mark Saito, Ursula Schauer, Peter Schlosser, Robert M. Sherrell, Alan M. Shiller, Hans Slagter, Jeroen E Sonke, Collin Stedmon, Ryan J. Woosley, **Ole Valk**, Jan van Ooijen, Ruifeng Zhang. 2020. The Transpolar Drift as a Source of Riverine and Shelf-Derived Trace Elements to the Central Arctic Ocean. *Journal of Geophysical Research: Oceans* 125 (5), e2019JC015920. https://doi.org/10.1029/2019JC015920

Mariia V Petrova, Stephan Krisch, Pablo Lodeiro, **Ole Valk,** Aurelie Dufour, Micha J. A. Rijkenberg, Eric P. Achterberg, Benjamin Rabe, Michiel M. Rutgers van der Loeff, Bruno Hamelin, Jeroen E. Sonke, Cédric Garnier, Lars-Eric Heimbürger-Boavida. 2020. Mercury species export from the Arctic to the Atlantic Ocean. *Marine Chemistry* 225, 103855. https://doi.org/10.1016/j.marchem.2020.103855

Javier A. Tesán Onrubia, Mariia V. Petrova, Viena Puigcorbé, Erin E. Black, **Ole Valk**, Aurelie Dufour, Bruno Hamelin, Ken O. Buesseler, Pere Masqué, Frédéric A. C. Le Moigne, Jeroen E. Sonke, Michiel M. Rutgers van der Loef, Lars-Eric Heimbürger-Boavida. 2020. Mercury Export Flux in the Arctic Ocean Estimated from $^{234}Th/^{238}U$ Disequilibria. *ACS Earth and Space Chemistry* 4 (5), 795-801. https://doi.org/10.1021/acsearthspacechem.0c00055

## References

Aagaard, K., 1981. On the deep circulation in the Arctic Ocean. Deep Sea Research Part A. Oceanographic Research Papers 28 (3), 251-268.

Aagaard, K., Coachman, L.K., Carmack, E.C., 1980. On the halocline of the Arctic Ocean*. Deep-Sea Research 1 28A, 529-545.

Aagaard, K., Swift, J.H., Carmack, E.C., 1985. Thermohaline Circulation in the Arctic Mediterranean Seas. Journal of Geophysical Research 90, 4833-4846.

Andersen, M.B., Stirling, C.H., Zimmermann, B., Halliday, A.N., 2010. Precise determination of the open ocean $^{234}U/^{238}U$ composition. Geochemistry, Geophysics, Geosystems 11 (12).

Anderson, R.F., Bacon, M.P., Brewer, P.G., 1983a. Removal of $^{230}Th$ and $^{231}Pa$ at ocean margins. Earth and Planetary Science Letters 66, 73-90.

Anderson, R.F., Bacon, M.P., Brewer, P.G., 1983b. Removal of $^{230}Th$ and $^{231}Pa$ from the open ocean. Earth and Planetary Science Letters 62, 7-23.

Anderson, R.F., Fleisher, M.Q., Robinson, L., Edwards, R.L., Hoff, J.A., Moran, S.B., Rutgers van der Loeff, M.M., Thomas, A.L., Roy-Barman, M., Francois, R., 2012. GEOTRACES intercalibration of $^{230}Th$, $^{232}Th$, $^{231}Pa$, and prospects for $^{10}Be$. Limnol. Oceanogr.: Methods 10, 179-213.

Ardyna, M., Babin, M., Gosselin, M., Devred, E., Bélanger, S., Matsuoka, A., Tremblay, J.É., 2013. Parameterization of vertical chlorophyll *a* in the Arctic Ocean: impact of the subsurface chlorophyll maximum on regional, seasonal, and annual primary production estimates. Biogeosciences 10 (6), 4383-4404.

Armitage, T.W.K., Bacon, S., Kwok, R., 2018. Arctic Sea Level and Surface Circulation Response to the Arctic Oscillation. Geophysical Research Letters 45 (13), 6576-6584.

Arrigo, K.R., Perovich, D.K., Pickart, R.S., Brown, Z.W., van Dijken, G.L., Lowry, K.E., Mills, M.M., Palmer, M.A., Balch, W.M., Bahr, F., Bates, N.R., Benitez-Nelson, C., Bowler, B., Brownlee, E., Ehn, J.K., Frey, K.E., Garley, R., Laney, S.R., Lubelczyk, L., Mathis, J., Matsuoka, A., Mitchell, B.G., Moore, G.W.K., Ortega-Retuerta, E., Pal, S., Polashenski, C.M., Reynolds, R.A., Schieber, B., Sosik, H.M., Stephens, M., Swift, J.H., 2012. Massive Phytoplankton Blooms Under Arctic Sea Ice. Science 336 (6087), 1408-1408.

Arrigo, K.R., Perovich, D.K., Pickart, R.S., Brown, Z.W., van Dijken, G.L., Lowry, K.E., Mills, M.M., Palmer, M.A., Balch, W.M., Bates, N.R., Benitez-Nelson, C.R., Brownlee, E., Frey, K.E., Laney, S.R., Mathis, J., Matsuoka, A., Greg Mitchell, B., Moore, G.W.K., Reynolds, R.A., Sosik, H.M., Swift, J.H., 2014. Phytoplankton blooms beneath the sea ice in the Chukchi sea. Deep Sea Research Part II: Topical Studies in Oceanography 105, 1-16.

Arrigo, K.R., van Dijken, G., Pabi, S., 2008. Impact of a shrinking Arctic ice cover on marine primary production. Geophysical Research Letters 35 (19), n/a-n/a.

Arrigo, K.R., van Dijken, G.L., 2015. Continued increases in Arctic Ocean primary production. Progress in Oceanography 136, 60-70.

Årthun, M., Eldevik, T., Smedsrud, L.H., 2019. The Role of Atlantic Heat Transport in Future Arctic Winter Sea Ice Loss. Journal of Climate 32 (11), 3327-3341.

Årthun, M., Ingvaldsen, R.B., Smedsrud, L.H., Schrum, C., 2011. Dense water formation and circulation in the Barents Sea. Deep Sea Research Part I: Oceanographic Research Papers 58 (8), 801-817.

Assmy, P., Fernández-Méndez, M., Duarte, P., Meyer, A., Randelhoff, A., Mundy, C.J., Olsen, L.M., Kauko, H.M., Bailey, A., Chierici, M., Cohen, L., Doulgeris, A.P., Ehn, J.K., Fransson, A., Gerland, S., Hop, H., Hudson, S.R., Hughes, N., Itkin, P., Johnsen, G., King, J.A., Koch, B.P., Koenig, Z., Kwasniewski, S., Laney, S.R., Nicolaus, M., Pavlov, A.K., Polashenski, C.M., Provost, C., Rösel, A., Sandbu, M., Spreen, G., Smedsrud, L.H., Sundfjord, A., Taskjelle, T., Tatarek, A., Wiktor, J., Wagner, P.M., Wold, A., Steen, H., Granskog, M.A., 2017. Leads in Arctic pack ice enable early phytoplankton blooms below snow-covered sea ice. Scientific Reports 7 (1), 40850.

Backman, J., Jakobsson, M., Lovlie, r., Polyak, L., Febo, L.A., 2004. Is the central Arctic Ocean a sediment starved basin? Quaternary Science Reviews 23, 1435-1454.

Bacon, M.P., Anderson, R.F., 1982. Distribution of Thorium Isotopes Between Dissolved and Particulate Forms in The Deep Sea. Journal of Geophysical Research 87, 2045-2056.

Bacon, M.P., Huh, C.-A., Moore, R.M., 1989. Vertical profiles of some natural radionuclides over the Alpha Ridge, Arctic Ocean. Earth and Planetary Science Letters 95, 15-22.

Bacon, M.P., Roether, W., Elderfield, H., Charnock, H., Lovelock, J.E., Liss, P.S., Whitfield, M., 1988. Tracers of chemical scavenging in the ocean: boundary effects and large-scale chemical fractionation. Philosophical Transactions of the Royal Society of London. Series A, Mathematical and Physical Sciences 325 (1583), 147-160.

Baker, E.T., Edmonds, H.N., Michael, P.J., Bach, W., Dick, H.J.B., Snow, J.E., Walker, S.L., Banerjee, N.R., Langmuir, C.H., 2004. Hydrothermal venting in magma deserts: The ultraslow-spreading Gakkel and Southwest Indian Ridges. Geochemistry, Geophysics, Geosystems 5 (8).

Beszczynska-Moeller, A., Woodgate, R., Lee, C., Melling, H., Karcher, M., 2011. A Synthesis of Exchanges Through the Main Oceanic Gateways to the Arctic Ocean. Oceanography (Washington D.C.) 24.

Beszczynska-Möller, A., Fahrbach, E., Schauer, U., Hansen, E., 2012. Variability in Atlantic water temperature and transport at the entrance to the Arctic Ocean, 1997–2010. ICES Journal of Marine Science 69 (5), 852-863.

Björk, G., Anderson, L.G., Jakobsson, M., Antony, D., Eriksson, B., Eriksson, P.B., Hell, B., Hjalmarsson, S., Janzen, T., Jutterström, S., Linders, J., Löwemark, L., Marcussen, C., Anders Olsson, K., Rudels, B., Sellén, E., Sølvsten, M., 2010. Flow of Canadian basin deep water in the Western Eurasian Basin of the Arctic Ocean. Deep Sea Research Part I: Oceanographic Research Papers 57 (4), 577-586.

Björk, G., Jakobsson, M., Rudels, B., Swift, J.H., Anderson, L., Darby, D.A., Backman, J., Coakley, B., Winsor, P., Polyak, L., Edwards, M., 2007. Bathymetry and deep-water exchange across the central Lomonosov Ridge at 88–89°N. Deep Sea Research Part I: Oceanographic Research Papers 54 (8), 1197-1208.

Björk, G., Winsor, P., 2006. The deep waters of the Eurasian Basin, Arctic Ocean: Geothermal heat flow, mixing and renewal. Deep Sea Research Part I: Oceanographic Research Papers 53 (7), 1253-1271.

Boetius, A., Albrecht, S., Bakker, K., Bienhold, C., Felden, J., Fernández-Méndez, M., Hendricks, S., Katlein, C., Lalande, C., Krumpen, T., Nicolaus, M., Peeken, I., Rabe, B., Rogacheva, A., Rybakova, E., Somavilla, R., Wenzhöfer, F., 2013. Export of Algal Biomass from the Melting Arctic Sea Ice. Science 339.

Boyd, P.W., Ellwood, M.J., 2010. The biogeochemical cycle of iron in the ocean. Nature Geosci 3 (10), 675-682.

Bruland, K.W., Donat, J.R., Hutchins, D.A., 1991. Interactive influences of bioactive trace metals on biological production in oceanic waters. Limnology and Oceanography 36 (8), 1555-1577.

Buesseler, K.O., 1998. The decoupling of production and particulate export in the surface ocean. GLOBAL BIOGEOCHEMICAL CYCLES 12 (2), 297-310.

Cai, P., Rutgers van der Loeff, M.M., Stimac, I., Nöthig, E.-M., Lepore, K., Moran, S.B., 2010. Low export flux of particulate organic carbon in the central Arctic Ocean as revealed by $^{234}$Th:$^{238}$U disequilibrium. Journal of Geophysical Research 115.

Casacuberta, N., Masqué, P., Henderson, G., Rutgers van-der-Loeff, M., Bauch, D., Vockenhuber, C., Daraoui, A., Walther, C., Synal, H.A., Christl, M., 2016. First $^{236}$U data from the Arctic Ocean and use of $^{236}$U/$^{238}$U and $^{129}$I/$^{236}$U as a new dual tracer. Earth and Planetary Science Letters 440, 127-134.

Charette, M.A., Kipp, L.E., Jensen, L.T., Dabrowski, J.S., Whitmore, L.M., Fitzsimmons, J.N., Williford, T., Ulfsbo, A., Jones, E., Bundy, R.M., Vivancos, S.M., Pahnke, K., John, S.G., Xiang, Y., Hatta, M., Petrova, M.V., Heimbürger-Boavida, L.-E., Bauch, D., Newton, R., Pasqualini, A., Agather, A.M., Amon, R.M.W., Anderson, R.F., Andersson, P.S., Benner, R., Bowman, K.L., Edwards, R.L., Gdaniec, S., Gerringa, L.J.A., González, A.G., Granskog, M., Haley, B., Hammerschmidt, C.R., Hansell, D.A., Henderson, P.B., Kadko, D.C., Kaiser, K., Laan, P., Lam, P.J., Lamborg, C.H., Levier, M., Li, X., Margolin, A.R., Measures, C., Middag, R., Millero, F.J., Moore, W.S., Paffrath, R., Planquette, H., Rabe, B., Reader, H., Rember, R., Rijkenberg, M.J.A., Roy-Barman, M., Rutgers van der Loeff, M., Saito, M., Schauer, U., Schlosser, P., Sherrell, R.M., Shiller, A.M., Slagter, H., Sonke, J.E., Stedmon, C., Woosley, R.J., Valk, O., van Ooijen, J., Zhang, R., 2020. The Transpolar Drift as a Source of Riverine and Shelf-Derived Trace Elements to the Central Arctic Ocean. Journal of Geophysical Research: Oceans 125 (5), e2019JC015920.

Chase, Z., Anderson, R.F., Fleisher, M.Q., Kubik, P.W., 2002. The influence of particle composition and particle flux on scavenging of Th, Pa and Be in the ocean. Earth and Planetary Science Letters 204, 215-229.

Chen, J.H., Lawrence Edwards, R., Wasserburg, G.J., 1986. $^{238}$U, $^{234}$U and $^{232}$Th in seawater. Earth and Planetary Science Letters 80 (3–4), 241-251.

Cheng, H., Edwards, R.L., Hoff, J., Gallup, C.D., Richards, D.A., Asmerom, Y., 2000. The half-lives of uranium-234 and thorium-230. Chemical Geology 169 (1–2), 17-33.

Clough, L.M., Ambrose, W.G., Kirk Cochran, J., Barnes, C., Renaud, P.E., Aller, R.C., 1997. Infaunal density, biomass and bioturbation in the sediments of the Arctic Ocean. Deep Sea Research Part II: Topical Studies in Oceanography 44 (8), 1683-1704.

Cochran, K., J., H.D., Livingston, H.D., Buesseler, K.O., Key, R.M., 1995. Natural and anthropogenic radionuclide distributions in the Nansen Basin, Artic Ocean: Scavenging rates and circulation timescales. Deep-Sea Research II 42, 1495-1517.

Codispoti, L.A., Flagg, C., Kelly, V., Swift, J.H., 2005. Hydrographic conditions during the 2002 SBI process experiments. Deep Sea Research Part II: Topical Studies in Oceanography 52 (24), 3199-3226.

Collins, M., Knutti, R., Arblaster, J., Dufresne, J.-L., Fichefet, T., Friedlingstein, P., Gao, X., Gutowski, W.J., Johns, T., Krinner, G., Shongwe, M., Tebaldi, C., Weaver, A.J., Wehner, M., 2014. Long-term Climate Change: Projections, Commitments and Irreversibility. . In: Intergovernmental Panel on Climate, C. (Ed.), Climate Change 2013 – The Physical Science Basis: Working Group I Contribution to the Fifth Assessment Report of the Intergovernmental Panel on Climate Change [Stocker, T.F., D. Qin, G.-K. Plattner, M. Tignor, S.K. Allen, J. Boschung, A. Nauels, Y. Xia, V. Bex and P.M. Midgley (eds.)]. Cambridge University Press, Cambridge, pp. 1029-1136.

Comiso, J.C., Meier, W.N., Gersten, R., 2017. Variability and trends in the Arctic Sea ice cover: Results from different techniques. Journal of Geophysical Research: Oceans 122 (8), 6883-6900.

Costa, K.M., Hayes, C.T., Anderson, R.F., Pavia, F.J., Bausch, A., Deng, F., Dutay, J.-C., Geibert, W., Heinze, C., Henderson, G., Hillaire-Marcel, C., Hoffmann, S., Jaccard, S.L., Jacobel, A.W., Kienast, S.S., Kipp, L., Lerner, P., Lippold, J., Lund, D., Marcantonio, F., McGee, D., McManus, J.F., Mekik, F., Middleton, J.L., Missiaen, L., Not, C., Pichat, S., Robinson, L.F., Rowland, G.H., Roy-Barman, M., Tagliabue, A., Torfstein, A., Winckler, G., Zhou, Y., 2020. $^{230}$Th Normalization: New Insights on an Essential Tool for Quantifying Sedimentary Fluxes in the Modern and Quaternary Ocean. Paleoceanography and Paleoclimatology 35 (2), e2019PA003820.

Dalpadado, P., Arrigo, K.R., van Dijken, G.L., Skjoldal, H.R., Bagøien, E., Dolgov, A.V., Prokopchuk, I.P., Sperfeld, E., 2020. Climate effects on temporal and spatial dynamics of phytoplankton and zooplankton in the Barents Sea. Progress in Oceanography 185, 102320.

de Steur, L., Hansen, E., Mauritzen, C., Beszczynska-Moeller, A., Fahrbach, E., 2014. Impact of recirculation on the East Greenland Current in Fram Strait: Results from moored current meter measurements between 1997 and 2009. Deep Sea Research Part I: Oceanographic Research Papers 92.

Delanghe, D., Bard, E., Hamelin, B., 2002. New TIMS constraints on the uranium-238 and uranium-234 in seawaters from the main ocean basins and the Mediterranean Sea1. Marine Chemistry 80 (1), 79-93.

Dukhovskoy, D., Johnson, M., Proshutinsky, A.Y., 2004. Arctic decadal variability: An auto-oscillatory system of heat and fresh water exchange. Geophys. Res. Lett. 31.

Edmonds, H.N., Michael, P.J., Baker, E.T., Connelly, D.P., Snow, J.E., Langmuir, C.H., Dick, H.J.B., Muhe, R., German, C.R., Graham, D.W., 2003. Discovery of abundant hydrothermal venting on the ultraslow-spreading Gakkel ridge in the Arctic Ocean. Nature 421 (6920), 252-256.

Edmonds, H.N., Moran, S.B., Cheng, H., Edwards, R.L., 2004. $^{230}$Th and $^{231}$Pa in the Arctic Ocean: implications for particle fluxes and basin-scale Th/Pa fractionation. Earth and Planetary Science Letters 227, 155-167.

Edmonds, H.N., Moran, S.B., Hoff, J.A., Smith, J.R., Edwards, R.L., 1998. Protactinium-231 and Thorium-230 Abundances and High Scavenging Rates in the Western Arctic Ocean. Science 280, 405-406.

Ekwurzel, B., Schlosser, P., Mortlock, R.A., Fairbanks, R.G., Swift, J.H., 2001. River runoff, sea ice meltwater, and Pacific water distribution and mean residence times in the Arctic Ocean. Journal of Geophysical Research: Oceans 106 (C5), 9075-9092.

Fahl, K., Nöthig, E.-M., 2007. Lithogenic and biogenic particle fluxes on the Lomonosov Ridge (central Arctic Ocean) and their relevance for sediment accumulation: Vertical vs. lateral transport. Deep-Sea Research I 54, 1256-1272.

Fitzsimmons, J.N., Boyle, E.A., Jenkins, W.J., 2014. Distal transport of dissolved hydrothermal iron in the deep South Pacific Ocean. Proceedings of the National Academy of Sciences 111 (47), 16654-16661.

Gard, G., 1993. Late Quaternary coccoliths at the North Pole: Evidence of ice-free conditions and rapid sedimentation in the central Arctic Ocean. Geology 21 (3), 227-230.

Gardner, W., Richardson, M., Mishonov, A., 2020. Global Transmissometer Database V3 (Coupled with CTD data).

Gaye, B., Fahl, K., Kodina, L.A., Lahajnar, N., Nagel, B., Unger, D., Gebhardt, A.C., 2007. Particulate matter fluxes in the southern and central Kara Sea compared to sediments: Bulk fluxes, amino acids, stable carbon and nitrogen isotopes, sterols and fatty acids. Continental Shelf Research 27 (20), 2570-2594.

Gdaniec, S., Roy-Barman, M., Foliot, L., Thil, F., Dapoigny, A., Burckel, P., Garcia-Orellana, J., Masqué, P., Mörth, C.-M., Andersson, P.S., 2017. Thorium and protactinium isotopes as tracers of marine particle fluxes and deep water circulation in the Mediterranean Sea. Marine Chemistry.

Gdaniec, S., Roy-Barman, M., Levier, M., Valk, O., van der Loeff, M.R., Foliot, L., Dapoigny, A., Missiaen, L., Mörth, C.-M., Andersson, P.S., 2020. $^{231}$Pa and $^{230}$Th in the Arctic Ocean: Implications for boundary scavenging and $^{231}$Pa-$^{230}$Th fractionation in the Eurasian Basin. Chemical Geology 532, 119380.

Geibert, W., Usbeck, R., 2003. Adsorption of thorium and protactinium onto different particle types: Experimental findings. Geochimica et Cosmochimica Acta 68, 1486-1501.

Geibert, W., Usbeck, R., 2004. Adsorption of thorium and protactinium onto different particle types: experimental findings 11Associate editor: S. Krishnaswami. Geochimica et Cosmochimica Acta 68 (7), 1489-1501.

Geibert, W., 2018. Processes that Regulate Trace Element Distribution in the Ocean. Elements 14 (6), 391-396.

German, C.R., Casciotti, K.A., Dutay, J.-C., Heimbürger, L.E., Jenkins, W.J., Measures, C.I., Mills, R.A., Obata, H., Schlitzer, R., Tagliabue, A., Turner, D.R., Whitby, H., 2016. Hydrothermal impacts on trace element and isotope ocean biogeochemistry. Philosophical Transactions of the Royal Society A: Mathematical, Physical and Engineering Sciences 374 (2081).

German, C.R., Colley, S., Palmer, M.R., Khripounoff, A., Klinkhammer, G.P., 2002. Hydrothermal plume-particle fluxes at 13°N on the East Pacific Rise. Deep Sea Research Part I: Oceanographic Research Papers 49 (11), 1921-1940.

German, C.R., Fleer, A.P., Bacon, M.P., M., E.J., 1991. Hydrothermal scavenging at the Mid-Atlantic Ridge: radionuclide distributions. Earth and Planetary Science Letters 105, 170-181.

Goldberg, E.D., 1954. Marine Geochemistry 1. Chemical Scavengers of the Sea. The Journal of Geology 62 (3), 249-265.

Granskog, M.A., Stedmon, C.A., Dodd, P.A., Amon, R.M.W., Pavlov, A.K., de Steur, L., Hansen, E., 2012. Characteristics of colored dissolved organic matter (CDOM) in the Arctic outflow in the Fram Strait: Assessing the changes and fate of terrigenous CDOM in the Arctic Ocean. Journal of Geophysical Research: Oceans 117 (C12).

Grenier, M., François, R., Soon, M., Rutgers van der Loeff, M., Yu, X., Valk, O., Not, C., Moran, S.B., Edwards, R.L., Lu, Y., Lepore, K., Allen, S.E., 2019. Changes in Circulation and Particle Scavenging in the Amerasian Basin of the Arctic Ocean over the Last Three Decades Inferred from the Water Column Distribution of Geochemical Tracers. Journal of Geophysical Research: Oceans 124 (12), 9338-9363.

Günther, F., Overduin, P.P., Sandakov, A.V., Grosse, G., Grigoriev, M.N., 2013. Short- and long-term thermo-erosion of ice-rich permafrost coasts in the Laptev Sea region. Biogeosciences 10 (6), 4297-4318.

Haas, C., Eicken, H., 2001. Interannual variability of summer sea ice thickness in the Siberian and central Arctic under different atmospheric circulation regimes. Journal of Geophysical Research: Oceans 106 (C3), 4449-4462.

Haine, T.W.N., Curry, B., Gerdes, R., Hansen, E., Karcher, M., Lee, C., Rudels, B., Spreen, G., de Steur, L., Stewart, K.D., Woodgate, R., 2015. Arctic freshwater export: Status, mechanisms, and prospects. Global and Planetary Change 125, 13-35.

Haine, T.W.N., Martin, T., 2017. The Arctic-Subarctic sea ice system is entering a seasonal regime: Implications for future Arctic amplification. Scientific Reports 7 (1), 4618-4618.

Hayes, C.T., Anderson, R.F., Fleisher, M.Q., Huang, K.F., Robinson, L.F., Lu, Y., Cheng, H., Edwards, R.L., Moran, S.B., 2015a. $^{230}$Th and $^{231}$Pa on GEOTRACES GA03, the U.S. GEOTRACES North Atlantic transect, and implications for modern and paleoceanographic chemical fluxes. Deep-Sea Research Part II: Topical Studies in Oceanography 116, 29-41.

Hayes, C.T., Anderson, R.F., Fleisher, M.Q., Vivancos, S.M., Lam, P.J., Ohnemus, D.C., Huang, K.-F., Robinson, L., Lu, Y., Cheng, H., Edwards, R.L., Moran, S.B., 2015b. Intensity of Th and Pa scavenging partitioned by particle chemistry in the North Atlantic Ocean. Marine Chemistry 170, 49-60.

Henderson, G.M., Heinze, C., Anderson, R.F., Winguth, A.M.E., 1999. Global distribution of the $^{230}$Th flux to ocean sediments constrained by GCM modelling. Deep-Sea Research I 46, 1861-1893.

Hoffmann, S., McManus, J., 2007. Is there a $^{230}$Th deficit in Arctic sediments? Earth and Planetary Science Letters 258 (3), 516-527.

Hoffmann, S., McManus, J., Curry, W.B., Brown-Leger, S.L., 2013. Persistent export of $^{231}$Pa from the deep central Arctic Ocean over the past 35,000 years. Nature 497, 603-607.

Holden, N.E., 1990. Total half-lives for selected nuclides. Pure and Applied Chemistry 62 (5), 941-958.

Honeyman, B.D., Balistrieri, L.S., Murray, J.W., 1988. Oceanic trace metal scavenging: the importance of particle concentration. Deep Sea Research Part A. Oceanographic Research Papers 35 (2), 227-246.

Honjo, S., Krishfield, R.A., Eglinton, T.I., Manganini, S.J., Kemp, J.N., Doherty, K., Hwang, J., McKee, T.K., Takizawa, T., 2010. Biological pump processes in the cryopelagic and hemipelagic Arctic Ocean: Canada Basin and Chukchi Rise. Progress in Oceanography 85 (3–4), 137-170.

Hsieh, Y.-T., Henderson, G.M., Thomas, A.L., 2011. Combining seawater $^{232}$Th and $^{230}$Th concentrations to determine dust fluxes to the surface ocean. Earth and Planetary Science Letters 312, 280-290.

Huh, C.-A., Kelley, J.M., Murray, J.W., Wei, C.-L., 1994. Water column distribution of $^{230}$Th and $^{232}$Th in the Black Sea. Deep Sea Research Part I: Oceanographic Research Papers 41 (1), 101-112.

Huh, C.-A., Pisias, N., Kelley, J.M., C., M.T., Grantz, A., 1997. Natural radionuclides and plutonium in sediments from the western Arctic Ocean: sedimentation rates and pathways of radionuclides. Deep-Sea Research II 44, 1725-1743.

Hwang, J., Eglinton, T.I., Krishfield, R.A., Manganini, S.J., Honjo, S., 2008. Lateral organic carbon supply to the deep Canada Basin. Geophysical Research Letters 35 (11), n/a-n/a.

Hwang, J., Kim, M., Manganini, S.J., McIntyre, C.P., Haghipour, N., Park, J., Krishfield, R.A., Macdonald, R.W., McLaughlin, F.A., Eglinton, T.I., 2015. Temporal and spatial variability of particle transport in the deep Arctic Canada Basin. Journal of Geophysical Research: Oceans 120 (4), 2784-2799.

Ingvaldsen, R., Loeng, H., Asplin, L., 2002. Variability in the Atlantic inflow to the Barents Sea based on a one-year time series from moored current meters. Continental Shelf Research, 505-519.

Jakobsson, M., Grantz, A., Kristoffersen, Y., Macnab, R., 2003. Physiographic provinces of the Arctic Ocean seafloor. GSA Bulletin 115 (12), 1443-1455.

Jansen, E., Christensen, J.H., Dokken, T., Nisancioglu, K.H., Vinther, B.M., Capron, E., Guo, C., Jensen, M.F., Langen, P.L., Pedersen, R.A., Yang, S., Bentsen, M., Kjær, H.A., Sadatzki, H., Sessford, E., Stendel, M., 2020. Past perspectives on the present era of abrupt Arctic climate change. Nature Climate Change 10 (8), 714-721.

Jeandel, C., Rutgers van der Loeff, M., Lam, P.J., Roy-Barman, M., Sherrell, R.M., Kretschmer, S., German, C., Dehairs, F., 2015. What did we learn about ocean particle dynamics in the GEOSECS–JGOFS era? Progress in Oceanography 133, 6-16.

Jensen, L.T., Morton, P., Twining, B.S., Heller, M.I., Hatta, M., Measures, C.I., John, S., Zhang, R., Pinedo-Gonzalez, P., Sherrell, R.M., Fitzsimmons, J.N., 2020. A comparison of marine Fe and Mn cycling: U.S. GEOTRACES GN01 Western Arctic case study. Geochimica et Cosmochimica Acta.

Jerome, S., Bobin, C., Cassette, P., Dersch, R., Galea, R., Liu, H., Honig, A., Keightley, J., Kossert, K., Liang, J., Marouli, M., Michotte, C., Pommé, S., Röttger, S., Williams, R., Zhang, M., 2020. Half-life determination and comparison of activity standards of $^{231}$Pa. Applied Radiation and Isotopes 155, 108837.

Jones, E.P., Rudels, B., Anderson, L.G., 1995. Deep waters of the Arctic Ocean: origins and circulation. Deep-Sea Research 1 42, 737-760.

Kadko, D., Aguilar-Islas, A., Bolt, C., Buck, C.S., Fitzsimmons, J.N., Jensen, L.T., Landing, W.M., Marsay, C.M., Rember, R., Shiller, A.M., Whitmore, L.M., Anderson, R.F., 2019.

The residence times of trace elements determined in the surface Arctic Ocean during the 2015 US Arctic GEOTRACES expedition. Marine Chemistry 208, 56-69.

Karcher, M., Beszczynska-Möller, A., Kauker, F., Gerdes, R., Heyen, S., Rudels, B., Schauer, U., 2011. Arctic Ocean warming and its consequences for the Denmark Strait overflow. Journal of Geophysical Research 116.

Karcher, M., Smith, J.N., Kauker, F., Gerdes, R., Smethie Jr., W.M., 2012. Recent changes in Arctic Ocean circulation revealed by iodine-129 observations and modeling. Journal of Geophysical Research 117.

Karcher, M.J., Gerdes, R., Kauker, F., Köberle, C., 2003. Arctic warming: Evolution and spreading of the 1990s warm event in the Nordic seas and the Arctic Ocean. Journal of Geophysical Research: Oceans 108 (C2).

Kipp, L.E., Charette, M.A., Moore, W.S., Henderson, P.B., Rigor, I.G., 2018. Increased fluxes of shelf-derived materials to the central Arctic Ocean. Science Advances 4 (1).

Klinkhammer, G., Bender, M., Weiss, R.F., 1977. Hydrothermal manganese in the Galapagos Rift. Nature 269 (5626), 319-320.

Klunder, M.B., Bauch, D., Laan, P., de Baar, H.J.W., Van Heuven, S.M.A.C., Ober, S., 2012a. Dissolved iron in the Arctic shelf seas and surface waters of the central Arctic Ocean: Impact of Arctic river water and ice-melt. Journal of Geophysical Research 117.

Klunder, M.B., Laan, P., Middag, R., de Baar, H.J.W., Bakker, K., 2012b. Dissolved iron in the Arctic Ocean: Important role of hydrothermal sources, shelf input and scavenging removal. Journal of Geophysical Research-Oceans 117 (C4).

Knight, G.B., Macklin, R.L., 1948. Half-Life of $UX_1$ ($Th_{234}$). Physical Review 74 (10), 1540-1541.

Kretschmer, S., Geibert, W., Rutgers van der Loeff, M.M., Schnabel, C., Xu, S., Mollenhauer, G., 2011. Fractionation of $^{230}$Th, $^{231}$Pa, and $^{10}$Be induced by particle size and composition within an opal-rich sediment of the Atlantic Southern Ocean. Geochimica et Cosmochimica Acta 75, 6971–6987.

Krishnaswami, S., Lal, D., Somayajulu, B.L.K., Weiss, R.F., Craig, H., 1976. Large-volume in-situ filtration of deep Pacific waters: Mineralogical and radioisotope studies. Earth and Planetary Science Letters 32 (2), 420-429.

Krumpen, T., Belter, H.J., Boetius, A., Damm, E., Haas, C., Hendricks, S., Nicolaus, M., Nöthig, E.-M., Paul, S., Peeken, I., Ricker, R., Stein, R., 2019. Arctic warming interrupts the Transpolar Drift and affects long-range transport of sea ice and ice-rafted matter. Scientific Reports 9 (1), 5459.

Kuzyk, Z.Z.A., Gobeil, C., Macdonald, R.W., 2013. $^{210}$Pb and $^{137}$Cs in margin sediments of the Arctic Ocean: Controls on boundary scavenging. GLOBAL BIOGEOCHEMICAL CYCLES 27 (2), 422-439.

Lal, D., 1977. The Oceanic Microcosm of Particles. Science 198 (4321), 997-1009.

Leblond, P.H., 1980. On the Surface Circulation in Some Channels of the Canadian Arctic Archipelago. ARCTIC 33 (1), 189-197.

Letscher, R.T., Hansell, D.A., Kadko, D., 2011. Rapid removal of terrigenous dissolved organic carbon over the Eurasian shelves of the Arctic Ocean. Marine Chemistry 123 (1), 78-87.

Lippold, J., Luo, Y., Francois, R., Allen, S.E., Gherardi, J., Pichat, S., Hickey, B., Schulz, H., 2012. Strength and geometry of the glacial Atlantic Meridional Overturning Circulation. nature geoscience 5 (11), 813-816.

Liu, J., Song, M., Horton, R.M., Hu, Y., 2013. Reducing spread in climate model projections of a September ice-free Arctic. Proceedings of the National Academy of Sciences 110 (31), 12571-12576.

Lund-Hansen, L.C., Bendtsen, J., Stratmann, T., Tonboe, R., Olsen, S.M., Markager, S., Sorrell, B.K., 2020. Will low primary production rates in the Amundsen Basin (Arctic Ocean) remain low in a future ice-free setting, and what governs this production? Journal of Marine Systems 205, 103287.

Luo, Y., Francois, R., Allen, S.E., 2010. Sediment $^{231}Pa/^{230}Th$ as a recorder of the rate of the Atlantic meridional overturning circulation: insights from a 2-D model. Ocean Science 6, 381-400.

Marchal, O., Francois, R., Stocker, T.F., Joos, F., 2000. Ocean thermohaline circulation and sedimentary $^{231}Pa/^{230}Th$ ratio. Palaeogeography 15, 625-641.

McClelland, J.W., Holmes, R.M., Dunton, K.H., Macdonald, R.W., 2012. The Arctic Ocean Estuary. Estuaries and Coasts 35 (2), 353-368.

McManus, J.F., Francois, R., Gherardi, J.M., Keigwin, L.D., Brown-Leger, S.L., 2004. Collapse and rapid resumption of Atlantic meridional circulation linked to deglacial climate changes. Nature 428, 834-837.

Middag, R., de Baar, H.J.W., Laan, P., Bakker, K., 2009. Dissolved aluminium and the silicon cycle in the Arctic Ocean. Marine Chemistry 115 (3–4), 176-195.

Middag, R., de Baar, H.J.W., Laan, P., Klunder, M.B., 2011. Fluvial and hydrothermal input of manganese into the Arctic Ocean. Geochimica et Cosmochimica Acta 75 (9), 2393-2408.

Moore, W.S., Sackett, W.M., 1964. Uranium and thorium series inequilibrium in sea water. Journal of Geophysical Research (1896-1977) 69 (24), 5401-5405.

Moran, S.B., Shen, C.-C., Edwards, R.L., Edmonds, H.N., Scholten, J.C., Smith, J.N., Ku, T.-L., 2005. $^{231}Pa$ and $^{230}Th$ in surface sediments of the Arctic Ocean: Implications for $^{231}Pa/^{230}Th$ fractionation, boundary scavenging, and advective export. Earth and Planetary Science Letters 234, 235-248.

Morison, J., Kwok, R., Peralta-Ferriz, C., Alkire, M., Rigor, I., Andersen, R., Steele, M., 2012. Changing Arctic Ocean freshwater pathways. Nature 481 (7379), 66-70.

Morison, J., Steele, M., Kikuchi, T., Falkner, K., Smethie, W., 2006. Relaxation of central Arctic Ocean hydrography to pre-1990s climatology. Geophysical Research Letters 33 (17).

Münchow, A., Melling, H., Falkner, K.K., 2006. An Observational Estimate of Volume and Freshwater Flux Leaving the Arctic Ocean through Nares Strait. Journal of Physical Oceanography 36 (11), 2025-2041.

Mysak, L.A., 2001. Patterns of Arctic Circulation. Science 293 (5533), 1269-1270.

Newton, R., Pfirman, S., Tremblay, B., DeRepentigny, P., 2017. Increasing transnational sea-ice exchange in a changing Arctic Ocean. Earth's Future 5 (6), 633-647.

Nittrouer, C.A., Wright, L.D., 1994. Transport of particles across continental shelves. Reviews of Geophysics 32 (1), 85-113.

Nöthig, E.-M., Lalande, C., Fahl, K., Metfies, K., Salter, I., Bauerfeind, E., 2020. Annual cycle of downward particle fluxes on each side of the Gakkel Ridge in the central Arctic Ocean.

Philosophical Transactions of the Royal Society A: Mathematical, Physical and Engineering Sciences 378 (2181), 20190368.

Nozaki, Y., Horibe, Y., Tsubota, H., 1981. The water column distributions of thorium isotopes in the western North Pacific. Earth and Planetary Science Letters 54 (2), 203-216.

Nozaki, Y., Yang, H.-S., Yamada, M., 1987. Scavenging of thorium in the ocean. Journal of Geophysical Research: Oceans 92 (C1), 772-778.

O'Brien, M.C., Macdonald, R.W., Melling, H., Iseki, K., 2006. Particle fluxes and geochemistry on the Canadian Beaufort Shelf: Implications for sediment transport and deposition. Continental Shelf Research 26 (1), 41-81.

Orvik, K.A., Niiler, P., 2002. Major pathways of Atlantic water in the northern North Atlantic and Nordic Seas toward Arctic. Geophysical Research Letters 29 (19), 2-1-2-4.

Owens, S.A., Buesseler, K.O., Sims, K.W.W., 2011. Re-evaluating the $^{238}$U-salinity relationship in seawater: Implications for the $^{238}$U–$^{234}$Th disequilibrium method. Marine Chemistry 127 (1), 31-39.

Oziel, L., Baudena, A., Ardyna, M., Massicotte, P., Randelhoff, A., Sallée, J.-b., Ingvaldsen, R., Devred, E., Babin, M., 2020. Faster Atlantic currents drive poleward expansion of temperate phytoplankton in the Arctic Ocean. Nature Communications 11.

Pavia, F., Anderson, R., Vivancos, S., Fleisher, M., Lam, P., Lu, Y., Cheng, H., Zhang, P., Lawrence Edwards, R., 2018. Intense hydrothermal scavenging of $^{230}$Th and $^{231}$Pa in the deep Southeast Pacific. Marine Chemistry 201, 212-228.

Perovich, D., 2011. The Changing Arctic Sea Ice Cover. Oceanography 24, 162-173.

Perovich, D.K., Meier, W., Tschudi, M., Farrell, S., Hendricks, S., Gerland, S., Haas, C., Krumpen, T., Polashenski, C., Ricker, R., Webster, M., 2019. [The Arctic] sea ice cover [in "State of the Climate in 2018"]. Bulletin of the American Meteorological Society 100 (9), 146-150.

Perovich, D.K., Richter-Menge, J.A., 2009. Loss of Sea Ice in the Arctic. Annual Review of Marine Science 1 (1), 417-441.

Peterson, B.J., Holmes, R.M., McClelland, J.W., Vörösmarty, C.J., Lammers, R.B., Shiklomanov, A.I., Shiklomanov, I.A., Rahmstorf, S., 2002. Increasing River Discharge to the Arctic Ocean. Science 298 (5601), 2171-2173.

Pfirman, S.L., Kögeler, J.W., Rigor, I., 1997. Potential for rapid transport of contaminants from the Kara Sea. Science of the Total Environment 202 (1), 111-122.

Piontek, J., Galgani, L., Nöthig, E.-M., Peeken, I., Engel, A., 2020. Organic matter composition and heterotrophic bacterial activity at declining summer sea ice in the central Arctic Ocean. Limnology and Oceanography n/a (n/a).

Pistone, K., Eisenman, I., Ramanathan, V., 2014. Observational determination of albedo decrease caused by vanishing Arctic sea ice. Proceedings of the National Academy of Sciences 111 (9), 3322-3326.

Polyakov, I.V., Beszczynska, A., Carmack, E.C., Dmitrenko, I.A., Fahrbach, E., Frolov, I.E., Gerdes, R., Hsansen, E., Holfort, J., Ivanov, V.V., Johnson, M.A., Karcher, M., Kauker, F., Morison, J., Orvik, K.A., Schauer, U., Simmons, H.L., Skagseth, O., Sokolov, V.T., Steele, M., Timokhov, L.A., Walsh, D., Walsh, J.E., 2005. One more step toward a warmer Arctic. Geophysical Research Letters 32.

Polyakov, I.V., Pnyushkov, A.V., Alkire, M.B., Ashik, I.M., Baumann, T.M., Carmack, E.C., Goszczko, I., Guthrie, J., Ivanov, V.V., Kanzow, T., Krishfield, R., Kwok, R., Sundfjord, A., Morison, J., Rember, R., Yulin, A., 2017. Greater role for Atlantic inflows on sea-ice loss in the Eurasian Basin of the Arctic Ocean. Science 356 (6335), 285-291.

Proshutinsky, A.Y., Dukhovskoy, D., Timmermans, M.-L., Krishfield, R., Bamber, J.L., 2015. Arctic circulation regimes. Philosophical Transactions of the Royal Society A: Mathematical, Physical and Engineering Sciences 373 (2052), 20140160.

Proshutinsky, A.Y., Johnson, M.A., 1997. Two circulation regimes of the wind-driven Arctic Ocean. JOURNAL OF GEOPHYSICAL RESEARCH, 102, 12493-12514.

Proshutinsky, A.Y., Polyakov, I.V., Johnson, M.A., 1999. Climate states and variability of Arctic ice and water dynamics during 1946–1997. Polar Research 18 (2), 135-142.

Rabe, B., Karcher, M., Kauker, F., Schauer, U., Toole, J.M., Krishfield, R.A., Pisarev, S., Kikuchi, T., Su, J., 2014. Arctic Ocean basin liquid freshwater storage trend 1992–2012. Geophysical Research Letters 41 (3), 961-968.

Randelhoff, A., Sundfjord, A., 2017. Short Commentary on Marine Productivity at Arctic Shelf Breaks: Upwelling, Advection and Vertical Mixing. Ocean Science Discussions, 1-11.

Resing, J.A., Sedwick, P.N., German, C.R., Jenkins, W.J., Moffett, J.W., Sohst, B.M., Tagliabue, A., 2015. Basin-scale transport of hydrothermal dissolved metals across the South Pacific Ocean. Nature 523 (7559), 200-203.

Riedel, C., Schlindwein, V., 2010. Did the 1999 earthquake swarm on Gakkel Ridge open a volcanic conduit? A detailed teleseismic data analysis. Journal of Seismology 14 (3), 505-522.

Rigor, I.G., Wallace, J.M., Colony, R.L., 2002. Response of Sea Ice to the Arctic Oscillation. Journal of Climate 15 (18), 2648-2663.

Rijkenberg, M.J.A., Slagter, H.A., Rutgers van der Loeff, M., van Ooijen, J., Gerringa, L.J.A., 2018. Dissolved Fe in the Deep and Upper Arctic Ocean With a Focus on Fe Limitation in the Nansen Basin. Frontiers in Marine Science 5 (88).

Robinson, L.F., Belshaw, N.S., Henderson, G.M., 2004. U and Th concentrations and isotope ratios in modern carbonates and waters from the Bahamas. Geochimica et Cosmochimica Acta 68, 1777-1789.

Rothrock, D.A., Yu, Y., Maykut, G.A., 1999. Thinning of the Arctic sea-ice cover. Geophysical Research Letters 26 (23), 3469-3472.

Roy-Barman, M., 2009. Modelling the effect of boundary scavenging on Thorium and Protactinium profiles in the ocean. Biogeosciences 6, 3091-3107.

Roy-Barman, M., Chen, J.H., Wasserburg, G.J., 1996. $^{230}$Th-$^{232}$Th systematics in the central Pacific Ocean: The sources and the fates of thorium. Earth and Planetary Science Letters 139 (3), 351-363.

Roy-Barman, M., Jeandel, C., 2016. Marine Geochemistry: Ocean Circulation, Carbon Cycle and Climate Change. Oxford University Press, Oxford.

Rudels, B., 2009. Arctic Ocean Circulation A2 - Steele, John H. Encyclopedia of Ocean Sciences (Second Edition). Academic Press, Oxford, pp. 211-225.

Rudels, B., 2012. Arctic Ocean circulation and variability – advection and external forcing encounter constraints and local processes. Ocean Science 8, 261-286.

Rudels, B., 2015. Arctic Ocean circulation, processes and water masses: A description of observations and ideas with focus on the period prior to the International Polar Year 2007–2009. Progress in Oceanography 132, 22-67.

Rudels, B., Anderson, L.G., Jones, E.P., 1996. Formation and evolution of the surface mixed layer and halocline of the Arctic Ocean. Journal of Geophysical Research: Oceans 101 (C4), 8807-8821.

Rudels, B., Jones, E.P., Anderson, L.G., Kattner, G., 2013. On the Intermediate Depth Waters of the Arctic Ocean. The Polar Oceans and Their Role in Shaping the Global Environment. American Geophysical Union, pp. 33-46.

Rudels, B., Jones, E.P., Kattner, G., 1994. On the Intermediate Depth Waters of the Arctic Ocean. In: Johannessen, O.M., Muench, R.D., Overland, J.E. (Eds.), The Polar Oceans and Their Role in Shaping the Global Environment, pp. 33-46.

Rudels, B., Korhonen, M., Schauer, U., Pisarev, S., Rabe, B., Wisotzki, A., 2015. Circulation and transformation of Atlantic water in the Eurasian Basin and the contribution of the Fram Strait inflow branch to the Arctic Ocean heat budget. Progress in Oceanography 132 (0), 128-152.

Rutgers van der Loeff, M., Kipp, L., Charette, M.A., Moore, W.S., Black, E., Stimac, I., Charkin, A., Bauch, D., Valk, O., Karcher, M., Krumpen, T., Casacuberta, N., Smethie, W., Rember, R., 2018. Radium Isotopes Across the Arctic Ocean Show Time Scales of Water Mass Ventilation and Increasing Shelf Inputs. Journal of Geophysical Research: Oceans 0 (0).

Rutgers van der Loeff, M., Venchiarutti, C., Stimac, I., van Ooijen, J., Huhn, O., Rohardt, G., Strass, V., 2016. Meridional circulation across the Antarctic Circumpolar Current serves as a double $^{231}$Pa and $^{230}$Th trap. Earth and Planetary Science Letters 455, 73-84.

Rutgers van der Loeff, M.M., Geibert, W., 2008. Chapter 7 U- and Th-Series Nuclides as Tracers of Particle Dynamics, Scavenging and Biogeochemical Cycles in the Oceans. In: Krishnaswami, S., Cochran, J.K. (Eds.), Radioactivity in the Environment. Elsevier, pp. 227-268.

Saito, M.A., Noble, A.E., Tagliabue, A., Goepfert, T.J., Lamborg, C.H., Jenkins, W.J., 2013. Slow-spreading submarine ridges in the South Atlantic as a significant oceanic iron source. nature geoscience 6, 775-779.

Sakshaug, E., 2004. Primary and Secondary Production in the Arctic Seas. In: Stein, R., MacDonald, R.W. (Eds.), The Organic Carbon Cycle in the Arctic Ocean. Springer Berlin Heidelberg, Berlin, Heidelberg, pp. 57-81.

Schauer, U., Beszczynska-Moeller, A., 2009. Problems with estimating oceanic heat transport – conceptual remarks for the case of Fram Strait in the Arctic Ocean. Ocean Science Discussions (OSD) 6.

Schauer, U., Fahrbach, E., Osterhus, S., Rohardt, G., 2004. Arctic warming through the Fram Strait: Oceanic heat transport from 3 years of measurements. Journal of Geophysical Research: Oceans 109 (C6).

Schlindwein, V., Riedel, C., 2010. Location and source mechanism of sound signals at Gakkel ridge, Arctic Ocean: Submarine Strombolian activity in the 1999–2001 volcanic episode. Geochemistry, Geophysics, Geosystems 11 (1).

Schlitzer, R., 2016. Ocean Data View. http://odv.awi.de.

Schlosser, P., Bauch, D., Fairbanks, R., Bönisch, G., 1994. Arctic river-runoff: mean residence time on the shelves and in the halocline. Deep Sea Research Part I: Oceanographic Research Papers 41 (7), 1053-1068.

Schlosser, P., Kromer, B., Ekwurzel, B., Bönisch, G., McNichol, A., Schneider, R., von Reden, K., Östlund, H.G., Swift, J.H., 1997. The first trans-Arctic 14C section: comparison of the mean ages of the deep waters in the Eurasian and Canadian basins of the Arctic Ocean. Nuclear Instruments and Methods in Physics Research Section B: Beam Interactions with Materials and Atoms 123 (1), 431-437.

Scholten, J.C., Fietzke, J., Mangini, A., Garbe-Schönberg, C.-D., Eisenhauer, A., Schneider, R., Stoffers, P., 2008. Advection and scavenging: Effects on $^{230}$Th and $^{231}$Pa distribution off Southwest Africa. Earth and Planetary Science Letters 271, 159-169.

Scholten, J.C., Rutgers van der Loeff, M.M., Michel, A., 1995. Distribution of $^{230}$Th and $^{231}$Pa in the water column in relation to the ventilation of the deep Arctic basins. Deep-Sea Research II 42, 1519-1531.

Schuur, E.A.G., Abbott, B.W., Bowden, W.B., Brovkin, V., Camill, P., Canadell, J.G., Chanton, J.P., Chapin, F.S., Christensen, T.R., Ciais, P., Crosby, B.T., Czimczik, C.I., Grosse, G., Harden, J., Hayes, D.J., Hugelius, G., Jastrow, J.D., Jones, J.B., Kleinen, T., Koven, C.D., Krinner, G., Kuhry, P., Lawrence, D.M., McGuire, A.D., Natali, S.M., O'Donnell, J.A., Ping, C.L., Riley, W.J., Rinke, A., Romanovsky, V.E., Sannel, A.B.K., Schädel, C., Schaefer, K., Sky, J., Subin, Z.M., Tarnocai, C., Turetsky, M.R., Waldrop, M.P., Walter Anthony, K.M., Wickland, K.P., Wilson, C.J., Zimov, S.A., 2013. Expert assessment of vulnerability of permafrost carbon to climate change. Climatic Change 119 (2), 359-374.

Schuur, E.A.G., McGuire, A.D., Schädel, C., Grosse, G., Harden, W.J., Hayes, D.J., Hugelius, G., Koven, C.D., Kuhry, P., Lawrence, D.M., Natali, S.M., Olefeldt, D., Romanovsky, V.E., Schaefer, K., Turetsky, M.R., Treat, C.C., Vonk, J.E., 2015. Climate change and the permafrost carbon feedback. Nature 520, 171-179.

Serreze, M.C., Barrett, A.P., Stroeve, J.C., Kindig, D.N., Holland, M.M., 2009. The emergence of surface-based Arctic amplification. The Cryosphere 3 (1), 11-19.

Serreze, M.C., Francis, J.A., 2006. The Arctic Amplification Debate. Climatic Change 76 (3), 241-264.

Serreze, M.C., Holland, M.M., Stroeve, J., 2007. Perspectives on the Arctic's Shrinking Sea-Ice Cover. Science 315 (5818), 1533-1536.

Slagstad, D., Wassmann, P.F.J., Ellingsen, I., 2015. Physical constrains and productivity in the future Arctic Ocean. Frontiers in Marine Science 2 (85).

Smethie, W.M., Jr., 2017. CFC-11, CFC-12, CFC-113, and SF6 measured on water bottle samples during POLARSTERN cruise PS94 (ARK-XXIX/3) to the Arctic Ocean in 2016. PANGAEA.

Smethie, W.M., Jr., Chipman, D.W., Swift, J.H., Koltermann, K.P., 1988. Chlorofluoromethanes in the Arctic Mediterranean seas: evidence for formation of bottom water in the Eurasian Basin and deep-water exchange through Fram Strait. Deep-Sea Research 35, 347-369.

Smith, J.N., McLaughlin, F.A., Smethie, W.M., Moran, S.B., Lepore, K., 2011. Iodine-129, $^{137}$Cs, and CFC-11 tracer transit time distributions in the Arctic Ocean. Journal of Geophysical Research: Oceans 116 (C4), n/a-n/a.

Smith, J.N., Moran, S.B., Macdonald, R.W., 2003. Shelf–basin interactions in the Arctic Ocean based on $^{210}$Pb and Ra isotope tracer distributions. Deep Sea Research Part I: Oceanographic Research Papers 50 (3), 397-416.

Sohn, R.A., Willis, C., Humphris, S., Shank, T.M., Singh, H., Edmonds, H.N., Kunz, C., Hedman, U., Helmke, E., Jakuba, M., Liljebladh, B., Linder, J., Murphy, C., Nakamura, K.-i., Sato, T., Schlindwein, V., Stranne, C., Tausenfreund, M., Upchurch, L., Winsor, P., Jakobsson, M., Soule, A., 2008. Explosive volcanism on the ultraslow-spreading Gakkel ridge, Arctic Ocean. Nature 453 (7199), 1236-1238.

Stein, R., Grobe, H., Washner, M., 1994. Organic carbon, carbonate, and clay mineral distributions in eastern central Arctic Ocean surface sediments. Marine Geology 119, 269-285.

Tanhua, T., Jones, E.P., Jeansson, E., Jutterström, S., Smethie, W.M., Wallace, D.W.R., Anderson, L.G., 2009. Ventilation of the Arctic Ocean: Mean ages and inventories of anthropogenic CO2 and CFC-11. Journal of Geophysical Research: Oceans 114 (C1), n/a-n/a.

Terhaar, J., Kwiatkowski, L., Bopp, L., 2020. Emergent constraint on Arctic Ocean acidification in the twenty-first century. Nature 582 (7812), 379-383.

Timmermans, M.-L., Marshall, J., 2020. Understanding Arctic Ocean Circulation: A Review of Ocean Dynamics in a Changing Climate. Journal of Geophysical Research: Oceans 125 (4), e2018JC014378.

Timmermans, M.-L., Winsor, P., Whitehead, J.A., 2005. Deep-Water Flow over the Lomonosov Ridge in the Arctic Ocean. Journal of Physical Oceanography 35 (8), 1489-1493.

Tremblay, J.-É., Gagnon, J., 2009. The effects of irradiance and nutrient supply on the productivity of Arctic waters: a perspective on climate change. Springer Netherlands, Dordrecht, pp. 73-93.

Trimble, S.M., Baskaran, M., Porcelli, D., 2004. Scavenging of thorium isotopes in the Canada Basin of the Arctic Ocean. Earth and Planetary Science Letters 222, 915-932.

Turner, D.R., Whitfield, M., Dickson, A., 1981. The equilibrium speciation of dissolved components in freshwater and sea water at 25°C and 1 atm pressure. Geochimica et Cosmochimica Acta 45, 855-881.

Ulfsbo, A., Jones, E.M., Casacuberta, N., Korhonen, M., Rabe, B., Karcher, M., Heuven, S.M.A.C., 2018. Rapid Changes in Anthropogenic Carbon Storage and Ocean Acidification in the Intermediate Layers of the Eurasian Arctic Ocean: 1996–2015. GLOBAL BIOGEOCHEMICAL CYCLES 32 (9), 1254-1275.

Våge, K., Pickart, R.S., Pavlov, V., Lin, P., Torres, D.J., Ingvaldsen, R., Sundfjord, A., Proshutinsky, A.Y., 2016. The Atlantic Water boundary current in the Nansen Basin: Transport and mechanisms of lateral exchange. Journal of Geophysical Research: Oceans 121 (9), 6946-6960.

Venchiarutti, C., Rutgers van der Loeff, M.M., Stimac, I., 2011. Scavenging of $^{231}$Pa and thorium isotopes based on dissolved and size-fractionated particulate distributions at Drake Passage (ANTXXIV-3). Deep-Sea Research II 58, 2767-2784.

Venchiarutti, C., Jeandel, C., Roy-Barman, M., 2008. Particle dynamics study in the wake of Kerguelen Island using thorium isotopes. Deep Sea Research Part I: Oceanographic Research Papers 55 (10), 1343-1363.

Walter, H.-J., Rutgers van der Loeff, M.M., François, R., 1999. Reliability of the $^{231}Pa$ /$^{230}Th$ Activity Ratio as a Tracer for Bioproductivity of the Ocean. In: Fischer, G., Wefer, G. (Eds.), Use of Proxies in Paleoceanography: Examples from the South Atlantic. Springer Berlin Heidelberg, Berlin, Heidelberg, pp. 393-408.

Woodgate, R., 2013. Arctic Ocean Circulation: Going Around At the Top Of the World. Nature Education Knowledge 4 (8), 8.

Woodgate, R.A., Aagaard, K., Muench, R.D., Gunn, J., Björk, G., Rudels, B., Roach, A.T., Schauer, U., 2001. The Arctic Ocean Boundary Current along the Eurasian slope and the adjacent Lomonosov Ridge: Water mass properties, transports and transformations from moored instruments. Deep Sea Research Part I: Oceanographic Research Papers 48 (8), 1757-1792.

Woodgate, R.A., Aagaard, K., Weingartner, T.J., 2005. A year in the physical oceanography of the Chukchi Sea: Moored measurements from autumn 1990–1991. Deep Sea Research Part II: Topical Studies in Oceanography 52 (24), 3116-3149.

Woodgate, R.A., Fahrbach, E., Rohardt, G., 1999. Structure and transports of the East Greenland Current at 75°N from moored current meters. Journal of Geophysical Research: Oceans 104 (C8), 18059-18072.

Woodgate, R.A., Weingartner, T., Lindsay, R., 2010. The 2007 Bering Strait oceanic heat flux and anomalous Arctic sea-ice retreat. Geophysical Research Letters 37 (1).

Xiang, Y., Lam, P.J., 2020. Size-Fractionated Compositions of Marine Suspended Particles in the Western Arctic Ocean: Lateral and Vertical Sources. Journal of Geophysical Research: Oceans 125 (8), e2020JC016144.

Yu, E.-F., Francois, R., Rutgers van der Loeff, M.M., 1996. Similar rates of modern and last-glacial ocean thermohaline circulation inferred from radiochemical data. Nature 379, 689-694.

Yu, X., Allen, S.E., François, R., Grenier, M., Myers, P.G., Hu, X., 2020. Modeling Dissolved and Particulate Th in the Canada Basin: Implications for Recent Changes in Particle Flux and Intermediate Circulation. Journal of Geophysical Research: Oceans 125 (2), e2019JC015640.

# CHAPTER 2: Importance of Hydrothermal Vents in Scavenging Removal of $^{230}$Th in the Nansen Basin

**Ole Valk[1], Michiel M. Rutgers van der Loeff[1], Walter Geibert[1], Sandra Gdaniec[2], Micha. J. A. Rijkenberg[3], S. Bradley Moran[4], Kate Lepore[5], Richard Lawrence Edwards[6], Yanbin Lu[7], Viena Puigcorbé[8]**

[1]Alfred-Wegener-Institute Helmholtz Centre for Polar and Marine Research, 27570 Bremerhaven, Germany

[2]Stockholm University, Department of Geological Sciences, 106 91, Stockholm, Sweden

[3]Department of Ocean Systems, NIOZ Royal Institute for Sea Research and Utrecht University, Den Burg, The Netherlands

[4]College of Fisheries and Ocean Sciences, University of Alaska Fairbanks, Fairbanks, AK 99775, USA

[5]Mount Holyoke College, South Hadley, MA 01075, USA

[6]University of Minnesota, Minneapolis, MN 55455, USA

[7]Nanyang Technological University, 639798, Singapore

[8]School of Science, Edith Cowan University, Joondalup, WA 6027, Australia

**Key Point:**

• The first $^{230}$Th time series in the Arctic shows that a hydrothermal event caused scavenging removal of $^{230}$Th in the Nansen Basin.

Manuscript published in *Geophysical Research Letters*, 45, 10,539–10,548. https://doi.org/10.1029/2018GL079829

Received; 3 August 2018
Accepted: 17 September 2018
Accepted article online: 19 September 2018

**Abstract**

In this study we present dissolved and particulate $^{230}$Th and $^{232}$Th results, as well as particulate $^{234}$Th data, obtained as part of the GEOTRACES central Arctic Ocean sections GN04 (2015) and IPY11 (2007). Samples were analysed following GEOTRACES methods, and compared to previous results from 1991. We observe significant decreases in $^{230}$Th concentrations in the deep waters of the Nansen Basin. We ascribe this non-steady state removal process to a variable release and scavenging of trace metals near an ultra-slow spreading ridge. This finding demonstrates that hydrothermal scavenging in the deep-sea may vary on annual time scales and highlights the importance of repeated GEOTRACES sections.

**Plain Language Summary**

This study presents new results of thorium isotopes from the central Arctic Ocean. Thorium-230 is produced continuously in seawater by radioactive decay of $^{234}$U and subsequently removed by particle scavenging. We show that observed changes in $^{230}$Th concentrations compared to earlier times are related to submarine volcanic eruptions. We use $^{230}$Th data from three different expeditions conducted in 1991, 2007 and 2015. The Nansen Basin is part of the Eurasian Basin of the Arctic Ocean. It is divided from the Amundsen Basin by the Gakkel Ridge. The Gakkel Ridge is a region where the Eurasian and the North American plates spread apart, triggering volcanism. Submarine volcanos and hydrothermal vents release trace elements such as iron. Iron is known to be oxidized to particles that react with $^{230}$Th. Thus, when iron particles sink they remove $^{230}$Th from the water column. In the Nansen Basin this process took place between 2007 and 2015, triggered by earthquake-induced volcanic eruptions in 2001. In this study, we present a conceptual hydrothermal scavenging process and plume dispersal by deep water circulation.

## 1. Introduction

$^{230}$Th ($t_{1/2}$ = 75,690 yrs) is produced in the ocean by the radioactive decay of dissolved $^{234}$U and removed from the water column by scavenging onto sinking particles (Bacon and Anderson, 1982). Its water column distribution is the result of scavenging, circulation and in-growth (Henderson *et al.*, 1999; Scholten *et al.*, 1995). $^{232}$Th ($t_{1/2}$ = 1.4 x $10^{10}$ yrs) in seawater is supplied by lithogenic materials (Santschi *et al.*, 2006). Thorium isotopes are widely used tracers for particle fluxes and water mass advection (Coppola *et al.*, 2006; Roy-Barman *et al.*, 2002).

A recent study shows the importance of hydrothermal activity in Th removal in the South East Pacific (Pavia *et al.*, 2017). Hydrothermal plumes are sources of many trace elements, e.g. Fe and Mn (Klinkhammer *et al.*, 1977; Resing *et al.*, 2015; Saito *et al.*, 2013) and sinks for others,

including Th, due to scavenging onto particles or mineral co-precipitation (German *et al.*, 2002; German *et al.*, 1991). Hydrothermal particulate Fe scavenges $^{230}$Th (Hayes *et al.*, 2015). Hydrothermal plumes can travel over large distances (Fitzsimmons *et al.*, 2014) and can cause $^{230}$Th deficits even several thousand kilometers off axis (Pavia *et al.*, 2017).

The ultra-slow spreading Gakkel Ridge (Schlindwein, 2012) separates the Nansen- and the Amundsen Basins. Hydrothermal vents release trace metals (Edmonds *et al.*, 2003) constantly (Baker *et al.*, 2004). Additionally, sporadic explosive eruptions occur (Sohn *et al.*, 2008); the biggest known such event was in 1999 at the 85°E volcanic complex (Schlindwein, 2012) and continued as earthquake swarms until 2001 (Schlindwein and Riedel, 2010). Eruptive phases are rare but can last over decades (Schmid *et al.*, 2017). Deep water circulation disperses hydrothermal plumes. Deep waters in the Nansen Basin flow cyclonically while the general circulation direction in the Amundsen Basin is westwards (Fig. 3) (Rudels, 2009). The only deep water pathway to the Atlantic Ocean is through Fram Strait, which has a less than 2500 m sill depth.

Deep water in the central Nansen Basin has been reported to have lower particulate and higher dissolved $^{230}$Th concentrations than over the slope region (Cochran *et al.*, 1995). Residence times of $^{230}$Th were reported to be 18-19 years in the central Nansen Basin and 10-12 years on the Barents Sea slope (Scholten *et al.*, 1995). Almost 90% of the in-situ produced $^{230}$Th is estimated to be removed within the Arctic by scavenging (Moran *et al.*, 2005).

We present dissolved, particulate and total $^{230}$Th and $^{232}$Th results, as well as particulate $^{234}$Th data, from expedition ARKXXIX/3 (GEOTRACES section GN04) conducted in 2015 and dissolved and total $^{230}$Th data from expedition ARKXXII/2 (GIPY11) in 2007 and compare our results with those from 1991 (Scholten *et al.*, 1995). We further investigate whether hydrothermal activity at the Gakkel Ridge leads to similar observations as in the Pacific, and provide a new interpretation of how changes in this activity may affect trace element distributions in the Arctic Ocean. The first $^{230}$Th time series allows us to assess the variability of hydrothermal scavenging over time.

## 2 Materials and Methods

### 2.1 Sampling and Analysis of Th in Samples collected in 2007

Dissolved samples were filtered directly from the 24 L CTD-Niskin® bottles into cubitainers (LDPE) using 0.45 µm pore size Acropaks®. Samples were collected in volumes of 1 L, 2 L, and 10 L and acidified with concentrated ultraclean $HNO_3$. Seawater for the analysis of total $^{230}$Th

was sampled without filtration. The analyses were done at the University of Minnesota, Minneapolis, following methods described by Shen *et al.* (2003). The concentrations were measured using Inductively Coupled Plasma Mass Spectrometry (ICP-MS, Thermo Finnigan, Neptune) equipped with an secondary electron multiplier (SEM) and a Retarding Potential Quadrupole (RPQ) energy filter.

### 2.2. Sampling and Analysis of Th in Samples collected in 2015

Analysis of $^{230}$Th and $^{232}$Th were performed in clean laboratories of the Alfred-Wegener-Institute (AWI), following GEOTRACES methods (Anderson *et al.*, 2012). Water samples were filtered directly from the 24 L CTD-Niskin® bottles into cubitainers (LDPE) using 0.45 µm pore size Acropaks®. Seawater was sampled in volumes of 10 L (>2000 m) and 20 L (<2000 m), according to the expected concentrations (Nozaki *et al.*, 1981).

Seawater samples were spiked with $^{229}$Th and $^{236}$U to prepare the isotope dilution analyses by ICP-MS. Spikes were calibrated against the reference standard material UREM11, a material in state of radioactive equilibrium (Hansen and Ring, 1983).

Particles were sampled using in-situ pumps (McLane and Challenger Oceanic). 208 L to 772 L seawater were pumped through a 142 mm ⌀, 0.45 µm pore size Supor® (polyether sulfone) filter (Anderson *et al.*, 2012). Filters were cut aboard for subsamples under a laminar flow hood on a cutting board using tweezers and scalpels. 5/6 of the filters were used for Thorium and $^{231}$Pa (not shown in this study) analysis. A subsample (23mm ⌀) was dried, placed onto plastic mounts, covered with Mylar and aluminum foil and directly measured by beta decay counting of $^{234}$Th ($t_{1/2}$ = 24.1 days) for at least 12 h. Background measurements were performed six months later.

Filters were leached following the procedure described by Gdaniec *et al.* (2017). Filters were cut into pieces using ceramic scissors and placed into Teflon® beakers and then leached in 25 – 30 mL of 3 M HCl in ultrasonic baths). Samples were spiked with $^{233}$Pa, $^{229}$Th and $^{236}$U before leaching. After leaching, the sample solution was evaporated to less than 1 mL. Organic substances were dissolved by adding 8 M $HNO_3$ and $H_2O_2$ to the samples. Any remaining particles were separated by centrifugation and dissolved in concentrated HF. The two solutions were mixed and passed through anionic exchange columns following the protocol described in (Anderson *et al.*, 2012). Measurements were performed using an ICP-MS (Thermo Scientific™ ELEMENT-2™) equipped with an Apex-Q (Elemental Scientific®).

## 3 Results

$^{230}$Th results are unsupported excess $^{230}$Th ($^{230}Th_{xs}$); for simplification, here $^{230}$Th refers to $^{230}Th_{xs}$. Corrections were done following Hayes *et al.* (2015).

### 3.1 Dissolved Th Concentrations

Concentrations of dissolved $^{230}$Th are listed in Table A1. Both 2015 Nansen Basin profiles at stations 50 and 58 show a linear increase down to 2000 m, followed by a sharp decrease below this depth (Fig. 1A). Station 68/69 (2015) from the Gakkel Ridge shows a similar feature; high concentrations down to 1500 m followed by a sharp decrease (Fig. 1B). In 2015, dissolved $^{230}$Th concentrations from the Amundsen Basin (station 81 and 117) increased linearly (Fig. 1C) over the entire water column. Results from the Nansen Basin at station 260 (2007) show a similar profile compared to 2015, without a decrease below 2000 m. Concentrations from three stations in the Makarov Basin in 2015 (shown as a scatter plot against dissolved iron (DFe) in Fig. 2A) increased with depth and were much higher than in the Eurasian Basin (Fig 2A).

### 3.2 Particulate and Total Th Concentrations

Particulate $^{230}$Th concentrations from 2015 are only available for station 50 (Fig. 1D). At this station, up to 50% (3000 m) of total $^{230}$Th was particulate. The profile shows the highest values in the deep water (> 2000 m), reaching up to 6.5 fg/kg. Particulate $^{234}$Th from 2015 (station 50) is shown as the relative amount of particulate $^{234}$Th (Fig. 1F), calculated from $^{238}$U activities, assuming equilibrium of $^{234}$Th with total $^{238}$U in deep water (Owens *et al.*, 2011). Between 2600 m and 3500 m the particulate fraction is higher than above.

Total $^{230}$Th concentrations (dissolved + particulate) decreased noticeably with depth in the Nansen Basin below 2000 m in 2015 (Fig. 1E). Station 260 (2007) shows a similar profile to 2015, without the decrease below 2000 m. Total $^{232}$Th at station 50 (2015) is lower and relatively constant below 2000 m towards the ocean bottom (Fig. 1G).

### 3.3 Changes in $^{230}$Th Distributions Between 1991, 2007 and 2015

We compare data from 1991 (Scholten *et al.*, 1995) with our 2007 and 2015 data (Fig. 1A). Dissolved $^{230}$Th concentrations in the Nansen Basin are generally lower in 2015 (station 50, 58) compared to 1991 and 2007. Only at 2000 m depth at station 50 are dissolved $^{230}$Th concentrations higher compared to samples from 1991 and 2007. The decrease in dissolved $^{230}$Th concentrations in 2015 compared to 1991 and 2007 is most prominent below 2000 m (Fig. 1A).

Particulate $^{230}$Th concentrations at station 50 (2015) were similar to those from station 239 (1991) (Scholten *et al.*, 1995) (Fig. 1D). Data from 2015 only exceed the 1991 data in the

deepest samples (>3000 m). Changes in total $^{230}$Th in the Nansen Basin reveal almost the same pattern as dissolved $^{230}$Th: above 2000 m values observed in 2007 and 2015 are similar to or lower than those from 1991. Values below 2000 m from 2007 were in the range of the 1991 values. Values in 2015 were much lower (Fig. 1E).

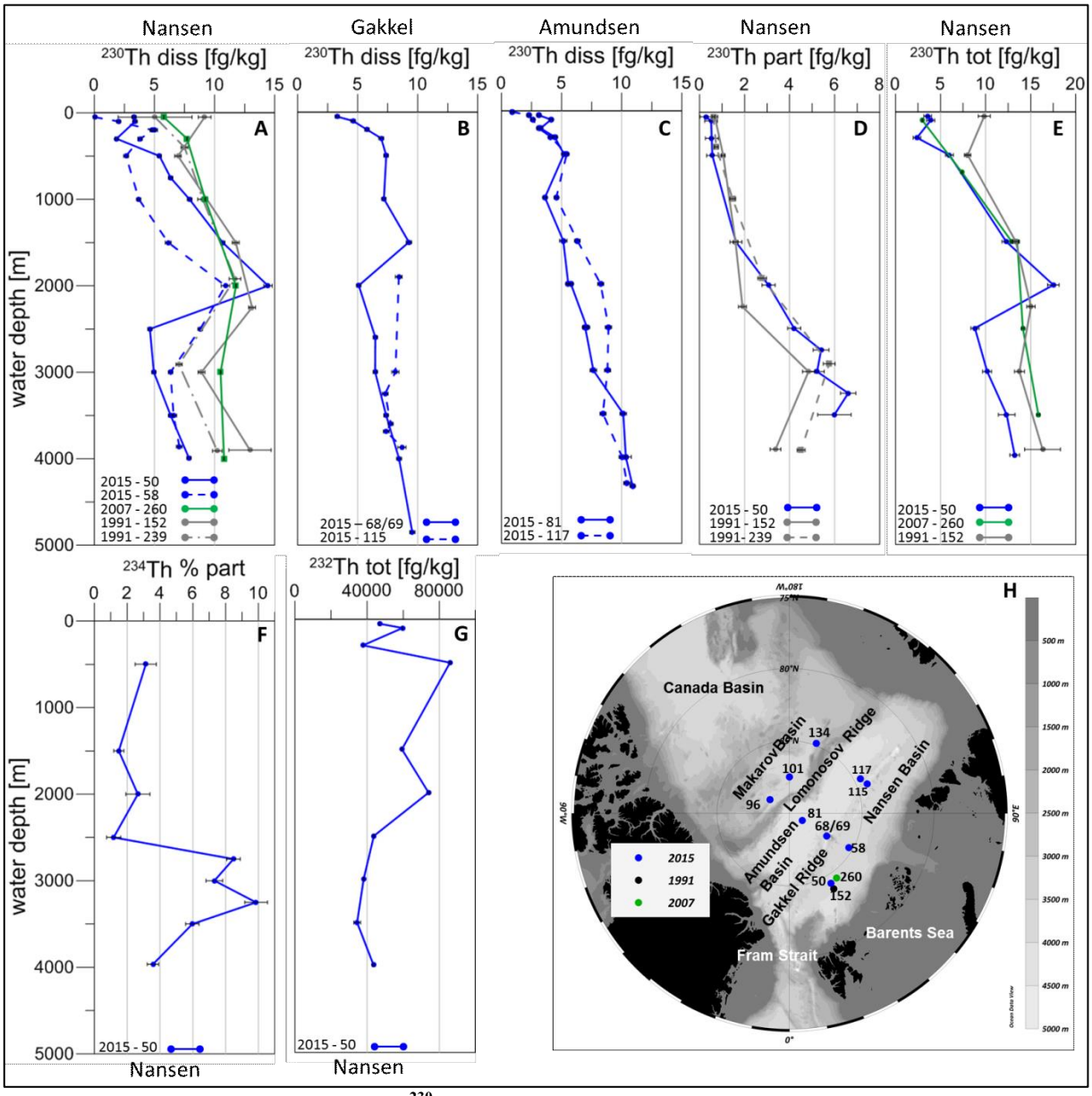


**Figure 6: (A) Nansen Basin dissolved $^{230}$Th concentrations from 1991, 2007 and 2015. (B) Gakkel Ridge dissolved $^{230}$Th data from 2015. (C) Amundsen Basin dissolved $^{230}$Th data from 2015. (D) Nansen Basin particulate $^{230}$Th data from 1991 and 2015. (E) Total $^{230}$Th data from 1991, 2007 and 2015. (F) Nansen Basin particulate $^{234}$Th as a percentage of total $^{234}$Th. (G) Total $^{232}$Th data from 2015 (station 50). (H) Map of the location of the profiles shown in figures 1A-G ; 1991 data are from Scholten *et al.* (1995).**

## 4 Discussion

### 4.1 Possible Reasons for Temporal Changes

Total $^{230}$Th in the Nansen Basin below 2000 m decreased significantly after 2007 (Fig. 1E). Advection could cause this decrease. We rule out advection from the Amundsen Basin as the reason, because dissolved $^{230}$Th concentrations below 2000 m in the Amundsen Basin are higher than at station 50 in the Nansen Basin. Moreover, deep waters in the Nansen Basin have lower CFC-11 concentrations than in the Amundsen Basin (Smethie, 2017). We exclude enhanced biological productivity because no significantly elevated net community production was found in the central Nansen Basin in 2011 (Ulfsbo *et al.*, 2014). Scavenging removal induced by surface generated particles would evoke removal over the whole water column. We only observe depletion below 2000 m.

Alternative particle sources are the Barents Sea shelf and slope. Sea ice formation in the Barents Sea produces dense waters (Rudels *et al.*, 2000) that mix with the boundary current, collecting particles from slope sediments (Moran and Moore, 1991; Rudels *et al.*, 2000). CFC-11 data shows no evidence for shelf water cascading at station 50, in fact values were even slightly lower compared to respective depths of surrounding stations (Smethie, 2017). We also do not observe an enhancement in the fraction shelf/slope waters as indicated by radium isotopes. At 3000 m, the $^{228}$Ra/$^{226}$Ra activity ratio at station 50 was 0.017 ± 0.004 (Rutgers van der Loeff *et al.*, 2018) and similar to prior measurements by Rutgers van der Loeff *et al.* (1995).

At station 50, the relative amount of particulate $^{234}$Th and $^{230}$Th below 2000 m was higher than above (Fig. 1D, F) indicating relatively high particle load at depth. Scholten *et al.* (1995) already reported elevated particulate $^{230}$Th, interpreted, together with a slight decrease in dissolved $^{230}$Th, as a consequence of periodically occurring nepheloid layers. This change did not affect total $^{230}$Th (Scholten *et al.*, 1995). In our study, a sudden increase in particle load will affect a shift of $^{230}$Th distribution on the time scale set by its scavenging coefficient, but for $^{234}$Th the time scale is controlled by the time scale of $^{234}$Th decay. The particle load at the time of sampling will be reflected rather by the particulate $^{234}$Th profile. These are signals on the time scale of $^{234}$Th decay, very ephemeral in comparison with the distribution of $^{230}$Th which is controlled by the cumulative scavenging effect of particles during the years preceding sampling. The larger particulate/dissolved ratio of $^{230}$Th compared to $^{234}$Th shows that $^{230}$Th adsorption occurs on a much longer time scale. The difference in depth distribution therefore illustrates the variability of particle loads. We conclude that a lateral supply of suspended particles at depth

does play a role in Th scavenging in the Nansen Basin but we see no evidence for an increase in this process.

Dissolved $^{230}$Th concentrations in the Makarov Basin are much higher than in the Nansen Basin, which implies a low scavenging regime in the Makarov Basin due to low particle inputs in addition to long water mass residence time (Scholten *et al.*, 1995). In 2007, Klunder *et al.* (2012) observed that dissolved iron (DFe) was lower in the Makarov- than in the Eurasian Basin and explained this by the absence of Fe sources that affect the Nansen Basin. High concentrations of DFe coincide with low concentrations of dissolved $^{230}$Th (Figure 2A), pointing at different scavenging regimes in the Eurasian- and Makarov Basin. The higher inputs of DFe in the Eurasian Basin enhance Fe oxy-hydroxide production and subsequent scavenging of particle reactive elements. We cannot conclude that the two scavenging regimes are only due to the presence or absence of hydrothermal vents, but we argue that the difference is controlled by DFe inputs. Therefore any additional Fe input would change the scavenging situation.

Continuous hydrothermal venting at the Gakkel Ridge (Baker *et al.*, 2004; Edmonds *et al.*, 2003; Michael *et al.*, 2003) is reflected by a small DFe containing hydrothermal plume at Station 68/69 (Gakkel Ridge) in 2015 in the immediate vicinity of a known vent (Rijkenberg *et al.*, 2018). Hence we assume that continuous venting is part of the background steady state situation as observed in 1991. We interpret the decrease at depth in $^{230}$Th at Station 68/69 as a consequence of scavenging by this steady venting. This decrease fits to observations from the East Pacific Rise (Pavia *et al.*, 2017). Since DFe was much higher in 2007 and dispersed over a larger area than in 2015 we conclude that the 2007 plume must have had another source than permanent venting and we hypothesize that it was caused by explosive volcanic eruptions at the Gakkel Ridge (Sohn *et al.*, 2008).

$^{230}$Th decreased below 2000 m at station 50, consistent with the plume depth from the eruptions in 2001 (Baker *et al.*, 2004; Stranne *et al.*, 2010). These eruptions release large amounts of material (Sohn *et al.*, 2008) and can cause “mega plumes” (Cann and Strens, 1989; Clague *et al.*, 2009). Hence explosive eruptions may overprint the steady state situation.

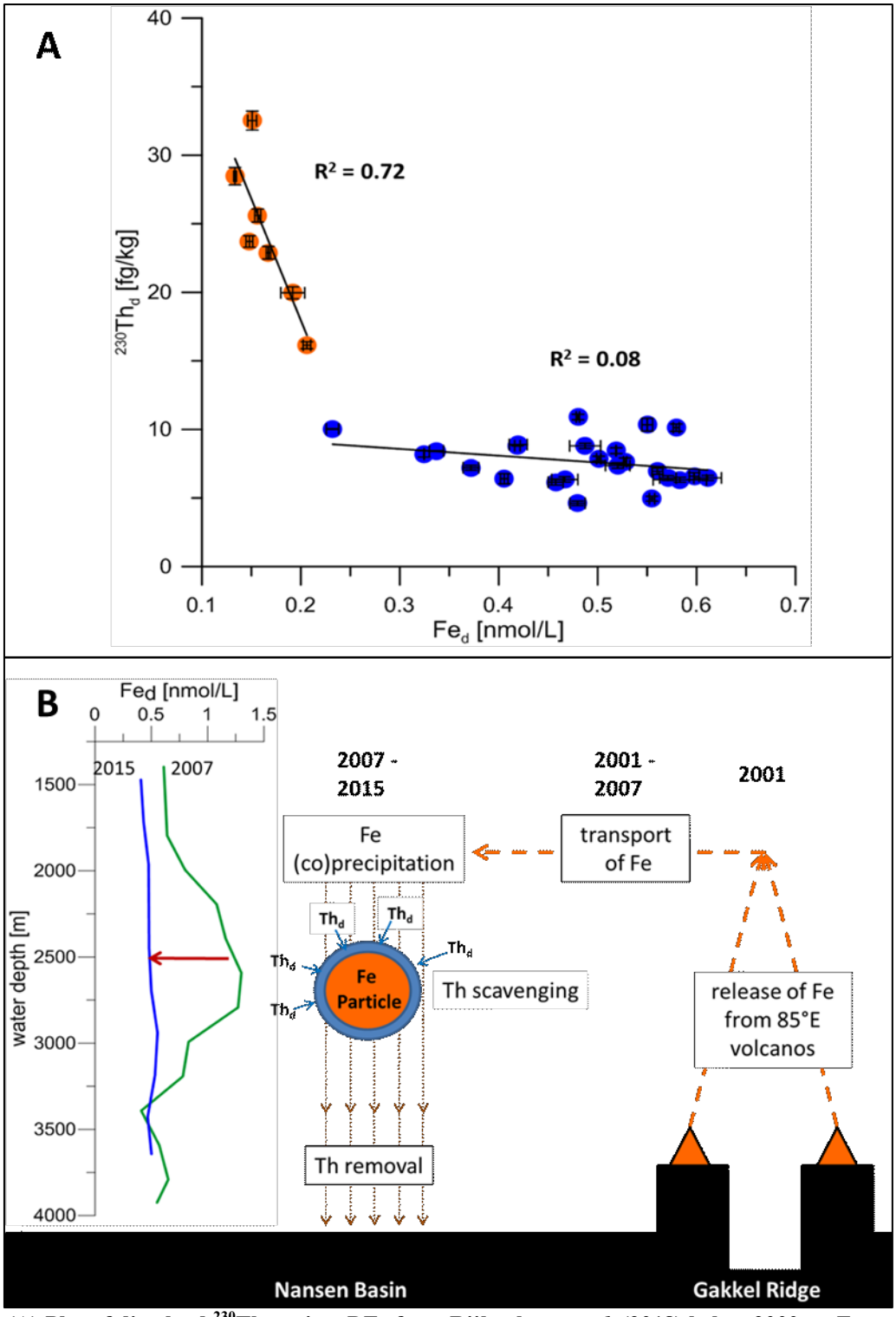


**Figure 7: (A) Plot of dissolved $^{230}$Th against DFe from Rijkenberg *et al.* (2018) below 2000 m. Eurasian Basin is blue and Makarov Basin is orange. Quality of relationships is given $R^2$ values. (B) Conceptual model of hydrothermal removal process: Fe is released by the vents (Edmonds *et al.*, 2003) and stabilized as dissolved or dissolved and micro particles, which allows it to circulate around the Nansen Basin. Later, oxidation forms Fe oxy-hydroxide-particles or Fe reacts with particles being there, which scavenge and remove Th. (Left) DFe from station 50 (2015, blue) and 260 (2007, green) (Klunder *et al.*, 2012).**

### 4.2 Hypothesis of Transient Scavenging by Eruptional Hydrothermal Fe

Elevated DFe concentrations at discrete depth horizons in the Eurasian Basin in 2007 with highest concentrations at the Gakkel Ridge and in the south western Nansen Basin in 2000-3500 m were described as a hydrothermal plume from continuous venting (Klunder *et al.*, 2012; Middag *et al.*, 2011). Based on our $^{230}$Th time series and new DFe from 2015 we interpret the high DFe data from 2007 as a plume released by huge eruptions. That means that after dispersal of the eruptive plume the scavenging regime in the Nansen Basin was no longer in a steady state. After 2007 until 2015, when only much smaller Fe peaks were observed and $^{230}$Th decreased below 2000 m, a scavenging event must have taken place.

We hypothesize that formation of Fe oxy-hydroxides by e.g. precipitation or co-precipitation caused by the Fe input increased particle concentration and changed their composition. Therefore we think that DFe removal triggered $^{230}$Th scavenging. Between 2007 and 2015 scavenging of $^{230}$Th occurred and resulted in DFe and $^{230}$Th removal by 2015. Figure 2B shows a conceptual model about this process.

The negative imprint of removed $^{230}$Th persists for many years, as production from $^{234}$U and supply from above 2000 m is only 2.34 fg/kg in 4 years (half the time between 2007 and 2015), following the approach of Pavia *et al.* (2017), and using the difference in $^{230}$Th flux into and out of the plume (2000-3990 m) and a settling rate from Rutgers van der Loeff *et al.* (2018).

By 2015 the additional eruptive Fe has been removed together with parts of dissolved $^{230}$Th. Particulate $^{230}$Th in 2015 is similar to 1991, while total and dissolved $^{230}$Th are significantly lower now. The extreme DFe peaks vanished but DFe is still higher in the Nansen- than in Makarov Basin. Our Nansen Basin $^{230}$Th profile from 2007 suggests that any additional scavenging caused by removal of eruptive Fe had not yet caused $^{230}$Th removal by 2007.

While measurements of particulate iron (PFe) and other potential scavengers in the plume are not available, we can estimate their contribution to adsorption of $^{230}$Th from analogies to the South East Pacific (GEOTRACES Section GP16), based on the observed distribution of DFe in the Arctic in 2007 and 2015. To this end we establish a PFe/DFe ratio within and outside the plume in the Pacific and apply this to the Arctic. With this estimate of PFe in the Arctic, we use published estimates of distribution coefficients for Th in the presence of natural $Fe(OH)_3$ to determine the possible contribution of PFe to $^{230}$Th scavenging. DFe data from the Arctic are quite comparable to GP 16 in the distant plume: For 2007, Klunder *et al.* (2012) report ~1.25 nmol/L, similar to the Pacific plume (Fitzsimmons *et al.*, 2014). For 2015, 0.5 nmol/L is reported, similar to background concentration at the depth of the plume at GP16. PFe/DFe ratios

at GP16 range from unity to three, both at the distant plume sites and for the background below 2500 m (Fitzsimmons *et al.*, 2014; Lam *et al.*, 2018). This results in an estimated PFe concentration in the deep Nansen Basin of 1.25-3.75 nM (2007) and 0.5-1.5 nM (2015) corresponding to Fe(OH)3 concentrations of 134-402 ng/L PFe for 1.25 nM DFe (2007), or 53.5-160.5 ng/L PFe for 0.5 nM DFe (2015). We now apply the Kd-value of $^{230}$Th for $Fe(OH)_3$ from Hayes *et al.* (2015) of $32.8*10^7$, and learn that 4.4%-13.2% of $^{230}$Th in 2007 (1.75%-5.25% in 2015) would be expected to be found on particles in the Arctic, solely due to PFe.

In 2007, about 25% of $^{230}$Th is particulate (based on the difference of total and dissolved $^{230}$Th from alternating depths), which means that the above estimate (up to 13.2% of $^{230}$Th on the $Fe(OH)_3$ phase) explains up to half of particulate $^{230}$Th. In 2015, the high fraction of particulate Th isotopes, up to 50% particulate $^{230}$Th at the plume depth, indicates the presence of a suspended particulate phase with either high mass concentrations or with a very high $K_d$. The high percentage particulate $^{230}$Th cannot be explained by $Fe(OH)_3$ scavenging using the analogy to GP16. In this year, hydrothermal $Fe(OH)_3$ can only explain a small fraction of $^{230}$Th removal and the precise mechanisms which have led to the situation observed in 2015 remain unclear and require further investigation of other potential scavengers, e.g. $MnO_2$.

### 4.3 Plume Dispersal

Klunder *et al.* (2012) reported a vent at 37°E or a plume from probably 85°E as a possible plume source. Klunder *et al.* (2012) and Middag *et al.* (2011) explained the horizontal dispersion of the plume as a combination of eddy diffusion and scavenging removal following the 1-dimensional first-order scavenging model of Weiss (1977). Their best fit was achieved using 5-15 years scavenging residence time for Fe (Klunder *et al.*, 2012) and 0.4-2 years for Mn (Middag *et al.*, 2011) on basis of the horizontal eddy diffusion coefficient $K_h = 5 \times 10^6$ $cm^2s^{-1}$ (Weiss, 1977). They explained the much longer residence time of Fe compared to Mn by Fe complexation with organic ligands (Thuróczy *et al.*, 2011). Their models show that the basin wide dispersal could be due to horizontal diffusion from a single source over many years, although deep water circulation and multiple plume sources (Baker *et al.*, 2004; Edmonds *et al.*, 2003) complicate their calculations. They assumed a steady state distribution and based their calculations on the model of Weiss (1977), developed to describe the Mn field around a constant vent. Our new $^{230}$Th data are in conflict with a scavenging process at steady state.

### 4.4 Plume Dispersal by Deep Water Circulation

Until 2015, the eruptive plume affected water masses must have spread over larger areas of the Nansen Basin by eddy diffusion and (re)circulation within the basin. We interpret our 2015 data from station 50 and 58 as fully affected by the plume. Figure 2B shows a theoretical concept of how plume intensity and subsequent scavenging can differ between Amundsen- and Nansen Basins due to circulation. Fe from eruptions in 2001 was dispersed, by the deep water circulation (Fig. 3). There might be recirculation (dashed white arrows in Fig. 3) within the Nansen Basin that retains hydrothermally influenced water masses in this basin (yellow dashed oval in Fig. 3). Plume signals in the Amundsen Basin in 2007 could be due to eddy diffusion, smaller plume branches, or both, and could have given rise to some hydrothermal scavenging. But the major part of the plume in the Amundsen Basin is expected to be transported out of the basin towards Fram Strait (Fig. 3). Therefore $^{230}$Th profiles from the Amundsen Basin do not represent hydrothermal scavenging as those from the Nansen Basin (Fig. 1B).

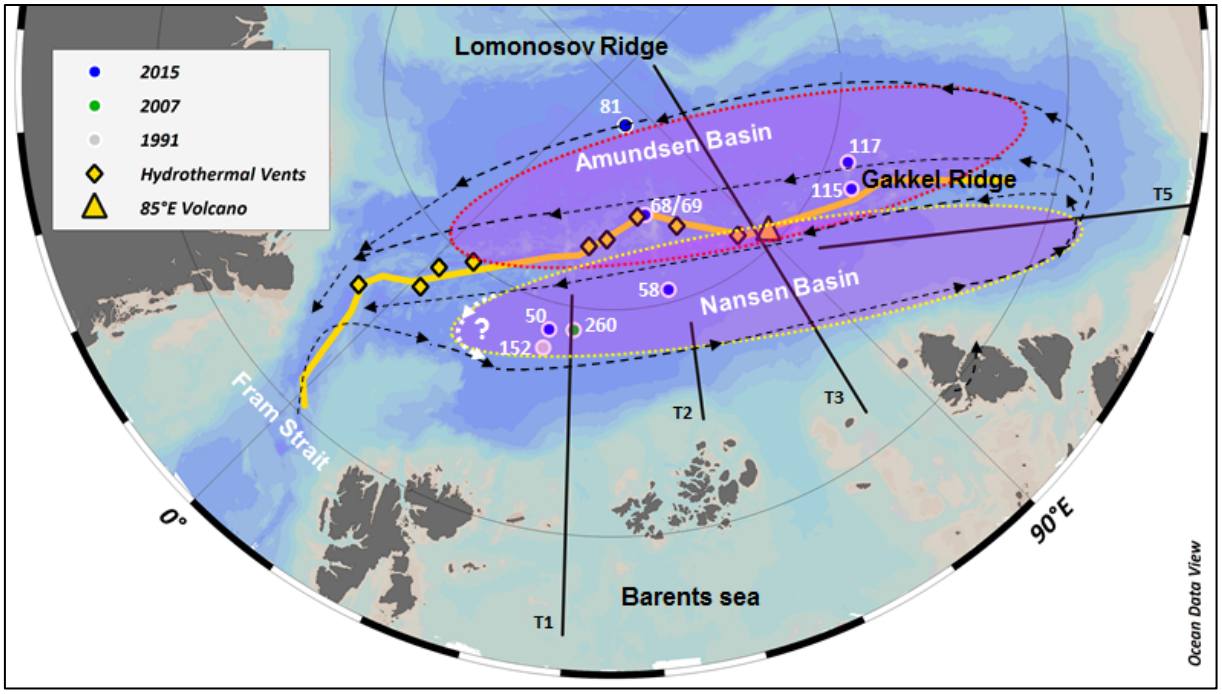


**Figure 3: Model of plume dispersal and Eurasian Basin deep water circulation (black dashed lines (Rudels, 2009)) including potential recirculation (white dashed line). Locations of stations from 2015, 2007 and 1991 are indicated with colored dots (see legend). Solid black lines are transects where in 2007 elevated Fe concentrations were observed (Klunder *et al.*, 2012). Two plume circulation pathways are presented: the yellow dashed line represents a plume circulation confined to the Nansen Basin, and the red dashed line shows a plume dispersal to the Amundsen Basin where the plume is removed faster by circulation. Map was created using Ocean Data View (Schlitzer, 2016).**

## 5 Conclusions

We provide evidence in support of hydrothermal activity as a potential trigger mechanism for scavenging of particle reactive elements in the Nansen Basin. Specifically, $^{230}$Th activities below 2000 m have changed between 2007 and 2015 as a result of a scavenging event, interpreted as hydrothermally induced. The $^{230}$Th time series suggests that Th scavenging in the Nansen Basin is not in steady state following submarine volcanic eruptions. The mechanism explaining the dispersal of the hydrothermal plume throughout the Nansen Basin will require further investigation, as well as the precise mechanism of eruptive Fe cycling leading to the 2015 situation. This proposed role of episodic hydrothermal input provides new insights on the nature of hydrothermal scavenging in the Arctic and how other trace elements may be removed from the Arctic. Submarine volcanic eruptions may also influence the distribution of other trace elements in the Nansen Basin, perhaps more than in other oceans, due to the small size and enclosed nature of the Eurasian Basins. The concurrence of geochemical and geophysical data may also improve interpretations of other trace element distributions from the Eurasian Arctic Ocean. Time variable signals, as seen in $^{230}$Th and DFe, complicate the interpretation of tracer data in the Arctic as being at steady state and show the value of repeated GEOTRACES occupations in understanding variability of scavenging processes in the deep ocean.

## Acknowledgements

We thank the Captain and crew of RV Polarstern for their help during expeditions ARKXXIX/3 and ARKXXII/2. We would like to thank Ronja Paffrath for help on board as well as Loes Gerringa, Vera Schlindwein and Ursula Schauer for helpful discussions. Ingrid Stimac is thanked for invaluable technical support and help in the laboratory. We thank Matthieu Roy-Barman for providing 5 In-situ-pumps in 2015. This work was partially supported by a U.S. NSF grant (OCE 143886) to RLE**.** Finally we thank two anonymous reviewers for very helpful and constructive comments, which helped to improve the manuscript.

**References**

Anderson, R.F., Fleisher, M.Q., Robinson, L., Edwards, R.L., Hoff, J.A., Moran, S.B., Rutgers van der Loeff, M.M., Thomas, A.L., Roy-Barman, M., Francois, R., 2012. GEOTRACES intercalibration of $^{230}$Th, $^{232}$Th, $^{231}$Pa, and prospects for $^{10}$Be. Limnol. Oceanogr.: Methods 10, 179-213.

Bacon, M.P., Anderson, R.F., 1982. Distribution of Thorium Isotopes Between Dissolved and Particulate Forms in The Deep Sea. Journal of Geophysical Research 87, 2045-2056.

Baker, E.T., Edmonds, H.N., Michael, P.J., Bach, W., Dick, H.J.B., Snow, J.E., Walker, S.L., Banerjee, N.R., Langmuir, C.H., 2004. Hydrothermal venting in magma deserts: The ultraslow-spreading Gakkel and Southwest Indian Ridges. Geochemistry, Geophysics, Geosystems 5 (8).

Beszczynska-Moeller, A., Woodgate, R., Lee, C., Melling, H., Karcher, M., 2011. A Synthesis of Exchanges Through the Main Oceanic Gateways to the Arctic Ocean. Oceanography (Washington D.C.) 24.

Cann, J.R., Strens, M.R., 1989. Modeling periodic megaplume emission by black smoker systems. Journal of Geophysical Research: Solid Earth 94 (B9), 12227-12237.

Charette, M.A., Kipp, L.E., Jensen, L.T., Dabrowski, J.S., Whitmore, L.M., Fitzsimmons, J.N., Williford, T., Ulfsbo, A., Jones, E., Bundy, R.M., Vivancos, S.M., Pahnke, K., John, S.G., Xiang, Y., Hatta, M., Petrova, M.V., Heimbürger-Boavida, L.-E., Bauch, D., Newton, R., Pasqualini, A., Agather, A.M., Amon, R.M.W., Anderson, R.F., Andersson, P.S., Benner, R., Bowman, K.L., Edwards, R.L., Gdaniec, S., Gerringa, L.J.A., González, A.G., Granskog, M., Haley, B., Hammerschmidt, C.R., Hansell, D.A., Henderson, P.B., Kadko, D.C., Kaiser, K., Laan, P., Lam, P.J., Lamborg, C.H., Levier, M., Li, X., Margolin, A.R., Measures, C., Middag, R., Millero, F.J., Moore, W.S., Paffrath, R., Planquette, H., Rabe, B., Reader, H., Rember, R., Rijkenberg, M.J.A., Roy-Barman, M., Rutgers van der Loeff, M., Saito, M., Schauer, U., Schlosser, P., Sherrell, R.M., Shiller, A.M., Slagter, H., Sonke, J.E., Stedmon, C., Woosley, R.J., Valk, O., van Ooijen, J., Zhang, R., 2020. The Transpolar Drift as a Source of Riverine and Shelf-Derived Trace Elements to the Central Arctic Ocean. Journal of Geophysical Research: Oceans 125 (5), e2019JC015920.

Clague, D.A., Paduan, J.B., Davis, A.S., 2009. Widespread strombolian eruptions of mid-ocean ridge basalt. Journal of Volcanology and Geothermal Research 180 (2), 171-188.

Cochran, K., J., H.D., Livingston, H.D., Buesseler, K.O., Key, R.M., 1995. Natural and anthropogenic radionuclide distributions in the Nansen Basin, Artic Ocean: Scavenging rates and circulation timescales. Deep-Sea Research II 42, 1495-1517.

Coppola, L., Roy-Barman, M., Mulsow, S., Povinec, P., Jeandel, C., 2006. Thorium isotopes as tracers of particles dynamics and deep water circulation in the Indian sector of the Southern Ocean (ANTARES IV). Marine Chemistry 100, 299-313.

Edmonds, H.N., Michael, P.J., Baker, E.T., Connelly, D.P., Snow, J.E., Langmuir, C.H., Dick, H.J.B., Muhe, R., German, C.R., Graham, D.W., 2003. Discovery of abundant hydrothermal venting on the ultraslow-spreading Gakkel ridge in the Arctic Ocean. Nature 421 (6920), 252-256.

Fitzsimmons, J.N., Boyle, E.A., Jenkins, W.J., 2014. Distal transport of dissolved hydrothermal iron in the deep South Pacific Ocean. Proceedings of the National Academy of Sciences 111 (47), 16654-16661.

Gdaniec, S., Roy-Barman, M., Foliot, L., Thil, F., Dapoigny, A., Burckel, P., Garcia-Orellana, J., Masqué, P., Mörth, C.-M., Andersson, P.S., 2017. Thorium and protactinium isotopes as tracers of marine particle fluxes and deep water circulation in the Mediterranean Sea. Marine Chemistry.

German, C.R., Colley, S., Palmer, M.R., Khripounoff, A., Klinkhammer, G.P., 2002. Hydrothermal plume-particle fluxes at 13°N on the East Pacific Rise. Deep Sea Research Part I: Oceanographic Research Papers 49 (11), 1921-1940.

German, C.R., Fleer, A.P., Bacon, M.P., M., E.J., 1991. Hydrothermal scavenging at the Mid-Atlantic Ridge: radionuclide distributions. Earth and Planetary Science Letters 105, 170-181.

Grenier, M., François, R., Soon, M., Rutgers van der Loeff, M., Yu, X., Valk, O., Not, C., Moran, S.B., Edwards, R.L., Lu, Y., Lepore, K., Allen, S.E., 2019. Changes in Circulation and Particle Scavenging in the Amerasian Basin of the Arctic Ocean over the Last Three Decades Inferred from the Water Column Distribution of Geochemical Tracers. Journal of Geophysical Research: Oceans 124 (12), 9338-9363.

Hansen, R.G., Ring, E.J., 1983. The preparation and certification of a uranium reference material. Council for Mineral Technology, Randburg, South Africa.

Hayes, C.T., Anderson, R.F., Fleisher, M.Q., Vivancos, S.M., Lam, P.J., Ohnemus, D.C., Huang, K.-F., Robinson, L., Lu, Y., Cheng, H., Edwards, R.L., Moran, S.B., 2015. Intensity of Th and Pa scavenging partitioned by particle chemistry in the North Atlantic Ocean. Marine Chemistry 170, 49-60.

Henderson, G.M., Heinze, C., Anderson, R.F., Winguth, A.M.E., 1999. Global distribution of the $^{230}$Th flux to ocean sediments constrained by GCM modelling. Deep-Sea Research I 46, 1861-1893.

Klinkhammer, G., Bender, M., Weiss, R.F., 1977. Hydrothermal manganese in the Galapagos Rift. Nature 269 (5626), 319-320.

Klunder, M.B., Laan, P., Middag, R., de Baar, H.J.W., Bakker, K., 2012. Dissolved iron in the Arctic Ocean: Important role of hydrothermal sources, shelf input and scavenging removal. Journal of Geophysical Research-Oceans 117 (C4).

Lam, P.J., Lee, J.-M., Heller, M.I., Mehic, S., Xiang, Y., Bates, N.R., 2018. Size-fractionated distributions of suspended particle concentration and major phase composition from the U.S. GEOTRACES Eastern Pacific Zonal Transect (GP16). Marine Chemistry 201, 90-107.

Lerner, P., Marchal, O., Lam, P.J., Gardner, W., Richardson, M.J., Mishonov, A., 2020. A model study of the relative influences of scavenging and circulation on $^{230}$Th and $^{231}$Pa in the western North Atlantic. Deep Sea Research Part I: Oceanographic Research Papers 155, 103159.

Michael, P.J., Langmuir, C.H., Dick, H.J.B., Snow, J.E., Goldstein, S.L., Graham, D.W., Lehnert, K., Kurras, G., Jokat, W., Muhe, R., Edmonds, H.N., 2003. Magmatic and amagmatic seafloor generation at the ultraslow-spreading Gakkel ridge, Arctic Ocean. Nature 423 (6943), 956-961.

Middag, R., de Baar, H.J.W., Laan, P., Klunder, M.B., 2011. Fluvial and hydrothermal input of manganese into the Arctic Ocean. Geochimica et Cosmochimica Acta 75 (9), 2393-2408.

Moran, S.B., Moore, R.M., 1991. The potential source of dissolved aluminum from resuspended sediments to the North Atlantic Deep Water. Geochimica et Cosmochimica Acta 55 (10), 2745-2751.

Moran, S.B., Shen, C.-C., Edwards, R.L., Edmonds, H.N., Scholten, J.C., Smith, J.N., Ku, T.-L., 2005. $^{231}$Pa and $^{230}$Th in surface sediments of the Arctic Ocean: Implications for $^{231}$Pa/$^{230}$Th fractionation, boundary scavenging, and advective export. Earth and Planetary Science Letters 234, 235-248.

Nozaki, Y., Horibe, Y., Tsubota, H., 1981. The water column distributions of thorium isotopes in the western North Pacific. Earth and Planetary Science Letters 54 (2), 203-216.

Owens, S.A., Buesseler, K.O., Sims, K.W.W., 2011. Re-evaluating the $^{238}$U-salinity relationship in seawater: Implications for the $^{238}$U–$^{234}$Th disequilibrium method. Marine Chemistry 127 (1), 31-39.

Pavia, F., Anderson, R., Vivancos, S., Fleisher, M., Lam, P., Lu, Y., Cheng, H., Zhang, P., Lawrence Edwards, R., 2017. Intense hydrothermal scavenging of $^{230}$Th and $^{231}$Pa in the deep Southeast Pacific. Marine Chemistry.

Resing, J.A., Sedwick, P.N., German, C.R., Jenkins, W.J., Moffett, J.W., Sohst, B.M., Tagliabue, A., 2015. Basin-scale transport of hydrothermal dissolved metals across the South Pacific Ocean. Nature 523 (7559), 200-203.

Rijkenberg, M.J.A., Slagter, H.A., Rutgers van der Loeff, M., van Ooijen, J., Gerringa, L.J.A., 2018. Dissolved Fe in the Deep and Upper Arctic Ocean With a Focus on Fe Limitation in the Nansen Basin. Frontiers in Marine Science 5 (88).

Roy-Barman, M., Coppola, L., Souhaut, M., 2002. Thorium isotopes in the western Mediterranean Sea: an insight into the marine particle dynamics. Earth and Planetary Science Letters 196, 161-174.

Rudels, B., 2009. Arctic Ocean Circulation A2 - Steele, John H. Encyclopedia of Ocean Sciences (Second Edition). Academic Press, Oxford, pp. 211-225.

Rudels, B., Muench, R.D., Gunn, J., Schauer, U., Friedrich, H.J., 2000. Evolution of the Arctic Ocean boundary current north of the Siberian shelves. Journal of Marine Systems 25 (1), 77-99.

Rutgers van der Loeff, M.M., Geibert, W., 2008. Chapter 7 U- and Th-Series Nuclides as Tracers of Particle Dynamics, Scavenging and Biogeochemical Cycles in the Oceans. In: Krishnaswami, S., Cochran, J.K. (Eds.), Radioactivity in the Environment. Elsevier, pp. 227-268.

Rutgers van der Loeff, M.M., Key, R.M., Scholten, J., Bauch, D., Michel, A., 1995. $^{228}$Ra as a tracer for shelf water in the Arctic Ocean. Deep-Sea Research II 42, 1533-1553.

Rutgers van der Loeff, M.M., Kipp, L.E., Charette, M.A., Moore, W.S., Black, E., Stimac, I., Charkin, A., Bauch, D., Valk, O., Karcher, M., Krumpen, T., Casacuberta, N., Smethie Jr, W.M., Rember, R., 2018. Radium Isotopes across the Arctic Ocean show Time Scales of Water Mass Ventilation and Increasing Shelf Inputs. Journal of Geophysical Research Oceans.

Saito, M.A., Noble, A.E., Tagliabue, A., Goepfert, T.J., Lamborg, C.H., Jenkins, W.J., 2013. Slow-spreading submarine ridges in the South Atlantic as a significant oceanic iron source. nature geoscience 6, 775-779.

Santschi, P.H., Murray, J.W., Baskaran, M., Benitez-Nelson, C.R., Guo, L.D., Hung, C.-C., Lamborg, C., Moran, S.B., Passow, U., Roy-Barman, M., 2006. Thorium speciation in seawater. Marine Chemistry 100, 250-268.

Schlindwein, V., 2012. Teleseismic earthquake swarms at ultraslow spreading ridges: indicator for dyke intrusions? Geophysical Journal International 190 (1), 442-456.

Schlindwein, V., Riedel, C., 2010. Location and source mechanism of sound signals at Gakkel ridge, Arctic Ocean: Submarine Strombolian activity in the 1999–2001 volcanic episode. Geochemistry, Geophysics, Geosystems 11 (1).

Schlitzer, R., 2016. Ocean Data View. http://odv.awi.de.

Schmid, F., Schlindwein, V., Koulakov, I., Plötz, A., Scholz, J.-R., 2017. Magma plumbing system and seismicity of an active mid-ocean ridge volcano. 7, 42949.

Scholten, J.C., Rutgers van der Loeff, M.M., Michel, A., 1995. Distribution of $^{230}$Th and $^{231}$Pa in the water column in relation to the ventilation of the deep Arctic basins. Deep-Sea Research II 42, 1519-1531.

Shen, C.-C., Cheng, H., Edwards, R.L., Moran, S.B., Edmonds, H.N., Hoff, J.A., Thomas, R.B., 2003. Measurement of Attogram Quantities of $^{231}$Pa in Dissolved and Particulate Fractions of Seawater by Isotope Dilution Thermal Ionization Mass Spectroscopy. analytical chemistry 75 (5), 1075-1079.

Smethie, W.M., Jr., 2017. CFC-11, CFC-12, CFC-113, and SF6 measured on water bottle samples during POLARSTERN cruise PS94 (ARK-XXIX/3) to the Arctic Ocean in 2016. PANGAEA.

Sohn, R.A., Willis, C., Humphris, S., Shank, T.M., Singh, H., Edmonds, H.N., Kunz, C., Hedman, U., Helmke, E., Jakuba, M., Liljebladh, B., Linder, J., Murphy, C., Nakamura, K.-i., Sato, T., Schlindwein, V., Stranne, C., Tausenfreund, M., Upchurch, L., Winsor, P., Jakobsson, M., Soule, A., 2008. Explosive volcanism on the ultraslow-spreading Gakkel ridge, Arctic Ocean. Nature 453 (7199), 1236-1238.

Stranne, C., Sohn, R.A., Liljebladh, B., Nakamura, K.-i., 2010. Analysis and modeling of hydrothermal plume data acquired from the 85°E segment of the Gakkel Ridge. Journal of Geophysical Research: Oceans 115 (C6), n/a-n/a.

Thuróczy, C.E., Gerringa, L.J.A., Klunder, M., Laan, P., Le Guitton, M., de Baar, H.J.W., 2011. Distinct trends in the speciation of iron between the shallow shelf seas and the deep basins of the Arctic Ocean. Journal of Geophysical Research: Oceans 116 (C10).

Ulfsbo, A., Cassar, N., Korhonen, M., van Heuven, S., Hoppema, M., Kattner, G., Anderson, L.G., 2014. Late summer net community production in the central Arctic Ocean using multiple approaches. GLOBAL BIOGEOCHEMICAL CYCLES 28 (10), 1129-1148.

Weiss, R.F., 1977. Hydrothermal manganese in the deep sea: Scavenging residence time and Mn/3He relationships. Earth and Planetary Science Letters 37 (2), 257-262.

# CHAPTER 3: Decrease in $^{230}$Th in the Amundsen Basin since 2007: Far-Field Effect of Increased Scavenging on the Shelf?

**Ole Valk[1], Michiel M. Rutgers van der Loeff[1], Walter Geibert[1], Sandra Gdaniec[2], S. Bradley Moran[3], Kate Lepore[4], Richard Lawrence Edwards[5], Yanbin Lu[6], Viena Puigcorbé[7], Nuria Casacuberta[8,9], Ronja Paffrath[10] William Smethie[11], Matthieu Roy-Barman[12]**

[1]Alfred-Wegener-Institute Helmholtz Centre for Polar and Marine Research, 27570 Bremerhaven, Germany

[2]Stockholm University, Department of Geological Sciences, 106 91, Stockholm, Sweden

[3]College of Fisheries and Ocean Sciences, University of Alaska Fairbanks, Fairbanks, AK 99775, USA

[4]Mount Holyoke College, South Hadley, MA 01075, USA

[5]University of Minnesota, Minneapolis, MN 55455, USA

[6]Nanyang Technological University, 639798, Singapore

[7]Center for Marine Ecosystem Research, School of Science, Edith Cowan University, Joondalup, WA 6027, Australia

[8]Laboratory of Ion Beam Physics, ETH Zurich, 8093 Zurich, Switzerland

[9]Institute of Biogeochemistry and Pollutant Dynamics, Environmental Physics, ETH Zurich, 8092 Zurich, Switzerland

[10]Max Planck Research Group for Marine Isotope Geochemistry, Institute for Chemistry and Biology of the Marine Environment, University of Oldenburg, 26129, Oldenburg, Germany

[11]Lamont-Doherty Earth Observatory, Palisades, NY 10964-8000, USA

[12]Laboratoire des Sciences du Climat et de l'Environnement, LSCE/IPSL, CEA – CNRS – UVSQ, Université Paris-Saclay, 91191 Gif-sur-Yvette, France

Manuscript published in *Ocean Science*, 16, 221–234, 2020. https://doi.org/10.5194/os-16-221-2020

Received: 8 May 2019 – Discussion started: 14 June 2019
Revised: 8 November 2019 – Accepted: 12 December 2019 – Published: 14 February 2020

**Abstract.** This study provides dissolved and particulate $^{230}$Th and $^{232}$Th results as well as particulate $^{234}$Th data collected during expeditions to the central Arctic Ocean on ARK-XXIX/3 (2015) and ARK-XXII/2 (2007) (GEOTRACES sections GN04 and GIPY11, respectively). Constructing a time-series of dissolved $^{230}$Th from 1991 to 2015 enables the identification of processes that control the temporal development of $^{230}$Th distributions in the Amundsen Basin. After 2007, $^{230}$Th concentrations decreased significantly over the entire water column, particularly between 300 m and 1500 m. This decrease is accompanied by a circulation change, evidenced by a concomitant increase in salinity. Potentially increased inflow of water of Atlantic origin with low dissolved $^{230}$Th concentrations leads to the observed depletion in dissolved $^{230}$Th in the central Arctic. Because atmospherically derived tracers (CFC, SF6) do not reveal an increase in ventilation rate, it is suggested that these interior waters have undergone enhanced scavenging of Th during transit from the Fram Strait and the Barents Sea to the central Amundsen Basin. The $^{230}$Th depletion propagates downward in the water column by settling particles and reversible scavenging.

## 1 Introduction

The Arctic Ocean is one of the most rapidly changing parts of the Earth's ocean-atmosphere system as a result of climate change. Underlying the potential anthropogenic changes is a large natural variability of the Arctic. Due to the limited observations in this extreme environment, establishing datasets that allow an assessment of its variability is important. Natural tracers of physical, chemical and biological processes provide an integrated description of the changing state of the system. They are therefore key tools to investigate processes, monitor environmental changes, and provide an observational baseline against which models can be tested.

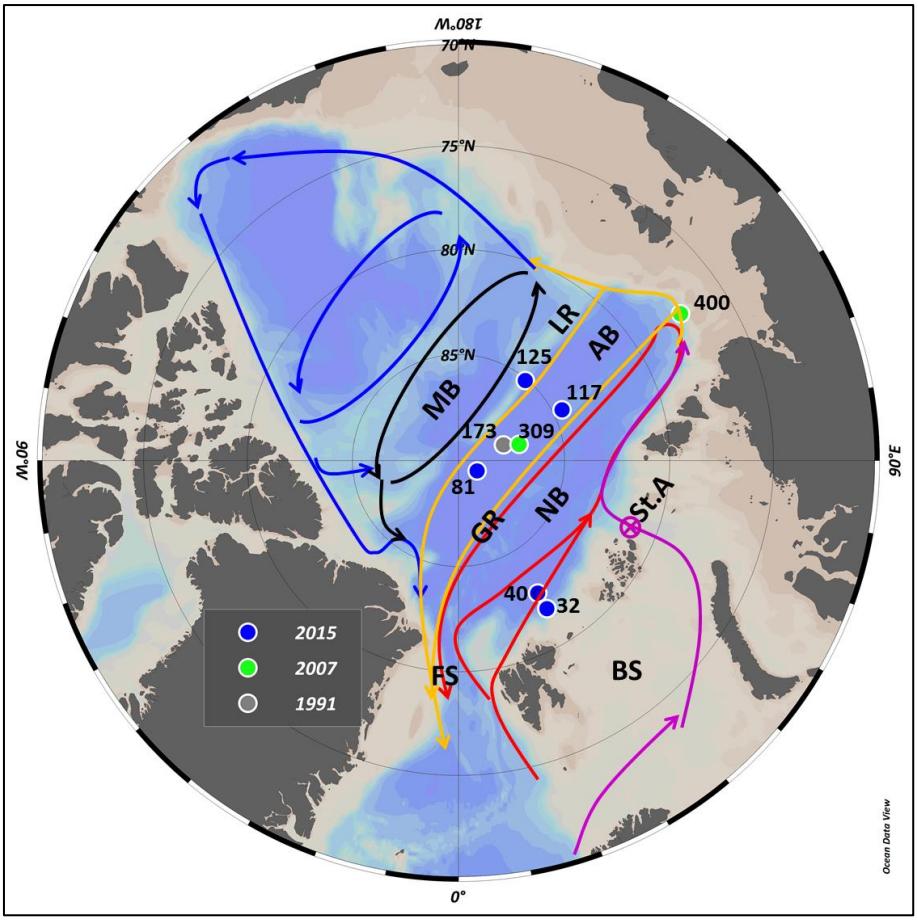


**Figure 8: Map of the Arctic Ocean and station overview. AB = Amundsen Basin, NB = Nansen Basin, GR = Gakkel Ridge, MB = Makarov Basin. BS = Barents Sea, FS = Fram Strait, LR = Lomonosov Ridge, (X) = subduction at St. Anna Trough (St.A) with intermediate water circulation patterns after Rudels (2009). Red is the Atlantic inflow through Fram Strait (FSBW) and return flow through the Nansen Basin; purple is the inflow through the Barents Sea (BSBW). Atlantic layer circulation in the Amundsen Basin (orange), the Makarov Basin (black) and Canada Basin (blue) are indicated as arrows.**

## 1.1 Hydrography and Circulation Patterns of the Central Arctic Ocean

The central Arctic Ocean is divided into the Amerasian Basin and Eurasian Basin by the Lomonosov Ridge (Fig. 1). The Gakkel Ridge separates the Eurasian Basin further into the Nansen Basin and the Amundsen Basin, while the Amerasian Basin is separated into the Makarov and Canada Basin by the Alpha-Mendeleev Ridge.

Water masses of the Arctic Ocean are commonly distinguished as five layers (Rudels, 2009). The uppermost low salinity Polar Mixed Layer (PML) varies in thickness between winter and summer, due to melting and freezing of sea ice. Salinity ranges from 30 to 32.5 (Amerasian Basin) to 32-34 (Eurasian Basin). Below the PML is a 100–250-m-thick halocline in which salinity increases sharply from approximately 32.5 to 34.5. The underlying Atlantic Layer is characterized in salinity and temperature by waters of Atlantic origin and is usually found between 400 m and 700 m water depth. Its salinity is 34.5-35. Intermediate waters down to 1500

m, with a salinity of 34.87-34.92, are still able to exchange over the Lomonosov Ridge. In contrast, deep and bottom waters differ between the Eurasian Basin (salinity: 34.92-34.945) and the Amerasian Basin (salinity: 34.92-34.96) due to the topographic barrier.

Atlantic waters from the Norwegian Atlantic Current enter the Arctic Ocean via the Fram Strait and the Barents Sea. Fram Strait Branch Water (FSBW) is supplied through the West Spitsbergen Current (WSC) (Rudels, 2012) (Fig. 1). Barents Sea Branch Water (BSBW) enters through the Barents Sea and consists of Atlantic water that undergoes strong modifications in Barents- and Kara Seas by cooling down and mixing with continental runoff and meltwater (Rudels *et al.*, 2015). The BSBW enters the Nansen Basin through the Santa Anna Trough, where limited mixing with the FSBW occurs. Once in the polar ocean, surface waters follow wind driven ice motion (Aagaard *et al.*, 1980), whereas deeper Atlantic water branches (FSBW and BSBW) flow cyclonically to the east forming a boundary current along the continental slopes of the Nansen and Amundsen basins.

BSBW (around approx. 1025 m depth, Tanhua, 2009) and FSBW (approx. 425 m) return in the Atlantic and Intermediate water layers along the Lomonosov Ridge towards Fram Strait (Rudels *et al.*, 2013) (Fig. 1) and a second branch crosses the Lomonosov Ridge entering the Canada Basin following the Arctic Ocean Boundary Current (AOBC) (Rudels, 2009).

Deep waters of the Arctic Ocean have similar structure, with a thick intermediate layer stratified in temperature but with salinity almost constant with depth (Rudels, 2009). Yet, the Amerasian Basin deep water is warmer, saltier and less dense than the Eurasian Basin Deep Water (EBDW) (Aagaard, 1981;Worthington, 1953). The deepest exchange of Makarov Basin water, part of the Amerasian Basin, with Eurasian Basin water occurs through a depression of the ridge, called the Intra-Basin with sill depth of approximately 1800 m (Björk *et al.*, 2007; Jones *et al.*, 1995; Björk *et al.*, 2010). Water from the Amundsen Basin flows over the Lomonosov Ridge into the deep Makarov Basin and in the reverse direction (Middag *et al.*, 2009).

Another important component of the Arctic Ocean is the freshwater content, coming from the melting of sea-ice and from river runoff. The fresh water content of the central Arctic Ocean is currently at the highest level since the early 1980s, and is expected to increase in the future (Rabe *et al.*, 2014) which could lead to a stronger stratification of the water column. This process is supported by sea ice decline, as observed in the Beaufort Gyre (Wang *et al.*, 2018). Karcher *et al.* (2012) suggest a reversal in flow direction of Atlantic Water in the Canada Basin at intermediate water depths on basis of $^{129}$I observations and modelling. This could lead to a decoupling of flow regimes in the Canada and Eurasian Basins and reduce exchange times between the two major basins of the Arctic Ocean (Karcher *et al.*, 2012).

### 1.2 Particle Fluxes, Shelf Input and Biological Productivity

Biological productivity in the central Arctic Ocean and related particle fluxes are lower than in other oceans due to the perennial sea ice cover (Clark and Hanson, 1983). This is expected to change in the future when light limitation is relieved by sea ice retreat (Pabi *et al.*, 2008). Arctic sea-ice extent is declining (Serreze *et al.*, 2016) and ice is becoming thinner (Serreze and Stroeve, 2015). Biological productivity may increase and begin earlier in the year, at least in the Pacific part of the Arctic, depending on nutrient supply (Hill *et al.*, 2017). Recent studies show that productivity is still low in the central Arctic Ocean, limited by both light and nutrient availability (Arrigo and van Dijken, 2015). Highest net community production (NCP) is found at the ice edge of the Nansen Basin and over the shelves, while the Amundsen Basin shows the lowest NCP (Ulfsbo *et al.*, 2014). Apart from the possible effect on NCP, the declining sea-ice cover will also enhance ice derived particle fluxes (Arrigo *et al.*, 2008; Boetius *et al.*, 2013). The Arctic Ocean has the largest relative amount of shelves of all World Ocean, approximately 50% of area in total (Jakobsson, 2002). Shelf sediments and large volumes of riverine input add trace metals and carbon among other terrestrial components to Arctic shelf areas, some of which are transported to the central Arctic by the Transpolar Drift (TPD) (Wheeler *et al.*, 1997; Rutgers van der Loeff *et al.*, 2018; Rutgers van der Loeff *et al.*, 1995). On the basis of an increase of $^{228}$Ra supply to the interior Arctic Ocean, Kipp *et al.* (2018) suggested that the supply of shelf derived materials is increasing with a following change in trace metal, nutrient and carbon balances. Thawing permafrost and subsequent increasing coastal erosion (Günther *et al.*, 2013) may increase terrestrial input to the central Arctic Ocean (Schuur *et al.*, 2013; Schuur *et al.*, 2015).

### 1.3 Th as a Tracer of Water Circulation and Particle Fluxes

Thorium isotopes have been extensively used to study and model physical oceanographic processes, such as advection, water mass mixing and particle flux (Bacon and Anderson, 1982; Rutgers van der Loeff and Berger, 1993; Roy-Barman, 2009; Rempfer *et al.*, 2017). In seawater, $^{230}$Th ($t_{1/2}$=75380 yrs) is produced by the radioactive decay of dissolved $^{234}$U. Without lateral transport by currents, the vertical distribution of $^{230}$Th in the water column is controlled by reversible exchange with sinking particles and increases with depth (Bacon and Anderson, 1982; Nozaki *et al.*, 1981). Deviations from a linear increase with depth profile of $^{230}$Th (Bacon and Anderson, 1982) suggest that oceanic currents transport $^{230}$Th away from the production area, or that ventilation, upwelling, or depth-dependent scavenging processes play a role for the $^{230}$Th

distribution in the water column (e.g., Rutgers van der Loeff and Berger, 1993; Moran *et al.* 1995; Roy-Barman, 2009).

$^{232}$Th ($t_{1/2}$=1.405x10$^{10}$ yrs) is known as a tracer for shelf/continental derived signatures (Hsieh *et al.*, 2011), while $^{234}$Th ($t_{1/2}$=24.1 d) serves as a tracer for particle flux (Moran and Smith, 2000).

### 1.3.1 $^{230}$Th in the Arctic Ocean

Several studies have addressed the regional distribution of dissolved $^{230}$Th in the Arctic Ocean in relation to particle fluxes and water mass residence time over the past decades. Yet several key points related to removal processes of dissolved $^{230}$Th are not entirely understood and the sensitivity of dissolved $^{230}$Th to environmental changes is still not explained sufficiently.

Bacon *et al.* (1989) hypothesized that scavenging of reactive elements in the central Arctic Ocean was significantly lower than in other parts of the world to explain the high $^{230}$Th concentrations observed at the Alpha Ridge and the northern Makarov Basin (Bacon *et al.*, 1989). Edmonds *et al.* (1998), later confirmed by Trimble *et al.* (2004), showed that $^{230}$Th activities in the deep southern Canada Basin were much lower, and residence times correspondingly shorter, than observed by Bacon *et al.* (1989) at the Alpha Ridge.

Cochran *et al.* (1995) calculated residence times of dissolved $^{230}$Th of 18-19 years in the central Nansen Basin and 10-12 years on the Barents Sea slope. $^{230}$Th concentrations in the Nansen Basin were found to be lower than those from the Alpha Ridge reported by Bacon *et al.* (1989) and deep water in the central Nansen Basin had lower particulate and higher dissolved $^{230}$Th concentrations than near the slopes (Cochran *et al.*, 1995). Scholten *et al.* (1995) found that the shallower Eurasian Basin Deep Water (EBDW) is influenced by ventilation, in contrast to the deeper Eurasian Basin Bottom Water (EBBW) and suggested resuspension as the cause for the increased scavenging rates in the EBBW. Valk *et al.* (2018) showed that the deep Nansen Basin is influenced by volcanic and hydrothermal inputs that lead to scavenging removal of $^{230}$Th over several years, at least episodically.

Sedimentary $^{231}Pa_{xs}/^{230}Th_{xs}$ from the Canada Basin provided new insights into the relevance of scavenging removal and the horizontal redistribution of these tracers as well as the fractionation between the low productivity, sea ice covered interior basins and the seasonally high particle flux areas at the margins. Low surface sediment $^{231}Pa_{xs}/^{230}Th_{xs}$ ratios were interpreted as a result of chemical fractionation of $^{230}$Th and $^{231}$Pa in the water column resulting in preferred $^{231}$Pa export out of the Arctic. Almost all of the $^{230}$Th produced in-situ (ca. 90 %) was estimated to be removed within the Arctic by scavenging onto particles (Moran *et al.*, 2005), while Hoffmann *et*

*al.* (2013) suggested that the deep waters of the Arctic are exchanged through the Fram Strait on centennial timescales.

Roy-Barman (2009) presented a boundary scavenging profile model, showing that linear $^{230}$Th concentration profiles do not necessarily imply that circulation is negligible. They suggested that the difference between the Arctic and other oceans is a considerable lateral transport of $^{230}$Th from the interior to the margins.

### 1.4 Motivation

Global warming is triggering profound changes in the ocean, and the Arctic Ocean is especially vulnerable to such environmental forcing. Summer ice cover is rapidly declining, while the supply of terrestrial material (Günther *et al.*, 2013) and particle flux (Boetius *et al.*, 2013) increases and ocean circulation is changing (Karcher *et al.*, 2012). These developments are expected to leave an imprint on the distribution of particle-reactive radionuclides, such as Th isotopes. A central motivation for this GEOTRACES study is to use the Th isotopes to depict changes in circulation and particle fluxes in the Arctic Ocean from 1991 to 2015. The basis of this study is a time series consisting of natural radionuclide data from various previous studies combined with new data from 2007 and 2015.

## 2 Methods

### 2.1 Sampling and Analysis of Th in Samples collected in 2007

Sea water samples were filtered directly from the 24 L CTD-Niskin® bottles into acid cleaned cubitainers (LDPE) using 0.45 µm pore size Acropaks®. Samples were collected in volumes of 1 L, 2 L, and 10 L and acidified with concentrated ultraclean $HNO_3$. Samples for the analysis of total $^{230}$Th were taken without filtration. Analyses were performed at the University of Minnesota, Minneapolis, following methods from Shen *et al.* (2003). Measurements were done using Inductively Coupled Plasma Mass Spectrometry (ICP-MS, Thermo Finnigan, Neptune) equipped with a Secondary Electron Multiplier (SEM) and a Retarding Potential Quadrupole (RPQ) energy filter.

### 2.2 Sampling and Analysis of Dissolved Th samples collected in 2015

Samples were filtered directly from the 24 L CTD-Niskin® bottles into cubitainers (LDPE) through 0.45 µm pore size Acropaks® in volumes of 10 L (>2000 m) and 20 L (<2000 m), according to the expected concentrations (Nozaki *et al.*, 1981). Acropaks® were used for half of

the cruise and then replaced by new ones. Subsequently water samples were acidified to a pH of 1.5-2 by addition of 1 mL (acid)/L (seawater) of concentrated double distilled $HNO_3$.

Preconcentration and analysis of $^{230}$Th and $^{232}$Th were performed following GEOTRACES methods in clean laboratories of the Alfred-Wegener-Institute (AWI), (Anderson *et al.*, 2012). Samples were spiked with $^{229}$Th and $^{236}$U, calibrated against the reference standard material UREM11, a material in radioactive equilibrium (Hansen *et al.*, 1983), followed by addition of a purified Fe-carrier solution ($FeCl_3$). The next day, the pH of the samples was raised to 8.5 by adding double-distilled $NH_4OH$, to induce $Fe(OH)_3$ precipitation. After 72 h, when the $Fe(OH)_3$ had settled to the bottom of the cubitainer, the precipitate was transferred from the cubitainers to acid cleaned 1 L Teflon® bottles, after syphoning off the supernatant water. After dissolution of the sample in concentrated HCl, the pH was raised again to 8.5 to allow the $Fe(OH)_3$ precipitate and settle. The supernatant water was syphoned off and the preticipate was transferred into acid cleaned 50 mL Falcon® tubes the following day. The samples were then washed by centrifugation four times at 4000 rpm for 12 minutes, where the supernatant was decanted before addition of new ultrapure Milli-Q® water. Finally, the precipitation was dissolved in concentrated HCl and evaporated to a drop (>10 µL) in an acid cleaned 15 mL Savillex® beaker. After evaporation, the fractions of Pa, Th, U and Nd were separated using chromatographic columns filled with anion exchange resin (AG1X8, 100-200 mesh) according to GEOTRACES methods (Anderson *et al.*, 2012). All fractions were collected in acid cleaned 15 mL Savillex® beakers and columns were washed and conditioned before the samples were loaded onto the columns using concentrated HCl and $HNO_3$.

Procedural blanks for $^{230}$Th and $^{232}$Th were run with each batch of 10-15 samples. Average $^{230}$Th and $^{232}$Th blank corrections are 0.24 fg/kg and 0.003 pmol/L, respectively. At station 81, a sample (2000 m) was divided into two samples and resulted in different dissolved $^{232}$Th concentrations, probably due to Th attached to the walls of the original cubitainer. Here, an average value considering the volumes of both parts of the divided samples was calculated.

### 2.3 Sampling and Analysis of Particulate $^{234}$Th Samples collected in 2015

Particulate samples were taken using in-situ pumps (McLane and Challenger Oceanic). 268 L to 860 L seawater were pumped through a 142 mm ⌀, 0.45 µm pore size Supor® (polyether sulfone) filter (Anderson *et al.*, 2012). Filters were cut aboard for subsamples under a laminar flow hood using tweezers and scalpels. Subsamples (23 mm ⌀) were dried, put on plastic mounts, covered with Mylar and aluminium foil and directly measured by beta decay counting of $^{234}$Th for at least 12 h. Six months later, background measurements were performed at the AWI in Bremerhaven.

### 2.4 Model

The model of Rutgers van der Loeff *et al.* (2018) was used to analyse the downward propagation of a ventilation signal in the Atlantic layer by settling particles and radioactive ingrowth. The $^{230}$Th model is based on the reversible exchange model of Bacon and Anderson (1982) and Nozaki *et al.* (1981) and solved with programming language R. We first let the $^{230}$Th model run with the base parameters as given for the Amundsen Basin in Table 1 of Rutgers van der Loeff *et al.* (2018), but without exchange with the Kara Sea, until dissolved $^{230}$Th reaches a linear steady state profile. We then simulate a hypothetical strong ventilation of the intermediate water with $^{230}$Th-depleted shelf water by introducing an exchange process down to 1500 m with a $^{230}$Th-free water mass on a time scale of 4 years, which causes a rapid reduction of $^{230}$Th in this upper layer. The $^{230}$Th profile is determined over the full water column over time since the beginning of this ventilation. Parameter values used in the simulation are listed in Table 1.

**Table 1: Parameters of the Profile Model adapted from Rutgers van der Loeff *et al.*, 2018, representing transient $^{230}$Th in the Amundsen Basin**

| Parameter | Symbol | Value | Unit |
|---|---|---|---|
| Vertical Eddy Diffusion Coefficient | $K_z$ | 4100 | $m^2\ y^{-1}$ |
| Exchange Time 0-1500m with Kara Sea | | | |
| Initial | $t_K$ | $\infty$ | y |
| During Ventilation | $t_K$ | 4 | y |
| $^{230}$Th Kara Sea | $^{230}Th_K$ | 0 | fg/L |
| $C_p/C_d$ $^{230}$Th (*) | $K_{230}$ | 0.5 | -.- |
| $C_p/C_d$ $^{234}$Th (*) | $K_{234}$ | 0.12 | -.- |
| Adsorption Rate Constant | $k_1$ | 1.59 | $y^{-1}$ |
| Desorption Rate Constant | $k_{-1}$ | 3.18 | $y^{-1}$ |
| Particle Settling Rate | S | 582 | $m\ y^{-1}$ |

*Valk *et al.* (2018)
$C_p$ = particulate concentration; $C_d$ = dissolved concentration

## 3. Results

$^{230}$Th results are expressed as unsupported excess $^{230}$Th ($^{230}Th_{xs}$); for simplification, hereinafter $^{230}$Th refers to $^{230}Th_{xs}$. Excess corrections were done following Hayes *et al.* (2015). $^{230}$Th concentrations are corrected for a proportion of $^{230}$Th released by dissolution of lithogenic particles. This is based on parallel measurements of $^{232}$Th, considering a lithogenic ratio $^{230}Th/^{232}Th = 4.0\times10^{-6}$ mol/mol (Roy-Barman *et al.*, 2009).

### 3.1 Dissolved $^{230}$Th in 1991, 2007 and 2015

Data obtained in 1991 by Scholten *et al.* (1995) constitute the baseline for the time series presented in this study (Fig. 2A). Dissolved $^{230}$Th activities increased with depth in the Amundsen Basins in 1991, 2007 and 2015.

Station 400 (2007), located at the south eastern margin of the Eurasian Basin showed lower concentrations than the open ocean stations.

### 3.2 Dissolved $^{232}$Th in 2007 and 2015

The concentrations of dissolved $^{232}$Th from 2007 and 2015 were similar. In 2015, dissolved $^{232}$Th concentrations observed in the Amundsen Basin showed a decreasing trend with depth. Surface concentrations were relatively high at station 117 (100 pg/kg) and 125 (>200 pg/kg). At station 81, dissolved $^{232}$Th showed a relatively constant depth distribution, where surface $^{232}$Th concentrations were lower compared to station 117 and 125. At stations 125 and 117 dissolved $^{232}$Th decreased as well slightly with depth, with station 117 showing a mid-depth maximum at 2000 m (Fig. 2C). 2007 values (station 309) decreased with depth until 2500 m and then slightly increased towards 4500 m. Close to the shelf (at station 400) concentrations were lower than in the open basin in 2007.

### 3.3 Particulate $^{234}$Th from 2015

Particulate $^{234}$Th from 2015 is shown as the relative amount of particulate $^{234}$Th (Fig. 2D) compared to total $^{234}$Th, calculated from $^{238}$U activities, assuming equilibrium of total $^{234}$Th with $^{238}$U in deep water (Owens *et al.*, 2011). All profiles show rather low concentrations of particulate $^{234}$Th in the Amundsen Basin. Especially below 2000 m particulate $^{234}$Th is much higher in the Nansen Basins (Valk *et al.*, 2018).

## 4 Discussion

### 4.1 Temporal Evolution of Dissolved $^{230}$Th in the Amundsen Basin

Figure 2A shows $^{230}$Th concentrations from 2015 and the temporal development since 1991. Temporal changes are manifest over the entire water column since 2007. With one exception, the 2015 concentration range is below 2007 and 1991 (Scholten *et al.*, 1995). This difference is larger than the concentration range for the three 2015 profiles (Fig. 2A). The three stations from 2015 (81, 117 and 125) are distributed over a wide area of the Amundsen Basin (Fig. 1). Because all stations show lower concentrations in 2015, this points to a temporal rather than a regional variability over the entire basin. The decrease in dissolved $^{230}$Th in the Amundsen Basin started after 2007, considering the similar concentrations in 1991 and 2007. Dissolved $^{230}$Th decreased by 0.32 fg/k/y in 300-500 m water depth, and by 0.52 fg/kg/y in 1000-1500 m. $^{230}$Th is known to respond to particle fluxes as well as ocean circulation (Anderson *et al.*, 1983b, a). A reduction in dissolved $^{230}$Th concentrations can therefore be caused by either increased

scavenging (Anderson *et al.*, 1983b) or by changing circulation (Anderson *et al.*, 1983a).

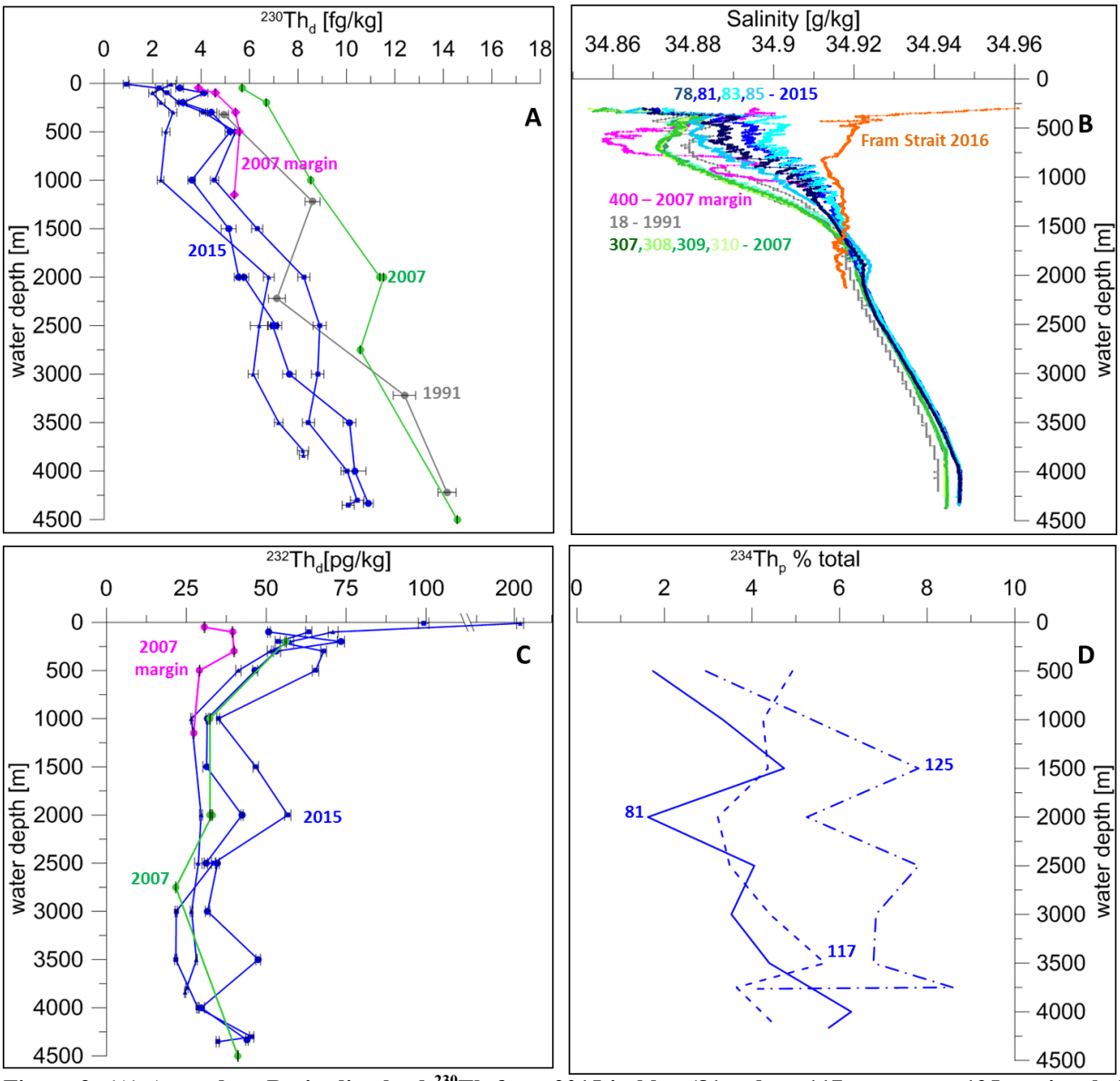


**Figure 9: (A) Amundsen Basin dissolved $^{230}$Th from 2015 in blue (81 = dots, 117 = squares, 125 = triangles), 2007 in green (309), 2007 margin in pink and 1991 in grey (173). (B) Amundsen Basin salinity profiles from 2015 (Rabe *et al.*, 2016), 2007 (Schauer and Wisotzki, 2010), 1991 (Rudels, 2010) and Fram Strait 2016 (Kanzow *et al.*, 2017). (C) Dissolved $^{232}$Th from 2015 (81 = dashed, 117 = dashed dotted, 125 = solid) and 2007 (309 = green) and 2007 margin (400 = pink) (D) Particulate $^{234}$Th from 2015 in percent of total $^{234}$Th.**

### 4.2 Scavenging in the Central Amundsen Basin

Biological production in the central Arctic Ocean in 2011 was not higher than in 2007 (Ulfsbo *et al.*, 2014). Therefore, enhanced biological production in the Amundsen Basin and subsequent sinking particles can be excluded as a reason for the changing Th distributions. Enhanced scavenging by lithogenic material at these stations can also be excluded because for all three stations from 2015, dissolved $^{232}$Th values at 1000 m are in the same range or lower than

observed in 2007 (Fig. 2C). Low dissolved $^{232}$Th is taken here as an indicator of low amounts of lithogenic material. Enhanced particle loads would result in high concentrations of particulate $^{234}$Th, as observed in the deep Nansen Basin where particulate $^{234}$Th ranges between 3.3 and 9.1 % of total $^{234}$Th (Valk *et al.*, 2018). In the Amundsen Basin only station 125 (2015), located at the slope of the Lomonosov Ridge shows relatively high values of particulate $^{234}$Th in the deep water from 1500m downwards (Fig. 2D). This feature could be explained by the resuspension of slope sediments along the Lomonosov Ridge, as no increased scavenging was observed in the deep Amundsen Basin (Slagter *et al.*, 2017). Slagter *et al.* (2017) argue that similar riverine surface influence of humic substances in the Amundsen Basin and in the Makarov Basin did not lead to increased scavenging at depth in the Amundsen Basin, even at stations influenced by the TPD (e.g. station 125) (Slagter *et al.*, 2017; Rutgers van der Loeff *et al.*, 2018). This is in contrast to the Makarov Basin, where they observed a slight increase of dissolved Fe-binding organic ligand concentrations, and reduced dissolved Fe concentrations that may point to more intense scavenging or lower Fe inputs (Slagter *et al.*, 2017; Klunder *et al.*, 2012), while the high $^{232}$Th observed at the surface of station 125 points to a notable continental component, a signal that is not observed below (Fig. 2C). Hence, our observations are consistent with Slagter *et al.* (2017). To summarize, dissolved $^{232}$Th generally did not increase since 2007, except for station 117 at 2000 m and station 81 at 3500 m. Recent studies about Ra isotopes, Fe binding ligands, NCP estimates and the particulate data ($^{234}$Th, $^{232}$Th) do not point at enhanced particle fluxes in the central Amundsen Basin. Therefore, and putting all these different parameters together, it can be concluded that scavenging of $^{230}$Th within the Amundsen Basin is unlikely to be the primary factor for the observed reduction between 2007 and 2015 in the Amundsen Basin.

### 4.3 500-1500 m: Intermediate Water Mass Changes

The decrease of dissolved $^{230}$Th at depths between 500 m and 1500 m for stations 81, 117 and 125 in the Amundsen Basin (2015) is most prominent at 1000 m, where concentrations decreased to half of the value in 2007 (Fig. 2A). This depth range in the Amundsen Basin is ventilated on considerably shorter time scales than in the Nansen and Makarov Basin by a westward boundary circulation (Tanhua *et al.*, 2009).

The drop in dissolved $^{230}$Th at 1000 m corresponds to an increase in the $^{129}$I/$^{236}$U ratio (Figure 3), implying a higher Atlantic influence of younger waters (Casacuberta *et al.*, 2018), which in turn is in agreement with an increase in the circulation/ventilation rate between 750 and 1500 m. For station 81, in the central Amundsen Basin, Rutgers van der Loeff *et al.* (2018) estimated a ventilation age based on $SF_6$ data of 15-18 years at 1000 m. This estimate fits to time scales

based on $^{228}$Ra data and is supported independently by the $^{129}$I/$^{236}$U ratio (Rutgers van der Loeff *et al.*, 2018).

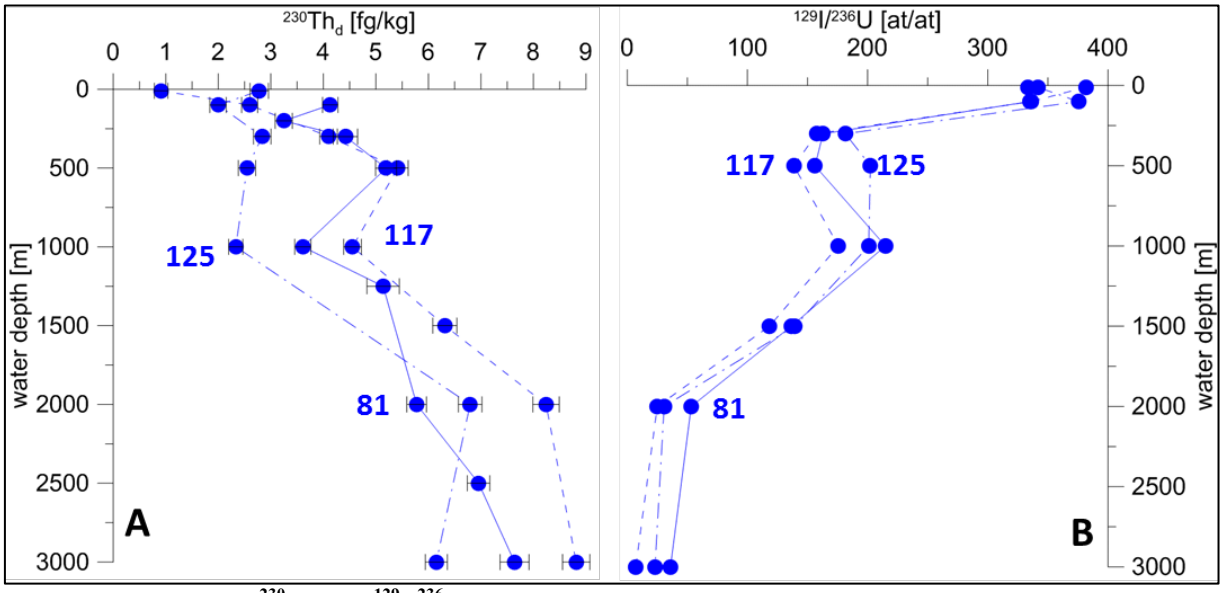


**Figure 3: (A) Dissolved $^{230}$Th. (B) $^{129}$I/$^{236}$U (Casacuberta *et al.*, 2018) from the Amundsen Basin, 2015**

While anthropogenic radionuclides (Fig. 3) imply exchange with young shelf waters of Atlantic influence, it is unclear to what extent the change in $^{230}$Th may be caused by exchange with the Makarov Basin. Tanhua *et al.* (2009) found notable changes in CFC tracer ages at the North Pole, indicating older waters in 1994 compared to 1991 and 2005 at 400 m; a change that was also documented in silicate concentrations (Tanhua *et al.*, 2009). This feature probably reflected a shift in the front of Eurasian and Canada Basin water around the year 1994, with Canadian Basin water penetrating deeper into the central Amundsen Basin (Tanhua *et al.*, 2009). Unfortunately, there is no $^{230}$Th data from this phase of penetration of Canada Basin water around 1994. If the $^{230}$Th data from 1991 are connected to CFC data from the same year, while the $^{230}$Th data from 2007 are connected to CFC data of 2005 (Tanhua *et al.*, 2009) they are both representative of periods of low intrusion of Canada Basin water over the Lomonosov Ridge. Renewed intrusion of Canada Basin water in 2015 can be excluded as mechanism for the observed change in $^{230}$Th because this would increase rather than decrease dissolved $^{230}$Th concentrations in the Amundsen Basin (Scholten *et al.*, 1995; Edmonds *et al.*, 2004; this study). Moreover, intrusion of Canada Basin water would not match the ventilation age estimated by Rutgers van der Loeff *et al.* (2018), since the Canada Basin water is known to be much older than Amundsen Basin water at this depth (Tanhua *et al.*, 2009). Hence, it is suggested that the changes in the Amundsen Basin cannot be explained by interaction with the Makarov Basin. On the contrary, salinity distributions imply that the influence of Atlantic waters in the Amundsen

Basin has increased at 500-1500 m by 2015 indicating that water masses have changed after 2007 (Fig. 2B). Figure 2B shows salinity profiles for three stations from the Amundsen Basin from 2007 (Schauer and Wisotzki, 2010), three from 2015 (Rabe *et al.*, 2016), one from 1994 (Swift, 2006a) and one from 1991 (Rudels, 2010). In 2015, the intermediate waters of the Amundsen Basin have a stronger Atlantic contribution (Polyakov *et al.*, 2017; Rabe *et al.*, 2016). This change is correlated with the decrease in dissolved $^{230}$Th.

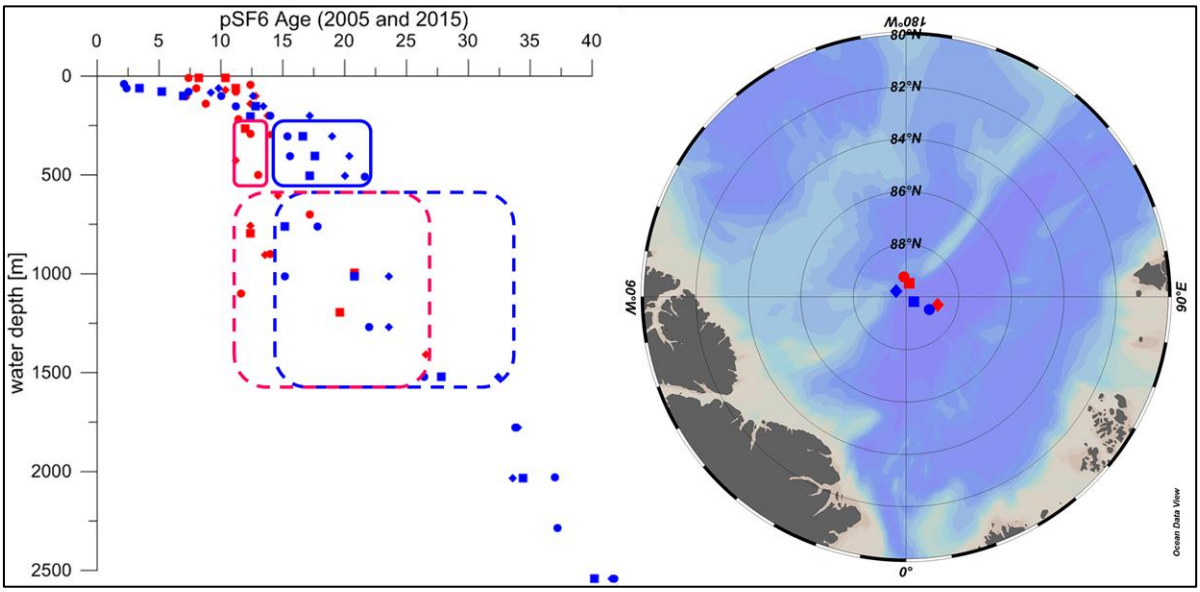


**Figure 4: Comparison of pCFC and pSF$_6$ ages from 2005 (red) and 2015 (blue) in the Amundsen Basin at stations located in the return flow along the Lomonosov Ridge, distinguishing the depth ranges of FSBW (solid box) and BSBW (dashed box). Locations of 2015 stations are marked in the map as blue symbols (81 = dots, 85 = squares, 89 = diamonds) and 2005 stations in red (41 = dots, 42 = squares, 46 = diamonds).**

Anthropogenic tracers can help determine whether the increased Atlantic water contribution had resulted in increased ventilation rates of the intermediate waters in the Amundsen Basin. A comparison of CFC and SF$_6$ ages between 2005 and 2015 (Fig. 4) shows that both the FSBW (approx. 425m) and the BSBW (approx. 1025m) ventilation age did not decrease after 2005. SF$_6$ age for the Atlantic Water (BSBW around 1000 m) at the northern end of the section in figure 4 is 12-15 years in 2005 and 15-18 years in 2015, suggesting perhaps a slowdown of transport of Atlantic Water in the boundary current. That would indicate that a change in scavenging along the flow path of the Atlantic water must be responsible for the observed decrease in dissolved $^{230}$Th, rather than a change in ventilation.

### 4.4 $^{230}$Th Removal Process in Intermediate Waters on Circulation Pathways

In order to judge the scavenging intensity it is useful to compare dissolved $^{230}$Th concentrations at various locations along the flow paths of the Atlantic waters. Arctic Intermediate Water (AIW) is comprised of water from the Greenland Sea and the Nordic Sea via the West Spitzbergen Current (WSC) (Rudels, 2009). In the North East Atlantic at 25°N (GEOTRACES section GA03_W, station 20), dissolved $^{230}$Th concentrations are 8.23 fg/kg at 1000 m and 13.17 fg/kg at 1500 m (Hayes *et al.*, 2015) (Fig. 5). At 55°N, dissolved $^{230}$Th concentrations in 1995 were 3.47 fg/kg at 500 m and 6.8 fg/kg at 1625 m (Vogler *et al.*, 1998) (station L3). In the Norwegian Sea, dissolved $^{230}$Th concentrations in 1993 were 5.81 fg/kg at 872 m and 7.04 fg/kg at 1286 m (Moran *et al.*, 1995) (station 13). These values are above the highest value of dissolved $^{230}$Th at 1000 m in the Amundsen Basin in 2015 (5 fg/kg). That means that these waters have lost $^{230}$Th during their transit to the central Amundsen Basin, through the productive North Atlantic, the Fram Strait (FSBW) and over the Barents Sea shelf (BSBW). These pathways are influenced by an increased input of terrestrial matter (Günther *et al.*, 2013) and/or increased primary production at the shelf and the ice edge compared to previous years (Arrigo and van Dijken, 2015; Ulfsbo *et al.*, 2018). Relatively high concentrations of Fe at the margin indicate the possibility of enhanced scavenging by iron oxides (Rijkenberg *et al.*, 2018).

At station 400, located at the south eastern margin of the Eurasian Basin, the deepest water is in the influence of BSBW, downstream of the Barents and Kara Sea shelf and slope. At the largest depth of ~1200m, $^{230}$Th the concentration is low and similar to concentrations in the central Amundsen Basin in 2015. This is consistent with the hypothesis that Atlantic waters that were depleted in $^{230}$Th on the shelf contribute to the decrease in dissolved $^{230}$Th in the central Amundsen Basin. Such a relic scavenging signal implies that scavenging occurs on pathways of inflow waters along the shelves rather than locally within the central basin. The high surface values of dissolved $^{230}$Th at station 400 are in line with low export production at this station compared to shallower stations over the shelf (Cai *et al.* 2010).

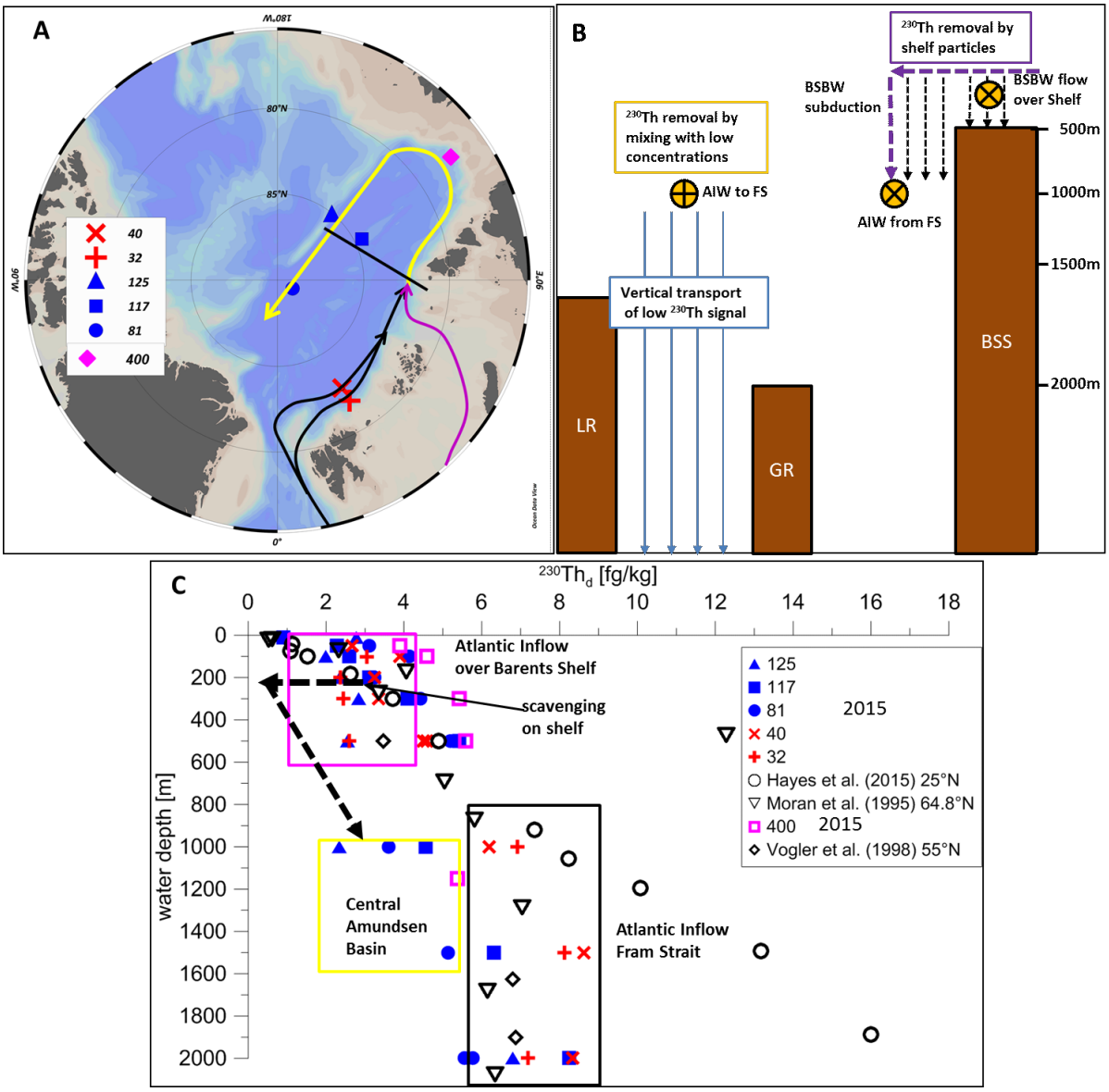


**Figure 5: (A) Circulation pathways of Atlantic waters to the central Amundsen Basin. (B) Conceptual drawing of scavenging and mixing of water masses close to St Anna Trough (black line in A represents the section of B). LR = Lomonosov Ridge, GR = Gakkel Ridge, BSS = Barents Sea Shelf, FS = Fram Strait). (C) Development of dissolved $^{230}$Th concentrations from the North Atlantic to the Amundsen Basin. Atlantic values: (open symbols, Hayes *et al.*, 2015; Vogler *et al.*, 1998; Moran *et al.*, 1995) represented by a deep box flowing in through Fram Strait and a shallow box with lower activities flowing in over the Barents shelf and exposed to additional scavenging on the shelf (horizontal black arrow) before it is subducted and mixed with deeper Atlantic inflow to form the observed reduced concentrations in the central Amundsen Basin. Stations 32 and 40 (red) are from Gdaniec *et al.* (2020).**

Hence, the observed reduction in dissolved $^{230}$Th in the intermediate water of the Amundsen Basin is attributed to a combination of scavenging and advection. Scavenging takes place locally on the shelves and along the slopes of the Barents, Kara and Laptev Seas, causing the removal of $^{230}$Th observed downstream in the central Amundsen Basin. Figure 5 shows pathways of intermediate waters and dissolved $^{230}$Th profiles from 2015, illustrating the mechanisms controlling the relatively low dissolved $^{230}$Th concentrations observed in the central Amundsen

Basin. Atlantic waters flowing over the Barents and Kara shelves lose $^{230}$Th by increased scavenging. $^{230}$Th depleted BSBW is subducted and gradually mixes with deeper Atlantic inflow. The closer the stations are to the Lomonosov Ridge, the younger the ventilation age (Fig. 5), and the more the salinities are shifted towards Atlantic values. Variability in temperature and salinity plots indicates that this branch interacts with ambient waters (Rudels *et al.*, 1994). This is consistent with dissolved $^{230}$Th concentrations observed at stations 81, 117 and 125 (2015), with station 125, located in the TPD and closest to the Lomonosov Ridge, showing the lowest concentrations. The low $^{230}$Th concentrations at station 125 may also be affected by additional scavenging due to resuspension on the slope of the Lomonosov Ridge.

### 4.5 Vertical Transport of Circulation derived $^{230}$Th Scavenging Signal and Effects in Deep Waters

Intermediate waters in the central Amundsen Basin have a lower dissolved $^{230}$Th in the depth range up to 1500 m, due to increased scavenging during transport of Atlantic water over the shelves and along the slope. The time series data also reveal changing conditions below the intermediate waters, indicated by a decrease of dissolved $^{230}$Th in the deeper water column (Fig. 2A).

This raises the question as to whether a change, as observed for 500-1500 m, might cause a decrease in concentrations in the water column below that depth within just 8 years. Theoretically, such a decreasing signal could be manifest by sinking particles via reversible scavenging of sinking particles. With particle settling rates of 582 m/y (Rutgers van der Loeff *et al.*, 2018) an average particle needs approximately six years from the depth of strongest depletion (1000 m) to reach the bottom of the water column. That would match the time scale of the decrease in $^{230}$Th observed between 2007 and 2015. The time for particle transport to depth is the limiting step, because the time scale for particle settling is longer than for adsorption and desorption of thorium (Rutgers van der Loeff *et al.*, 2018). On the basis of these parameters, Rutgers van der Loeff *et al.* (2018) created a model to illustrate the development of $^{228}$Ra and $^{228}$Th over time. This model is modified here to simulate how the full water column profile of dissolved $^{230}$Th in the Amundsen Basin reacts to a sudden change in circulation transport of water with low $^{230}$Th into the intermediate depth layer (Tab. 1). The model should be seen as a description of the downwards penetration of the removal signal, rather than a precise retrace of profiles from the central Amundsen Basin. The exchange process used to introduce the ventilated water mass is not meant to reproduce the actual ventilation with water from Kara/Barents Seas, but merely serves the purpose to create a rapid reduction of $^{230}$Th in the

upper 1500m in order to model the downward propagation of such a signal by reversible scavenging. The model results in figure 6 show how fast a decrease of $^{230}$Th in the ventilated layer (500-1500 m) is propagated into the deep water. Uncertainties in the model assumptions, such as particle sinking speed and exchange between dissolved and particulate phases might cause the difference between model and data. This may also explain why the downward penetration of the ventilation signal is slower in the model, where it has not yet reached the seafloor after 8 years (Fig. 6) than in the observed data. But the model results underpin the notion of a dissolved $^{230}$Th decrease due to circulation and scavenging along the circulation pathways, and account for the reduction of dissolved $^{230}$Th below the circulation influence. This temporal change can therefore be explained by a significant reduction in the input of low-$^{230}$Th waters from shallower depths, even if the scavenging rate in the deep basin remains constant.

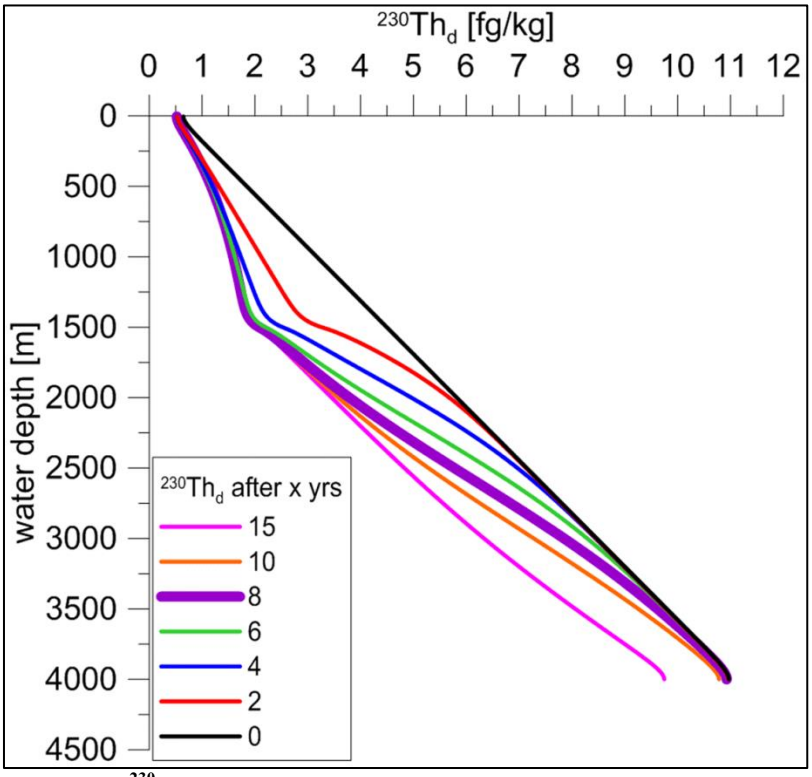


**Figure 6: Modelled dissolved $^{230}$Th distribution in the Amundsen Basin, 0, 2, 4, 6, 8, 10, 15, 20 years after reduction of concentration in upper layer (0-1500 m) by continuous exchange with $^{230}$Th-free surface water. Model was modified after Rutgers van der Loeff *et al.* (2018).**

Hydrothermal plumes released by volcanoes at the Gakkel Ridge could also decrease dissolved $^{230}$Th efficiently and periodically, as suggested by Valk *et al.* (2018) for the deep Nansen Basin. However, these plumes probably do not affect the Amundsen Basin as much as the Nansen Basin, due to recirculation in the Nansen Basin that retains most of the hydrothermal plume affected waters in the Nansen Basin (Valk *et al.*, 2018). Additionally, the depths where the major changes occurred in the Amundsen Basin are too shallow (the hydrothermal scavenging starts

below 2000 m) and the deep water decrease of dissolved $^{230}$Th in the Amundsen Basin since 2007 is much weaker than in the Nansen Basin (Valk *et al.*, 2018).

## 5. Conclusion

Concentrations of dissolved $^{230}$Th throughout the entire water column in the Amundsen Basin decreased since 2007. There is no indication of increased scavenging removal of $^{230}$Th due to increased particle flux within the Amundsen Basin. An increase in salinity of intermediate water (at 500 - 1500m) points to the influence of Atlantic derived waters, though $SF_6$ data suggest that the ventilation of this layer has not increased. The reduction in dissolved $^{230}$Th concentration in the Amundsen Basin intermediate waters is therefore attributed to increased scavenging from source waters and transport of this relict scavenging signature by advection. Thus, these downstream waters reflect a scavenging history over the Siberian shelves and slope that results in a reduction of $^{230}$Th relative to Atlantic source waters and, in turn, reduced dissolved $^{230}$Th in the central Amundsen Basin. The low-$^{230}$Th signal is propagated to deeper central Arctic Ocean waters by reversible scavenging. These findings highlight the close interaction of horizontal transport by advection and particle scavenging removal, which combine to generate far-field distributions of reactive trace elements.

**Author Contribution**

MRvdL, OV and WG designed and planned the study. OV, MRvdL, SG, KL, YL, RP, SBM and VP conducted sampling at sea. RLE and YL analysed the 2007 samples, while OV, VP and SG analysed the 2015 samples. NC provided I/U data, WS provided and interpreted SF6 data. All authors contributed to writing of the manuscript.

**Competing Interests**

The authors declare that they have no conflict of interest.

**Data Availability**

Data are available at https://doi.pangaea.de/10.1594/PANGAEA.908068 and at ttps://doi.pangaea.de/10.1594/PANGAEA.893871.

**Acknowledgement**

We thank the Captain and crew of RV Polarstern for their help during expeditions ARKXXIX/3 and ARKXXII/2. We would like to thank Ronja Paffrath for help on board**.** Ingrid Stimac is thanked for invaluable technical support and help in the laboratory. This work was partially supported by a U.S. NSF grant (OCE 143886) to RLE. Finally we thank the two anonymous reviewers for very thoughtful and constructive comments, which helped to improve the manuscript.

**References**

Aagaard, K., Coachman, L. K., and Carmack, E. C.: On the halocline of the Arctic Ocean*, Deep-Sea Research 1, 28A, 529-545, 1980.

Aagaard, K.: On the deep circulation in the Arctic Ocean, Deep Sea Research Part A. Oceanographic Research Papers, 28, 251-268, http://dx.doi.org/10.1016/0198-0149(81)90066-2, 1981.

Aksenov, Y., Ivanov, V. V., Nurser, A. J. G., Bacon, S., Polyakov, I. V., Coward, A. C., Naveira-Garabato, A. C., and Beszczynska-Moeller, A.: The Arctic Circumpolar Boundary Current, Journal of Geophysical Research: Oceans, 116, doi:10.1029/2010JC006637, 2011.

Anderson, R. F., Bacon, M. P., and Brewer, P. G.: Removal of $^{230}$Th and $^{231}$Pa from the open ocean, Earth and Planetary Science Letters, 62, 7-23, 1983a.

Anderson, R. F., Bacon, M. P., and Brewer, P. G.: Removal of $^{230}$Th and $^{231}$Pa at ocean margins, Earth and Planetary Science Letters, 66, 73-90, 1983b.

Anderson, R. F., Fleisher, M. Q., Robinson, L., Edwards, R. L., Hoff, J. A., Moran, S. B., Rutgers van der Loeff, M. M., Thomas, A. L., Roy-Barman, M., and Francois, R.: GEOTRACES intercalibration of $^{230}$Th, $^{232}$Th, $^{231}$Pa, and prospects for $^{10}$Be, Limnol. Oceanogr.: Methods, 10, 179-213, 2012.

Arrigo, K. R., van Dijken, G., and Pabi, S.: Impact of a shrinking Arctic ice cover on marine primary production, Geophysical Research Letters, 35, n/a-n/a, 10.1029/2008GL035028, 2008.

Arrigo, K. R., and van Dijken, G. L.: Continued increases in Arctic Ocean primary production, Progress in Oceanography, 136, 60-70, http://dx.doi.org/10.1016/j.pocean.2015.05.002, 2015.

Bacon, M. P., and Anderson, R. F.: Distribution of Thorium Isotopes Between Dissolved and Particulate Forms in The Deep Sea, Journal of Geophysical Research, 87, 2045-2056, 1982.

Bacon, M. P., Huh, C.-A., and Moore, R. M.: Vertical profiles of some natural radionuclides over the Alpha Ridge, Arctic Ocean, Earth and Planetary Science Letters, 95, 15-22, 1989.

Björk, G., Jakobsson, M., Rudels, B., Swift, J. H., Anderson, L., Darby, D. A., Backman, J., Coakley, B., Winsor, P., Polyak, L., and Edwards, M.: Bathymetry and deep-water exchange across the central Lomonosov Ridge at 88–89°N, Deep Sea Research Part I: Oceanographic Research Papers, 54, 1197-1208, http://dx.doi.org/10.1016/j.dsr.2007.05.010, 2007.

Björk, G., Anderson, L. G., Jakobsson, M., Antony, D., Eriksson, B., Eriksson, P. B., Hell, B., Hjalmarsson, S., Janzen, T., Jutterström, S., Linders, J., Löwemark, L., Marcussen, C., Anders Olsson, K., Rudels, B., Sellén, E., and Sølvsten, M.: Flow of Canadian basin deep water in the Western Eurasian Basin of the Arctic Ocean, Deep Sea Research Part I: Oceanographic Research Papers, 57, 577-586, http://dx.doi.org/10.1016/j.dsr.2010.01.006, 2010.

Boetius, A., Albrecht, S., Bakker, K., Bienhold, C., Felden, J., Fernández-Méndez, M., Hendricks, S., Katlein, C., Lalande, C., Krumpen, T., Nicolaus, M., Peeken, I., Rabe, B.,

Rogacheva, A., Rybakova, E., Somavilla, R., and Wenzhöfer, F.: Export of Algal Biomass from the Melting Arctic Sea Ice, Science, 339, 2013.

Cai, P., Rutgers van der Loeff, M. M., Stimac, I., Nöthig, E.-M., Lepore, K., and Moran, S. B.: Low export flux of particulate organic carbon in the central Arctic Ocean as revealed by $^{234}$Th:$^{238}$U disequilibrium, Journal of Geophysical Research, 115, 2010.

Casacuberta, N., Christl, M., Vockenhuber, C., Wefing, A.-M., Wacker, L., Masqué, P., Synal, H.-A., and Rutgers van der Loeff, M.: Tracing the Three Atlantic Branches Entering the Arctic Ocean With $^{129}$I and $^{236}$U, Journal of Geophysical Research: Oceans, 0, doi:10.1029/2018JC014168, 2018.

Clark, D. L., and Hanson, A.: Central Arctic Ocean Sediment Texture: A Key to Ice Transport Mechanisms, in: Glacial-Marine Sedimentation, edited by: Molnia, B. F., Springer US, Boston, MA, 301-330, 1983.

Cochran, K., J., H. D., Livingston, H. D., Buesseler, K. O., and Key, R. M.: Natural and anthropogenic radionuclide distributions in the Nansen Basin, Artic Ocean: Scavenging rates and circulation timescales, Deep-Sea Research II, 42, 1495-1517, 1995.

Edmonds, H. N., Moran, S. B., Hoff, J. A., Smith, J. R., and Edwards, R. L.: Protactinium-231 and Thorium-230 Abundances and High Scavenging Rates in the Western Arctic Ocean, Science, 280, 405-406, 1998.

Edmonds, H. N., Moran, S. B., Cheng, H., and Edwards, R. L.: $^{230}$Th and $^{231}$Pa in the Arctic Ocean: implications for particle fluxes and basin-scale Th/Pa fractionation, Earth and Planetary Science Letters, 227, 155-167, 2004.

Günther, F., Overduin, P. P., Sandakov, A. V., Grosse, G., and Grigoriev, M. N.: Short- and long-term thermo-erosion of ice-rich permafrost coasts in the Laptev Sea region, Biogeosciences, 10, 4297-4318, 10.5194/bg-10-4297-2013, 2013.

Hansen, R. G., Ring, E. J., Council for Mineral, T., and Analytical Chemistry, D.: The preparation and certification of a uranium reference material, Council for Mineral Technology, Randburg, South Africa, 1983.

Hayes, C. T., Anderson, R. F., Fleisher, M. Q., Vivancos, S. M., Lam, P. J., Ohnemus, D. C., Huang, K.-F., Robinson, L., Lu, Y., Cheng, H., Edwards, R. L., and Moran, S. B.: Intensity of Th and Pa scavenging partitioned by particle chemistry in the North Atlantic Ocean, Marine Chemistry, 170, 49-60, 2015.

Hill, V., Ardyna, M., Lee, S. H., and Varela, D. E.: Decadal trends in phytoplankton production in the Pacific Arctic Region from 1950 to 2012, Deep Sea Research Part II: Topical Studies in Oceanography, https://doi.org/10.1016/j.dsr2.2016.12.015, 2017.

Hoffmann, S. S., McManus, J. F., Curry, W. B., and Brown-Leger, S. L.: Persistent export of $^{231}$Pa from the deep central Arctic Ocean over the past 35,000 years, Nature, 497, 603-607, 2013.

Hsieh, Y.-T., Henderson, G. M., and Thomas, A. L.: Combining seawater $^{232}$Th and $^{230}$Th concentrations to determine dust fluxes to the surface ocean, Earth and Planetary Science Letters, 312, 280-290, 2011.

Jakobsson, M., 2002. Hypsometry and volume of the Arctic Ocean and its constituent seas. Geochemistry, Geophysics, Geosystems 3 (5), 1-18.

Jones, E. P., Rudels, B., and Anderson, L. G.: Deep waters of the Arctic Ocean: origins and circulation, Deep-Sea Research 1, 42, 737-760, 1995.

Kanzow, T; von Appen, W-J; Schaffer, J *et al.* (2017): Physical oceanography measured with CTD/Large volume Watersampler-system during POLARSTERN cruise PS100 (ARK-XXX/2)

Karcher, M., Smith, J. N., Kauker, F., Gerdes, R., and Smethie Jr., W. M.: Recent changes in Arctic Ocean circulation revealed by iodine-129 observations and modelling, Journal of Geophysical Research, 117, 2012.

Kipp, L. E., Charette, M. A., Moore, W. S., Henderson, P. B., and Rigor, I. G.: Increased fluxes of shelf-derived materials to the central Arctic Ocean, Science Advances, 4, 10.1126/sciadv.aao1302, 2018.

Lien, V. S., and Trofimov, A. G.: Formation of Barents Sea Branch Water in the north-eastern Barents Sea, Polar Research, 32, 18905, 10.3402/polar.v32i0.18905, 2013.

Middag, R., de Baar, H. J. W., Laan, P., and Bakker, K.: Dissolved aluminium and the silicon cycle in the Arctic Ocean, Marine Chemistry, 115, 176-195, http://dx.doi.org/10.1016/j.marchem.2009.08.002, 2009.

Moran, S. B., Hoff, J. A., Buesseler, K. O., and Edwards, R. L.: High precision $^{230}$Th and $^{232}$Th in the Norwegian Sea and Denmark by thermal ionization mass spectrometry, Geophysical Research Letters, 22, 2589-2592, 10.1029/95GL02652, 1995.

Moran, S. B., and Smith, J. N.: $^{234}$Th as a tracer of scavenging and particle export in the Beaufort Sea, Continental Shelf Research, 20, 153-167, https://doi.org/10.1016/S0278-4343(99)00065-5, 2000.

Moran, S. B., Shen, C.-C., Edwards, R. L., Edmonds, H. N., Scholten, J. C., Smith, J. N., and Ku, T.-L.: $^{231}$Pa and $^{230}$Th in surface sediments of the Arctic Ocean: Implications for $^{231}$Pa/$^{230}$Th fractionation, boundary scavenging, and advective export, Earth and Planetary Science Letters, 234, 235-248, 2005.

Nozaki, Y., Horibe, Y., and Tsubota, H.: The water column distributions of thorium isotopes in the western North Pacific, Earth and Planetary Science Letters, 54, 203-216, http://dx.doi.org/10.1016/0012-821X(81)90004-2, 1981.

Pabi, S., van Dijken, G. L., and Arrigo, K. R.: Primary production in the Arctic Ocean, 1998–2006, Journal of Geophysical Research: Oceans, 113, doi:10.1029/2007JC004578, 2008.

Polyakov, I. V., Pnyushkov, A. V., Alkire, M. B., Ashik, I. M., Baumann, T. M., Carmack, E. C., Goszczko, I., Guthrie, J., Ivanov, V. V., Kanzow, T., Krishfield, R., Kwok, R., Sundfjord, A., Morison, J., Rember, R., and Yulin, A.: Greater role for Atlantic inflows on sea-ice loss in the Eurasian Basin of the Arctic Ocean, Science, 356, 285-291, 10.1126/science.aai8204, 2017.

Owens, S. A., K. O. Buesseler, and K. W. W. Sims (2011), Re-evaluating the $^{238}$U-salinity relationship in seawater: Implications for the $^{238}$U–$^{234}$Th disequilibrium method, Marine Chemistry, 127(1), 31-39.

Rabe, B., Karcher, M., Kauker, F., Schauer, U., Toole, J. M., Krishfield, R. A., Pisarev, S., Kikuchi, T., and Su, J.: Arctic Ocean basin liquid freshwater storage trend 1992–2012, Geophysical Research Letters, 41, 961-968, 10.1002/2013GL058121, 2014.

Rabe, B.; Schauer, U., Ober, S., Horn, M., Hoppmann, M., Korhonen, M., Pisarev, S., Hampe, H., Villacieros, N., Savy, J.P., Wisotzki, A. (2016): Physical oceanography during POLARSTERN cruise PS94 (ARK-XXIX/3). Alfred Wegener Institute, Helmholtz Center

for Polar and Marine Research, Bremerhaven, PANGAEA, https://doi.org/10.1594/PANGAEA.859558

Rempfer, J., Stocker, T. F., Joos, F., Lippold, J., and Jaccard, S. L.: New insights into cycling of $^{231}$Pa and $^{230}$Th in the Atlantic Ocean, Earth and Planetary Science Letters, 468, 27-37, http://dx.doi.org/10.1016/j.epsl.2017.03.027, 2017.

Rijkenberg, M. J. A., Slagter, H. A., Rutgers van der Loeff, M., van Ooijen, J., and Gerringa, L. J. A.: Dissolved Fe in the Deep and Upper Arctic Ocean With a Focus on Fe Limitation in the Nansen Basin, Frontiers in Marine Science, 5, 10.3389/fmars.2018.00088, 2018.

Roy-Barman, M.: Modelling the effect of boundary scavenging on Thorium and Protactinium profiles in the ocean, Biogeosciences, 6, 3091-3107, 2009.

Rudels, B., Jones, E. P., Anderson, L. G., and Kattner, G.: On the Intermediate Depth Waters of the Arctic Ocean, in: The Polar Oceans and Their Role in Shaping the Global Environment, edited by: Johannessen, O. M., Muench, R. D., and Overland, J. E., 1994.

Rudels, B.: Arctic Ocean Circulation A2 - Steele, John H, in: Encyclopedia of Ocean Sciences (Second Edition), Academic Press, Oxford, 211-225, 2009.

Rudels, B.: Arctic Ocean circulation and variability – advection and external forcing encounter constraints and local processes, Ocean Science, 8, 261-286, 2012.

Rudels, B., Schauer, U., Björk, G., Korhonen, M., Pisarev, S., Rabe, B., and Wistotzki, A.: Observations of water masses and circulation with focus on the Eurasian Basin of the Arctic Ocean from the 1990s to the late 2000s, Ocean Science 9, 147-169, 2013.

Rudels, B., Korhonen, M., Schauer, U., Pisarev, S., Rabe, B., and Wisotzki, A.: Circulation and transformation of Atlantic water in the Eurasian Basin and the contribution of the Fram Strait inflow branch to the Arctic Ocean heat budget, Progress in Oceanography, 132, 128-152, http://dx.doi.org/10.1016/j.pocean.2014.04.003, 2015.

Rutgers van der Loeff, M., Kipp, L., Charette, M. A., Moore, W. S., Black, E., Stimac, I., Charkin, A., Bauch, D., Valk, O., Karcher, M., Krumpen, T., Casacuberta, N., Smethie, W., and Rember, R.: Radium Isotopes Across the Arctic Ocean Show Time Scales of Water Mass Ventilation and Increasing Shelf Inputs, Journal of Geophysical Research: Oceans, 0, doi:10.1029/2018JC013888, 2018.

Rutgers van der Loeff, M. M., and Berger, G. W.: Scavenging of $^{230}$Th and $^{231}$Pa near the Antarctic Polar Front in the South Atlantic, Deep-Sea Research 1, 40, 339-357, 1993.

Rutgers van der Loeff, M. M., Key, R. M., Scholten, J., Bauch, D., and Michel, A.: $^{228}$Ra as a tracer for shelf water in the Arctic Ocean, Deep-Sea Research II, 42, 1533-1553, 1995.

Scholten, J. C., Rutgers van der Loeff, M. M., and Michel, A.: Distribution of $^{230}$Th and $^{231}$Pa in the water column in relation to the ventilation of the deep Arctic basins, Deep-Sea Research II, 42, 1519-1531, 1995.

Schuur, E. A. G., Abbott, B. W., Bowden, W. B., Brovkin, V., Camill, P., Canadell, J. G., Chanton, J. P., Chapin, F. S., Christensen, T. R., Ciais, P., Crosby, B. T., Czimczik, C. I., Grosse, G., Harden, J., Hayes, D. J., Hugelius, G., Jastrow, J. D., Jones, J. B., Kleinen, T., Koven, C. D., Krinner, G., Kuhry, P., Lawrence, D. M., McGuire, A. D., Natali, S. M., O'Donnell, J. A., Ping, C. L., Riley, W. J., Rinke, A., Romanovsky, V. E., Sannel, A. B. K., Schädel, C., Schaefer, K., Sky, J., Subin, Z. M., Tarnocai, C., Turetsky, M. R., Waldrop, M. P., Walter Anthony, K. M., Wickland, K. P., Wilson, C. J., and Zimov, S. A.:

Expert assessment of vulnerability of permafrost carbon to climate change, Climatic Change, 119, 359-374, 10.1007/s10584-013-0730-7, 2013.

Schuur, E. A. G., McGuire, A. D., Schädel, C., Grosse, G., Harden, W. J., Hayes, D. J., Hugelius, G., Koven, C. D., Kuhry, P., Lawrence, D. M., Natali, S. M., Olefeldt, D., Romanovsky, V. E., Schaefer, K., Turetsky, M. R., Treat, C. C., and Vonk, J. E.: Climate change and the permafrost carbon feedback, Nature, 520, 171-179, 2015.

Serreze, M. C., and Stroeve, J.: Arctic sea ice trends, variability and implications for seasonal ice forecasting, Philosophical Transactions of the Royal Society A: Mathematical, Physical and Engineering Sciences, 373, 10.1098/rsta.2014.0159, 2015.

Serreze, M. C., Stroeve, J., Barrett, A. P., and Boisvert, L. N.: Summer atmospheric circulation anomalies over the Arctic Ocean and their influences on September sea ice extent: A cautionary tale, Journal of Geophysical Research: Atmospheres, 121, 11,463-411,485, doi:10.1002/2016JD025161, 2016.

Shen, C.-C., Cheng, H., Edwards, R. L., Moran, S. B., Edmonds, H. N., Hoff, J. A., and Thomas, R. B.: Measurement of Attogram Quantities of $^{231}$Pa in Dissolved and Particulate Fractions of Seawater by Isotope Dilution Thermal Ionization Mass Spectroscopy, Analytical Chemistry, 75, 1075-1079, 10.1021/ac026247r, 2003.

Slagter, H. A., Reader, H. E., Rijkenberg, M. J. A., Rutgers van der Loeff, M., de Baar, H. J. W., and Gerringa, L. J. A.: Organic Fe speciation in the Eurasian Basins of the Arctic Ocean and its relation to terrestrial DOM, Marine Chemistry, 197, 11-25, https://doi.org/10.1016/j.marchem.2017.10.005, 2017.

Swift, J. (2006): Physical oceanography at CTD station AOS94/35-1. Scripps Institution of Oceanography, UC San Diego, PANGAEA, https://doi.org/10.1594/PANGAEA.476073

Swift, J. (2006): Physical oceanography at CTD station AOS94/25-1. Scripps Institution of Oceanography, UC San Diego, PANGAEA, https://doi.org/10.1594/PANGAEA.476051

Tanhua, T., Jones, E. P., Jeansson, E., Jutterström, S., Smethie, W. M., Wallace, D. W. R., and Anderson, L. G.: Ventilation of the Arctic Ocean: Mean ages and inventories of anthropogenic CO2 and CFC-11, Journal of Geophysical Research: Oceans, 114, n/a-n/a, 10.1029/2008JC004868, 2009.

Trimble, S. M., Baskaran, M., and Porcelli, D.: Scavenging of thorium isotopes in the Canada Basin of the Arctic Ocean, Earth and Planetary Science Letters, 222, 915-932, 2004.

Ulfsbo, A., Cassar, N., Korhonen, M., van Heuven, S., Hoppema, M., Kattner, G., and Anderson, L. G.: Late summer net community production in the central Arctic Ocean using multiple approaches, Global Biogeochemical Cycles, 28, 1129-1148, 10.1002/2014GB004833, 2014.

Ulfsbo, A., Jones, E. M., Casacuberta, N., Korhonen, M., Rabe, B., Karcher, M., and van Heuven, S. M. A. C.: Rapid changes in anthropogenic carbon storage and ocean acidification in the intermediate layers of the Eurasian Arctic Ocean: 1996-2015, Global Biogeochemical Cycles, 0, doi:10.1029/2017GB005738, 2018.

Valk, O., Rutgers van der Loeff, M. M., Geibert, W., Gdaniec, S., Rijkenberg, M. J. A., Moran, S. B., Lepore, K., Edwards, R. L., Lu, Y., and Puigcorbé, V.: Importance of Hydrothermal Vents in Scavenging Removal of $^{230}$Th in the Nansen Basin, Geophysical Research Letters, 0, doi:10.1029/2018GL079829, 2018.

Vieira, L. H., Achterberg, E. P., Scholten, J., Beck, A. J., Liebetrau, V., Mills, M. M., and Arrigo, K. R.: Benthic fluxes of trace metals in the Chukchi Sea and their transport into the Arctic Ocean, Marine Chemistry, https://doi.org/10.1016/j.marchem.2018.11.001, 2018.

Vogler, S., Scholten, J., Rutgers van der Loeff, M., and Mangini, A.: $^{230}$Th in the eastern North Atlantic: the importance of water mass ventilation in the balance of $^{230}$Th, Earth and Planetary Science Letters, 156, 61-74, http://dx.doi.org/10.1016/S0012-821X(98)00011-9, 1998.

Wang, Q., Wekerle, C., Danilov, S., Koldunov, N., Sidorenko, D., Sein, D., Rabe, B., and Jung, T.: Arctic Sea Ice Decline Significantly Contributed to the Unprecedented Liquid Freshwater Accumulation in the Beaufort Gyre of the Arctic Ocean, Geophysical Research Letters, 45, 4956-4964, doi:10.1029/2018GL077901, 2018.

Wheeler, P. A., Watkins, J. M., and Hansing, R. L.: Nutrients, organic carbon and organic nitrogen in the upper water column of the Arctic Ocean: implications for the sources of dissolved organic carbon, Deep Sea Research Part II: Topical Studies in Oceanography, 44, 1571-1592, http://dx.doi.org/10.1016/S0967-0645(97)00051-9, 1997.

Worthington, L. V.: Oceanographic results of project Skijump I and Skijump II in the Polar Sea, 1951–1952, Eos, Transactions American Geophysical Union, 34, 543-551, 10.1029/TR034i004p00543, 1953.

# CHAPTER 4: Short-Term vs. Long-Term Removal Processes of dissolved $^{230}$Th and $^{231}$Pa in the Eurasian Basin

**Ole Valk[1], Michiel M. Rutgers van der Loeff[1], Walter Geibert[1], Sandra Gdaniec[2], S. Bradley Moran[4], Kate Lepore[5], Richard Lawrence Edwards[6], Yandbin Lu[7], Ingrid Stimac[1], Ronja Paffrath[8]**

[1]Alfred-Wegener-Institute Helmholtz Centre for Polar and Marine Research, 27570 Bremerhaven, Germany

[2]Stockholm University, Department of Geological Sciences, 106 91, Stockholm, Sweden

[3]Laboratoire des Sciences du Climat et de l'Environnement, LSCE/IPSL, CEA – CNRS – UVSQ, Université Paris-Saclay, 91191 Gif-sur-Yvette, France [4]College of Fisheries and Ocean Sciences,

[4]University of Alaska Fairbanks, Fairbanks, AK 99775, USA

[5]Mount Holyoke College, South Hadley, MA 01075, USA

[6]University of Minnesota, Minneapolis, MN 55455, USA

[7]Xi'an Jiaotong University, Beilin, Shaanxi 710000–710090, China

[8]Max Planck Research Group for Marine Isotope Geochemistry, Institute for Chemistry and Biology of the Marine Environment, University of Oldenburg, 26129, Oldenburg, Germany

**Keywords:**

- Dissolved $^{230}$Th and $^{231}$Pa budgets
- Variability of $^{230}$Th and $^{231}$Pa inventories
- Boundary scavenging of $^{230}$Th
- Increased $^{231}$Pa scavenging

Manuscript in preparation for submission to *Geochemistry, Geophysics, Geosystems*.

**Abstract**

The Arctic Ocean experiences changes in particle fluxes and particle composition, due to changing environmental conditions related to climate change. Particle reactive tracers $^{230}$Th and $^{231}$Pa can reveal consequences of these changes on scavenging behaviour and removal of particle reactive elements. Distribution and concentrations of dissolved $^{230}$Th and $^{231}$Pa can change significantly within less than ten years in the central Arctic Ocean. In this study we present new budgets for dissolved $^{230}$Th and $^{231}$Pa, as well as box models to illustrate scavenging removal and sedimentation patterns for these tracers, based on a water column time series from 1991 over 2007 to 2015. Based on GEOTRACES data we find indications for boundary scavenging of $^{230}$Th and partly $^{231}$Pa in the Eurasian Basin, contrasting previous studies. The conclusions of the models and their discussion are that $^{231}$Pa advective export from the Arctic Ocean might be less important than previously thought and that the margins of the Nansen Basin are a sink for Arctic $^{230}$Th and possibly $^{231}$Pa. While increased scavenging removal due to changing environmental conditions can be fully observed in the 2015 $^{230}$Th data, those developments are not yet visible in a dissolved $^{231}$Pa reduction, since changing $^{231}$Pa scavenging removal might be in an initial stage. Climate change triggered or intensified removal processes of $^{230}$Th and $^{231}$Pa in the Arctic Ocean cause reduced export of $^{230}$Th to the GIN Seas. Implications for sedimentary $^{231}$Pa/$^{230}$Th activity ratios in the Arctic or GIN Seas depend on the timescales and duration of the identified and hypothesised processes.

## 1. Introduction

### 1.1 $^{231}$Pa/$^{230}$Th in the Arctic Ocean

$^{235}$U and $^{234}$U are homogeneously distributed in seawater, their radioactive decay produces $^{231}$Pa and $^{230}$Th, respectively, at a constant ratio of 0.093. The $^{231}$Pa/$^{230}$Th sedimentary ratio is a well-known and frequently applied paleoceanographic tool. In addition to the age information it provides, it can serve as a proxy for particle fluxes and composition, biological productivity or overturning advective circulation (Chase *et al.*, 2002; Walter *et al.*, 1999; Yu *et al.*, 1996). In the Arctic Ocean, some studies have applied the $^{231}$Pa/$^{230}$Th sedimentary ratio for identifying basin wide fractionation (Moran *et al.*, 2005), boundary scavenging (Edmonds *et al.*, 2004), advective export in relation to the production of $^{230}$Th and $^{231}$Pa (Moran *et al.*, 2005), scavenging rates (Edmonds *et al.*, 2004) or past advective export (Hoffmann *et al.*, 2013). Open questions remain, such as why there is a $^{231}$Pa deficit in Arctic sediments (Gdaniec *et al.*, 2020; Moran *et al.*, 2005).

### 1.2 Increased Particle Fluxes at Margins and Boundary Scavenging

Previous $^{230}$Th and $^{231}$Pa budgets were primarily based on $^{231}$Pa/$^{230}$Th sedimentary ratios and production estimates (Hoffmann and McManus, 2007; Hoffmann *et al.*, 2013; Luo and Lippold, 2015; Moran *et al.*, 2005). These studies tried to the answer the question what the sedimentary ratio of $^{230}$Th/$^{231}$Pa reveals about boundary scavenging and circulation in the Arctic Ocean and the Nordic Seas. A major finding was that 39% of the in situ produced $^{231}$Pa are removed from the Arctic Ocean by advection through the Fram Strait, and 61% are removed by scavenging within the Arctic Ocean, while only 10% of the produced $^{230}$Th are exported by advection (Moran *et al.*, 2005). Huh *et al.* (1997) estimated that about one third of the $^{230}$Th produced in the Arctic Ocean was removed by scavenging within the central Arctic Ocean and two thirds at the margins. Therefore Moran *et al.* (2005) concluded that short ventilation times were responsible for the advection removal of $^{231}$Pa while $^{230}$Th was removed primarily at the margins by boundary scavenging. However, a new interpretation of the data of Huh *et al.* (1997) showed that there is no evidence for basin scale removal of $^{230}$Th to the margins by boundary scavenging (Hoffmann and McManus, 2007).

The margins of the Eurasian Basin (Nansen Basin slope and Barents Sea) experience increased particle fluxes, due to permafrost thawing (Günther *et al.*, 2013) and sea ice melt (Dalpadado *et al.*, 2020). It is expected that such changes are reflected in scavenging of $^{230}$Th and $^{231}$Pa. Scavenging of $^{230}$Th is elevated at the Nansen Basin slope relative to the central basins (Gdaniec *et al.*, 2020), probably due to increased mobilization of trace metals in Arctic shelves and slopes (Jensen *et al.*, 2020). Gdaniec *et al.* (2020) confirmed that boundary scavenging of $^{230}$Th does occur at the margins of the Eurasian Basin, and also concluded that the Barents Sea and the Nansen Basin margins can be a sink for the in-situ produced $^{231}$Pa amounts, assumed to be missing in Arctic deep-sea sediments. Similarly, there is evidence for increasing boundary scavenging along the margins of the Amerasian Basin of the Arctic Ocean, based on margin sedimentary $^{210}$Pb and $^{137}$Cs (Kuzyk *et al.*, 2013). Recent studies on $^{230}$Th and $^{231}$Pa in the Arctic Ocean water column (Gdaniec *et al.*, 2020; Grenier *et al.*, 2019; Valk *et al.*, 2020) indicate that the extent of boundary scavenging may not follow the sedimentary record used by Huh *et al.* (1997) and *Hoffmann and McManus*, 2007, but may indeed be changing. Therefore an important point in this study is discussing whether the observed scavenging behaviour of Th and Pa is in line with recent environmental changes in the Arctic Ocean. The $^{230}$Th, $^{231}$Pa scavenging removal models in this study will therefore be used to evaluate different boundary scavenging scenarios.

### 1.3 Aim of Paper

Time series of water column observations have shown that $^{230}$Th and $^{231}$Pa concentrations have changed significantly over decadal timescales. The water column inventory of $^{230}$Th decreased over the last three decades in the Eurasian Basin (Valk *et al.*, 2020; Valk *et al.*, 2018). Some changes were related to changing hydrothermal activities (Valk *et al.*, 2018) while others were related to climate change through increased particle fluxes at the margins (Gdaniec *et al.*, 2020; Valk *et al.*, 2020) or, in the Amerasian Basin, increased particle fluxes due to sea ice retreat and transport of shelf particles to the central basins (Grenier *et al.*, 2019; Yu *et al.*, 2020).

In this study we connect time series of water column observations from the Eurasian Basin as reported in Valk *et al.* (2018) and in Valk *et al.* (2020) to calculate inventories and inventory changes of dissolved $^{230}$Th and $^{231}$Pa in the various basins, in order to identify sources and sinks of these radionuclides and to determine regional budgets. As not all parts of the budgets are known, we consider two scenarios based on a simple box model to test the plausibility of different assumptions on the Arctic system. These scenarios then enable us to better predict the effect of a changing environment on the proxy record of the Eurasian Basin and the Greenland-Iceland and Norwegian Seas (GIN Seas).

## 2. Methods

### 2.1 $^{231}$Pa Analyses and Sampling

This section describes the sampling and analyses of unpublished dissolved $^{231}$Pa data in 2007 and 2015. Procedures for dissolved $^{230}$Th are described in published manuscripts (Gdaniec *et al.*, 2020; Grenier *et al.*, 2019; Valk *et al.*, 2020; Valk *et al.*, 2018).

#### 2.1.1 Dissolved $^{231}$Pa Sampling and Analyses in 2015

During Polarstern cruise PS94 (GEOTRACES Section GN04) sampling was performed according to the GEOTRACES standard methods (Anderson *et al.*, 2012). Sea water was filtrated directly from the 24 L Niskin®-bottles into pre-cleaned cuitainers (LDPE, 10 L >2000 m and 20 L <2000 m) using 0.45 µm pore size Acropaks®. Samples were acidified to a pH of 1.5-2 using concentrated double distilled $HNO_3$ and subsequently were sealed with Parafilm® in double plastic bags and stored until analyses.

Analyses were performed following GEOTRACES methods (*Anderson et al.*, 2012). Pre-concentration and analysis of dissolved $^{231}$Pa were performed following GEOTRACES methods (Anderson *et al.*, 2012) in the clean laboratories of the *Alfred-Wegener-Institute (AWI)*. Samples

were spiked with $^{229}$Th, $^{233}$Pa and $^{236}$U, calibrated against the reference standard material UREM11. Purified $FeCl_3$ was used added and after 24 h double-distilled $NH_4OH$ was added, to induce $Fe(OH)_3$ precipitation. 72 h later the precipitate was transferred from the cubitainers to acid cleaned 1 L Teflon® bottles. After dissolution of the sample in concentrated double distilled HCl, the pH was raised again to 8.5 and the $Fe(OH)_3$ precipitate was transferred into acid cleaned 50 mL Falcon® tubes. Samples then were washed in ultrapure Milli-Q® water four times by centrifuging (4000 rpm for 12 minutes) and decanting of the supernatant in between. Afterwards samples were dissolved in double distilled concentrated HCl and evaporated to >10 µL in an acid cleaned 15 mL Savillex® beakers. Pa, Th, U and Nd were separated using chromatographic columns filled with anion exchange resin (AG1X8, 100-200 mesh) according to GEOTRACES methods (Anderson *et al.*, 2012). All fractions were collected in acid cleaned 15 mL Savillex® beakers and columns were washed and conditioned before the samples were loaded onto the columns using double distilled concentrated HCl and $HNO_3$.

### 2.1.2 Dissolved $^{231}$Pa Sampling and Analyses in 2007

In 2007, during RV Polarstern expedition ARKXXII/2, water samples were collected along all transects of the cruise. Samples for total $^{231}$Pa and $^{230}$Th were collected at 6 stations, and samples for dissolved $^{231}$Pa and $^{230}$Th were collected at 9 stations. Stations were distributed across the basins and margins visited during ARKXXII/2 (figure 1). Samples were collected in volumes of 1L, 2L, and 10L and acidified with ultraclean concentrated $HNO_3$. Analyses were performed according to Shen *et al.* (2003). Measurements were done using a Finnigan MAT-262 equipped with an electron multiplier and a Retarding Potential Quadroupole (RPQ) energy filter (Shen *et al.*, 2003).

## 2.2 Budget Calculations and Results

Inventory calculations were performed for three time periods: the period until 1991, assumed to be in steady state; 1991-2007 and 2007-2015. These periods define the time which is referred to when later applying scenarios, which represent environmental settings. Dissolved $^{230}$Th data from the Nansen- and Amundsen Basin (2007 and 2015) were taken from (Valk *et al.*, 2020; Valk *et al.*, 2018), obtained during GEOTRACES cruises IPY11 and GN03. The 1991 data originate from Scholten *et al.* (1995). Dissolved $^{231}$Pa data from the Nansen- and Amundsen Basin (2007 and 2015) were obtained during the same cruises. 1991 $^{231}$Pa data are from (Scholten *et al.*, 1995). Dissolved $^{231}$Pa data from stations 32 and 50 are from Gdaniec *et al.* (2020). Volumes of the Nansen- and Amundsen Basin were calculated in a simplified way:

surface areas were defined, with the shelf-break serving as an outer boundary and the Gakkel Ridge as an internal one. An average depth of 4000 m was chosen and narrowing by the slopes ignored. The models are divided into three main boxes: the upper Eurasian Basin (<2000 m) (EUB), the deep Amundsen- (AB) and the deep Nansen Basin (NB) (>2000 m). The 2000 m depth division follows the deepest sill of the Lomonosov Ridge, separating the Amerasian- and Eurasian Basin, preventing exchange between the two major basins below ~1870 m (Björk *et al.*, 2007), while waters above can exchange freely (Rudels, 2009). Furthermore hydrothermal scavenging of $^{230}$Th was only detected below 2000 m (Valk *et al.*, 2018), while direct consequences of $^{230}$Th depleted inflowing waters were observed above (Valk *et al.*, 2020). Different $^{230}$Th developments in the deep Nansen- and Amundsen Basin (Valk *et al.*, 2020; Valk *et al.*, 2018), as well as a restriction of the hydrothermal plume to the Nansen Basin, due to recirculation in the deep Nansen Basin (Valk *et al.*, 2018), indicate that the deep basins can be seen as isolated, in a simplified illustration of the Eurasian Basin.

Calculating a budget requires the sources and sink terms, hence quantification of in- and outflow. As inflowing $^{230}$Th and $^{231}$Pa concentrations we chose average North Atlantic concentrations in 0-500 m water depth for the Barents Sea inflow ($^{230}$Th: 2.80 fg/kg, $^{231}$Pa: 0.70 fg/kg) and average concentrations down to 2000 m for the Fram Strait inflow ($^{230}$Th: 8.65 fg/kg, $^{231}$Pa: 2.35 fg/kg) (Hayes *et al.*, 2015). Outflow concentrations are dissolved $^{230}$Th and $^{231}$Pa concentrations above 2000 m from the respective time periods from the central Amundsen Basin. This outflow is expected to represent the Eurasian Basin outflow out of the Arctic Ocean.

Water fluxes are 1.5 Sv for the Barents Sea inflow ($BS_{in}$), 6.7 Sv for the Fram Strait inflow ($FS_{in}$) and 8.2 Sv for the Fram Strait outflow ($FS_{out}$) (Beszczynska-Möller *et al.*, 2012). Exchange through both the Canadian Archipelago and the Bering Strait were neglected, due to low volumes and lack of data. These exchanges are limited to shallow waters. Surface concentrations of $^{230}$Th and $^{231}$Pa are much lower than in deep waters (Nozaki *et al.*, 1981), hence these straits do not affect the budgets significantly. In- and outflow $^{230}$Th and $^{231}$Pa concentrations converted to total fluxes in kg/y are shown in table 1. Another source is the in-situ production (ISP) of dissolved $^{230}$Th and $^{231}$Pa. It was calculated (in dpm/m$^3$/y) using the U-Salinity relationship in seawater ($^{238}$U = (0.100 x S − 0.326), (Owens *et al.*, 2011) and adapted to the respective Volumes (V). Salinities are from Rabe *et al.* (2016) and Wisotzki (2008):

$$ISP\ ^{230}Th: \qquad {}^{238}U \times \lambda_{234} \times \frac{^{234}U}{^{238}U_{Seawater}} \times V$$

*($^{234}U/^{238}U_{Seawater}$ = 6.26 x 10$^{-5}$ (mol/mol) (Andersen et al., 2010))*

$$ISP\ ^{231}Pa: \quad {}^{238}U \times \lambda_{235} \times \frac{^{235}U}{^{238}U} \times {}_{Natural} \times V$$

*($^{235}U/^{238}U_{Natural}$= 1/137.88 (mol/mol) (Condon et al., 2010))*

Where $\lambda_{234}$ and $\lambda_{235}$ are the decay constants of $^{234}$U and $^{235}$U: 2.79$^{-6}$ (y$^{-1}$) and 9.72$^{-10}$ (y$^{-1}$), respectively.

### 2.2.1 Description of the Budget Box Model

The basis for the $^{230}$Th and $^{231}$Pa scavenging removal calculations are concentration changes between the sampling years (1991, 2007 and 2015), given as inventory changes, shown in figure 1 and summarized in table 1. Concentrations were summed up in average concentrations per basin and depth range. Inventory changes are:

$$Eq.1: Inventory\ changes = Inventory\ period\ A - Inventory\ period\ B$$

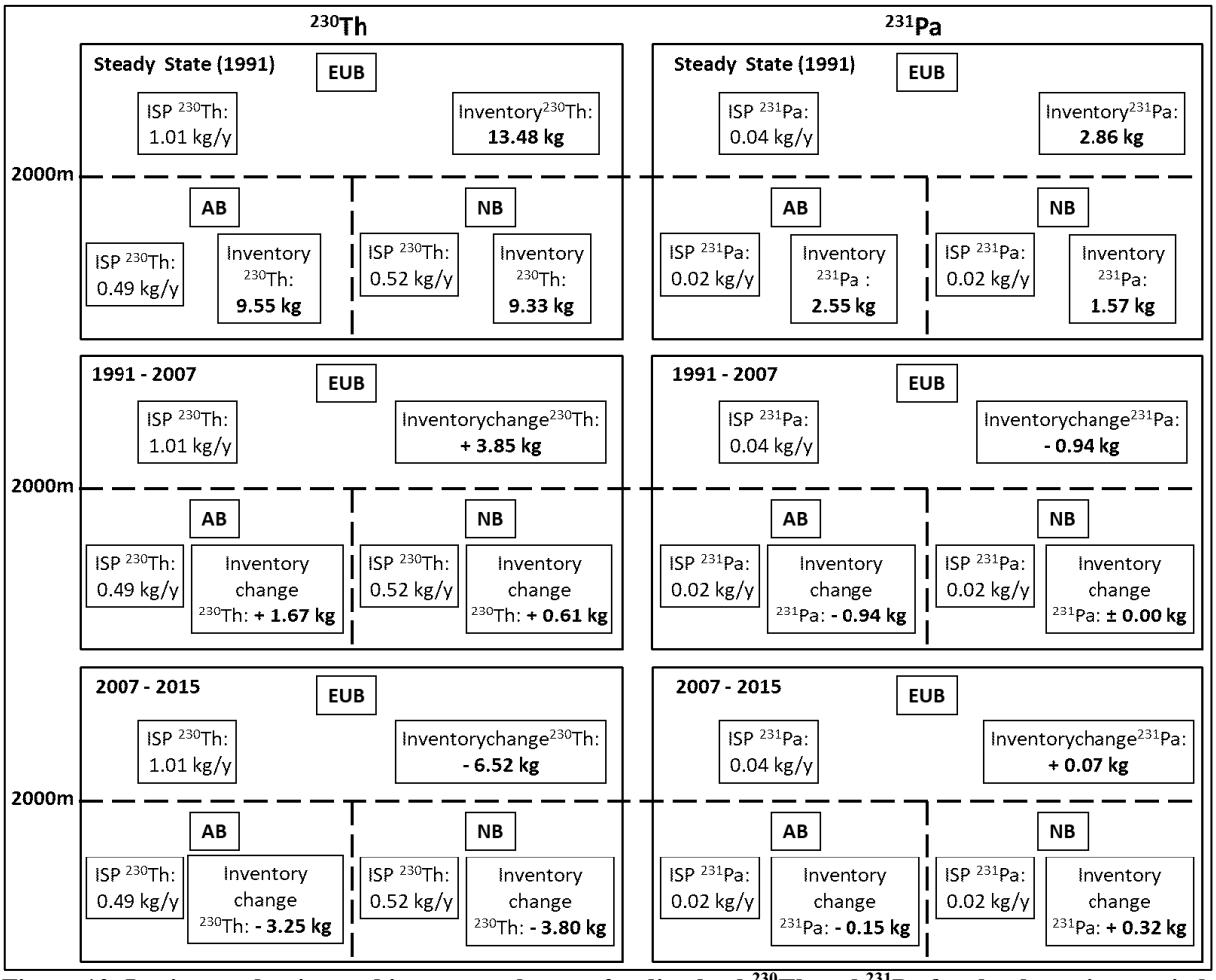


**Figure 10: In-situ production and inventory changes for dissolved $^{230}$Th and $^{231}$Pa for the three time periods.**

### 2.2.2 Total $^{230}$Th Removal Rates and Locations

The total removal rate of $^{230}$Th has increased over time. In the upper Eurasian Basin (<2000 m) the dissolved $^{230}$Th inventory decreased by - 6.52 kg (- 0.82 kg/y) between 2007 and 2015 (figure 1). From 1991 to 2015 dissolved $^{230}$Th removal doubled, with an intermediate reduction of removal from 1991-2007 and then increased threefold from 2007 to 2015.Removal rates of dissolved $^{230}$Th and $^{231}$Pa, as well as underlying data for the calculations are summarized in table 1.

Volumes of shelf waters are small compared to the volume of the central Eurasian Basin, even when restricting it to 2000 m depth. Furthermore there is no evidence in the sedimentary record for any appreciable boundary scavenging in the Arctic Ocean (Hoffmann and McManus, 2007). Hence the obvious area of $^{230}$Th removal is within the deep basins. This scavenging removal situation is represented by a box model where all of the $^{230}$Th scavenging removal happens within the central basins. This setting, **scenario-a,** is applied to all time periods, steady state, 1991-2007 and 2007-2015. **Scenario-a** requires a large or even dramatic change in scavenging flux in the central basin. However no direct evidence for the increased particle fluxes or concentrations, that could explain the dissolved $^{230}$Th decrease after 2007, were observed in the Amundsen Basin and particle fluxes are expected to be similar to previous years (Valk *et al.*, 2020).

Additionally no increase of ventilation times after 2007 is evident from circulation and ventilation tracers such as CFCs (Smethie, 2017) and $^{129}$I/$^{236}$U (Casacuberta *et al.*, 2018) in the Eurasian Basin. Hence the depletion of dissolved $^{230}$Th after 2007 is most likely due to mixing with inflowing Atlantic waters that have lost a significant part of dissolved $^{230}$Th while traveling along the Nansen Basin margin and through the Barents Sea. In these areas increased particle fluxes are expected due to permafrost thawing (Günther *et al.*, 2013) induced increasing terrestrial input to the Arctic Ocean (Schuur *et al.*, 2013; Schuur *et al.*, 2015) and sea ice melt triggered release of particulate matter to the water column (Arrigo *et al.*, 2008; Boetius *et al.*, 2013; Dalpadado *et al.*, 2020). Especially in the Barents Sea long term observations show that decreasing sea ice cover prolongs the growing season and increases the annual NPP since the late 1990s (Dalpadado *et al.*, 2020).

Increasing release of Fe and Mn from the shelves leads to increased scavenging of other trace metals throughout the water column, due to the mobilization of these redox-sensitive metals (Jensen *et al.*, 2020). At the Nansen Basin margin particles contain Fe-rich particles or aggregates, which are effective $^{230}$Th scavengers (Geibert and Usbeck, 2003; Pavia *et al.*, 2018),

indicated by relatively high dFe values (Rijkenberg *et al.*, 2018). High particulate $^{230}$Th and $^{232}$Th values close to Svalbard (Gdaniec *et al.*, 2020) indicate particles transported by glacier and coastal erosion causing $^{230}$Th scavenging. Elevated particulate $^{232}$Th concentrations at the Nansen Basin slope (Gdaniec *et al.*, 2020), indicate $^{230}$Th scavenging removal by particles from Barents Sea or resuspended slope sediments along the Fram Strait inflow passage. Figure 2 shows a transmission section rom the Barents Sea shelf to the central Nansen Basin (Gardner *et al.*, 2020), where elevated particle freight above 2000 m is visible close to the slopes of the Nansen Basin.

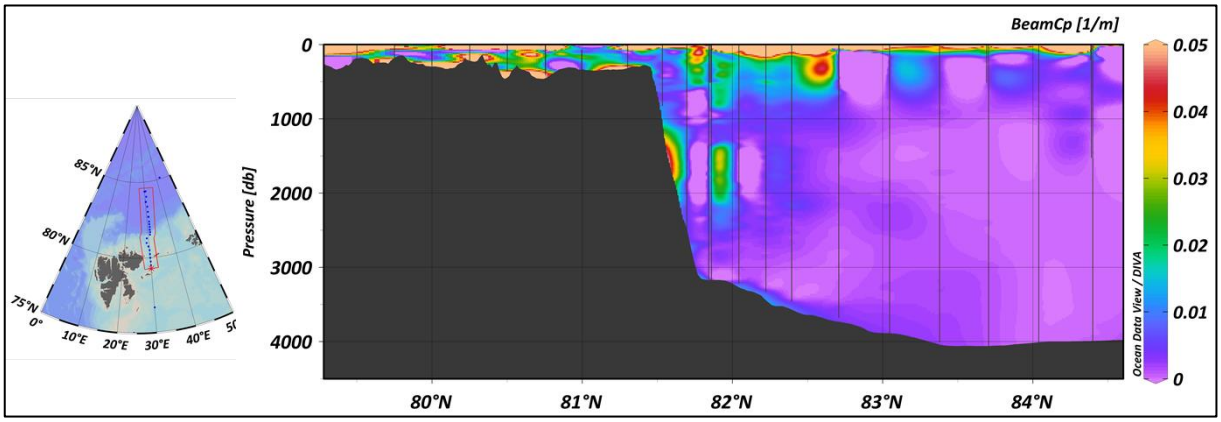


**Figure 2: Beam attenuation section from the Barents Sea shelf to the central Nansen Basin from PS94 (2015) (Gardner *et al.*, 2020). The figure was created using Ocean Data View® (Schlitzer, 2016).**

Therefore Valk *et al.* (2020) argued that the decrease of dissolved $^{230}$Th in the central Amundsen Basin is due to mixing with $^{230}$Th depleted waters, after undergoing increased scavenging removal at the inflow pathways of Atlantic Waters. Since no increased scavenging removal within the central basin is evident, removal must have occurred along the inflow passages of Atlantic Waters, the Barents Sea and along the Nansen Basin margin, referred to as removal on the margins. Therefore, we propose a second scenario for the 2007-2015 period, **scenario-b**. **Scenario-b** shall represent a climate change influenced "modern" scavenging removal situation assuming that boundary scavenging of $^{230}$Th occurs in the Eurasian Basin (Costa *et al.*, 2020; Gdaniec *et al.*, 2020). In **scenario-b** vertical particle fluxes to the deep basins are assumed to be similar to the 1991-2007 period, and the associated radionuclide scavenging flux was consequently derived from the flux in the 1991-2007 period, reduced by the factor of the inventory decrease above 2000 m between 1991-2007 and 2007-2015 (- 38%).The underlying assumptions of **scenario-b** are increasing particle fluxes at the margins, as stated above, as well as a potential increase of exchange between the margins and the central basin, explained in the following. It is possible that the exchange between the central basins and the margins changes over time. The Arctic Oceans' wind driven surface circulation is controlled by the stages of the

Arctic Ocean Oscillation Index (AOOI) (Dukhovskoy *et al.*, 2004; Proshutinsky and Johnson, 1997; Proshutinsky *et al.*, 1999). The AOOI decides whether the Arctic Ocean is dominated by Cyclonic- (CCR) or Anti-Cyclonic (ACCR) circulation regimes (Proshutinsky *et al.*, 2015). Since 1997 the AOOI is in a positive (ACCR) stage. Surface waters flow southwards along the Barents Sea shelf break in ACCR stages (Dukhovskoy *et al.*, 2006). Additionally upwelling of interior basin waters (ca. down to 500 m) to the shelves, during ACCR stages (Proshutinsky and Johnson, 1997; Randelhoff and Sundfjord, 2017) might contribute to an $^{230}$Th decrease when these waters undergo scavenging removal while creeping up the slopes. The intensity of FSBW flow through the St. Anna trough into the Kara/Barents Sea and back is also increased in ACCR phases (Lind and Ingvaldsen, 2012). All of this could contribute to enhanced boundary scavenging in ACCR phases, or even to the establishment of it. **Scenario-b** contains a boundary scavenging component in contrast to **scenario-a.**

### 2.2.3 Scavenging Removal and Sedimentation Calculations: Scenario-a

#### 2.2.3.1 Steady State Period

Boxes without volume and ISP for the Barents Sea the Nansen Basin margin illustrating scavenging removal before waters enter the Eurasian Basin, were added to the model. Scavenging removal in the upper 2000 m of the Eurasian Basin must balance in- and outflow and ISP:

$$Eq.2: Scavenging\ Removal\ EUB = ISP(EUB < 2000m) + FS_{in} + BS_{in} - FS_{out}$$

This scavenging removal is divided into two fractions. One is transported vertically to the deep basins. The other fraction is removed at the margins. **Scenario-a** represents a no boundary scavenging setting, following Hoffmann and McManus (2007). In **scenario-a** 100% of $^{230}$Th scavenging removal in the Eurasian Basin occurs within the central basin and 0% at the margins. The fraction that goes to the deep part of each basin (scavenging removal in figure 3) is half of the EUB scavenging removal adapted by the fraction assumed to be scavenged within each basin. For $^{230}$Th, the Amundsen- and Nansen Basin fractions, *fAB* and *fNB*, were calculated assuming that the particulate vertical nuclide flux at 2000 m is proportional to the dissolved concentration at 2000 m:

$$fNB = \frac{conc.^{230}Th_{2000m}(NB)}{conc.^{230}Th_{2000m}(AB + NB)}$$

$$fAB = \frac{conc.^{230}Th_{2000m}(AB)}{conc.^{230}Th_{2000m}(AB + NB)}$$

$^{231}$Pa was treated the same way. The flux to the deep parts of each basin is:

$$Eq.3: Flux\ to\ deep(NB) = \frac{Scavenging\ Removal\ EUB}{2}\ x\ 1.0\ x\ fNB$$

$$Eq.3.1: Flux\ to\ deep(AB) = \frac{Scavenging\ Removal\ EUB}{2}\ x\ 1.0\ x\ fAB$$

For the deep NB and AB (>2000 m) we estimate that all of the dissolved $^{230}$Th and $^{231}$Pa produced in these boxes is scavenged and removed there, assuming that lateral exchange with the Atlantic Ocean or the margins at this depth is negligible. ISP (> 2000 m) plus the flux from above 2000 m yields the amount of $^{230}$Th and $^{231}$Pa buried in deep basin sediments:

$$Eq.4: deep\ central\ (NB) sedimentation\ = ISP(NB > 2000m) + Flux\ to\ deep(NB)$$

$$Eq.4.1: deep\ central\ (AB) sedimentation = ISP(AB > 2000m) + Flux\ to\ deep(AB)$$

Figure 3 shows $^{230}$Th and $^{231}$Pa steady state box models under **scenario-a.** The net sum of scavenging removal from inflowing waters and scavenging removal by exchange between the central Eurasian Basin and the margin is given as “Net inflow and scavenging removal margin exchange flux”.

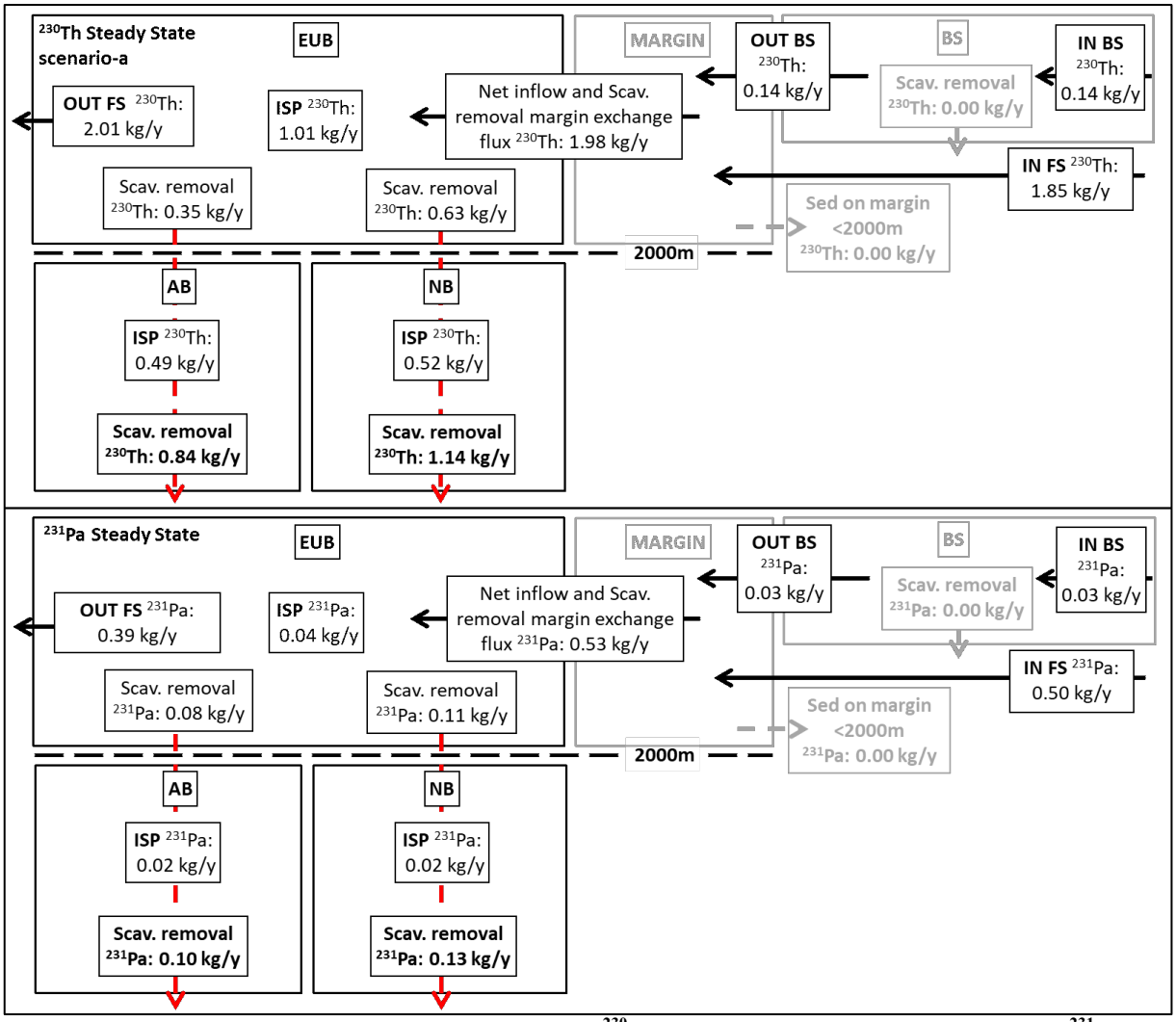


**Figure 3: Box model for the steady state situation for $^{230}$Th under scenario-a (upper panel) and $^{231}$Pa (lower panel) in the Eurasian Basin. Red arrows indicate scavenging removal or sedimentation fluxes, black arrows indicate net transport. Sed. = sedimentation, scav. = scavenging, FS = Fram Strait.**

### 2.2.3.2 1991-2007 Period:

Dissolved $^{230}$Th inventory changes (figure 1) are calculated using *Eq.1* and yield an increase of + 3.85 kg in the EUB (<2000 m), an increase of + 0.61 kg in the deep NB (>2000 m) and an increase of +1.67 kg in the AB (>2000 m). Dissolved $^{231}$Pa decreased in the entire Eurasian Basin except in the deep Nansen Basin. Scavenging removal of dissolved $^{230}$Th and $^{231}$Pa from the upper EUB is calculated after *Eq.2*, including the inventory change:

$$Eq.5: Scavenging\ Removal\ EUB(91-07) = ISP(NB > 2000m) + FS_{in} + BS_{in} - FS_{out} + Inventorychange(91-07)$$

The inclusion of the inventory change also applies to the deep basin scavenging removal where sedimentation is:

$$Eq.\,6\text{: }deep\ central\ (NB)\ sedimentation = ISP(NB > 2000m) + Flux\ to\ deep(NB) + Inventorychange(91-07)$$

$$Eq.\,6.1\text{: }deep\ central\ (AB)\ sedimentation = ISP(AB > 2000m) + Flux\ to\ deep(AB) + Inventorychange(91-07)$$

Fluxes from the EUB (<2000 m) to the deep basins are calculated similarly to the steady state situation using the fractionation factor for the 1991-2007 period, *fAB91-07* and *fNB91-07*. All other scavenging removal and sedimentation fluxes are calculated as for the steady state. Figure 4 shows the $^{230}$Th and $^{231}$Pa box models for 1991-2007.

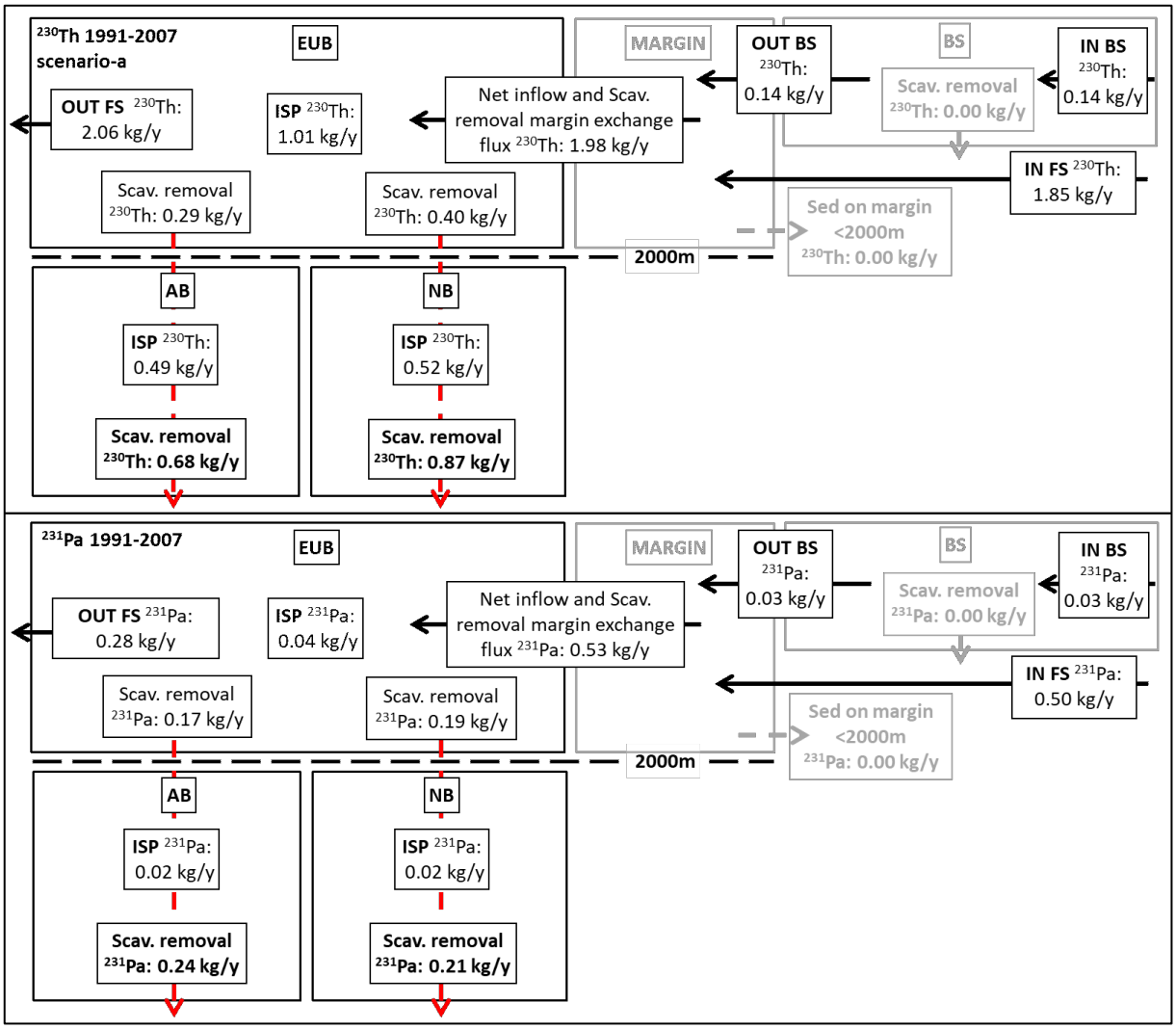


**Figure 4: Box model for the 1991-2007 situation for $^{230}$Th under scenario-a (upper panel) and $^{231}$Pa (lower panel) in the Eurasian Basin. Red arrows indicate scavenging removal or sedimentation fluxes, black arrows indicate net transport. Sed. = sedimentation, scav. = scavenging, FS = Fram Strait.**

### 2.2.3.3 2007-2015 Period:

Between 2007 and 2015 dissolved $^{230}$Th decreased significantly in the Eurasian Basin (figure 1) above and below 2000 m. Dissolved $^{231}$Pa increased marginally above 2000 m and decreased in the deep Amundsen Basin, while it increased in the deep Nansen Basin between 2007 and 2015. Figure 5 shows the $^{230}$Th and $^{231}$Pa box model.

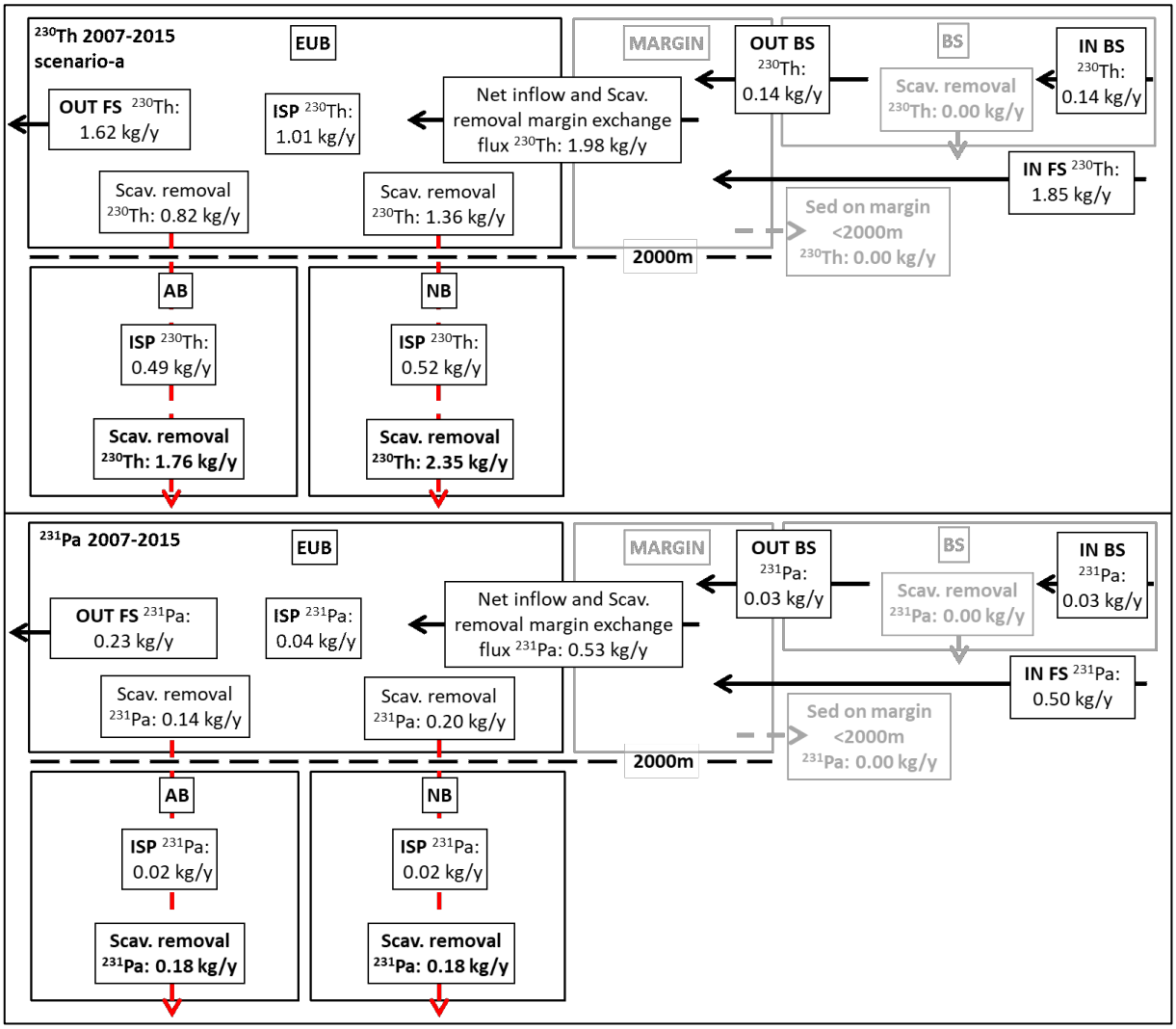


**Figure 5: Box model for the 2007-2015 situation for $^{230}$Th under scenario-a (upper panel) and $^{231}$Pa (lower panel) in the Eurasian Basin. Red arrows indicate scavenging removal or sedimentation fluxes, black arrows indicate net transport. Sed. = sedimentation, scav. = scavenging, FS = Fram Strait.**

**Table 1: Summary of data used in the models and calculated removal rates of dissolved $^{230}$Th and $^{231}$Pa in the upper 2000 m. $^{230}$Th, $^{231}$Pa data in inflow are from Hayes *et al.* (2015), water fluxes are from Beszczynska-Möller *et al.* (2012), 1991(steady state) $^{231}$Pa and $^{230}$Th are from Scholten *et al.* (1995).**

| | period | Inventory | change since previous | $BS_{in}$ | $FS_{in}$ | $FS_{out}$ | ISP | removal rate since previous |
|---|---|---|---|---|---|---|---|---|
| | | kg | kg/y | kg/y | kg/y | kg/y | kg/y | kg/y |
| $^{230}$Th | **Steady State** | 13.48 | 0.00 | 0.14 | 1.85 | 2.01 | 1.01 | **0.98** |
| | **1991-2007** | 17.35 | 0.24 | 0.14 | 1.85 | 2.06 | 1.01 | **0.69** |
| | **2007-2015** | 10.81 | -0.82 | 0.14 | 1.85 | 1.62 | 1.01 | **2.18** |
| $^{231}$Pa | **Steady State** | 2.86 | 0.00 | 0.03 | 0.50 | 0.39 | 0.04 | **0.19** |
| | **1991-2007** | 1.92 | -0.06 | 0.03 | 0.50 | 0.28 | 0.04 | **0.36** |
| | **2007-2015** | 1.99 | 0.01 | 0.03 | 0.50 | 0.23 | 0.04 | **0.34** |

### 2.2.3.4 Scavenging Removal and Sedimentation in 2007-2015: Scenario-b

In **scenario-b** we calculated the basin/margin scavenging removal ratio that yields vertical fluxes from the EUB (<2000 m) to the deep basins similar to the 1991-2007 period, only changed by the inventory change above 2000 m (- 38%). Distribution of dissolved $^{230}$Th between the NB and the AB above 2000 m has shifted towards the Nansen Basin in 2015 from a ~50/50 distribution in 1991 and 2007. The vertical flux in the AB serves a reference for these adapted fluxes in **scenario-b,** as the effects of increased margin scavenging and the lack of increased particle fluxes in the central basin was mainly described for the Amundsen Basin (Valk *et al.*, 2020). Under these assumptions the margin scavenging fraction during 2007-2015 must have been 78% to achieve a vertical flux from 1991-2007 reduced by ~38%. Therefore a basin/margin scavenging ratio of 78%/22% was applied, causing a reduction of vertical $^{230}$Th fluxes by - 38% in the AB and - 25% in the NB. Vertical fluxes to the deep basins under **scenario-b** are:

$$Eq.7: Flux\ to\ deep\ (NB) = \frac{Scavenging\ Removal\ EUB}{2}\ x\ 0.22\ x\ fNB15$$

$$Eq.7.1: Flux\ to\ deep\ (AB) = \frac{Scavenging\ Removal\ EUB}{2}\ x\ 0.22\ x\ fAB15$$

The fraction that is buried in margin and shelf sediments is:

$$Eq.8: Flux\ to\ margin\ = Scavenging\ Removal\ EUB - Flux\ to\ deep(AB + NB)$$

This flux is further divided into a Nansen Basin margin and a Barents Sea fraction, using the relation of inflowing water volumes (V) ($FS_{in}$ and $BS_{in}$) and applying $^{230}Th_{(p/d)}$ ratios, the ratio between particulate and dissolved $^{230}$Th, from the NB margin and the BS from 2015 (Gdaniec *et al.*, 2020), in order to precise scavenging removal areas for dissolved $^{230}$Th, called $fNB_{margin}$ and *fBS*. For $^{231}$Pa we assume no margin scavenging.

$$Eq.9: Flux\ to\ NB_{margin} = flux\ to\ margin\ x\ fNB_{margin}\ x\ V\ \frac{FS_{in}}{FS_{in} + BS_{in}}$$

$$Eq.9.1: Flux\ to\ BS = flux\ to\ margin\ x\ fBS\ x\ V\ \frac{BS_{in}}{FS_{in} + BS_{in}}$$

Both are the amounts of $^{230}$Th removed from inflowing waters, shown in figure 3 as scavenging removal and sedimentation in the BS and the margin box. **Scenario-b** is illustrated in figure 6. Table 2 summarises basin/margin scavenging estimates, as well as scavenging removal and sedimentation fluxes for both scenarios.

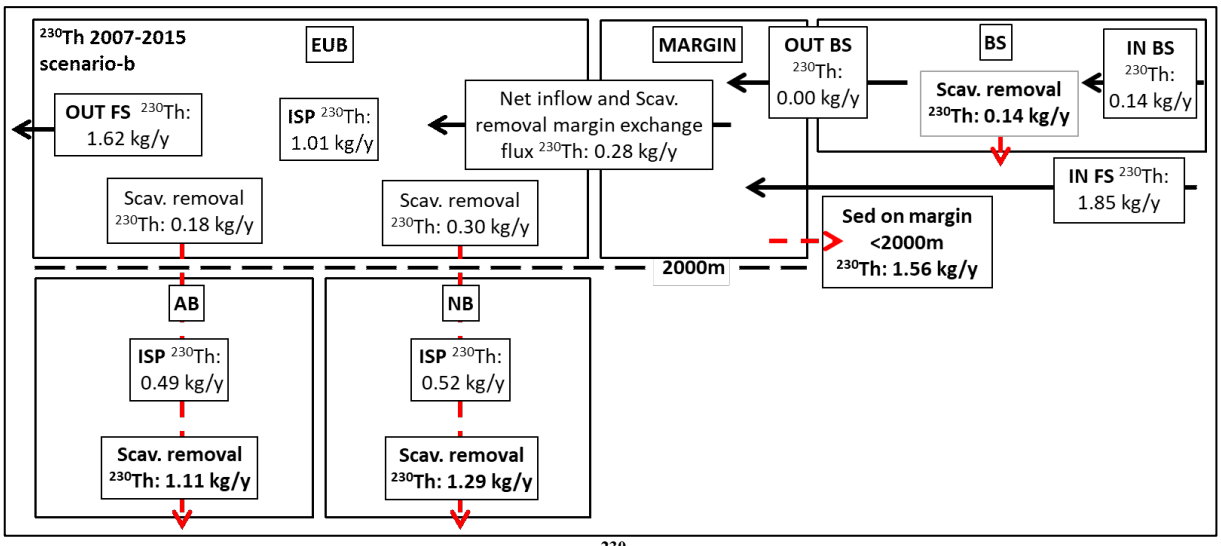


**Figure 6: Box model for the 2007-2015 situation of $^{230}$Th under scenario-b. Red arrows indicate scavenging removal or sedimentation fluxes, black arrows indicate net transport. Sed. = sedimentation, scav. = scavenging, FS = Fram Strait.**

**Table 2: Basin/margin percental scavenging removal ratios, scavenging removal and sedimentation fluxes for dissolved $^{230}$Th and $^{231}$Pa.**

| | period | scenario | basin/margin scavenging removal | vertical flux EUB at 2000m | | $^{230}$Th shelf/slope sedimentation | | $^{230}$Th deep sedimentation | |
|---|---|---|---|---|---|---|---|---|---|
| | | | | NB | AB | BS | $NB_{margin}$ | NB | AB |
| | | | % | kg/y | kg/y | kg/y | kg/y | kg/y | kg/y |
| $^{230}$Th | Steady state | a | 100/0 | 0.63 | 0.35 | 0.00 | 0.00 | **1.14** | **0.84** |
| | 1991-2007 | a | 100/0 | 0.40 | 0.29 | 0.00 | 0.00 | **0.87** | **0.68** |
| | 2007-2015 | a | 100/0 | 1.36 | 0.82 | 0.00 | 0.00 | **2.35** | **1.76** |
| | 2007-2015 | b | 22/78 | 0.30 | 0.18 | 0.14 | 1.56 | **1.29** | **1.11** |
| $^{231}$Pa | Steady state | a | 100/0 | 0.11 | 0.08 | 0.00 | 0.00 | **0.11** | **0.08** |
| | 1991-2007 | a | 100/0 | 0.19 | 0.17 | 0.00 | 0.00 | **0.19** | **0.17** |
| | 2007-2015 | a | 100/0 | 0.20 | 0.14 | 0.00 | 0.00 | **0.20** | **0.14** |

## 3. Discussion

### 3.1. Scenario Discussion

#### 3.1.1 Factors controlling $^{230}$Th Scavenging Removal

$^{230}$Th inventories can change on decadal time scales or even less in the central Arctic Ocean. Especially in the Eurasian Basin inventories decreased by up to 40% within only 8 years, e.g. in the deep Nansen Basin (Grenier *et al.*, 2019; Valk *et al.*, 2020; Valk *et al.*, 2018). Different processes are responsible for inventory changes in different parts of the Eurasian Basin, from hydrothermal scavenging in the deep Nansen Basin (Valk *et al.*, 2018), over inflow scavenging removal affecting the central Amundsen Basin above 2000 m to the consequence from the latter for deep waters by reversible scavenging (Valk *et al.*, 2020). Hence climate changes as well as seismic processes change concentrations and distributions of dissolved $^{230}$Th rapidly in the Eurasian Basin. The in our calculations fixed amounts of $^{230}$Th and $^{231}$Pa entering the Arctic partly control how much $^{230}$Th and $^{231}$Pa is removed per year in the EUB (0-2000 m). The most decisive factor in terms of where scavenging removal occurs in our scenarios is the basin/margin scavenging removal variable that decides if removal occurs in the central basins or at the margins, expressed as a relative fraction. In **scenario-a**, all removal takes place in the deep basins. In **scenario-b** a large fraction of $^{230}$Th scavenging removal occurs at the margins. Part of this margin removal is in fact scavenging in inflowing waters on the margins, as discussed in Valk *et al.* (2020), because waters trespass an area and undergo scavenging removal, but do not pass there again, as in the Barents Sea. But especially in the FSBW, removal in the inflow and removal related to basin-margin exchange cannot be distinguished, implying that **scenario-b** includes actual boundary scavenging.

#### 3.1.2 Scenarios vs. Reality

It is an ongoing discussion to which extent $^{230}$Th is subject to boundary scavenging in the Arctic Ocean. The two scenarios were introduced to investigate what boundary conditions are actually compatible with the observed spatial and temporal structure of the particle-reactive radionuclides $^{230}$Th and $^{231}$Pa. **Scenario-a** is based on the assumption that no boundary scavenging occurs in the Arctic Ocean (Hoffmann and McManus, 2007), contradicting the assumption that 62% of $^{230}$Th is removed at the margins (Huh *et al.*, 1997). In **scenario-a**, inventory changes of $^{230}$Th can only be due to removal within the central basins, corresponding to a 100%/0% basin/margin scavenging removal ratio.

No scavenging removal in the Barents Sea and at the margins seems unlikely given the, relative to the central basin, particle rich margins of the Arctic Ocean in general (Wells *et al.*, 2006), and specifically the Nansen Basin margin (Gdaniec *et al.*, 2020; Nöthig *et al.*, 2020b), the Fram Strait (Nöthig *et al.*, 2020b; Sanchez-Vidal *et al.*, 2015) and the Barents Sea (Dalpadado *et al.*, 2020; Schuur *et al.*, 2015). Moreover, $^{234}$Th analyses show that Thorium removal is more efficient in the Barents Sea and Laptev Sea than in the central basin (Cai *et al.*, 2010; Coppola *et al.*, 2002). This might indicate that our scenario a does not represent the steady state situation, unless the previous stated particle fluxes increased significantly after 1991.

**Scenario-b**, only presented for the 2007-2015 period, shall illustrate modern climate change conditions. We included a basin/margin scavenging removal ratio for $^{230}$Th, matching the margin removal process from Valk *et al.* (2020). Therefore **scenario-b** is based on increasing scavenging removal of $^{230}$Th at the margins, due to the aforementioned increased particle fluxes (Arrigo *et al.*, 2008; Boetius *et al.*, 2013; Dalpadado *et al.*, 2020; Schuur *et al.*, 2013; Schuur *et al.*, 2015) and potentially increased exchange between the margins and central basins. This is represented by applying a 22%/78% basin/margin scavenging removal ratio, an even more pronounced boundary scavenging than the 38%/62% from Huh *et al.* (1997). Nevertheless, 22%/78% ratio in **scenario-b** does not necessary contradict Hoffmann and McManus (2007), given the different time scales represented by sediment and water column data. Phases of more pronounced boundary scavenging, or even only phases of high scavenging rates at the margins, can be overprinted and hidden in bulk sediments by longer phases without boundary scavenging. **Scenario-b** provides a change in scavenging removal patterns compared to **scenario-a**. There is significant scavenging removal in the Barents Sea and the Nansen Basin margin, removing most inflowing $^{230}$Th directly at the inflow passages and a small amount by exchange with the central basin.

### 3.1.3 Comparison of Model Parameters with Moran *et al.* (2005)

The chosen inflow concentrations of dissolved $^{231}$Pa and $^{230}$Th are important for the outcome of the model calculations, especially for $^{231}$Pa. Since we did not include a margin scavenging removal component for $^{231}$Pa in the model calculations, all $^{231}$Pa removal occurs within the deep basins. Therefore the scavenging removal fluxes and sedimentation of $^{231}$Pa is more uncertain than for $^{230}$Th.

Inflowing $^{231}$Pa concentrations used in this study are not too different from those used by Moran *et al.* (2005), 2.35 fg/kg for $FS_{in}$ (this study) and 0.7 fg/kg in the much less voluminous $BS_{in}$ (this

study) compared to 2.33 fg/kg (Moran *et al.*, 2005). Inflowing concentrations of $^{230}$Th are different, 8.65 fg/kg ($FS_{in}$, this study) and 2.8 fg/kg ($BS_{in}$, this study) versus 7.04 fg/kg (Moran *et al.*, 2005). We chose concentrations from recent GEOTRACES cruises (GA_03) from Hayes *et al.* (2015) in order to make the data more consistent in terms of sampling years with the 2015 Arctic GEOTRACES data.

Moran *et al.* (2005) focused on intermediate and deep waters below 1000 m entering and exiting the Arctic Ocean and used concentrations from the GIN Seas obtained in 1993 as a reference. They neglected shallower inflows, such as the Barents Sea. In this study we include shallow inflow through the Barents Sea and Fram Strait leading to different in- and outflow volumes, based on newer results of Fram Strait and Barents Sea water fluxes from Beszczynska-Möller *et al.* (2012). In this study the shallow inflow through the Barents Sea and Fram Strait was included because we put a focus on scavenging removal of $^{230}$Th and $^{231}$Pa in inflowing waters and have indications that these processes are important for the central basin inventories, due to a depletion signal they carry when looping around the Arctic and mixing after sinking to greater depth with Arctic ambient waters (Valk *et al.*, 2020), hence these waters matter because of their reducing concentrations. (Moran *et al.*, 2005) additionally already suggested that scavenging over the Barents Sea shelves would further reduce the radionuclide content of inflowing waters, which might gain importance due to changing particle input at the shelves and therefore will be discussed in this study as a factor contributing to $^{230}$Th and $^{231}$Pa removal in the Arctic Ocean. Gdaniec *et al.* (2020) report dissolved $^{230}$Th concentrations in the Barents Sea, close to its Opening to the Atlantic, in the same range as in the north eastern Atlantic, supporting the decision to use those values. Outflowing concentrations in this study differ from those used by Moran *et al.* (2005) who used average intermediate/deep water dissolved radionuclide activities from the entire central Arctic Ocean, here converted to concentration units, of 13.86 fg/kg for $^{230}$Th and 2.33 fg/kg for $^{231}$Pa. In this study we use intermediate depth Amundsen Basin concentrations as averages from the respective periods. This might be an advantage compared to the previous budget, given the quite high regional variance in $^{230}$Th and $^{231}$Pa concentrations in the central Arctic Ocean. Makarov Basin dissolved $^{230}$Th concentrations are twice as high from below 500 m throughout the water column as in the Eurasian Basin and Makarov $^{231}$Pa concentrations being two to four times higher than in the Eurasian Basin below 1000 m (Grenier *et al.*, 2019; Valk *et al.*, 2018). The Eurasian Basin itself shows a rather ununiform distribution of dissolved $^{230}$Th and $^{231}$Pa concentrations, with on average lower concentrations of $^{230}$Th in the Amundsen Basin than in the Nansen Basin, above 2000 m, and lower values in the Nansen Basin

below 2000 m. This continues within the individual Basins of the Eurasian Basin, where two stations from the same Basin can show notable different concentrations, due to their location and rather locally restricted processes (Valk *et al.*, 2020; Valk *et al.*, 2018). Additionally $^{129}$I/$^{236}$U derived circulation times show much faster circulation times for intermediate waters in the Amundsen Basin than in the Amerasian Basin, indicating a faster transport of the FSBW than the BSBW (Wefing *et al.*, 2020), hence a higher contribution of waters from the Amundsen Basin than from the Amerasian Basin in the Fram Strait outflow. Additional to the decision of how to define outflow concentrations, there is no depth division in the model from Moran *et al.* (2005)**,** which could lead to an overestimate of outflow concentrations when averaging concentrations of $^{230}$Th and $^{231}$Pa below 1000 m for the entire central Arctic Ocean. The sill depth of the Lomonosov Ridge of maximum 1870 m (Björk *et al.*, 2007) prevents deeper waters from the Makarov or Canada Basin to flow into the Eurasian Basin and towards the Fram Strait, hence the highest concentrations of $^{231}$Pa and $^{230}$Th in the Arctic Ocean do not contribute to outflowing $^{230}$Th and $^{231}$Pa values. Additionally the sill depth of the Fram Strait hinders waters below 2500 m from leaving the Arctic by advective export through the Fram Strait. Hence a part of the in-situ produced $^{230}$Th and $^{231}$Pa is excluded from export by advection.

Of course the chosen inflow values influence the budgets and their outcome. Since we use the same inflow concentrations for each period, our results are more suitable to estimate rates and patterns of changes rather than finding concrete values for sedimentation fluxes. The aim of this study is to investigate changes over the past 24 years, with a focus on the past decade, therefore we include inflow waters flowing through areas where changes in particle flux or composition are expected to occur first.

### 3.2 Scavenging Removal and Sedimentation

Results of the models will be discussed in context of the influence of removal processes of $^{230}$Th in the Eurasian Basin on sedimentary $^{230}$Th accumulation in the Eurasian Basin and the GIN Seas to evaluate their effects on the paleo-oceanographic interpretation of those records. We focus on the 2007-2015 period under **scenario-b**. Figure 7 sums up scavenging removal, sedimentation fluxes and removal processes for the 2007-2015 period following **scenario-b**. Developments of $^{231}$Pa will then be compared to $^{230}$Th and $^{231}$Pa/$^{230}$Th sedimentary activity ratios will be discussed.

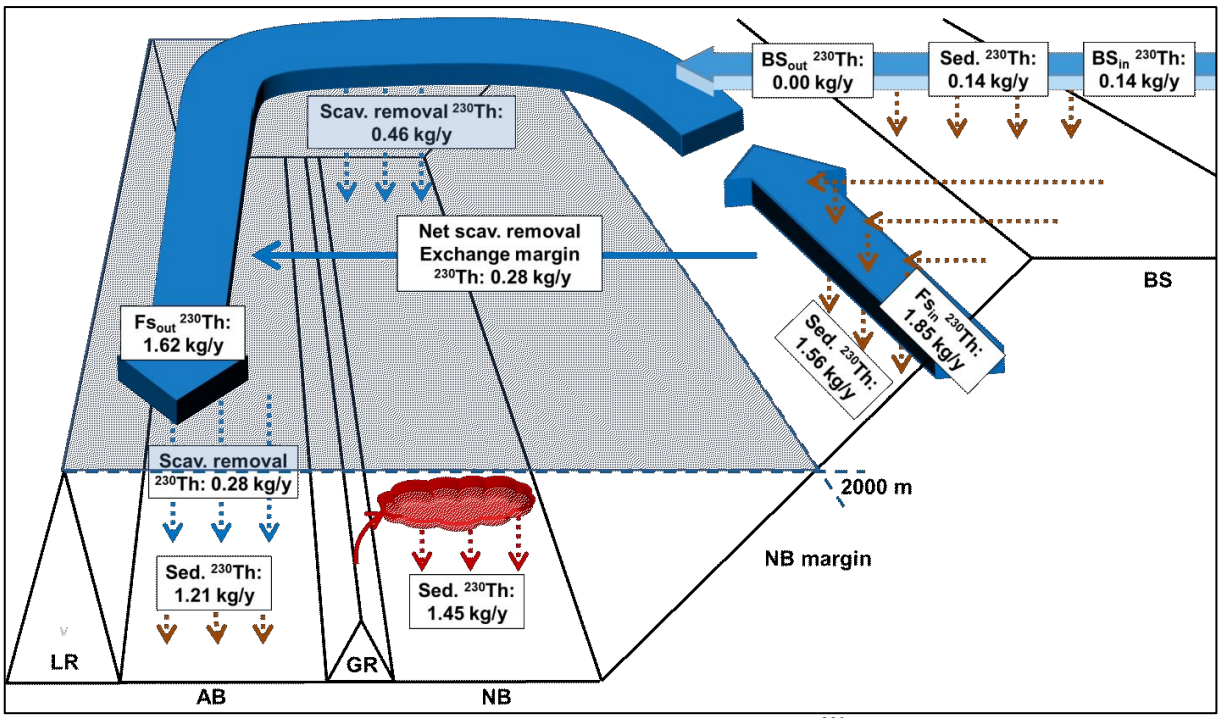


**Figure 7: Scavenging removal processes and sedimentation fluxes of $^{230}$Th between 2007 and 2015 in the Eurasian Basin under scenario-b. LR = Lomonosov Ridge, GR = Gakkel Ridge. Circulation patterns from Rudels (2009).**

### 3.2.1 The Eurasian Basin (<2000 m)

#### 3.2.1.1 $^{230}$Th

Dissolved $^{230}$Th decreased from 1991 to 2015 with an intermediate increase in 2007. Increased scavenging removal of $^{230}$Th from 2007 (0.69 kg/y) to 2015 (2.18 kg/y) reduced the $^{230}$Th inventory in the EUB (<2000 m).

1.70 kg/y of the 2.18 kg/y are removed at the Nansen Basin margin and in the Barents Sea. In the Barents Sea 0.14 kg/y $^{230}$Th of the 1.70 kg/y are removed from inflowing waters to sediments. 1.56 kg/y $^{230}$Th are removed along the Nansen Basin margin from inflowing waters, causing a net flow of 0.28 kg/y dissolved $^{230}$Th from the Nansen Basin margin and the Barents Sea into the central Eurasian Basin, shown in figure 6 and 7 as “net scavenging removal margin exchange”. $^{230}$Th outflow into the GIN Seas decreased from 2.06 kg/y (1991-2007) to 1.62 kg/y (2007-2015), following the inventory decrease. Therefore, following the model calculations and the findings of Valk *et al.* (2020), a recent increase of particle fluxes in the Barents Sea and at the Nansen Basin margin has made these areas a sink for $^{230}$Th. The intensity of this process likely depends on short term climate changes. On longer time scales, exceeding the time series by far, eustatic and even isostatic sea level changes can influence the intensity of this process given the high sensitivity of arctic surface circulation patterns to sea level changes, due to the vast shelves (Jakobsson *et al.*, 2004).

#### 3.2.1.2 $^{230}$Th vs. $^{231}$Pa

Advective export of $^{231}$Pa through the Fram Strait is considered to be of high importance for $^{231}$Pa distribution in the Arctic sediments (Hoffmann *et al.*, 2013). Earlier work had concluded that fractionation of $^{230}$Th and $^{231}$Pa in the Arctic Ocean is due to preferential export of $^{231}$Pa by advection of about 39% of the in-situ produced $^{231}$Pa, contrasting advective export of only 10% of $^{230}$Th from in-situ production (Moran *et al.*, 2005). Now we discuss if this has changed, due to changing environmental conditions.

The dissolved $^{231}$Pa development in recent years (2007-2015) in the upper Eurasian Basin is opposite to $^{230}$Th. Dissolved $^{230}$Th scavenging removal increased reducing inventories, while dissolved $^{231}$Pa inventories in the EUB (<2000 m) increased slightly by + 0.08 kg between 2007 and 2015, implying little change in $^{231}$Pa scavenging after 2007. Apparently, $^{231}$Pa scavenging removal in the Arctic Ocean reacts differently to the processes controlling the removal of $^{230}$Th. The assumed export of 39% of $^{231}$Pa from ISP (Moran *et al.*, 2005) is in contrast to our results. Besides the aforementioned differences in budget calculations this is due to the 30% decrease in $^{231}$Pa inventories from 1991 to 2015. Due to this inventory change scavenging removal from the upper Eurasian Basin, as well as outflow through the Fram strait decreased by more than 40% since 1991. An obvious explanation for the inventory change from 1991 to 2007, 2015 would be increased scavenging removal of $^{231}$Pa, either within the central basin or at the margins, as assumed for $^{230}$Th. Valk *et al.* (2020) could not find evidence for increased particle fluxes within the central basin that would explain the decrease of $^{230}$Th from 2007 to 2015. Hence increased scavenging removal of $^{231}$Pa within the central basins seems to be unlikely. Furthermore no change in ventilation or circulation times, which could affect $^{231}$Pa export, was found as summarized in Valk *et al.* (2020).

Another option which could theoretically explain the temporal discrepancies in $^{230}$Th and $^{231}$Pa developments, worth discussing, is a change in particle composition. Diatoms built from biogenic opal are effective scavengers of $^{231}$Pa (Chase *et al.*, 2002; Lao *et al.*, 1992; Walter *et al.*, 1997). Diatoms contribute up to more than 40% of sea ice released algae in the central Nansen- and Amundsen Basin (Boetius *et al.*, 2013). Exclusively ice-associated algae, including Arctic diatoms *Nitzschia frigida* or *Melosira arctica,* make up a large proportion of annual Phytoplankton Carbon (PPC) fluxes in the central Eurasian Basin (Lalande *et al.*, 2019), but only play a minor role at Arctic slopes and shelves (Juul-Pedersen *et al.*, 2010). Elevated presence of sea-ice diatoms transported by the Trans-Polar-Drift (TPD) (Nöthig *et al.*, 2020), contributing up to70% of the annual new primary production in the Eurasian Basin (Roca-Martí *et al.*, 2018)

could give a possible explanation for the decreasing dissolved $^{231}$Pa inventories in the Eurasian Basin over time.

Additionally the Amundsen Basin receives larger lateral input from the BSBW than the Nansen Basin (Rudels *et al.*, 2004; Schauer *et al.*, 2002). The BSBW could transport diatoms from Barents Sea, known for its diatom blooms (Wassmann *et al.*, 1990), into the Amundsen Basin, causing enhanced, albeit just slightly enhanced, scavenging removal of $^{231}$Pa, both above and below 2000 m. Based on $\delta^{30}$Si-DSi and $\delta^{30}$Si-b$SiO_2$ Liguori *et al.* (2020) argue that waters in the Amundsen Basin indeed show a diatom production signature. It is possible that this increased opal flux is not represented in some particulate tracers, such as particulate $^{234}$Th, because diatom shells can efficiently form rapidly sinking aggregates. Therefore we might observe a consequence of enhanced biogenic silica particle fluxes which were not present at the time of sampling, maybe due to the seasonality of blooms. Theoretically it is possible that in 2015 or before, waters carrying a signal from the Barents Sea NPP peak in 2007, 2008 (Dalpadado *et al.*, 2020) reached the central Amundsen Basin, given surface tracer ages, evident from $^{129}$I/$^{236}$U of 7-9 years (Wefing *et al.*, 2020). Unfortunately this explanation falls apart for two reasons.

First of all, if diatoms contribute to scavenging of $^{231}$Pa they also must affect dissolved $^{230}$Th. This could indicate that the assumption that vertical particle fluxes remained equal in the central Eurasian Basin between 1991-2007 and 2007-2015 is incorrect. A significant increase in diatom shell fluxes would also be represented in particulate $^{234}$Th, which was not the case in 2015 (Valk *et al.*, 2020). One could conclude therefore that $^{231}$Pa scavenging within the central basins did not change due to higher abundance of diatoms. Second, the distribution and concentrations of $^{230}$Th and $^{231}$Pa in the Arctic Ocean are much more variable than maybe thought previously, not only in time, as shown by the time series, but also in their spatial distribution. To simplify the budget calculations we chose to present the upper 2000 m of the Eurasian Basin as one box e.g. (figure 1). This could indicate a caveat of the models. Nevertheless, given the lack of information about exchange between the upper Amundsen and Nansen Basin we chose to combine them into one basin. In order to identify processes controlling the distribution of $^{231}$Pa, or how it reacts to processes driving $^{230}$Th distribution we might now have to look in detail at the two basins (Nansen and Amundsen) separately before we discuss if there are indications for $^{231}$Pa scavenging in the central Eurasian Basin or even a pronounced margin scavenging.

Dissolved $^{231}$Pa did not decrease above 2000 m in the Eurasian Basin seen as a single basin between 2007 and 2015 but decreased by 18% in the upper Amundsen Basin (<2000 m), contrasting to its 24% increase in the upper Nansen Basin (<2000 m). A development similar to $^{230}$Th, which decreased in both basins above 2000 m, but much more in the Amundsen Basin (-

50% AB vs. - 26% NB). For both basins no evidence for increased particle presence relative to 2007 above 2000 m was found in 2015 data. Particulate $^{234}$Th and $^{230}$Th (Nansen Basin) (Valk *et al.*, 2018) were not higher than in 2007 and the particulate fraction of $^{234}$Th was generally well below 5% in the Amundsen Basin in 2015 (Valk *et al.*, 2020), besides one station (125), located close to the Lomonosov Ridge and in the influence of the TPD. This station 125 rather shows an input of lithogenic material, given its high surface dissolved $^{232}$Th concentrations (Valk *et al.*, 2020). Hence an increase of diatom fluxes is unlikely.

Another option explaining the Amundsen Basin decrease of $^{231}$Pa is scavenging removal of $^{231}$Pa at the margins, as reported for $^{230}$Th (Gdaniec *et al.*, 2020; Valk *et al.*, 2020). The Barents Sea is known for diatom blooms (Wassmann *et al.*, 1990) and sea ice retreat enhances algae growth (Arrigo and van Dijken, 2015). Hence scavenging removal of $^{231}$Pa there would be likely, as already suggested by Moran *et al.* (2005). Though, detailed temporal trends indicate that total diatom production in the Barents Sea increases less than total NPP (Dalpadado *et al.*, 2020; Orkney *et al.*, 2020). Likewise, spatial distribution of diatom blooms shows that inflow of Atlantic waters at both the Fram Strait and the Barents Sea rather leads through areas with decreasing diatom abundances (Orkney *et al.*, 2020). Nevertheless this option needs to be discussed in detail, since margin scavenging removal of both radionuclides is of huge importance for the model calculations.

Fractionation factors $F_{(Th/Pa)}$ $((^{230}Th/^{231}Pa)_p/(^{230}Th/^{231}Pa)_d)$ are 11.80 at the Nansen Basin margin (station 32) above 2000 m and 6.30 (one outlier sample at 1000 m was excluded) in the central Nansen Basin above 2000 m (Gdaniec *et al.*, 2020). Taking only the uppermost 500 m of the water column yield $F_{(Th/Pa)}$ of 3.43 at the margin and 4.33 in the central basin. $^{231}$Pa/$^{230}$Th activity ratios in suspended particles above 2000 m in 2015 were 0.04 at the margin and 0.05 in the central Nansen Basin (Gdaniec *et al.*, 2020). This could indicate that, besides the uppermost 500 m that Th/Pa fractionation is lower in the central Nansen Basin than on the margins.

A $F_{(Th/Pa)}$ of 10 represents lithogenic particles (Moran *et al.*, 2002), while a $F_{(Th/Pa)}$ of <5 represents significant admixture of diatoms. 40% diatoms of sinking particles cause a $F_{(Th/Pa)}$ of 1.86 ± 0.43 (Walter *et al.*, 1997). This would fit to the $F_{(Th/Pa)}$ of 6.30 above 2000 m and to the 4.33 above 500 m, since Arctic particles contain a significant proportion of terrestrial material, e.g. from the TPD (Charette *et al.*, 2020) but still contain a notable diatom proportion there.

The different $F_{(Th/Pa)}$ above 2000 m at the margin and the central Nansen Basin might indicate that indeed scavenging removal of $^{231}$Pa occurs rather in the central basins, while $^{230}$Th is scavenged at the margins, due to different particle composition. Furthermore particle size and

moreover settling speed could fractionate $^{230}$Th and $^{231}$Pa, with $^{231}$Pa being less prone to react on fast settling particles (Kretschmer *et al.*, 2011). This could in turn indicate that the assumption that vertical particle fluxes remained equal between 1991-2007 and 2007-2015 is not correct or that the $F_{(Th/Pa)}$, given no reduction in dissolved $^{231}$Pa over time, is rather the beginning of a future development, also suggested by Nöthig *et al.* (2020) who suggest that ice algae fluxes will increase. This development would first affect the Amundsen Basin where a reduction of dissolved $^{231}$Pa after 2007 was observed. This would make sense to some degree, given that $^{231}$Pa needs more time than $^{230}$Th to adapt to increasing or changing particle fluxes and due to the seasonality of diatom fluxes, which rather is less pronounced for terrigenous particle inputs at the margins. Hence removal of $^{230}$Th from inflowing waters would likely affect the entire Eurasian Basins $^{230}$Th inventories, while $^{231}$Pa is more regionally affected, by diatom blooms and the TPD location. Then even a slight increase of diatom fluxes per year, by either higher export or prolonged export seasons, would affect dissolved $^{231}$Pa there, while dissolved $^{230}$Th also reacts to this change, but it might be less visible in the case of $^{230}$Th, due to the much stronger decrease at the margins upstream. Hence elevated diatom fluxes would affect both $^{231}$Pa and $^{230}$Th, but would be more crucial for scavenging removal of $^{231}$Pa.

Even if the assumption that particles in the central Eurasian Basin maintain their 1991-2007 vertical fluxes is not correct, it would still mean that scavenging removal of $^{230}$Th happens mostly at the margins, due to high particle fluxes in combination with particle composition favouring $^{230}$Th over $^{231}$Pa. Vertical $^{230}$Th fluxes in the central basins would still be equal or even reduced compared to 1991-2007, due to the reduction of source $^{230}$Th in the upper 2000 m. $^{231}$Pa vertical fluxes in the central basins would increase, due to the lack of margin scavenging and higher diatom fluxes in the central basin than at the margins. Therefore increasing diatom fluxes can cause increased scavenging removal of $^{231}$Pa in the Eurasian Basin, but combining all findings and parameters this process is not yet fully in progress but might be crucial in the near future and currently we observe its consequences in an initial stage, and locally restricted. An extension of the $^{230}$Th and $^{231}$Pa time series might be required in order to investigate the continuity of observed changes as well as the effects on $^{231}$Pa, given that 8 years (2007-2015) might not be enough to fully observe the reaction of $^{231}$Pa to changes already affecting $^{230}$Th. Calculated scavenging residence times for $^{231}$Pa in the steady state in the upper Eurasian Basin are 15 years, which is in the order of circulation times of intermediate waters in the Amundsen Basin (Rutgers van der Loeff *et al.*, 2018; Smith *et al.*, 2011; Wefing *et al.*, 2020). This is in line with the implications from low sediment $^{231}$Pa/$^{230}$Th ratios, which were explained by advective export of $^{231}$Pa being its main removal mechanism in the Arctic Ocean (Moran *et al.*, 2005).

Suspended particles in the upper 2000 m of the central Nansen Basin (station 50) show an average $^{231}$Pa /$^{230}$Th activity ratio of 0.05 and a $F_{(Th/Pa)}$ of 6.30 (Gdaniec *et al.*, 2020). In the uppermost 500 m, the $F_{(Th/Pa)}$ is 4.33 and particulate $^{231}$Pa/$^{230}$Th slightly higher, 0.06. Particulate $^{231}$Pa/$^{230}$Th is below the production ratio in the central Nansen Basin and its slope above 2000 m, while dissolved $^{231}$Pa/$^{230}$Th is well above the production ratio, especially in the upper 2000 m of the Nansen Basin margin (station 32) (Gdaniec *et al.*, 2020). This can lead to the conclusion that $^{230}$Th is removed by scavenging along the margin in the FSBW, while $^{231}$Pa seems to be scavenged in the upper 500 m potentially in Barents sea derived waters, but these particles are not yet found in deep (>2000 m) particulate activity ratios, which are 0.03 m at the margin (Gdaniec *et al.*, 2020).

Interestingly, particulate $^{231}$Pa/$^{230}$Th activity ratios in the Barents Sea are 0.084 on average (0-~400 m), hence much higher than at the Nansen Basin margin (0.053, 0-500 m to 0.033, >2000 m). The highest particulate $^{231}$Pa/$^{230}$Th ratios in the Barents Sea are observed at the surface (0.125 on average) and close to the seafloor (0.14 on average) (Gdaniec *et al.*, 2020). $F_{(Th/Pa)}$ in the Barents Sea is 10.28 on average, with lower values towards the sea floor (6.22 and 8.85 in 350-400 m) (Gdaniec *et al.*, 2020). These high values of $F_{(Th/Pa)}$ indicate a high proportion of lithogenic material and only the deepest and the surface samples show indication for a significant diatom contribution. This might represent recent scavenging of $^{231}$Pa by present diatom blooms, but given the lower $^{231}$Pa/$^{230}$Th activity ratios between the surface and the bottom and the higher F values at intermediate depths, this might represent a seasonal feature, given the temporal variations of phytoplankton blooms in the Barents Sea. Over the growing season phytoplankton blooms change from diatom dominated blooms in May to coccolithophore blooms in August (Signorini and McClain, 2009). Hence during the Barents Sea sampling of GEOTRACES section GN_04 in October 2015 possibly the latter bloom was present in surface waters. Theoretically, the with depth decreasing $F_{(Th/Pa)}$, as well as the high particulate $^{231}$Pa/$^{230}$Th ratios in bottom waters around 350 m could be a relic of the May diatom blooms, where fast sinking diatom particles already made their way towards the seafloor. Gdaniec *et al.* (2020) calculated a particle settling rate of 600 m/y for the margins of the Eurasian Basin. Sinking velocities of diatoms can vary (Miklasz and Denny, 2010), but are often even much faster, especially when forming aggregates (Iversen and Ploug, 2013; Ploug and Grossart, 2000). This could point at a seasonal $^{231}$Pa scavenging and rather constant $^{230}$Th scavenging in the Barents Sea. Dissolved $^{231}$Pa/$^{230}$Th ratios at these stations are 1.029 on average (Gdaniec *et al.*, 2020), supporting the hypothesis of seasonal $^{231}$Pa scavenging and constant $^{230}$Th scavenging.

An explanation for this could be the much higher volumes of terrigenous material from erosion and riverine input relative to biomass from diatom production.

Surface sediment $^{231}$Pa/$^{230}$Th activity ratios in Barents Sea are even higher (0.4) than particulate ratios. It could indicate that the Nansen Basin margin and especially the Barents Sea could be a sink for Arctic $^{231}$Pa, on time scales longer than represented by suspended particles collected using in-situ pumps. Hence possibly the assumption that $^{231}$Pa is not preferentially removed at the margins and on the shelves could be wrong and inflow amounts to the central Eurasian Basin need to be adapted accordingly. If such a process can leave an imprint on the central basin $^{231}$Pa inventories depends on the scavenging removal residence times of $^{231}$Pa and water mass residence times. The latter is rather short in the Barents Sea, given an estimated circulation time scale for waters flowing through the Barents Sea of approximately 2 years (Smith *et al.*, 2011).

Individual dissolved $^{230}$Th profiles from 2015 in the Amundsen Basin show a negative peak at 1000 m correlating with a peak in $^{129}$I/$^{236}$U (Casacuberta *et al.*, 2018; Valk *et al.*, 2020) indicating a fast advective removal, which would be even more important in terms of $^{231}$Pa advective removal. This is due to faster circulation rates of the Amundsen Basin compared to the Nansen Basin (Tanhua *et al.*, 2009; Wefing *et al.*, 2020) and could transport any Barents Sea derived depletion signal relatively fast to the central Amundsen Basin. $^{231}$Pa therefore might be removed within the Barents Sea seasonally, while $^{230}$Th is removed along the margins of the Nansen Basin, probably all along its way around the Eurasian Basin along its margins and shelf breaks, as argued by Valk *et al.* (2020). The consequences on the central basin inventories therefore are much more pronounced for $^{230}$Th, due to the much higher inflowing volume through the Fram Strait, assuming that $^{230}$Th is scavenged there and $^{231}$Pa in the Barents Sea. Hence it might be possible that the $^{231}$Pa reduction since 2007 in the Amundsen Basin might be due to changing scavenging removal of $^{231}$Pa in the Barents Sea or waters derived from there.

As mentioned earlier, dissolved $^{231}$Pa did not decrease in the upper Nansen Basin, but increased by 24%. One explanation could be that, due to its slower circulation rates compared to the Amundsen Basin any depletion signal needs more time to arrive in the central Nansen Basin, which could explain lesser $^{230}$Th reduction between 2007 and 2015. The longer scavenging residence time of $^{231}$Pa could explain why no decrease of dissolved $^{231}$Pa was observed in the upper Nansen Basin whatsoever. It does not explain the increase of dissolved $^{231}$Pa in the upper Nansen Basin, though. One explanation, albeit highly speculative, for this opposite development in the two basins upper 2000 m water masses is recirculation.

Mean water mass ages based on Transient Tracer Distribution (TTD) based on anthropogenic radionuclide ratio $^{129}$I/$^{236}$U are older in the Nansen Basin than in the Amundsen Basin, even at stations located close to the tracer sources in the Fram Strait and the Barents Sea, pointing at recirculation in the Nansen Basin north of the Fram Strait (Wefing *et al.*, 2020). This could mean that the upper Nansen Basin receives a part of the dissolved $^{231}$Pa removed from the Amundsen Basin by advection, from recirculation before these waters leave the Arctic through the Fram Strait. This recirculation from the Amundsen Basin and/or the Nansen Basin would transport waters, carrying a strong $^{230}$Th depletion signal from margin scavenging removal in inflow waters back to the central Eurasian Basin (Nansen Basin). Those waters would have lost a major part of their dissolved $^{230}$Th content, but relatively less dissolved $^{231}$Pa, hence are relatively enriched in dissolved $^{231}$Pa. This would increase the time available for $^{231}$Pa to react with particles and subsequently to be removed from the dissolved phase. Therefore increased scavenging removal of $^{231}$Pa might be expected to occur in the near future. The longer circulation times of the Nansen Basin combined with recirculation would not change the assumption that removal of $^{231}$Pa in the Arctic is mainly controlled by circulation times rather than scavenging residence times of $^{231}$Pa (Moran *et al.*, 2005), but it would change the implications of it in terms of $^{231}$Pa export. The results and interpretation of our budget based on recent water column time series indicate that the response of $^{231}$Pa to circulation and variable particle fluxes in the Arctic Ocean might be more complex than previously assumed. Especially the change in distribution of $^{231}$Pa between the upper Amundsen and the upper Nansen Basin point at a deviation from the previously assumed export of $^{231}$Pa from the Arctic Ocean, at least in recent years.

### 3.2.2 The Deep Basins

#### 3.2.2.1 The Deep Nansen Basin

##### 3.2.2.1.1 $^{230}$Th

Hydrothermal activity can act as a sink for $^{230}$Th and $^{231}$Pa (Pavia *et al.*, 2018). Hydrothermal plumes can travel over large distances affecting an entire ocean basin (Fitzsimmons *et al.*, 2014). The ultra-slow spreading Gakkel Ridge, separating the Amundsen- and Nansen Basin, is the only hydrothermally active ridge in the Arctic Ocean. Constant venting (Baker *et al.*, 2004) but also explosive eruptions due to earthquakes can occur there (Schlindwein and Riedel, 2010; Sohn *et al.*, 2008). These explosive eruptions release huge amounts of dissolved and particulate

trace elements that cause significant scavenging removal of $^{230}$Th on over time (Valk *et al.*, 2018).

Dissolved $^{230}$Th increased during the 1991-2007 period by + 0.61 kg (+ 0.04 kg/y) in the deep Nansen Basin (>2000 m) and decreased by - 3.80 kg (- 0.48 kg/y) during 2007-2015 (figure 1). This results in a $^{230}$Th scavenging removal flux of 0.99 kg/y and a subsequent sedimentation of 1.29 kg/y. This hydrothermal scavenging event increased scavenging removal of $^{230}$Th significantly between 2007 and 2015 (Valk *et al.*, 2018). This event was restricted to the deep Nansen Basin, not affecting the deep Amundsen Basin (Valk *et al.*, 2018).

$^{230}$Th sedimentation during 1991-2007 was significantly higher than before, regardless which scenario is applied. Hence hydrothermal scavenging clearly increased $^{230}$Th scavenging removal and sedimentation fluxes in the deep NB in just 8 years. That implies that the total amount of $^{230}$Th buried in the deep Nansen Basin is significantly higher during or at the end of volcanic eruption phases at the Gakkel Ridge. It is important to distinguish between constant hydrothermal venting (Baker *et al.*, 2004), contributing to the steady state situation, and explosive eruptions (Sohn *et al.*, 2008), overprinting the steady state situation, causing the drastic inventory decrease of dissolved $^{230}$Th after 2007 (Valk *et al.*, 2018).

#### 3.2.2.1.2 The Deep Nansen Basin: $^{230}$Th vs. $^{231}$Pa

The dissolved $^{230}$Th inventory of the deep Nansen Basin decreased by almost 40% between 2007 and 2015, while the dissolved $^{231}$Pa inventory increased by 20%. The oppositional development of $^{230}$Th and $^{231}$Pa in this case is much more pronounced than e.g. in the EUB (<2000 m).

One explanation for the lack of $^{231}$Pa scavenging removal by the hydrothermal scavenging event that removed significant amounts of $^{230}$Th in the deep Nansen Basin between 2007 and 2015 (Valk *et al.*, 2018) is a temporal delay of $^{231}$Pa scavenging removal due its lower particle reactivity in general and its lesser preference for Fe oxy-hydroxide particles in hydrothermal plumes in particular (Pavia *et al.*, 2018).

Particulate $^{231}$Pa was indeed elevated in the Nansen Basin at station 50 below 2000 m, relative to the slope of the Nansen Basin but somehow did not yet reduce the dissolved concentrations, as observed for $^{230}$Th at the same station over the same time (Gdaniec *et al.*, 2020; Valk *et al.*, 2018). Particulate $^{231}$Pa/$^{230}$Th activity ratios in the deep Nansen Basin were 0.08 by the sampling time, higher than above 2000 m (0.05) (Gdaniec *et al.*, 2020), indicating a stronger $^{231}$Pa scavenging after $^{230}$Th was removed in the deep before. This is in contrast to the Nansen Basin slope where $^{231}$Pa/$^{230}$Th is lower below 2000 m than above. This excludes the option that $^{231}$Pa in the deep Nansen Basin is transported by deep water circulation towards areas with higher

particle fluxes, the Nansen Basin slope or the Fram Strait, and is removed there primarily. The 2015 particulate $^{231}$Pa profiles from the central Nansen Basin and the slope indicate that resuspended slope particles scavenge $^{230}$Th over $^{231}$Pa while the hydrothermal relic particles might now scavenge $^{231}$Pa. This could mean that after a strong $^{230}$Th scavenging removal event, which was over or in its dying phase in 2015, now relic particles from the submarine eruptions scavenge $^{231}$Pa. If this was the case we expect a decrease of dissolved $^{231}$Pa in the near future. Calculated scavenging residence times of $^{230}$Th and $^{231}$Pa in the deep Nansen Basin in a steady state are ~18 and 75 years respectively, assuming that vertical fluxes bypass the deep inventory. This supports the explanation of the absence of a dissolved $^{231}$Pa decrease compared to $^{230}$Th, by a delayed reaction of $^{231}$Pa, due to its relatively smaller particle reactivity. $F_{(Th/Pa)}$ at station 50 in the Nansen Basin shows an average value below 2000 m of 11.20 (Gdaniec *et al.*, 2020), which fits to exactly an $F_{(Th/Pa)}$ for $Fe(OH)_3$ (Hayes *et al.*, 2015). Despite the generally lower residence time of Mn compared to Fe in the ocean (Bruland *et al.*, 1994), pFe and pMn decouple with plume traveling distance and time and seem to have fundamentally different settling properties (Fitzsimmons *et al.*, 2017). This could mean that somehow after Fe particles scavenged $^{230}$Th a second scavenging phase with primarily $MnO_2$ particles will start in the near future, scavenging $^{231}$Pa, while $^{230}$Th, due to its higher particle reactivity is already removed and just a relic of this removal event is observed, maybe just before dissolved $^{231}$Pa also starts to decrease.

Another option could be that $^{231}$Pa just slightly reacted to the hydrothermally released particles, but is scavenged onto sinking silicate rich particles, from e.g. under ice diatom blooms. Due to reversible scavenging, it can cause an increase of particulate $^{231}$Pa, without a notable decrease in its dissolved phase. This could be supported by up to 35% diatoms from total taxonomic entities below 3000 m (Nöthig *et al.*, 2020). These particles would affect dissolved $^{230}$Th as well, but since a major part of it has been removed by hydrothermal particles before it might not be visible in a decrease of dissolved $^{230}$Th. However Liguori *et al.* (2020) did not find differences in Silicate isotopes, indicating diatom abundances, in deep waters between the Nansen Basin and its slope. Therefore it is unlikely that the elevated $^{231}$Pa particulate concentrations in the deep Nansen Basin are due to the presence of diatom shell particles, but rather to a, relative to $^{230}$Th, delayed consequence of hydrothermal particles.

#### 3.2.2.1.3 The Deep Nansen Basin: Influence of Deep Water Exchange with the Atlantic

We decided to limit the inflow of Atlantic waters to 2000 m for simplification reasons for the box model. Nevertheless it is important to discuss the potential influence of waters entering the Nansen Basin below 2000 m down to ca. 2500 m through the Fram Strait. Based on salinity and

temperature data from 2007 (Wisotzki, 2008) and 2015 (Rabe *et al.*, 2016) there are no indications for a shift of water masses in the central deep Nansen Basin, which could contribute to the decrease of dissolved $^{230}$Th. Especially an increase in temperature would be expected if significant changes in Arctic deep waters occurred due to advection flow from the Atlantic Ocean. Additionally North Atlantic (Hayes *et al.*, 2015) and Norwegian Sea (Moran *et al.*, 1995) deep water $^{230}$Th concentrations are higher than those from the deep Nansen Basin, where the major $^{230}$Th depletion was observed. Hence it is unlikely that a deep water inflow contributed significantly to the observed depletion.

#### 3.2.2.2 The Deep Amundsen Basin

##### 3.2.2.2.1 $^{230}$Th

The deep (>2000 m) Amundsen Basin $^{230}$Th scavenging situation has changed since 1991. Dissolved $^{230}$Th decreased between 2007 and 2015 by 3.25 kg (0.44 kg/y), while during the 1991-2007 period the dissolved $^{230}$Th inventory increased by 1.67 kg (figure 1). The decrease since 2007 was explained previously by scavenging removal at the margins and subsequent inflow of $^{230}$Th depleted waters above 2000 m leading to a reduction in the deep due to reversible scavenging, transporting the depletion signal downwards (Valk *et al.*, 2020).

$^{230}$Th scavenging removal in the deep AB has increased by a factor of more than two since 1991, and by more than 2.5 since 2007, following **scenario-a**. Even after applying **scenario-b** to the 2007-2015 period the sedimentation fluxes are still higher than in the steady state and 1991-2007 period under **scenario-a**. Hence even when removing a significant part of dissolved $^{230}$Th at the margins and therefore decreasing vertical fluxes from above 2000 m, the inventory changes of dissolved $^{230}$Th require increased scavenging removal at depth. This has not been considered by Valk *et al.* (2020). Maybe particle fluxes contribute slightly more to the inventory change than assumed, while still the reduced vertical input mainly contributes to the inventory change, with a potential deep water exchange. This scavenging removal by deep water circulation would be in conflict with the models, which do not represent such a process since Hoffmann and McManus (2007) neglect it and no further indications were found. Never the less ventilation of Eurasian Basin deep waters is slow, in the order of 250 years (Schlosser *et al.*, 1994), hence reduction of $^{230}$Th by deep water circulation or formation on decadal time scales can be ruled out.

##### 3.2.2.2.2 $^{230}$Th vs. $^{231}$Pa

Dissolved $^{231}$Pa inventories in the deep Amundsen Basin decreased since 2007 by ~10%, equal to 0.02 kg/y, which is in the order of ISP of $^{231}$Pa in the deep Amundsen Basin. Vertical input of

dissolved $^{231}$Pa decreased, as for $^{230}$Th, with the difference that vertical $^{230}$Th fluxes decreased due to a reduction in the source inventory above 2000 m, while vertical fluxes of $^{231}$Pa decreased because scavenging removal in the EUB above 2000 m was lower during 2007-2015 than before. Therefore the vertical input of $^{231}$Pa decreased and subsequently the deep water inventory as well. The deep Amundsen is the only box in the model where dissolved $^{231}$Pa decreased between 2007 and 2015. Since it is unlikely that increased vertical fluxes of opal containing particles are responsible for the observed depletion a potential explanation is that $^{231}$Pa is removed from the upper 2000 m of the water column by scavenging from inflowing waters in the Barents Sea, as discussed in *section 3.2.1.2*. This would result in lower $^{231}$Pa vertical fluxes in the Amundsen Basin. This margin removal would decrease the deep $^{231}$Pa inventory by reversible scavenging, similar as modelled for $^{230}$Th (Valk *et al.*, 2020), but takes more time to fully affect dissolved and particulate $^{231}$Pa profiles in the Amundsen Basin, which is represented by a deep water dissolved $^{230}$Th inventory decrease of 31% and just 10% for $^{231}$Pa.

## 3.3 Implications for Sedimentary $^{230}$Th, $^{231}$Pa and $^{231}$Pa/$^{230}$Th

Vertical and spatial distribution and concentrations of dissolved $^{230}$Th and $^{231}$Pa in the Arctic Ocean can change rather quickly, on decadal or even shorter time scales (Grenier *et al.*, 2019; Valk *et al.*, 2020; Valk *et al.*, 2018). Hence it might be taken into account that sedimentation of the two isotopes also differs regionally, at least on time scales shorter than average surface bulk sediments can reveal. The following sections conclude the discussed $^{230}$Th and $^{231}$Pa developments in the Eurasian Basin and put them in context to expected $^{230}$Th/$^{231}$Pa sedimentary activity ratios.

### 3.3.1 Nansen Basin Margin and Barents Sea

According to our calculations scavenging removal fluxes from the EUB (<2000 m) to the deep NB and AB show extremely high $^{231}$Pa /$^{230}$Th activity ratios of 1.54 (NB) and 1.76 (AB), way above the production ratio of 0.093. It is worth noting that this ratio strongly depends on the chosen inflow $^{231}$Pa and $^{230}$Th concentrations ($FS_{in}$ + $BS_{in}$), leading to a $^{231}$Pa/$^{230}$Th activity ratio of 0.61.

As a trend, following the model calculations $^{230}$Th, is preferentially removed from the water column and buried at the margins, while $^{231}$Pa is almost exclusively buried within the deep basins or exported by advection. The removal of $^{231}$Pa depends probably heavily on the abundance of biogenic opal particles in the central Eurasian Basin, while $^{230}$Th removal in the central upper Eurasian Basin is due to increased particle fluxes at the margins. However, there

are indications for a potential $^{231}$Pa margin removal in the Barents Sea during diatom blooms in spring. This possibility needs further investigation, since it could be important for temporal changes in $^{231}$Pa inventories, given that besides seasonal variations in diatom production there is also a large inter annual phytoplankton production variability in the Barents Sea (Dalpadado *et al.*, 2020; Ellingsen *et al.*, 2008).

### 3.3.2 Nansen Basin

Sporadically occurring submarine volcanic eruptions cause a reduction of dissolved $^{230}$Th in the deep Nansen Basin, but not on $^{231}$Pa. Hence these phases should contribute to sedimentary $^{231}$Pa/$^{230}$Th ratios with an input way below the production ratio in the deep Nansen Basin. This sedimentation flux ratio is, applying **scenario-b** for $^{230}$Th, 0.32 in 2007-2015. Sedimentary $^{231}$Pa/$^{230}$Th ratios in the Nansen Basin, accumulated over thousands of years, are in the order of 0.05, below their production ratio of 0.093 (Moran *et al.*, 2005). So the question where the "missing" $^{231}$Pa went is open. It could be that $^{231}$Pa is affected by deep water circulation and deposited somewhere else than $^{230}$Th, due to longer scavenging residence times. These deposition areas can be the margins of the Eurasian Basin, or beyond Fram Strait.

Explosive eruptions at ultra-slow spreading ridges are rare (Pontbriand *et al.*, 2012) but release huge volumes that build up volcanic formations (Cann and Smith, 2005; Cochran, 2008; Smith and Cann, 1993) and can last over decades (Schmid *et al.*, 2017). Hence this process probably does not affect the $^{231}$Pa/$^{230}$Th sedimentary ratio on timescales of tens or hundreds, not even thousands of years, due to the low sedimentation rates of the Eurasian Basin (1 cm/kyrs – 5 cm/kyrs) (Backman *et al.*, 2004; Gard, 1993) in addition to a bioturbation depth of approximately 2-10 cm (Clough *et al.*, 1997). Only if explosive eruptions occur more frequently or induce sporadically significantly increased sedimentation rates, then these scavenging events would also measurably affect sedimentary $^{230}$Th accumulation in the deep Nansen Basin and, due to the lower effect on $^{231}$Pa, potentially also their sedimentary ratio.

Hydrothermal plumes, containing trace metals such as Fe or Mn, can travel over long distances and times (Fitzsimmons *et al.*, 2014) before or while forming particles, scavenging $^{230}$Th, and cause $^{230}$Th deficits even several thousand kilometres off axis (Pavia *et al.*, 2018). Therefore these volcanic induced hydrothermal scavenging removal events might have to be considered when investigating sedimentary $^{231}$Pa/$^{230}$Th records in sediments of the Nansen Basin, even without an apparent layer of volcanic material. It is supposed that voluminous eruptions occurred at several sites along the Gakkel Ridge during the past 2 Ma (Cochran *et al.*, 2003) with a higher frequency than traditionally thought (Edwards *et al.*, 2001). Those eruptions might occur more

frequently in the future if the 1999-2001 earthquake swarms at the Gakkel Ridge has opened a volcanic conduit leading to more intense volcanism as proposed by Riedel and Schlindwein (2010) and maybe generally higher removal rates of $^{230}$Th in deep waters of the Nansen Basin.

### 3.3.3 Amundsen Basin

According to the models, sedimentation of $^{230}$Th in the Amundsen Basin increased since 1991, with an intermediate decrease in 2007. Since 2007 $^{230}$Th sedimentation increased by more than 40 % from 0.68 kg/y to 1.11 kg/y. While $^{231}$Pa sedimentation decreased from 0.24 kg/y to 0.18 kg/y in 2015 in the Amundsen Basin. If this situation remains in the future it will shift sedimentary $^{231}$Pa/$^{230}$Th ratios towards $^{230}$Th. Sedimentary $^{231}$Pa/$^{230}$Th in the Amundsen Basin are 0.061 – 0.089 (Scholten *et al.*, 1995). Sedimentation ratios according to our models are much higher, which is probably due to the absence of margin scavenging for $^{231}$Pa and a lower outflow out of the Arctic Ocean, potentially indicating a missing $^{231}$Pa removal process. Nevertheless the sedimentation developments of $^{230}$Th and $^{231}$Pa in the Amundsen Basin, evident from the time series, show that the deep Amundsen Basin will probably develop a $^{231}$Pa/$^{230}$Th ratio even lower than it is now reported. If there is actually a recirculation feature transporting a certain amount of $^{231}$Pa from the Amundsen Basin to the Nansen Basin than this could lead to higher $^{231}$Pa sedimentation at the Nansen Basin or at margin, but this is not yet visible in our inventories and in particulate and dissolved $^{231}$Pa data. Surface sediment $^{231}$Pa/$^{230}$Th activity ratios are above their production ratio at the margin of the Nansen Basin (0.18, station 32) (Gdaniec *et al.*, 2020). The only sediment $^{231}$Pa/$^{230}$Th ratio close to the production ratio reported by Scholten *et al.* (1995) is located close to the Fram Strait and significantly higher than ratios from the central Amundsen and Nansen Basins. This could indicate that $^{231}$Pa scavenging removal took place in this area already in the past. This sediment ratio would increase if there is an establishment of recirculation from the Amundsen Basin. This recirculation process could support an enhanced removal of $^{231}$Pa to sediments relative to $^{230}$Th on longer time scales. Until such a development is visible in sediment data it takes time, due to sedimentation rates and bioturbation, as well as due to the long $^{231}$Pa scavenging residence times.

## 3.4 Exchange with the GIN Seas and the Amerasian Basin

### 3.4.1 GIN Seas

Advective export of both dissolved $^{230}$Th and $^{231}$Pa from the Eurasian Basin to the GIN Seas was reduced by ~20% from the 1991-2007 period to 2007-2015. During the 2007-2015 period the outflow $^{231}$Pa/$^{230}$Th ratio was 0.32. Outflow concentrations in our calculations are average values per period. Taking only the respective years, 2007 and 2015, outflow $^{231}$Pa/$^{230}$Th ratios changed from 0.25 (2007) to 0.54 (2015), due to the decrease by 38% of dissolved $^{230}$Th and a small increase of dissolved $^{231}$Pa in the EUB (<2000 m). A potential future development of outflow $^{231}$Pa/$^{230}$Th ratios will probably increase to the 2015 ratio (0.54) or even higher if the trends from the 2007-2015 period maintain, or even increase. The decreasing $^{230}$Th inventories in the Eurasian Basin lead to a lower accumulation of $^{230}$Th in GIN Sea sediments.

Increased scavenging removal at arctic margins will affect the sedimentary inventory of $^{230}$Th far away from those scavenging removal areas, while export of $^{231}$Pa is affected differently or might react with a temporal delay in a similar manner. There are indications that $^{231}$Pa scavenging removal in the Barents Sea and areas affected by waters from the Barents Sea will increase. This would lead to a reduced export of $^{231}$Pa in the future. For all periods presented in this study there is no significant export of $^{231}$Pa, following the model calculations, not even for the 1991 situation. This is in contrast to previous budgets. This is due to in and outflow values based on recent water column data and the focus of the model on the Eurasian Basin. If this finding represents the reality it would have impact on the interpretation of $^{231}$Pa/$^{230}$Th sedimentary ratios in the Gin Seas.

$^{231}$Pa/$^{230}$Th ratios in surface sediments in the GIN Seas are below or around the production ratio of 0.093 (Scholten *et al.*, 1995), the Arctic component adding to it is well above the production ratio, according to the model calculations, and might shift even more towards $^{231}$Pa. Therefore we expect that climate change alters scavenging removal of $^{230}$Th in the Eurasian Basin, which leads to an increase of $^{231}$Pa/$^{230}$Th in outflowing waters from the Arctic Ocean. Even if the consequences of enhanced margin or boundary scavenging in the Arctic are not directly measurable in GIN Sea sediments, due to bioturbation and/or due to the relatively small volume of the Arctic Ocean outflow compared to the GIN Seas, it might be worth noting that such signals can be buried in sediments overprinted by larger scale processes and situations. That means that changing scavenging intensities or scavenging behaviour of $^{230}$Th at the margins of the Eurasian Basin may still affect the $^{231}$Pa/$^{230}$Th ratio of advective export to the GIN Seas on

longer time scales and total accumulation of $^{230}$Th on decadal time scales, especially under rapidly changing climate conditions, such as the current global warming.

Past changes could show such patterns of changed $^{231}$Pa/$^{230}$Th ratios in Arctic export, such changes as initial forming of continental ice sheets transporting erosion material to the Arctic Ocean and of course the melting phases of those when particle input and composition changes (Azetsu-Scott and Syvitski, 1999) and release particles from e.g. Greenland to the central Arctic Ocean (Gillard *et al.*, 2016). Maybe even phases of higher rainfalls in North Europe, North Asia and North America e.g. during the late Holocene (Berntsson *et al.*, 2014) which can change on decadal timescales (Zhan *et al.*, 2018) leading to higher riverine particle discharge to the Arctic Ocean, could cause a notable change in $^{230}$Th scavenging removal. All of which will only be visible in sediment core data if their duration is long enough to leave an imprint that is not buried under a background situation or mixed with it by bioturbation. Additionally it is possible that $^{230}$Th and $^{231}$Pa get removed by scavenging in the Fram Strait and in the East Greenland Current (EGC), due to particle input from the Greenland's shelves and higher biological production compared to the ice covered Arctic Ocean (Sanchez-Vidal *et al.*, 2015).

### 3.4.2 Exchange with Amerasian Basin

The division of the budget into two depth ranges is based on the assumption that the topography of the Lomonosov Ridge disconnects deep water exchange between the Eurasian- and the Amerasian Basin. The deepest connection between the two major basins is via the Intra Basin, located in the middle of the Lomonosov Ridge, with a sill depth shallower than 1870 m (Björk *et al.*, 2007). This is in contrast to circulation of shallow and intermediate waters, which are able to exchange between the Eurasian and the Amerasian Basin (Rudels, 2009).

The Amerasian Basin developments of $^{230}$Th and $^{231}$Pa show a decrease for both isotopes, especially in intermediate waters. This decrease is due to increased scavenging and variability in circulation and mixing. Especially the Canada Basin experiences an increasing margin-basin transport of lithogenic and terrigenous material and enhanced biological production due to sea ice retreat (Grenier *et al.*, 2019). This margin-basin transport might be comparable to the margin scavenging process from the Eurasian Basin. In the Amerasian Basin the particle transport from the margins to the central basin already caused a reduction of both $^{230}$Th and $^{231}$Pa until 2015. Increased scavenging removal is accompanied by increased mixing of water masses (Yu *et al.*, 2020). We assume that reduced $^{230}$Th and $^{231}$Pa concentrations from the Eurasian Basin add to a reduction of the two tracers in the Amerasian Basin by mixing with ambient waters. Yu *et al.* (2020) combined a modelling study, including a circulation model, with measured tracer data

from the 2015 GEOTRACES Arctic Ocean campaign (Grenier *et al.*, 2019) and discussed the influence of Atlantic Waters on $^{230}$Th developments. Such a valuable approach using a circulation model should be done for the Eurasian Basin and extended to the entire Arctic Ocean, in order to understand $^{230}$Th and $^{231}$Pa reactions to climate change on an Arctic Ocean wide scale and the connections between its two major basins. Additionally the impact of Trans Polar Drift carried riverine, coastal and shelf particulate material to the central Arctic Ocean (Charette *et al.*, 2020; Kipp *et al.*, 2018; Rutgers van der Loeff *et al.*, 2018) on $^{230}$Th and $^{231}$Pa on both sides near the Lomonosov Ridge needs to be investigated in further detail in order to understand the connection of variabilities in both the Amerasian and the Eurasian Basin in relation to $^{230}$Th and $^{231}$Pa developments.

## 4. Conclusions

Generally inventories of $^{230}$Th and $^{231}$Pa can change rather quickly in the Arctic Ocean. Especially $^{230}$Th is highly reactive to environmental changes and decreased significantly in just 8 years. $^{231}$Pa seems less dynamic, most likely due to its lower particle reactivity and could react to the same processes differently or with a temporal delay.

The central Eurasian Basin (>2000 m) experienced a significant depletion of the dissolved $^{230}$Th inventory due to increased scavenging at inflow pathways of Atlantic waters in only 8 years. Therefore the margins of the Eurasian Basin are a sink of $^{230}$Th in the Arctic Ocean. $^{231}$Pa is mainly removed within the central Eurasian Basin. Nevertheless dissolved $^{231}$Pa decreased only in the Amundsen Basin part of the Eurasian Basin above 2000 m. Shorter ventilation times than in the Nansen Basin are a possible explanation, together with a higher influence of BSBW, which has undergone, at least seasonally, scavenging of $^{231}$Pa. The developments of $^{231}$Pa relative to $^{230}$Th are more difficult to identify. If there is recirculation north of the Fram Strait of waters leaving the Amundsen Basin, it might lead to stronger scavenging removal of $^{231}$Pa relative to $^{230}$Th, which already has been removed from these waters upstream. Areas of high particle fluxes or export of diatoms from the Barents Sea where these waters pass can therefore be a possible sink for Arctic $^{231}$Pa. The increased scavenging removal of $^{230}$Th at the margins of the Nansen Basin could point at increased boundary scavenging or its onset, due to recent climate changes.

Scavenging removal and subsequent sedimentation of $^{230}$Th in the deep Nansen Basin increases during or after volcanic eruptions at the Gakkel Ridge. It is possible that $^{231}$Pa reacts in a later stage of the same process with a temporal delay and most likely to a lesser extent. Hence periodically the $^{231}$Pa/$^{230}$Th activity ratio in sediments of the deep Nansen Basin decreases

during these phases. Environmental changes, due to climate warming, in the Arctic Ocean cause a higher $^{231}$Pa/$^{230}$Th ratio in outflowing waters, due to strong decrease of dissolved $^{230}$Th, while $^{231}$Pa did not decrease and has partly even increased. This also indicates that the central Arctic Ocean and especially its margins are or become a sink for $^{230}$Th. Therefore export of $^{230}$Th reduced between 2007 and 2015 and will probably continue to decrease in the future, which would over longer time scales lead to reduced sedimentation of $^{230}$Th in the GIN Seas or the Fram Strait. The main result of our models and discussion is that we do not find indications for export of $^{231}$Pa in the order suggested by Moran *et al.* (2005) and rather conclude that the Arctic Ocean is or becomes a sink for $^{231}$Pa. This is not necessarily in contrast to Moran *et al.* (2005), given the different timescales of investigation, it rather points at changing environmental conditions and the importance of processes happening in the upper parts of the water column, such as scavenging removal in inflowing Atlantic Waters. The inclusion of shallow inflow as well as outflow concentrations averaged for time periods leads to the absence of $^{231}$Pa export through Fram Strait even for the 1991 situation, although export through the Canadian Archipelago is also neglected in this study.

A remaining question is where $^{231}$Pa is eventually buried in the Arctic Ocean or its neighbouring seas. Our model does not yield $^{231}$Pa sedimentation numbers that are consistent with published sediment core data. This can indicate a missing margin or boundary scavenging component of $^{231}$Pa in the Eurasian Basin and its margins or an unidentified removal process. Finally the $^{231}$Pa scavenging situation might be changing currently. Concluding the discussion of $^{231}$Pa scavenging removal in the upper 2000 m of the Eurasian Basin we hypothesize that the margins of the Eurasian Basin are a sink for Arctic $^{231}$Pa rather than advective export to the GIN Seas.

**Data Accessibility**

Data used in this study is available at https://doi.org/10.1594/PANGAEA.893871, https://doi.org/10.1594/PANGAEA.908068, https://doi.org/10.1016/j.chemgeo.2019.119380.

**References**

Andersen, M.B., Stirling, C.H., Zimmermann, B., Halliday, A.N., 2010. Precise determination of the open ocean 234U/238U composition. Geochemistry, Geophysics, Geosystems 11 (12).

Arrigo, K.R., van Dijken, G., Pabi, S., 2008. Impact of a shrinking Arctic ice cover on marine primary production. Geophysical Research Letters 35 (19), n/a-n/a.

Arrigo, K.R., van Dijken, G.L., 2015. Continued increases in Arctic Ocean primary production. Progress in Oceanography 136, 60-70.

Azetsu-Scott, K., Syvitski, J., 1999. Influence of melting icebergs on distribution, characteristics and transport of marine particles in an East Greenland fjord. Journal of Geophysical Research 104, 5321-5328.

Backman, J., Jakobsson, M., Lovlie, r., Polyak, L., Febo, L.A., 2004. Is the central Arctic Ocean a sediment starved basin? Quaternary Science Reviews 23, 1435-1454.

Baker, E.T., Edmonds, H.N., Michael, P.J., Bach, W., Dick, H.J.B., Snow, J.E., Walker, S.L., Banerjee, N.R., Langmuir, C.H., 2004. Hydrothermal venting in magma deserts: The ultraslow-spreading Gakkel and Southwest Indian Ridges. Geochemistry, Geophysics, Geosystems 5 (8).

Berntsson, A., Rosqvist, G.C., Velle, G., 2014. Late-Holocene temperature and precipitation changes in Vindelfjällen, mid-western Swedish Lapland, inferred from chironomid and geochemical data. The Holocene 24 (1), 78-92.

Beszczynska-Möller, A., Fahrbach, E., Schauer, U., Hansen, E., 2012. Variability in Atlantic water temperature and transport at the entrance to the Arctic Ocean, 1997–2010. ICES Journal of Marine Science 69 (5), 852-863.

Björk, G., Jakobsson, M., Rudels, B., Swift, J.H., Anderson, L., Darby, D.A., Backman, J., Coakley, B., Winsor, P., Polyak, L., Edwards, M., 2007. Bathymetry and deep-water exchange across the central Lomonosov Ridge at 88–89°N. Deep Sea Research Part I: Oceanographic Research Papers 54 (8), 1197-1208.

Boetius, A., Albrecht, S., Bakker, K., Bienhold, C., Felden, J., Fernández-Méndez, M., Hendricks, S., Katlein, C., Lalande, C., Krumpen, T., Nicolaus, M., Peeken, I., Rabe, B., Rogacheva, A., Rybakova, E., Somavilla, R., Wenzhöfer, F., 2013. Export of Algal Biomass from the Melting Arctic Sea Ice. Science 339.

Bruland, K.W., Orians, K.J., Cowen, J.P., 1994. Reactive trace metals in the stratified central North Pacific. Geochimica et Cosmochimica Acta 58 (15), 3171-3182.

Cai, P., Rutgers van der Loeff, M.M., Stimac, I., Nöthig, E.-M., Lepore, K., Moran, S.B., 2010. Low export flux of particulate organic carbon in the central Arctic Ocean as revealed by $^{234}$Th:$^{238}$U disequilibrium. Journal of Geophysical Research 115.

Cann, J.R., Smith, D.K., 2005. Evolution of volcanism and faulting in a segment of the Mid-Atlantic Ridge at 25°N. Geochemistry, Geophysics, Geosystems 6 (9).

Casacuberta, N., Christl, M., Vockenhuber, C., Wefing, A.-M., Wacker, L., Masqué, P., Synal, H.-A., Rutgers van der Loeff, M., 2018. Tracing the Three Atlantic Branches Entering the Arctic Ocean With $^{129}$I and $^{236}$U. Journal of Geophysical Research: Oceans 0 (0).

Charette, M.A., Kipp, L.E., Jensen, L.T., Dabrowski, J.S., Whitmore, L.M., Fitzsimmons, J.N., Williford, T., Ulfsbo, A., Jones, E., Bundy, R.M., Vivancos, S.M., Pahnke, K., John, S.G., Xiang, Y., Hatta, M., Petrova, M.V., Heimbürger-Boavida, L.-E., Bauch, D., Newton, R.,

Pasqualini, A., Agather, A.M., Amon, R.M.W., Anderson, R.F., Andersson, P.S., Benner, R., Bowman, K.L., Edwards, R.L., Gdaniec, S., Gerringa, L.J.A., González, A.G., Granskog, M., Haley, B., Hammerschmidt, C.R., Hansell, D.A., Henderson, P.B., Kadko, D.C., Kaiser, K., Laan, P., Lam, P.J., Lamborg, C.H., Levier, M., Li, X., Margolin, A.R., Measures, C., Middag, R., Millero, F.J., Moore, W.S., Paffrath, R., Planquette, H., Rabe, B., Reader, H., Rember, R., Rijkenberg, M.J.A., Roy-Barman, M., Rutgers van der Loeff, M., Saito, M., Schauer, U., Schlosser, P., Sherrell, R.M., Shiller, A.M., Slagter, H., Sonke, J.E., Stedmon, C., Woosley, R.J., Valk, O., van Ooijen, J., Zhang, R., 2020. The Transpolar Drift as a Source of Riverine and Shelf-Derived Trace Elements to the Central Arctic Ocean. Journal of Geophysical Research: Oceans 125 (5), e2019JC015920.

Chase, Z., Anderson, R.F., Fleisher, M.Q., Kubik, P.W., 2002. The influence of particle composition and particle flux on scavenging of Th, Pa and Be in the ocean. Earth and Planetary Science Letters 204, 215-229.

Clough, L.M., Ambrose, W.G., Kirk Cochran, J., Barnes, C., Renaud, P.E., Aller, R.C., 1997. Infaunal density, biomass and bioturbation in the sediments of the Arctic Ocean. Deep Sea Research Part II: Topical Studies in Oceanography 44 (8), 1683-1704.

Cochran, J.R., 2008. Seamount volcanism along the Gakkel Ridge, Arctic Ocean. Geophysical Journal International 174 (3), 1153-1173.

Cochran, J.R., Kurras, G.J., Edwards, M.H., Coakley, B.J., 2003. The Gakkel Ridge: Bathymetry, gravity anomalies, and crustal accretion at extremely slow spreading rates. Journal of Geophysical Research: Solid Earth 108 (B2), n/a-n/a.

Condon, D.J., McLean, N., Noble, S.R., Bowring, S.A., 2010. Isotopic composition ($^{238}$U/$^{235}$U) of some commonly used uranium reference materials. Geochimica et Cosmochimica Acta 74 (24), 7127-7143.

Coppola, L., Roy-Barman, M., Wassmann, P., Mulsow, S., Jeandel, C., 2002. Calibration of sediment traps and particulate organic carbon export using $^{234}$Th in the Barents Sea. Marine Chemistry 80, 11-26.

Costa, K.M., Hayes, C.T., Anderson, R.F., Pavia, F.J., Bausch, A., Deng, F., Dutay, J.-C., Geibert, W., Heinze, C., Henderson, G., Hillaire-Marcel, C., Hoffmann, S., Jaccard, S.L., Jacobel, A.W., Kienast, S.S., Kipp, L., Lerner, P., Lippold, J., Lund, D., Marcantonio, F., McGee, D., McManus, J.F., Mekik, F., Middleton, J.L., Missiaen, L., Not, C., Pichat, S., Robinson, L.F., Rowland, G.H., Roy-Barman, M., Tagliabue, A., Torfstein, A., Winckler, G., Zhou, Y., 2020. $^{230}$Th Normalization: New Insights on an Essential Tool for Quantifying Sedimentary Fluxes in the Modern and Quaternary Ocean. Paleoceanography and Paleoclimatology 35 (2), e2019PA003820.

Dalpadado, P., Arrigo, K.R., van Dijken, G.L., Skjoldal, H.R., Bagøien, E., Dolgov, A.V., Prokopchuk, I.P., Sperfeld, E., 2020. Climate effects on temporal and spatial dynamics of phytoplankton and zooplankton in the Barents Sea. Progress in Oceanography 185, 102320.

Dukhovskoy, D., Johnson, M., Proshutinsky, A.Y., 2004. Arctic decadal variability: An auto-oscillatory system of heat and fresh water exchange. Geophys. Res. Lett. 31.

Dukhovskoy, D., Johnson, M., Proshutinsky, A.Y., 2006. Arctic decadal variability from an idealized atmosphere-ice-ocean model : 2. Simulation of decadal oscillations. Journal of Geophysical Research 111.

Edmonds, H.N., Moran, S.B., Cheng, H., Edwards, R.L., 2004. $^{230}$Th and $^{231}$Pa in the Arctic Ocean: implications for particle fluxes and basin-scale Th/Pa fractionation. Earth and Planetary Science Letters 227, 155-167.

Edwards, M.H., Kurras, G.J., Tolstoy, M., Bohnenstiehl, D.R., Coakley, B.J., Cochran, J.R., 2001. Evidence of recent volcanic activity on the ultraslow-spreading Gakkel ridge. Nature 409 (6822), 808-812.

Ellingsen, I.H., Dalpadado, P., Slagstad, D., Loeng, H., 2008. Impact of climatic change on the biological production in the Barents Sea. Climatic Change 87 (1), 155-175.

Fitzsimmons, J.N., Boyle, E.A., Jenkins, W.J., 2014. Distal transport of dissolved hydrothermal iron in the deep South Pacific Ocean. Proceedings of the National Academy of Sciences 111 (47), 16654-16661.

Fitzsimmons, J.N., John, S.G., Marsay, C.M., Hoffman, C.L., Nicholas, S.L., Toner, B.M., German, C.R., Sherrell, R.M., 2017. Iron persistence in a distal hydrothermal plume supported by dissolved-particulate exchange. Nature Geosci 10 (3), 195-201.

Gard, G., 1993. Late Quaternary coccoliths at the North Pole: Evidence of ice-free conditions and rapid sedimentation in the central Arctic Ocean. Geology 21 (3), 227-230.

Gardner, W., Richardson, M., Mishonov, A., 2020. Global Transmissometer Database V3 (Coupled with CTD data).

Gdaniec, S., Roy-Barman, M., Levier, M., Valk, O., van der Loeff, M.R., Foliot, L., Dapoigny, A., Missiaen, L., Mörth, C.-M., Andersson, P.S., 2020. $^{231}$Pa and $^{230}$Th in the Arctic Ocean: Implications for boundary scavenging and $^{231}$Pa-$^{230}$Th fractionation in the Eurasian Basin. Chemical Geology 532, 119380.

Geibert, W., Usbeck, R., 2003. Adsorption of thorium and protactinium onto different particle types: Experimental findings. Geochimica et Cosmochimica Acta 68, 1486-1501.

Gillard, L.C., Hu, X., Myers, P.G., Bamber, J.L., 2016. Meltwater pathways from marine terminating glaciers of the Greenland ice sheet. Geophysical Research Letters 43 (20), 10,873-810,882.

Grenier, M., François, R., Soon, M., Rutgers van der Loeff, M., Yu, X., Valk, O., Not, C., Moran, S.B., Edwards, R.L., Lu, Y., Lepore, K., Allen, S.E., 2019. Changes in Circulation and Particle Scavenging in the Amerasian Basin of the Arctic Ocean over the Last Three Decades Inferred from the Water Column Distribution of Geochemical Tracers. Journal of Geophysical Research: Oceans 124 (12), 9338-9363.

Günther, F., Overduin, P.P., Sandakov, A.V., Grosse, G., Grigoriev, M.N., 2013. Short- and long-term thermo-erosion of ice-rich permafrost coasts in the Laptev Sea region. Biogeosciences 10 (6), 4297-4318.

Hayes, C.T., Anderson, R.F., Fleisher, M.Q., Huang, K.F., Robinson, L.F., Lu, Y., Cheng, H., Edwards, R.L., Moran, S.B., 2015. $^{230}$Th and $^{231}$Pa on GEOTRACES GA03, the U.S. GEOTRACES North Atlantic transect, and implications for modern and paleoceanographic chemical fluxes. Deep-Sea Research Part II: Topical Studies in Oceanography 116, 29-41.

Hoffmann, S., McManus, J., 2007. Is there a $^{230}$Th deficit in Arctic sediments? Earth and Planetary Science Letters 258 (3), 516-527.

Hoffmann, S., McManus, J., Curry, W.B., Brown-Leger, S.L., 2013. Persistent export of $^{231}$Pa from the deep central Arctic Ocean over the past 35,000 years. Nature 497, 603-607.

Huh, C.-A., Pisias, N., Kelley, J.M., C., M.T., Grantz, A., 1997. Natural radionuclides and plutonium in sediments from the western Arctic Ocean: sedimentation rates and pathways of radionuclides. Deep-Sea Research II 44, 1725-1743.

Iversen, M.H., Ploug, H., 2013. Temperature effects on carbon-specific respiration rate and sinking velocity of diatom aggregates - potential implications for deep ocean export processes. Biogeosciences 10 (6), 4073-4085.

Jakobsson, M., Grantz, A., Kristoffersen, Y., Macnab, R., MacDonald, R.W., Sakshaug, E., Stein, R., Jokat, W., 2004. The Arctic Ocean: Boundary Conditions and Background Information. In: Stein, R., MacDonald, R.W. (Eds.), The Organic Carbon Cycle in the Arctic Ocean. Springer Berlin Heidelberg, Berlin, Heidelberg, pp. 1-32.

Jensen, L.T., Morton, P., Twining, B.S., Heller, M.I., Hatta, M., Measures, C.I., John, S., Zhang, R., Pinedo-Gonzalez, P., Sherrell, R.M., Fitzsimmons, J.N., 2020. A comparison of marine Fe and Mn cycling: U.S. GEOTRACES GN01 Western Arctic case study. Geochimica et Cosmochimica Acta.

Juul-Pedersen, T., Michel, C., Gosselin, M., 2010. Sinking export of particulate organic material from the euphotic zone in the eastern Beaufort Sea. Marine Ecology-Progress Series 410, 55-70.

Kipp, L.E., Charette, M.A., Moore, W.S., Henderson, P.B., Rigor, I.G., 2018. Increased fluxes of shelf-derived materials to the central Arctic Ocean. Science Advances 4 (1).

Kretschmer, S., Geibert, W., Rutgers van der Loeff, M.M., Schnabel, C., Xu, S., Mollenhauer, G., 2011. Fractionation of $^{230}$Th, $^{231}$Pa, and $^{10}$Be induced by particle size and composition within an opal-rich sediment of the Atlantic Southern Ocean. Geochimica et Cosmochimica Acta 75, 6971–6987.

Kuzyk, Z.Z.A., Gobeil, C., Macdonald, R.W., 2013. $^{210}$Pb and $^{137}$Cs in margin sediments of the Arctic Ocean: Controls on boundary scavenging. GLOBAL BIOGEOCHEMICAL CYCLES 27 (2), 422-439.

Lalande, C., Nöthig, E.-M., Fortier, L., 2019. Algal Export in the Arctic Ocean in Times of Global Warming. Geophysical Research Letters 46 (11), 5959-5967.

Lao, Y., Anderson, R.F., Broecker, W.S., Trumbore, S.E., Hofmann, H.J., Wolfli, W., 1992. Transport and burial rates of $^{10}$Be and $^{231}$Pa in the Pacific Ocean during the Holocene period. Earth and Planetary Science Letters 113.

Liguori, B., Ehlert, C., Pahnke, K., 2020. The Influence of Water Mass Mixing and Particle Dissolution on the Silicon Cycle in the Central Arctic Ocean. Frontiers in Marine Science 7.

Lind, S., Ingvaldsen, R.B., 2012. Variability and impacts of Atlantic Water entering the Barents Sea from the north. Deep Sea Research Part I: Oceanographic Research Papers 62, 70-88.

Luo, Y., Lippold, J., 2015. Controls on $^{231}$Pa and $^{230}$Th in the Arctic Ocean. Geophysical Research Letters 42 (14), 5942-5949.

Miklasz, K.A., Denny, M.W., 2010. Diatom sinkings speeds: Improved predictions and insight from a modified Stokes' law. Limnology and Oceanography 55 (6), 2513-2525.

Moran, S.B., Hoff, J.A., Buesseler, K.O., Edwards, R.L., 1995. High precision $^{230}$Th and $^{232}$Th in the Norwegian Sea and Denmark by thermal ionization mass spectrometry. Geophysical Research Letters 22 (19), 2589-2592.

Moran, S.B., Shen, C.-C., Edmonds, H.N., Weinstein, S.E., Smith, J.N., Edwards, R.L., 2002. Dissolved and particulate $^{231}$Pa and $^{230}$Th in the Atlantic Ocean: constraints on

intermediate/deep water age, boundaryscavenging, and $^{231}$Pa/$^{230}$Th fractionation. Earth and Planetary Science Letters 203, 999-1014.

Moran, S.B., Shen, C.-C., Edwards, R.L., Edmonds, H.N., Scholten, J.C., Smith, J.N., Ku, T.-L., 2005. $^{231}$Pa and $^{230}$Th in surface sediments of the Arctic Ocean: Implications for $^{231}$Pa/$^{230}$Th fractionation, boundary scavenging, and advective export. Earth and Planetary Science Letters 234, 235-248.

Nöthig, E.-M., Lalande, C., Fahl, K., Metfies, K., Salter, I., Bauerfeind, E., 2020a. Annual cycle of downward particle fluxes on each side of the Gakkel Ridge in the central Arctic Ocean. Philosophical Transactions of the Royal Society A: Mathematical, Physical and Engineering Sciences 378 (2181), 20190368.

Nöthig, E.-M., Ramondenc, S., Haas, A., Hehemann, L., Walter, A., Bracher, A., Lalande, C., Metfies, K., Peeken, I., Bauerfeind, E., Boetius, A., 2020b. Summertime Chlorophyll a and Particulate Organic Carbon Standing Stocks in Surface Waters of the Fram Strait and the Arctic Ocean (1991–2015). Frontiers in Marine Science 7 (350).

Nozaki, Y., Horibe, Y., Tsubota, H., 1981. The water column distributions of thorium isotopes in the western North Pacific. Earth and Planetary Science Letters 54 (2), 203-216.

Orkney, A., Platt, T., Narayanaswamy, B.E., Kostakis, I., Bouman, H.A., 2020. Bio-optical evidence for increasing *Phaeocystis* dominance in the Barents Sea. Philosophical Transactions of the Royal Society A: Mathematical, Physical and Engineering Sciences 378 (2181), 20190357.

Owens, S.A., Buesseler, K.O., Sims, K.W.W., 2011. Re-evaluating the $^{238}$U-salinity relationship in seawater: Implications for the $^{238}$U–$^{234}$Th disequilibrium method. Marine Chemistry 127 (1), 31-39.

Pavia, F., Anderson, R., Vivancos, S., Fleisher, M., Lam, P., Lu, Y., Cheng, H., Zhang, P., Lawrence Edwards, R., 2018. Intense hydrothermal scavenging of $^{230}$Th and $^{231}$Pa in the deep Southeast Pacific. Marine Chemistry 201, 212-228.

Ploug, H., Grossart, H.-P., 2000. Bacterial growth and grazing on diatom aggregates: Respiratory carbon turnover as a function of aggregate size and sinking velocity. Limnology and Oceanography 45 (7), 1467-1475.

Pontbriand, C.W., Soule, S.A., Sohn, R.A., Humphris, S.E., Kunz, C., Singh, H., Nakamura, K.-i., Jakobsson, M., Shank, T., 2012. Effusive and explosive volcanism on the ultraslow-spreading Gakkel Ridge, 85°E. Geochemistry, Geophysics, Geosystems 13 (10).

Proshutinsky, A.Y., Dukhovskoy, D., Timmermans, M.-L., Krishfield, R., Bamber, J.L., 2015. Arctic circulation regimes. Philosophical Transactions of the Royal Society A: Mathematical, Physical and Engineering Sciences 373 (2052), 20140160.

Proshutinsky, A.Y., Johnson, M.A., 1997. Two circulation regimes of the wind-driven Arctic Ocean. JOURNAL OF GEOPHYSICAL RESEARCH, 102, 12493-12514.

Proshutinsky, A.Y., Polyakov, I.V., Johnson, M.A., 1999. Climate states and variability of Arctic ice and water dynamics during 1946–1997. Polar Research 18 (2), 135-142.

Rabe, B., Schauer, U., Ober, S., Horn, M., Hoppmann, M., Korhonen, M., Pisarev, S., Hampe, H., Villacieros, N., Savy, J.P., Wisotzki, A., 2016. Physical oceanography during POLARSTERN cruise PS94 (ARK-XXIX/3). PANGAEA.

Randelhoff, A., Sundfjord, A., 2017. Short Commentary on Marine Productivity at Arctic Shelf Breaks: Upwelling, Advection and Vertical Mixing. Ocean Science Discussions, 1-11.

Riedel, C., Schlindwein, V., 2010. Did the 1999 earthquake swarm on Gakkel Ridge open a volcanic conduit? A detailed teleseismic data analysis. Journal of Seismology 14 (3), 505-522.

Rijkenberg, M.J.A., Slagter, H.A., Rutgers van der Loeff, M., van Ooijen, J., Gerringa, L.J.A., 2018. Dissolved Fe in the Deep and Upper Arctic Ocean With a Focus on Fe Limitation in the Nansen Basin. Frontiers in Marine Science 5 (88).

Rudels, B., 2009. Arctic Ocean Circulation A2 - Steele, John H. Encyclopedia of Ocean Sciences (Second Edition). Academic Press, Oxford, pp. 211-225.

Rudels, B., Jones, E., Schauer, U., Eriksson, P., 2004. Atlantic sources of the Arctic Ocean surface and halocline waters. Polar Research 23, 181-208.

Rutgers van der Loeff, M., Kipp, L., Charette, M.A., Moore, W.S., Black, E., Stimac, I., Charkin, A., Bauch, D., Valk, O., Karcher, M., Krumpen, T., Casacuberta, N., Smethie, W., Rember, R., 2018. Radium Isotopes Across the Arctic Ocean Show Time Scales of Water Mass Ventilation and Increasing Shelf Inputs. Journal of Geophysical Research: Oceans 0 (0).

Sanchez-Vidal, A., Veres, O., Langone, L., Ferré, B., Calafat, A., Canals, M., Durrieu de Madron, X., Heussner, S., Mienert, J., Grimalt, J.O., Pusceddu, A., Danovaro, R., 2015. Particle sources and downward fluxes in the eastern Fram strait under the influence of the west Spitsbergen current. Deep Sea Research Part I: Oceanographic Research Papers 103, 49-63.

Schauer, U., Loeng, H., Rudels, B., Ozhigin, V.K., Dieck, W., 2002. Atlantic Water flow through the Barents and Kara Seas. Deep Sea Research Part I: Oceanographic Research Papers 49 (12), 2281-2298.

Schlosser, P., Kromer, B., Östlund, G., Ekwurzel, B., Bönisch, G., Loosli, H.H., Purtschert, R., 1994. On the $^{14}$C and $^{39}$Ar Distribution in the Central Arctic Ocean: Implications for Deep Water Formation. Radiocarbon 36 (3), 327-343.

Schlindwein, V., Riedel, C., 2010. Location and source mechanism of sound signals at Gakkel ridge, Arctic Ocean: Submarine Strombolian activity in the 1999–2001 volcanic episode. Geochemistry, Geophysics, Geosystems 11 (1).

Schlitzer, R., 2016. Ocean Data View. http://odv.awi.de.

Schmid, F., Schlindwein, V., Koulakov, I., Plötz, A., Scholz, J.-R., 2017. Magma plumbing system and seismicity of an active mid-ocean ridge volcano. 7, 42949.

Scholten, J.C., Rutgers van der Loeff, M.M., Michel, A., 1995. Distribution of $^{230}$Th and $^{231}$Pa in the water column in relation to the ventilation of the deep Arctic basins. Deep-Sea Research II 42, 1519-1531.

Schuur, E.A.G., Abbott, B.W., Bowden, W.B., Brovkin, V., Camill, P., Canadell, J.G., Chanton, J.P., Chapin, F.S., Christensen, T.R., Ciais, P., Crosby, B.T., Czimczik, C.I., Grosse, G., Harden, J., Hayes, D.J., Hugelius, G., Jastrow, J.D., Jones, J.B., Kleinen, T., Koven, C.D., Krinner, G., Kuhry, P., Lawrence, D.M., McGuire, A.D., Natali, S.M., O'Donnell, J.A., Ping, C.L., Riley, W.J., Rinke, A., Romanovsky, V.E., Sannel, A.B.K., Schädel, C., Schaefer, K., Sky, J., Subin, Z.M., Tarnocai, C., Turetsky, M.R., Waldrop, M.P., Walter Anthony, K.M., Wickland, K.P., Wilson, C.J., Zimov, S.A., 2013. Expert assessment of vulnerability of permafrost carbon to climate change. Climatic Change 119 (2), 359-374.

Schuur, E.A.G., McGuire, A.D., Schädel, C., Grosse, G., Harden, W.J., Hayes, D.J., Hugelius, G., Koven, C.D., Kuhry, P., Lawrence, D.M., Natali, S.M., Olefeldt, D., Romanovsky, V.E., Schaefer, K., Turetsky, M.R., Treat, C.C., Vonk, J.E., 2015. Climate change and the permafrost carbon feedback. Nature 520, 171-179.

Shen, C.-C., Cheng, H., Edwards, R.L., Moran, S.B., Edmonds, H.N., Hoff, J.A., Thomas, R.B., 2003. Measurement of Attogram Quantities of $^{231}$Pa in Dissolved and Particulate Fractions of Seawater by Isotope Dilution Thermal Ionization Mass Spectroscopy. analytical chemistry 75 (5), 1075-1079.

Signorini, S.R., McClain, C.R., 2009. Environmental factors controlling the Barents Sea spring-summer phytoplankton blooms. Geophysical Research Letters 36 (10).

Smethie, W.M., Jr., 2017. CFC-11, CFC-12, CFC-113, and SF6 measured on water bottle samples during POLARSTERN cruise PS94 (ARK-XXIX/3) to the Arctic Ocean in 2016. PANGAEA.

Smith, D.K., Cann, J.R., 1993. Building the crust at the Mid-Atlantic Ridge. Nature 365 (6448), 707-715.

Smith, J.N., McLaughlin, F.A., Smethie, W.M., Moran, S.B., Lepore, K., 2011. Iodine-129, 137Cs, and CFC-11 tracer transit time distributions in the Arctic Ocean. Journal of Geophysical Research: Oceans 116 (C4), n/a-n/a.

Sohn, R.A., Willis, C., Humphris, S., Shank, T.M., Singh, H., Edmonds, H.N., Kunz, C., Hedman, U., Helmke, E., Jakuba, M., Liljebladh, B., Linder, J., Murphy, C., Nakamura, K.-i., Sato, T., Schlindwein, V., Stranne, C., Tausenfreund, M., Upchurch, L., Winsor, P., Jakobsson, M., Soule, A., 2008. Explosive volcanism on the ultraslow-spreading Gakkel ridge, Arctic Ocean. Nature 453 (7199), 1236-1238.

Tanhua, T., Jones, E.P., Jeansson, E., Jutterström, S., Smethie, W.M., Wallace, D.W.R., Anderson, L.G., 2009. Ventilation of the Arctic Ocean: Mean ages and inventories of anthropogenic CO2 and CFC-11. Journal of Geophysical Research: Oceans 114 (C1), n/a-n/a.

Valk, O., Rutgers van der Loeff, M.M., Geibert, W., Gdaniec, S., Moran, S.B., Lepore, K., Edwards, R.L., Lu, Y., Puigcorbé, V., Casacuberta, N., Paffrath, R., Smethie, W., Roy-Barman, M., 2020. Decrease in $^{230}$Th in the Amundsen Basin since 2007: far-field effect of increased scavenging on the shelf? Ocean Sci. 16 (1), 221-234.

Valk, O., Rutgers van der Loeff, M.M., Geibert, W., Gdaniec, S., Rijkenberg, M.J.A., Moran, S.B., Lepore, K., Edwards, R.L., Lu, Y., Puigcorbé, V., 2018. Importance of Hydrothermal Vents in Scavenging Removal of $^{230}$Th in the Nansen Basin. Geophysical Research Letters 0 (0).

van Ooijen, J.C., Rijkenberg, M.J.A., Gerringa, L.J.A., Rabe, B., Rutgers van der Loeff, M.M., 2016. Inorganic nutrients measured on water bottle samples during POLARSTERN cruise PS94 (ARK-XXIX/3). PANGAEA.

Walter, H.-J., Rutgers van der Loeff, M.M., François, R., 1999. Reliability of the $^{231}$Pa /$^{230}$Th Activity Ratio as a Tracer for Bioproductivity of the Ocean. In: Fischer, G., Wefer, G. (Eds.), Use of Proxies in Paleoceanography: Examples from the South Atlantic. Springer Berlin Heidelberg, Berlin, Heidelberg, pp. 393-408.

Walter, H.J., Rutgers van der Loeff, M.M., Hoeltzen, H., 1997. Enhanced scavenging of $^{231}$Pa relative to $^{230}$Th in the South Atlantic south of the Polar Front: Implications for the use of

the $^{231}$Pa/$^{230}$Th ratio as a paleoproductivity proxy. Earth and Planetary Science Letters 149, 85-100.

Wassmann, P., Vernet, M., Mitchell, B.G., Rey, F., 1990. Mass sedimentation of Phaeocystis pouchelii the Barents Sea. Marine Ecology-progress Series - MAR ECOL-PROGR SER 66, 183-195.

Wefing, A.-M., Casacuberta, N., Christl, M., Gruber, N., Smith, J., 2020. Circulation timescales of Atlantic Waters in the Arctic Ocean determined from anthropogenic radionuclides.

Wells, L.E., Cordray, M., Bowerman, S., Miller, L.A., Vincent, W.F., Deming, J.W., 2006. Archaea in particle-rich waters of the Beaufort Shelf and Franklin Bay, Canadian Arctic: Clues to an allochthonous origin? Limnology and Oceanography 51 (1), 47-59.

Wisotzki, A., 2008. Physical oceanography measured on water bottle samples during POLARSTERN cruise ARK-XXII/2. In: Bakker, Karel; Wisotzki, Andreas (2009): Physical oceanography and hydrochemistry profiles measured on water bottle samples during POLARSTERN cruise ARK-XXII/2. Alfred Wegener Institute, Helmholtz Center for Polar and Marine Research, Bremerhaven, PANGAEA, https://doi.org/10.1594/PANGAEA.712157. PANGAEA.

Yu, E.-F., Francois, R., Rutgers van der Loeff, M.M., 1996. Similar rates of modern and last-glacial ocean thermohaline circulation inferred from radiochemical data. Nature 379, 689-694.

Yu, X., Allen, S.E., François, R., Grenier, M., Myers, P.G., Hu, X., 2020. Modeling Dissolved and Particulate Th in the Canada Basin: Implications for Recent Changes in Particle Flux and Intermediate Circulation. Journal of Geophysical Research: Oceans 125 (2), e2019JC015640.

Zhan, Y., Ren, G., Yang, S., 2018. Change in precipitation over the Asian continent from 1901 to 2016 based on a new multi-source dataset. Climate Research 76, 41–57.

# CHAPTER 5: $^{231}$Pa and $^{230}$Th in the Arctic Ocean: Implications for Boundary Scavenging and $^{231}$Pa-$^{230}$Th Fractionation in the Eurasian Basin

**Sandra Gdaniec[1,2,3], Matthieu Roy-Barman[3], Martin Levier[3], Ole Valk, Michiel M. Rutgers van der Loeff[4], Lorna Foliot[3], Arnaud Dapoigny[3], Lise Missiaen[3], Carl-Magnus Mörth[1], Per S. Andersson[1]**

[1]Stockholm University, Department of Geological Sciences, 106 91, Stockholm, Sweden

[2]Swedish Museum of Natural History, Department of Geosciences, Stockholm, Sweden

[3]Laboratoire des Sciences du Climat et de l'Environnement, LSCE/IPSL, CEA – CNRS – UVSQ, Université Paris-Saclay, 91191 Gif-sur-Yvette, France

[4]Alfred-Wegener-Institute Helmholtz Centre for Polar and Marine Research, 27570 Bremerhaven, Germany

**Keywords:**

• GEOTRACES

• Protactinium

• Thorium

• Arctic Ocean

• Boundary scavenging

Manuscript published in *Chemical Geology*, Volume 532, 2020, 119380, ISSN 0009-2541, https://doi.org/10.1016/j.chemgeo.2019.119380

Received: 23 April 2019,
Revised: 6 November 2019
Accepted: 7 November 2019
Available online: 9 November 2019.

**Abstract**

$^{231}$Pa, $^{230}$Th and $^{232}$Th were analysed in filtered seawater ($n$ = 70) and suspended particles ($n$ = 39) collected along a shelf-basin transect from the Barents shelf to the Makarov Basin in the Arctic Ocean during GEOTRACES section GN04 in 2015. The distribution of dissolved $^{231}$Pa and $^{230}$Th in the Arctic Ocean deviates from the linear increase expected from reversible scavenging. Higher $^{232}$Th concentrations were observed at the shelf, slope and in surface waters in the deep basin, pointing at lithogenic sources. Fractionation factors ($F_{Th/Pa}$) observed at the Nansen margin were higher compared to $F_{Th/Pa}$ in the central Nansen Basin, possibly due to the residual occurrence of hydrothermal particles in the deep central Nansen Basin. Application of a boundary scavenging model quantitatively accounts for the dissolved and particulate $^{230}$Th distributions in the Nansen Basin. Modelled dissolved $^{231}$Pa distributions were largely overestimated, which was attributed to the absence of incorporation of water exchange with the Atlantic Ocean in the model. $^{231}$Pa/$^{230}$Th ratios of the suspended particles of the Nansen Basin were below the $^{231}$Pa/$^{230}$Th production ratio, but top-core sediments of the Nansen margin and slope have high $^{231}$Pa/$^{230}$Th-ratios, suggesting that scavenging along the Nansen margin partly acts as a sink for the missing Arctic $^{231}$Pa.

## 1. Introduction

Particle reactive isotopes in the natural uranium and thorium decay series are useful tracers of particle flux and scavenging in the oceans (e.g. Edmonds *et al.*, 2004; Roy-Barman, 2009; Rutgers van der Loeff and Berger, 1993). In seawater, $^{231}$Pa and $^{230}$Th are produced at a constant rate by the decay of homogeneously distributed $^{235}$U and $^{234}$U, respectively. Both $^{231}$Pa and $^{230}$Th are particle reactive elements, which means that they get scavenged onto settling particles and removed from the water column to the sediments. However, due to differences in their particle reactivity, the $^{231}$Pa/$^{230}$Th ratio of seawater, marine particles and sediments often differs from that of the production ratio (Rutgers van der Loeff and Berger, 1993). The distribution and dispersion of $^{231}$Pa and $^{230}$Th in the water column and their ratio in sediments are of interest for processes controlling spatial and temporal variations in ocean biogeochemistry. The difference in the chemical behaviour of the two tracers can result in large scale deviation of the $^{231}$Pa/$^{230}$Th ratio of marine sediments compared to the production ratio of these nuclides in the overlying water column, with higher sedimentary $^{231}$Pa/$^{230}$Th ratios at ocean margin and lower $^{231}$Pa/$^{230}$Th to the inner ocean compared to the production ratio. Differences in particle concentration, composition and flux influence scavenging rates of $^{231}$Pa and $^{230}$Th in the water column (Chase *et al.*, 2002). Environments governed by high particle flux, such as ocean margins are very

effective sinks for $^{231}$Pa and $^{230}$Th (e.g. Scholten *et al.*, 1995; Gdaniec *et al.*, 2017). This process, usually referred to as boundary scavenging has previously been thought to be pronounced in the Arctic Ocean (Bacon *et al.*, 1989; Cochran *et al.*, 1995; Scholten *et al.*, 1995). However, despite the contrasted particle fluxes over large shelf areas (receiving high river inputs) and the inner Arctic with its perennial sea ice cover, the $^{231}$Pa/$^{230}$Th ratio of arctic sediment does not vary much and is on average lower than the production ratio (e.g. Edmonds *et al.*, 2004; Moran *et al.*, 2005). Not many studies have reported $^{231}$Pa/$^{230}$Th ratios slightly exceeding the production ratio (e.g. Luo and Lippold, 2015). The overall low $^{231}$Pa/$^{230}$Th ratios casted some doubts on mechanisms driving the boundary scavenging in the Arctic Ocean. While boundary scavenging does occur in the Arctic Ocean (Roy-Barman, 2009), the net export of $^{231}$Pa to the Atlantic Ocean through the Fram strait plays a key role in the Pa and Th budget of the Arctic Ocean (Edmonds *et al.*, 2004; Hoffmann *et al.*, 2013; Moran *et al.*, 2005). However, the low vertical resolution, the relatively large analytical uncertainties and sometimes lack of particulate data limits the water column constraints on boundary scavenging in Arctic Ocean (Bacon *et al.*, 1989; Cochran *et al.*, 1995; Edmonds *et al.*, 2004; Scholten *et al.*, 1995) and more data are required for a proper modelling of boundary scavenging (Luo and Lippold, 2015).

In this study, dissolved and particulate $^{231}$Pa, $^{230}$Th, and $^{232}$Th concentrations measured along GEOTRACES section GN04 in the Barents Sea, Nansen Basin, Amundsen Basin and Makarov Basin are presented. The objective was to explore the influence of boundary scavenging and shelf-basin interactions on the observed distribution of $^{231}$Pa and $^{230}$Th in the Arctic Ocean. We revisit boundary scavenging modelling using a model adapted from Roy-Barman (2009) that we compared to the current dataset and used to constrain the scavenging behaviour of Pa and Th between the Arctic margin and the inner ocean.

## 2. Methods

### 2.1. Sampling

Samples were collected on R/V Polarstern during expedition PS94 in 2015, at seven stations located in the Barents Sea, Nansen, Amundsen and Makarov Basins along the GEOTRACES GA04 section in the Arctic Ocean (Fig. 1). The samples were collected along a shelf-basin transect from the Barents shelf to the Makarov Basin to study the exchange between the margin and interior ocean. Stations 4, 161, 153 and 18 represent the shelf, station 32 represents the margin, while station 40, 50, 125 (Amundsen basin) and 101 (Makarov basin) represent the interior ocean.

Water samples were collected in 24 l Niskin® bottles mounted on a General Oceanic® rosette equipped with a Sea-Bird Electronics CTD system (SBE911plus). The CTD-system was equipped with sensors allowing measurements of salinity, temperature and transmission (Rabe *et al.*, 2016; van Ooijen *et al.*, 2016). For the analysis of dissolved $^{231}$Pa, $^{230}$Th and $^{232}$Th, 5l of water were filtered directly from the Niskin bottles into sampling containers using Acropak500™ cartridges (0.45 µm pore size), which were cleaned in between stations. After filtration, water samples were acidified using concentrated ultra-pure HCl (~1 ml of acid per 1 l of seawater). Samples were stored in double plastic bags until analysis.

Particulate samples were collected using in-situ pumps (McLane and Challenger Oceanic) at six stations along the GA04 section (Fig. 1). Particles (0.8 µm pore size) were collected on Supor® polyethersulfone filters with a diameter of 142 mm. At two locations (N 84° 6′ 51.64″, E 12° 4` 11.69″ and N 84° 31.40″, E 11° 6` 11.43″), "dirty ice" (ice rafted sediments incorporated into sea ice when it forms on the Arctic shelf) was collected from deck using a plastic spade and container. At station 161, 32 and 101, surface sediment cores were collected using a Multi-corer (Fig. 1). The top (0–1 cm interval) of each core was analysed for $^{238}$U, $^{234}$U, $^{231}$Pa, $^{232}$Th and $^{230}$Th at LSCE.

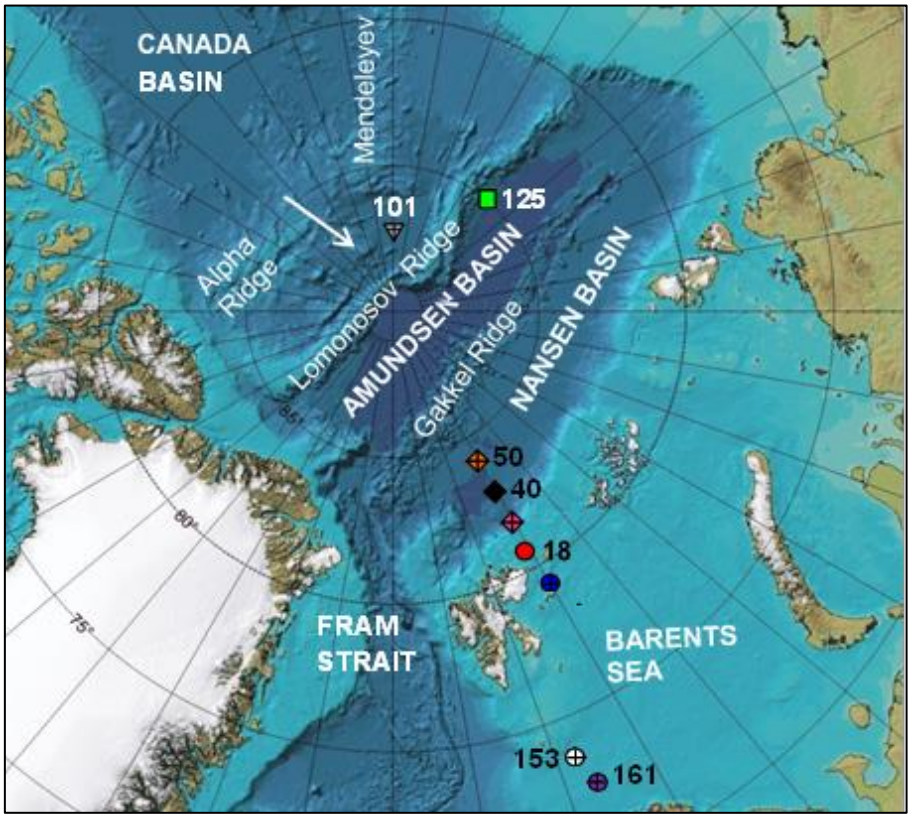


**Figure 1: Samples for the analysis of dissolved and particulate $^{231}$Pa, $^{230}$Th and $^{232}$Th were collected at 9 stations along the GEOTRACES GN04 section in the Arctic Ocean. Crossed symbols denote sampling for particulate and dissolved samples and non-crossed points are stations which were sampled for the analysis of dissolved concentrations.**

## 2.2. Chemical Preparation of Pa and Th in Seawater, Suspended Particles, Surface Sediments and Dirty Ice

$^{231}$Pa, $^{230}$Th and $^{232}$Th were determined by isotope dilution and mass spectrometry. Seawater samples were processed as described in (Gdaniec *et al.*, 2017). For filtered particles, approximately 1/5 (corresponding to ~25–200 l seawater) of the total filter material was cut on board in a laminar flow bench and used to determine the concentrations of $^{231}$Pa and Th isotopes in suspended particles. The leaching of filter samples was performed at the Swedish Museum of Natural history followed by spiking and analysis at LSCE. The filters were submerged in 3 N HCl and heated to > 50 °C to wash the particles off the filters without dissolving the filters. The leachate, containing the suspended particles, was then dissolved in a mixture of concentrated $HNO_3$ and HF following the method described in Gdaniec *et al.* (2017). Surface sediments were dried and an aliquot (0.2 g) of crushed bulk sediment was spiked with $^{233}$Pa, $^{229}$Th and $^{236}$U, followed by total dissolution in a $HNO_3$ and HF mixture. Pa, Th and U were separated by anion exchange chromatography (Guihou *et al.*, 2010). The dirty ice samples were melted and particles were separated by centrifugation at the clean laboratory of Laboratoire des Sciences de l'Environnement Marin (LEMAR). Total dissolution of the particles (~0.2 g) was carried out at the Swedish Museum of Natural History using microwave oven digestion using HF, $HNO_3$ and HCl followed by spiking, chemical separation and analysis of $^{231}$Pa, $^{230}$Th and $^{232}$Th at Laboratoire des Sciences du Climat et de l'Environnement (LSCE). $^{231}$Pa, $^{230}$Th and $^{232}$Th concentrations in seawater, particles and sediment samples were analysed at LSCE by Multi Collector Inductively Coupled Plasma Mass Spectrometry (MC-ICP-MS) on a Thermo Scientific™ Neptune Plus™ instrument equipped with an Aridus II™ desolvating nebulizer and a Jet interface (Burckel *et al.*, 2015, Gdaniec *et al.*, 2017).

Uranium concentrations in seawater were estimated using the bottle salinity measured from the CTD and the U-Salinity relationship in seawater (U = (0.100 * S − 0.326), Owens *et al.*, 2011). The conservative behaviour of uranium in the Arctic Ocean can be questioned due to the surface and mixed layer of the Arctic contain a significant portion of a mixture of river and ice melt water. However, in the study of Not *et al.* (2012) the investigators apply the U vs. salinity relation- ship over a salinity range of ~0–135, and showed that the U-salinity relationship exhibits the conservative behaviour over the entire range investigated.

Procedural blanks for seawater samples were determined by per- forming a complete chemical procedure on 3–11 bottles of 250 ml of Milli-Q® water with each batch of samples. Total procedural blanks for seawater samples ranged between 7.3 pg and 29.9 pg for $^{232}$Th (average = 15 ± 6 pg), 0.07 and 8.42 fg for $^{230}$Th (average = 1.02 ± 1.80 fg) and 0.05 and 0.26 fg for $^{231}$Pa

(average = 0.17 ± 0.18 fg). These blanks were equivalent to 0.9–14% of the measured $^{232}$Th, 0.2–21% of the measured $^{230}$Th and 0.1–42% of the measured $^{231}$Pa.

For particles, procedural blanks were prepared in the same way as for samples by using acid cleaned filters (0.5 N $HNO_3$) mounted onto the pump and deployed but not connected to the pumping system. Total procedural blanks ranged between 3.3 pg and 29.1 pg for $^{232}$Th (average = 4.3 ± 1.2 pg), 0.02 and 0.36 fg for $^{230}$Th (average = 0.15 ± 0.03 fg) and 0.004 and 0.7 fg for $^{231}$Pa (average = 0.27 ± 0.34 fg). These blanks were equivalent to 0.1–16% of the measured $^{232}$Th, 0.1–19% of the measured $^{230}$Th and 0.1–89% of the measured $^{231}$Pa.

All measured $^{231}$Pa and $^{230}$Th concentrations were corrected for the in-growth of $^{231}$Pa and $^{230}$Th by uranium decay during the time period between sample collection and the U-Th/Pa separation. All un- certainties are expressed as 2 standard errors on the mean (2 $\sigma_n$) including the propagated contribution from sample weighting, spike impurities, spike contributions, blank corrections and mass spectrometric measurements.

Replicates for dissolved $^{231}$Pa, $^{230}$Th and $^{232}$Th concentrations were measured (Table S1). It was initiated because the first analysis of $^{230}$Th at 1000 m depth for station 32 seemed obviously overestimated. An additional aliquot of the 1000 m sample was analysed and 2 additional samples (500 m depth at St. 32 and 40) were replicated to check the method reliability. They confirmed that the first analysis of $^{230}$Th at 1000 m depth had suffered from contamination, but showed a good agreement (within or close to analytical uncertainties) for the other $^{231}$Pa and $^{230}$Th measurements. The $^{232}$Th replicates can vary by as much as 30% indicating small $^{232}$Th contaminations, but it will have no significant impact on the discussion.

An inter-comparison of dissolved and particulate Pa-Th measurements between LSCE and AWI at stations 101 and 125 is given in Fig. ES1. Seawater samples at station 101 (GEOTRACES crossover station of the USCGC Healy HLY1502 (GN01) and R/V Polarstern PS94 (GN04) cruises) and station 125 were duplicated and analysed for dissolved $^{231}$Pa, $^{230}$Th and $^{232}$Th in order to provide an intercomparison between AWI and LSCE. These samples were obtained from the same casts, but not always the same bottle, so some differences in concentrations were expected (Fig. ES1). Concentrations of dissolved $^{231}$Pa, $^{230}$Th and $^{232}$Th at station 50 (Fig. 1) have been published in Valk *et al.*, 2018 and will be used here to investigate the relationship between the Nansen margin and interior. Moreover, an intercomparison of dissolved and particulate Pa-Th measurements with AWI (Alfred Wegener Institute), UMN (Minnesota University) and LDEO (*Lamont Doherty Earth Observatory*) at station 101 is in progress.

## 3. Results

### 3.1. General Circulation and Hydrography

The Arctic Mediterranean, like the Mediterranean Sea, transforms and exports Atlantic water of lower density entering from the adjacent ocean into high density intermediate and deep waters. The Arctic Ocean comprises two major basins, the Amerasian Basin and the Eurasian Basin, separated by the Lomonosov Ridge (Fig. 1). The Eurasian Basin is divided into the Nansen and Amundsen Basin by the Gakkel Ridge, while the Amerasian Basin is separated by the Alpha-Mendeleyev Ridge into the Makarov and the Canada Basins (Fig. 1). The inflow of Atlantic Water (AW) over the Barents Sea was re- cognized at stations 161 and 153, where high salinity (> 35.1) and high temperatures (~2–7.6 °C) were observed (Rabe *et al.*, 2016) (Fig. ES2). Close to the Barents Sea shelf break (St. 04 and 18), the polar waters (Polar Mixed Layer and Halocline) were significantly colder (≤0.8 °C) and fresher (≤34.8) compared to the inflow of AW (Fig. ES2). AW enters the central Arctic Ocean mainly by two branches; the Fram Strait Branch Water (FSBW) and the Barents Sea Branch Water (BSBW) (Rudels, 1994). The FSBW enters the Nansen Basin through the Fram Strait and then forms the Boundary current that flows around the Nansen Basin along the Gakkel Ridge (e.g. Rudels, 2009) (Fig. ES3). As AW enters the Arctic Basin, it encounters sea ice and the upper water masses cool (−1.8 °C) and become less saline (~34.9–35.0) compared to underlying waters (Fig. ES2). The BSBW flows over the Barents Sea shelf and enters the Nansen Basin through St. Anna Trough (~1000 m depth), where limited ex- change with FSBW occurs (e.g. Rudels, 2009) (Fig. ES3). At the eastern Siberian margin, the BSBW is divided into 3 branches: one branch flows into the Amundsen Basin while the second branch of the BSBW continues to flow towards the Fram Strait, as well as the ventilated inter- mediate water masses (Tanhua *et al.*, 2009) (Fig. ES3). The third part of the BSBW prolongs into the Makarov Basin as part of the Arctic Ocean Boundary Current that travels anti-cyclonically around the Arctic Ocean (Rudels, 1994; Rudels *et al.*, 2012). In the Nansen Basin (St. 32 and 40), the warm FSBW was observed between ~100 and ~1000 m (Rabe *et al.*, 2016) (Fig. ES2). In these waters, the Atlantic layer typically has maximum temperature of ~2.5 °C and the salinity ranges between 34.9 and 35.05 (Fig. ES2). Station 50, in the central Nansen Basin is influenced by the return flow of colder (−2 °C) and less saline FSBW along the Gakkel Ridge (Rabe *et al.*, 2016) (Fig. ES2).

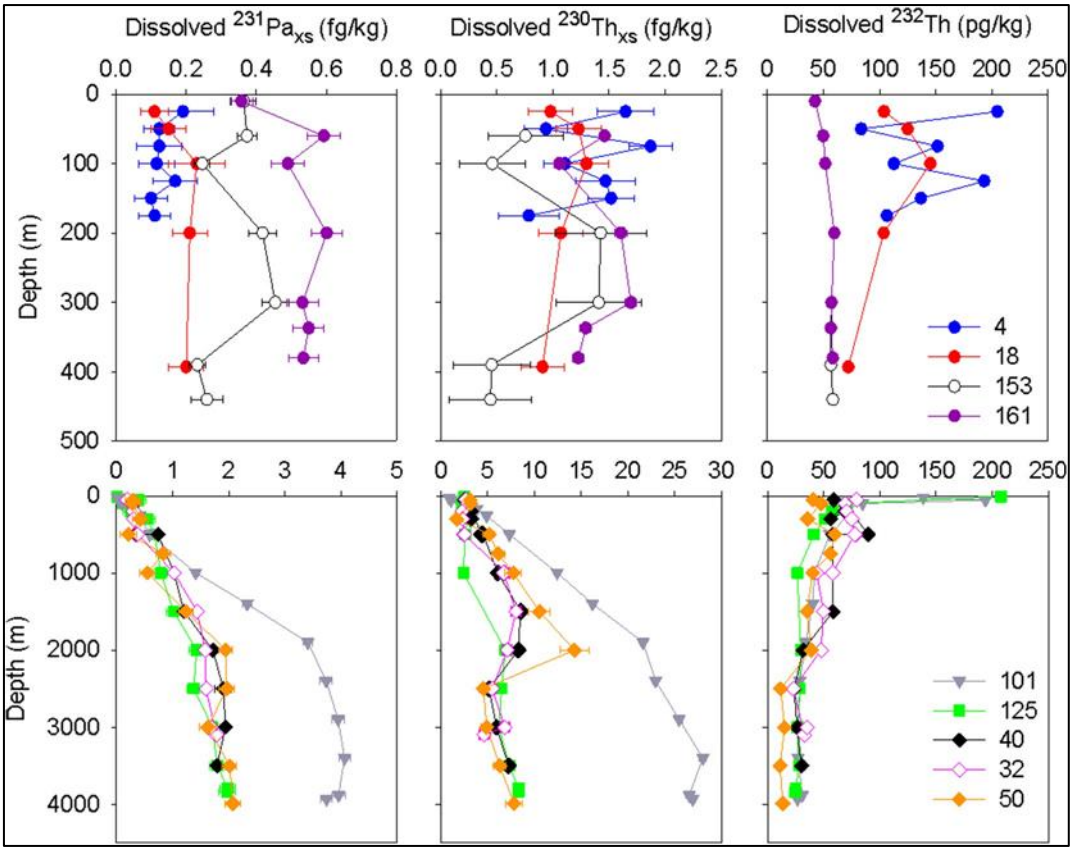


**Figure 2: Dissolved concentrations of $^{231}Pa_{xs}$, $^{230}Th_{xs}$ and $^{232}Th$ for shelf stations (upper panel) and deep stations (lower panel). Diamonds: Nansen Basin, squares: Amundsen basin, triangles: Makarov Basin and circles: shelf stations.**

The Eurasian Basin communicates with the Canada Basin through the boundary current that enters the Canada Basin north of Siberia and through the intra-Basin located at the central part of the Lomonosov Ridge, with a sill depth of ~1850 m (Björk *et al.*, 2007) (Fig. ES3). A reverse flow from the Makarov Basin to the Amundsen basin has also been identified (Björk *et al.*, 2010, 2007). Above 1700 m, stations 125 and 101 show similar water mass characteristics that fit to the BSBW (Rabe *et al.*, 2016) (Fig. ES2). Below this depth range, the deep waters of the Amerasian Basin are warmer and saltier compared to the Eurasian Basin Deep Water (EBDW) (Fig. ES2) (e.g. Aagaard *et al.*, 1981).The deep waters from the Eurasian Basin exit the Arctic through the Fram Strait and contribute to the deeper layers in the Nordic Seas (e.g. Rudels, 2015).

### 3.2. Dissolved and Particulate $^{232}$Th Concentrations

Concentrations of dissolved $^{232}$Th in the Arctic Ocean ranged between 11 and 205 pg/kg and were generally decreasing with depth (Fig. 2). Elevated concentrations of $^{232}$Th were observed close to the Nansen shelf break at station 04 and 18 (72–205 pg/kg) and in surface waters of station 101 (139–194 fg/kg). Below ~500 m depth, concentrations of dissolved $^{232}$Th were

higher closer to the Nansen margin (24–80 pg/kg) compared to the Nansen interior (11–60 pg/kg) (Fig. 2). Concentrations of particulate $^{232}$Th in the Barents Sea display elevated concentrations at depth, where concentrations up to ~2500 pg/ kg were observed at station 04 (Fig. 3). At the deep stations, particulate $^{232}$Th ranged between 10 pg/kg and ~80 pg/kg, where lower concentrations were observed at the ocean interior (St. 101 and 50) compared to the margin (St. 32) (Fig. 3).

### 3.3. Dissolved $^{231}Pa_{xs}$ and $^{230}Th_{xs}$ Concentrations

Measured concentrations of $^{231}$Pa and $^{230}$Th must be corrected for the presence of detrital components due to the presence of U in lithogenic particles. The concentration of lithogenic U is estimated from the measured concentrations of $^{232}$Th, which is entirely of lithogenic origin (Brewer *et al.*, 1980). As U is assumed to be at secular equilibrium in lithogenic phases, the unsupported $^{231}$Pa and $^{230}$Th ($^{231}Pa_{xs}$ and $^{230}Th_{xs}$) produced solely by radioactive decay of dissolved U-isotopes can be calculated**:**

$$^{230}Th_{xs} = {}^{230}Th_m - {}^{232}Th_m \times \left(\frac{^{230}Th}{^{232}Th}\right)_{Litho} \times \frac{M230}{M232} \quad (1)$$

$$^{231}Pa_{xs} = {}^{231}Pa_m - {}^{232}Th_m \times \left(\frac{^{230}Th}{^{232}Th}\right)_{Litho} \times \left(\frac{^{235}U}{^{238}U}\right)_{Nat} \times \frac{\lambda_{230}}{\lambda_{238}} \times \frac{\lambda_{235}}{\lambda_{231}} \times \frac{M231}{M232} \quad (2)$$

where the subscript *m* refers to measured concentrations of $^{231}$Pa, $^{230}$Th (fg/kg) and $^{232}$Th (pg/kg) in seawater and particles. The $(^{235}U/^{238}U)_{Nat}$ is the natural $^{235}$U/$^{238}$U ratio of 1/137.88 (atom/atom) (Condon *et al.*, 2010) and the $(^{230}Th/^{232}Th)_{Litho}$ was estimated from the average activity ratio [$^{238}$U/$^{232}$Th] = 0.6 ± 0.3. This range is relatively large compared to values used previously for the Arctic Ocean ([$^{238}$U/$^{232}$Th] = 0.6 ± 0.1, Moran *et al.*, 2005). It allows covering the high value ([$^{238}$U/$^{232}$Th] ≈ 0.9) deduced from the $^{230}$Th/$^{232}$Th (=4.75 × $10^{-6}$ mol/mol) measured in the dirty ice, as well as the low ratio ([$^{238}$U/$^{232}$Th] = 0.3) inferred from the filtered particles at station 04 to avoid "negative $^{231}Pa_{xs}$-values" in (see Section 3.4). The secular equilibrium in the lithogenic fraction of marine sediment is at has been questioned due to the possible loss of $^{234}$U (through $^{234}$Th, its parent isotope), $^{230}$Th and $^{231}$Pa (through $^{231}$Th, its parent isotope) by α-recoil (Bourne-Worster *et al.*, 2012).

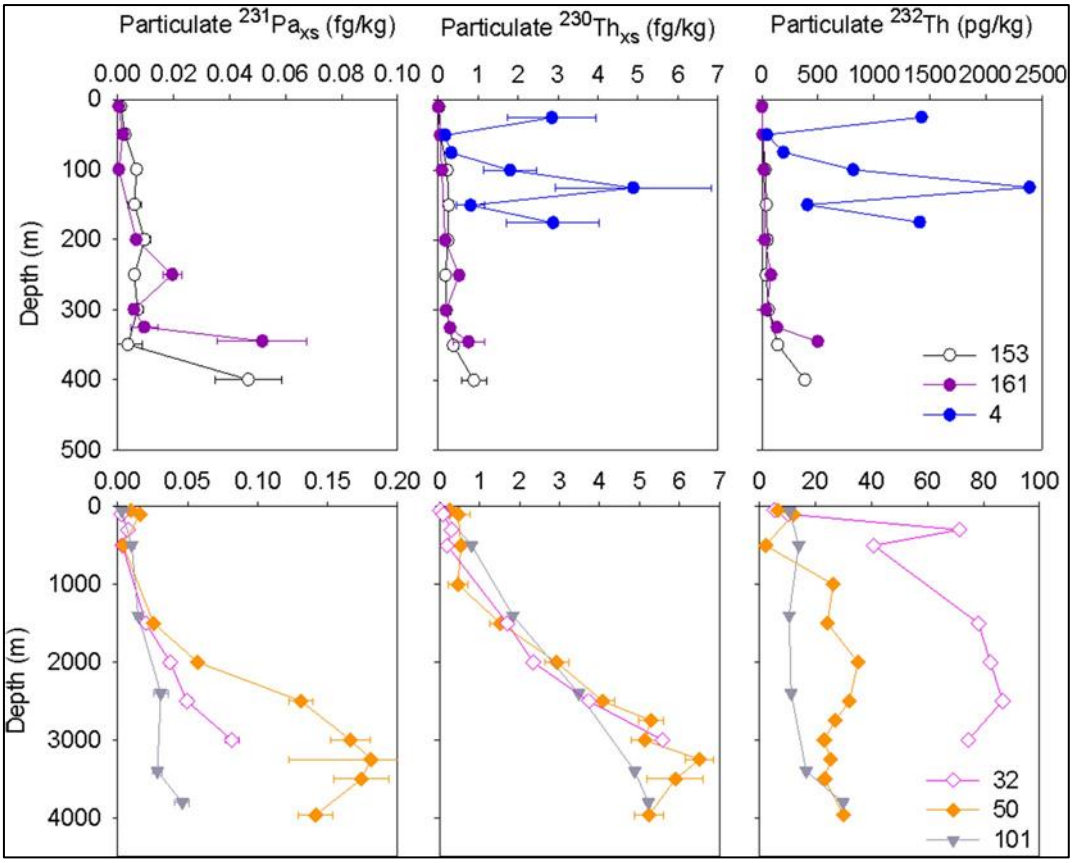


**Figure 3: Particulate concentrations of $^{231}Pa_{xs}$, $^{230}Th_{xs}$ and $^{232}Th$ for shelf stations (upper panel) and deep stations (lower panel). Diamonds: Nansen Basin, triangles: Makarov Basin and circles: shelf stations.**

At present, it is unclear if this process is sufficient to explain the discrepancy between the 2 estimates of the [$^{238}$U/$^{232}$Th] activity ratio presented here. Therefore, we conservatively consider the range [$^{238}$U/$^{232}$Th] = 0.6 ± 0.3 as possible and to propagate the resulting uncertainties. The same lithogenic corrections have been made for the dissolved concentrations of $^{231}$Pa and $^{230}$Th at stations 50 and 125 measured by Valk *et al.* (2018).

$\lambda_{230}$, $\lambda_{231}$, $\lambda_{235}$ and $\lambda_{238}$ are the decay constants for $^{230}$Th ($\lambda_{230}$ = 9.16 × $10^{-6}$ $y^{-1}$), $^{231}$Pa ($\lambda_{231}$ = 2.11 × $10^{-5}$ $y^{-1}$), $^{235}$U ($\lambda_{235}$ = 9.85 × $10^{-10}$ $y^{-1}$) and $^{238}$U ($\lambda_{238}$ = 1.55 × $10^{-10}$ $y^{-1}$), respectively (Cheng *et al.*, 1998; Condon *et al.*, 2010). *M230, M231* and *M232* are the atomic masses of $^{230}$Th (230.033 g/mol) $^{231}$Pa (231.036 g/mol) and $^{232}$Th (232.038 g/mol). The concentrations of $^{231}$Pa and $^{230}$Th can be converted to radioactivity units (μBq/kg) by using the conversion factors 0.5724 and 1.3110, respectively. $^{232}$Th concentrations can be converted to pmol/kg using the atomic mass of $^{232}$Th (232.038). Higher lithogenic content was observed in particles and seawater collected at the shelf, margin and in bottom waters of the deep basins. On average, the lithogenic contribution ranged between 0.04 and 33% for dissolved $^{231}$Pa, between 2.3 and 72% for particulate $^{231}$Pa, between 0.3 and 34% for dissolved $^{230}$Th and between 1.0 and 58% for particulate $^{230}$Th. In the deep Arctic Basin, the observed dissolved concentrations of $^{231}Pa_{xs}$ and

$^{230}Th_{xs}$ are increasing with depth until ~2000 m, followed by decreasing or invariant concentrations approaching the seafloor. This depletion at depth was more pronounced at the Nansen Basin stations (32, 40, 50) compared to the Makarov Basin station (101). The depletion of $^{230}Th_{xs}$ in the Nansen Basin was greater compared to the decrease of dissolved $^{231}Pa_{xs}$ in waters below 2000 m depth (Fig. 2). In the Makarov Basin, dissolved $^{231}Pa_{xs}$ ranged between 0.02 and 4.0 fg/kg and concentrations of dissolved $^{230}Th_{xs}$ ranged between 0.9 and 27.9 fg/kg. In contrast, lower concentrations of dissolved $^{231}Pa_{xs}$ (0.19–1.9 fg/kg) and $^{230}Th_{xs}$ (2.1–8.9 fg/kg) were observed at the deep stations of the Eurasian Basin (Fig. 2). In the Barents Sea, concentrations of dissolved $^{231}Pa_{xs}$ were lower in the polar waters of stations 04 and 18 (0.1–0.2 fg/kg) compared to the inflowing Atlantic Water stations 153 and 161 (0.23–0.6 fg/kg), while the dissolved $^{231}Pa_{xs}$ in shallow waters (< 500 m) over the slope (St 32) and in the Nansen Basin (stations 40 and 50) ($^{231}Pa_{xs}$ = 0.20–0.4 fg/kg) are intermediate between the Atlantic inflowing water (St. 153, 161) and close to Svalbard (St. 4). The distribution of dissolved $^{230}Th_{xs}$ was similar for all four shelf stations (0.5–1.99 fg/kg) (Fig. 2) and generally lower compared to water at corresponding depth of the interior basin (2.3–3.8 fg/kg) (Fig. 2). At station 125, located in the Amundsen Basin, the water column distribution of dissolved $^{231}$Pa was similar compared to the stations located in the Nansen Basin, while concentrations of dissolved $^{230}$Th in the Nansen Basin (St. 32, 40, 50) were similar or higher compared to the distribution of dissolved $^{230}$Th from 500 m to 2000 m depth at station 125 (Fig. 2).

### 3.4. Particulate $^{231}Pa_{xs}$ and $^{230}Th_{xs}$ Concentrations

The filtered particles from station 04 (Table ES2) and the dirty ice (Table ES3) were used to determine the range of [$^{238}$U/$^{232}$Th] activity ratios of the lithogenic material. There was a high abundance of lithogenic particles at station 04 ($^{232}$Th = 46–2400 pg/kg) and these particles have low $^{231}$Pa/$^{232}$Th ratios that must be supported by a [$^{238}$U/$^{232}$Th] activity ratio of ~ 0.3 (to avoid negative values of $^{231}Pa_{xs}$), a value that we take as the lower limit of the [$^{238}$U/$^{232}$Th] activity ratio of the lithogenic material. Ice rafted sediments embedded in sea ice (called “dirty ice”) are an important source of lithogenic particles in the Arctic Ocean (Pfirman and Thiede, 1987). As dirty ice is formed on the shelf, it may contain shelf sediments that have been incorporated into the ice as anchor ice or by sediment resuspension. This means that the dirty ice could contain some $^{230}Th_{xs}$ that has been scavenged over the shelf. Here, the $^{230}$Th/$^{232}$Th ratio (= $4.75 \times 10^{-6}$ mol/mol) of dirty ice is supported by a [$^{238}$U/$^{232}$Th] activity ratio of ~ 0.9, a value in good agreement with the estimate of the average continental crust suggesting that dirty ice is free of $^{230}Th_{xs}$. Therefore, we take 0.9 as the upper limit of the [$^{238}$U/$^{232}$Th] activity ratio of the

lithogenic material. Concentrations of particulate $^{231}Pa_{xs}$ and $^{230}Th_{xs}$ in the Arctic Ocean generally display an increasing trend with depth. Particulate concentrations of $^{231}Pa_{xs}$ ranged between 0.0004 and 0.08 fg/kg and particulate $^{230}Th_{xs}$ concentrations ranged between 0.001 and 5.6 fg/kg. Elevated particulate $^{231}Pa_{xs}$ and $^{230}Th_{xs}$ concentrations were observed close to the seafloor at stations 04, 153 and 161 and in deep waters of the Nansen and Makarov Basins (Fig. 3). Due to the high abundance of particulate $^{232}$Th at station 04 ($^{232}$Th = 46–2400 pg/kg), it was not possible to estimate the unsupported particulate $^{231}Pa_{xs}$ concentrations for this station (see above). In the interior Nansen (Station 50), the distribution of particulate $^{231}Pa_{xs}$ and $^{230}Th_{xs}$ displayed an increase with depth until ~3000 m, followed by a decrease in particulate concentrations approaching the seafloor. At station 32, concentrations of particulate $^{230}Th_{xs}$ ranged between 0.02 and 5.6 fg/kg, which was similar to concentrations observed at station 50 (0.28–5.9 fg/kg). In contrast, particulate $^{231}Pa_{xs}$ (> 2000 m) was lower at the slope (0.05–0.08 fg/kg) compared to the interior (0.13–0.18 fg/kg) (Fig. 3). The distribution of particulate $^{230}Th_{xs}$ observed at station 101 was very similar to the slope and interior of the Nansen Basin, while, below 1500 m, the particulate $^{231}Pa_{xs}$ concentrations were lower in the Makarov Basin compared to the stations located in the Nansen Basin (Fig. 3). As this manuscript was already submitted, the intercomparison work revealed that the particulate $^{231}$Pa concentrations at station 101 are ~ 50% lower than at the nearby station of the USCGC Healy HLY1502 (GN01) cruise in 2015 (while particulate Th isotopes are essentially similar at the 2 stations). Therefore, the interpretation of particulate Pa data requires caution Before we can compare particulate $^{230}Th_{xs}$ and $^{231}Pa_{xs}$ in the water column with measurements in the surface sediment, we must first evaluate if an age correction is required for the sediment samples, as the sedimentation rate in the Arctic Ocean can be very low. Sedimentation rate estimates in the Makarov Basin range from 0.4 to 4 cm/ky (e.g. Nowaczyk *et al.*, 2001). It corresponds at most to a mean age of 1.2 ky for the 1st cm of the sediment core, so that it is not necessary to correct the $^{231}Pa_{xs}/^{230}Th_{xs}$ ratio for radioactive decay in the sediment. The higher sedimentation rates encountered over the Barents Sea and slope make age corrections negligible (Ivanova *et al.*, 2002). We have determined the $^{238}$U and $^{234}$U content of the 3 sediments (Table ES3). The [$^{234}$U/$^{238}$U] activity ratio of the 3 sediments is slightly below equilibrium suggesting the absence of seawater derived U, in agreement other arctic sediments (Hillaire-Marcel *et al.*, 2017). Hence, we can estimate the [$^{231}Pa_{xs}/^{230}Th_{xs}$] activity ratio more precisely than based on the [$^{238}$U/$^{232}$Th] range determined for the suspended particles.

### 3.5. The Fractionation Factor

The fractionation factor ($F_{Th/Pa}$) was calculated as follows:

$$F_{Th/Pa} = (^{230}Th_{xs}/^{231}Pa_{xs})_p/(^{230}Th_{xs}/^{231}Pa_{xs})_d \quad (3)$$

Fractionation factors obtained in this study ranged between 2.7 and 25.4 (Fig. 4). They are comparable to values reported from other ocean basins (e.g. Hayes *et al.*, 2015a; Moran *et al.*, 2002, 2001; Scholten *et al.*, 2008). The distribution of $F_{Th/Pa}$ with depth was rather constant (Fig. 4). Below 1000 m depth, fractionation factors were consistently lower at station 50 in the interior of the Nansen Basin (2.7–13.3) compared to the Nansen margin (3.7–22.3) and the Makarov Basin (7.2–25.4) (Fig. 4).

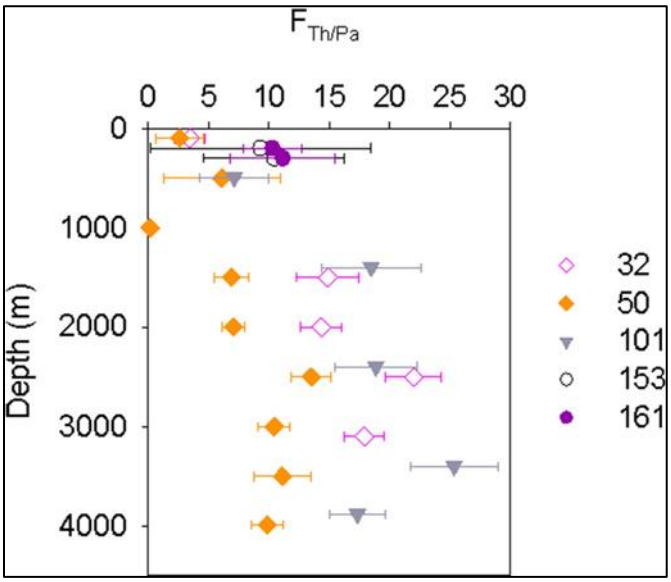


**Figure 4: Pa-Th Fractionation factors. Diamonds: Nansen Basin, triangles: Makarov Basin and circles: shelf stations.**

## 4. Discussion

### 4.1. $^{230}Th_{xs}$ and $^{232}Th$ Scavenging in the Arctic Ocean

Early studies of $^{210}Pb_{xs}$ and $^{230}Th_{xs}$ in Arctic sediments highlighted that their inventory in the sediments exceeded the supply from the overlying water column near the slopes and shelves and were greater at the margins compared to the interior basins (Huh *et al.*, 1997; Smith *et al.*, 2003). This process, usually referred to as boundary scavenging was expected to be pronounced in the Arctic Ocean due to the high proportion of shelf areas with the associated high particle flux versus the low particle flux regions in the ice-covered interior basins (Bacon *et al.*, 1989; Cochran *et al.*, 1995; Edmonds *et al.*, 2004; Scholten *et al.*, 1995). Early studies estimated the Th scavenging rates using a simple 1D production-vertical scavenging model (Bacon *et al.*,

1989; Edmonds, 1998; Scholten *et al.*, 1995), but this view was later challenged to include the effect of lateral transport, the effect of deep water ventilation (Scholten *et al.*, 1995) and boundary scavenging (Roy-Barman, 2009). Box-modelling using sedimentary and dissolved $^{230}Th_{xs}$ and $^{231}Pa_{xs}$ data suggests that ~90% of the in-situ produced $^{230}Th_{xs}$ was removed within the Arctic Ocean by particle scavenging and that a large fraction of the scavenged $^{230}Th_{xs}$ was removed by boundary scavenging along the Arctic margins (Moran *et al.*, 2005; Roy-Barman, 2009). The dataset presented here will be used to revisit our understanding of the scavenging processes in the Arctic Ocean. We start the discussion with $^{230}$Th because it is highly particle reactive (relative to Pa) and currently used to study and identify variations in scavenging intensity (e.g. Roy-Barman, 2009; Hayes *et al.*, 2015a, 2015b).

### 4.1.1. The Makarov Basin

When lateral transport can be neglected, the 1D reversible scavenging model predicts a linear increase of both dissolved $^{230}Th_{xs}$ ($^{230}Th_{xs\text{-}d)}$ and particulate $^{230}Th_{xs}$ ($^{230}Th_{xs\text{-}p)}$ concentrations with depth and consequently produces a constant $^{230}Th_{xs\text{-}p}/^{230}Th_{xs\text{-}d}$ ratio throughout the water column (Bacon and Anderson, 1982). Among all stations re- ported here, these conditions seem best fulfilled at station 101 in the Makarov Basin, particularly above 2000 m depth (Figs. 2 and 3). Station 101 is located in the Makarov Basin at high latitude isolated from continental margins. Therefore St. 101 can be used as a reference station to evaluate the effect of continental margins on the scavenging in the interior ocean. Neglecting horizontal transport, the $^{230}Th_{xs\text{-}p}$ concentration is a function of the settling rate (*S*) of small particles and of the water depth (*h)*:

$$S = \frac{P_{230Th} \times h}{^{230}Th_{xs-p}} \quad (4)$$

where the $P_{230Th}$ is the production rate of $^{230}$Th in the water column (0.56 fg/kg/y). The settling rate (*S*) of particles (> 0.8 μm) in the Makarov Basin ranged between 340 and 440 m/y, which is consistent with earlier estimates in the central Arctic Ocean (e.g. Edmonds *et al.*, 2004; Scholten *et al.*, 1995) and very close to new estimates e.g. S = 434 m/y (Rutgers Van Der Loeff *et al.*, 2018) However, it may represent an upper limit for the particle settling speed in the central Arctic, because this calculation neglects the possible role of boundary scavenging (Roy-Barman, 2009). The scavenging residence time of $^{230}Th_{xs}$ (~55 y) is much shorter than the water ventilation residence time in the Makarov Basin (e.g. Scholten *et al.*, 1995). Since particle fluxes in the Makarov Basin are low and the water residence time is high, dissolved $^{230}Th_{xs}$ concentrations have more time to build up by the decay of uranium and stay in solution (Fig. 2).

The particulate/total ratio of $^{230}Th_{xs}$ is relatively low (6–16%) and tends to increase with depth at station 101 (Fig. 5).

Below 2000 m depth, dissolved $^{230}Th_{xs}$ displayed more invariant concentrations followed by decreasing concentrations approaching the seafloor (Fig. 2). The ventilation of the deep Arctic could contribute to produce such concave profiles (Scholten *et al.*, 1995). However, the ventilation age of the deep Makarov Basin is hundreds of years, which is much longer compared to the $^{230}$Th scavenging residence time (e.g. Rutgers van der Loeff *et al.*, 2018). These depleted concentrations of dissolved $^{230}Th_{xs}$ and $^{232}$Th close to the seafloor were accompanied with elevated concentrations of particulate $^{230}Th_{xs}$ and $^{232}$Th (Fig. 3), suggesting enhanced removal of dissolved $^{230}Th_{xs}$ close to the seafloor. No benthic nepheloid layer was detected by transmission (Fig. ES4). However, even a slight increase in resuspended sediments (not detectable by the transmissometer) may be sufficient to enhance scavenging and removal of dissolved $^{230}$Th close to the seafloor.

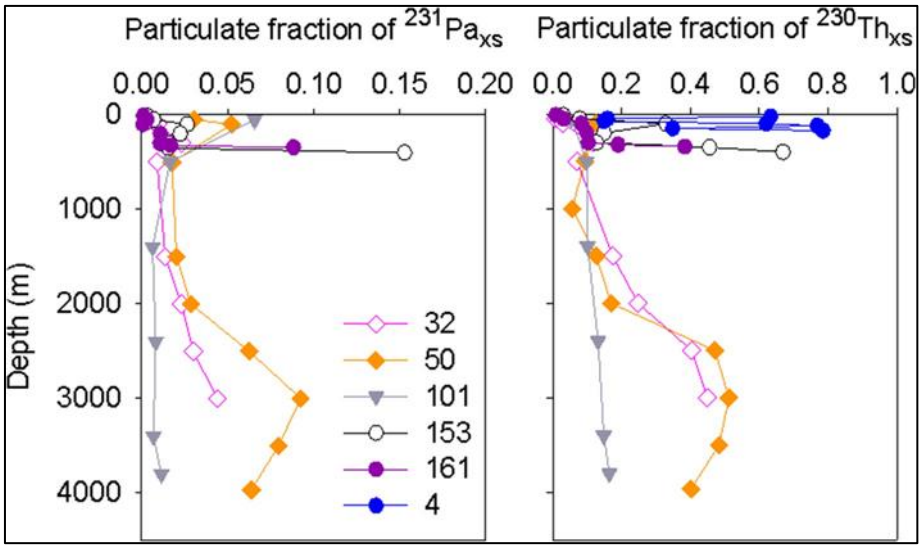


**Figure 5: Depth profiles of (a) the particulate/total ratios of $^{231}Pa_{xs}$ and (b) particulate/total ratios for $^{230}Th_{xs}$. Diamonds: Nansen Basin, triangles: Makarov Basin and circles: shelf stations.**

### 4.1.2. The Eurasian Basin

A sharp depletion of $^{230}Th_{xs}$ observed in deep waters (> 2000 m) of the Nansen was recently attributed to removal of $^{230}Th_{xs}$ related to release of dissolved iron from hydrothermal vents at the Gakkel Ridge (Valk *et al.*, 2018). Therefore, the following discussion will mainly be divided into water masses above and below 2000 m depth.

#### 4.1.2.1. Waters above 2000 m

On the Barents shelf, the temperature and salinity at station 153 and 161 clearly indicate the inflow of saltier and warmer AW (Fig. ES2). As a consequence, the dissolved $^{230}Th_{xs}$ concentrations (Fig. 2) compare well to surface concentrations from the northern Atlantic Ocean (Hayes *et al.*, 2015a). Close to the seafloor at station 153 and 161 elevated particulate $^{230}Th_{xs}$ and $^{232}$Th concentrations were observed (Fig. ES2). The increased particulate fraction of $^{230}Th_{xs}$ at the bottom of the water column accompanied with reduced dissolved $^{230}Th_{xs}$ indicates bottom scavenging over the shelf (Figs. 2 and 3). The low beam transmission (300–450 m depth) reflects resuspension of bottom sediments resulting in enhanced scavenging (Fig. ES4). This probably happens due to the inflow of AW over the Barents Sea shelf which disrupts the sediments close to the seafloor (Lukashin and Shcherbinin, 2007). At stations 04 and 18, the polar waters was less salty and colder compared to the Atlantic inflow, suggesting influence of ice melt and runoff close to the coast of Svalbard (Fig. 3). This was also reflected by the low beam transmission in the surface and bottom waters over the Barents shelf, indicating the presence of suspended particulate material (Fig. ES4). In addition, extremely high concentrations of particulate $^{232}$Th (up to ~2400 pg/kg) and elevated concentrations of dissolved $^{232}$Th (100–200 pg/kg) were observed at station 04 and 18, suggesting that the particulate material is dominated by lithogenic inputs and partial dissolution of these particles (Fig. 2). Nevertheless, the dissolved $^{230}Th_{xs}$ concentrations at stations 04 and 18 compare well with those of stations 153 and 161 suggesting that the water flow rate does not leave enough time for net scavenging to occur. Station 32 and 40 are located within the FSBW, where the modified Atlantic inflow (~2.5 °C) can be recognized between ~100 and 1000 m depth, followed by colder and less salty deep waters (Fig. ES2). Concentrations of dissolved $^{230}Th_{xs}$ in surface waters at station 32 and 40 (2.3–2.7 fg/kg) were within the range but on the high side of North Atlantic ($^{230}Th_{xs}$ = 0.76–3.4 fg/kg, Hayes *et al.*, 2015a, 2015b) and Norwegian Sea ($^{230}Th_{xs}$ = 0.6–2.3 fg/kg, Moran *et al.*, 1995) values. At station 32 and 40, dissolved $^{230}Th_{xs}$ increases linearly with depth until ~1500 m and then becomes constant (Fig. 2). This departure from the equilibrium profile suggests the possibility of enhanced scavenging at the margin. By contrast, Station 50 (Valk *et al.*, 2018) is located within the return flow of the FSBW (Fig. ES2 and ES3). Dissolved $^{230}Th_{xs}$ concentrations increase linearly down to 2000 m and they are higher than at station 32 and 40 indicating a lower scavenging rate. Surprisingly, the distribution of particulate $^{230}Th_{xs}$ was very similar at stations 32 and 50 (and also at station 101) (Fig. 3). Elevated concentrations of particulate $^{232}$Th at the

margin (St. 32) compared to the inner ocean (St. 50) are likely due to the advection of shelf waters (St. 4) transporting $^{232}$Th into the interior basin.

The dissolved $^{230}Th_{xs}$ concentrations were considerably lower in the Amundsen basin (station 125) compared to the Makarov basin (station 101) (Fig. 2), as shown previously (Scholten *et al.*, 1995; Valk *et al.*, 2018). This reflects the large difference in water residence times be- tween the Makarov and Amundsen Basins (Schlosser *et al.*, 1997), where the longer water residence time in the Makarov Basin allows the concentrations of $^{230}Th_{xs}$ to build up over time by the decay of U, whereas waters from the Amundsen Basin were submitted to boundary scavenging while flowing along the eastern Siberian margin.

Except the surface samples (< 100 m), the dissolved $^{230}Th_{xs}$ concentrations are significantly lower in the Nansen and Amundsen Basins (St. 50, 40, 32,125) compared to the Makarov Basin (St. 101). Within the Eurasian Basins (above 2000 m), a horizontal gradient of dissolved $^{230}Th_{xs}$ content between stations 125, 32, 40 and 50 was observed (Fig. 2). At station 50, dissolved $^{230}Th_{xs}$ concentrations were highest, followed by intermediate concentrations at the Nansen margin (St. 32, 40) and the lowest dissolved $^{230}Th_{xs}$ were observed at station 125. This suggests that $^{230}Th_{xs}$ is scavenged along the boundaries as the dissolved $^{230}Th_{xs}$ is decreasing towards the margin. The water at station 125 has probably experienced more scavenging on the Kara and Laptev shelf compared to the Barents shelf. Another possible reason for the low $^{230}Th_{xs}$ concentrations observed at 125 is scavenging onto particles carried by the TPD (Trans Polar Drift) (Charette, pers. com.).

#### 4.1.2.2. Below 2000 m

Below 2000 m, the $^{230}Th_{xs}$ concentrations are relatively constant and identical within the Eurasian Basin. The sharp decrease at station 50 is clearly due to hydrothermal scavenging (Valk *et al.*, 2018). In 2015, there was no sign of a strong hydrothermal activity in the beam transmission data suggesting that the hydrothermal event was over at the time of sampling and that the hydrothermal plume had faded away (Fig. ES4). The major part of the hydrothermal plume in the basin is expected to be transported out of the Nansen Basin along the Gakkel Ridge directly towards Fram Strait (Fig. ES3). Therefore, the distribution of dissolved $^{230}Th_{xs}$ at stations 32, 40 and 125 are not directly downstream of station 50 and their $^{230}Th_{xs}$ do not necessarily represent hydrothermal scavenging conditions. Valk *et al.* (2018) identified hydrothermal plume water by their high dissolved Fe content. The dis- solved Fe content of the deep waters at station 32 are higher than at station 50: it does not correspond to an hydrothermal

source, but to sediment resuspension at the slope as a source of dissolved Fe (Klunder *et al.*, 2012, Rijkenberg *et al.*, 2018).

An additional argument for deep enhanced scavenging comes from $^{232}$Th. In general, dissolved $^{232}$Th concentrations increases with depth in the deep ocean (e.g. Moran *et al.*, 2002; Scholten *et al.*, 2008; Okubo *et al.*, 2013). In the present study, $^{232}$Th decrease with depth, a feature that was already observed in the Arctic (Edmonds *et al.*, 2004), but remained unexplained. The lack of increasing dissolved $^{232}$Th concentrations towards the seafloor suggests enhanced bottom scavenging. The lowest dissolved $^{232}$Th in the deep basins occurs at station 50 suggesting the involvement of scavenging by the hydrothermal plume. However, low deep dissolved $^{232}$Th is also found in the Makarov Basin, where scavenging by a hydrothermal plume is not suspected. Note that the higher concentrations at station 32 do not necessarily represent a lower scavenging rate because a high scavenging rate can be balanced by a high input flux by particle resuspension/dissolution as suggested by the relatively low beam transmission and high particulate $^{232}$Th at this station.

#### 4.1.2.3. The Particulate Fraction

Despite different dissolved $^{230}Th_{xs}$ profiles at stations 32, 50 (Nansen Basin) and 101 (Makarov Basin), the particulate $^{230}Th_{xs}$ concentrations above 2500 m depth were similar at these stations (Fig. 3). By contrast, particulate $^{232}$Th concentrations were higher at station 32 compared to stations 50 and 101, highlighting the role of the continental margins in providing high levels of particulate matter into the low productivity interior ocean. The particulate fraction of $^{230}Th_{xs}$ increases with depth at stations 32 and 50 from 1% to 45% with a local maximum (20%) around 200 m (Fig. 5). This subsurface maximum particulate fraction can be related to the high $^{230}Th_{xs}$ particulate fractions associated to the bottom nepheloid layers on the shelf at station 153 and 04. Despite the high concentrations of particulate $^{230}Th_{xs}$ in the Makarov Basin, the $^{230}Th_{xs}$ particulate fractions are higher at stations 32 and 50 because the dis- solved $^{230}Th_{xs}$ concentrations are much lower in the Nansen Basin compared to the Makarov Basin. At station 32 and 101, the increased particulate fraction of $^{230}Th_{xs}$ at the bottom of the water column accompanied with reduced dissolved $^{230}Th_{xs}$ indicates bottom scavenging in deep waters of the open basin as it was already observed over the shelf (Figs. 2 and 3). At station 50, the increased $^{230}Th_{xs}$ particulate fraction of the bottom waters is the relic of a hydrothermal plume induced scavenging event, possibly at a stage where the steady state situation is being achieved again (Valk *et al.*, 2018).

### 4.2. Modelling $^{230}$Th Scavenging in the Arctic Ocean

Several features listed in previous sections of this paper (increasing $^{230}Th_{xs}$ particulate fraction with depth; decreasing dissolved $^{230}Th_{xs}$ content in the deepest waters of the ocean margin) are not consistent with the 1D scavenging models that predict a linear increase of dissolved and particulate $^{230}Th_{xs}$ concentrations with depth and a constant $^{230}Th_{xs}$ particulate fraction with depth (e.g. Bacon and Anderson, 1982, Roy-Barman *et al.*, 1996). They are not consistent with the boundary scavenging model of Roy-Barman (2009) either, because this model predicts a rather linear increase of dissolved $^{230}Th_{xs}$ with depth at the margin and a constant $^{230}Th_{xs}$ particulate fraction with depth. This is certainly due to an oversimplification of the particle dynamics: particles were assumed to have a constant vertical flux and their transport be- tween the margin and the ocean interior was neglected. To overcome these assumptions, we propose a boundary scavenging model where particles are introduced both at the ocean surface and also throughout the water column at the margin (hypothesis 1) and where particles are transported between the margin and the ocean interior (hypothesis 2). The input of particles at all depths of the ocean margin can be viewed as a result of nepheloid layers on the shelf or on the slope and/or to the chemical evolution of particles as they settle through the water column (precipitation of Fe-Mn oxyhydroxides at depth for example). A key point is that the particles introduced at depth are assumed to be free of $^{230}Th_{xs}$ and $^{231}Pa_{xs}$ when they are introduced in the water column, so that the input of particles will not be associated with an input of $^{230}Th_{xs.}$ and $^{231}Pa_{xs}$ (hypothesis 3). This means that the particles are not merely resuspended local bottom sediments, which are known to contain $^{230}Th_{xs}$. Instead, we hypothesize that nepheloid layers flow downward as turbidity currents along the slope with no or little mixing with sur- rounding waters so that they may not scavenge $^{230}$Th until they detach from the slope. Only then, particles spread and scavenge $^{230}Th_{xs}$ from the deep waters. This view differs from Rutgers van der Loeff and Boudreau (1997), who assumed equilibration between seawater and particles. Hypothesis (3) is required because a dissolved $^{230}Th_{xs}$ depletion compared to the equilibrium profile cannot be produced by resuspension of sediments that would already be "equilibrated" with overlying seawater. Hypothesis (3) is crucial for creating a water column $^{230}Th_{xs}$ profile as observed in this study. Transport of particles between the margin and the inner ocean (hypothesis 2) allows that most particles in the ice-covered central Arctic are advected from the margins.

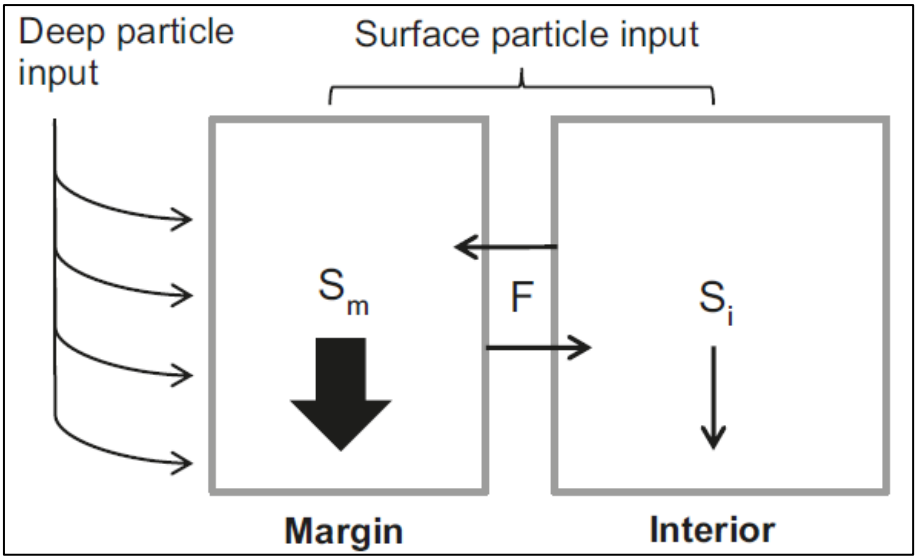


**Figure 6: Schematic representation of the boundary scavenging profile model: the margin and open ocean boxes exchange a total flux of water (F). Vertical mixing is neglected. Particles are introduced in the surface waters of the ocean margin and interior and at all depths in the margin box (bent arrows). Particles are then transported by currents between the margin and ocean interior.**

### 4.2.1. Transport of Water

In this box model, the Arctic Ocean is divided into 2 boxes: the ocean margin and the ocean interior (Fig. 6). The water volumes of the margin and of the ocean interior are $V_m$ and $V_i$ ($m^3$) (Jakobsson, 2002). These 2 boxes exchange a total flux of water F ($m^3/s$). For simplicity, we assume that the water flows horizontally between the boxes. Vertical mixing and ventilation of water by inputs through Fram strait and Barents Sea are neglected. Hence, at any depth in the water column the residence time of the water with respect to horizontal exchange is $\tau_m = V_m/F$ at the margin and $\tau_i = V_i/F$ at the ocean interior (Table 1). The time constant associated to water transport are $k_m = 1/\tau_m$ and $k = 1/\tau$. The time constant associated with water exchange between the ocean margin and the ocean interior are $k_m = 1/\tau_m$ for the ocean margin and $k = 1/\tau$ for the ocean interior.

### 4.2.2. Particle Transport

In this study, the concentration of particles was not measured. The particle concentration is embedded in the dissolved-particulate partition coefficient *K*, introduced in the following section. We scale the impact of particle concentration on the partition coefficient *K* with a parameter *m* assumed to be proportional to the particulate concentration:

$$m = P(z)/P^m(0) \quad (5)$$

where P is the particle concentration (at the margin or in the ocean interior) and $P^m(0)$ is the particle concentration in the surface water of the ocean margin.

**Table 1: Parameters of the boundary scavenging profile model.**

| Parameter | Ocean interior | Ocean margin |
|---|---|---|
| V ($m^3$) | $6.5 \times 10^{15}$ | V ($m^3$) |
| τ (y) | 50 | 10 |
| k | 0.02 | 0.1 |
| S (m/y) | 300 | 600 |
| $K^{230}Th$ | | 0.11 |
| $K^{231}Pa$ | 0.0075 | 0.0075 |
| $p^{230}Th$ ($fg/m^3/y$) | 0.056 | 0.056 |
| $p^{231}Pa$ ($fg/m^3/y$) | 0.025 | 0.025 |
| μ ($y^{-1}$) | | 0.5 |
| m (0) | 1.5 | 1 |

Hence, $m^m = 1$ in the surface water of the ocean margin and m is proportional to the particle concentration elsewhere. The conservation equations for $m^m$ and $m^i$ at the ocean margin and in the inner ocean include particle production throughout the water column at the margin (hypothesis 1) and particle transport between the margin and the inner ocean (hypothesis 2) and are given by:

$$\frac{dm^m}{dt} = -S^m \frac{dm^m}{dz} + k_m\left(m^i - m^m\right) + \mu \times m^m \quad (6)$$

$$\frac{dm^i}{dt} = -S^i \frac{dm^i}{dz} + k_i\left(m^m - m^i\right) \quad (7)$$

where $S^m$ and $S^i$ are the settling velocities of the particles at the margin and in the inner ocean. They are both assumed to be constant with depth. We expect higher particle settling rates at the margin compared to the interior due to increased production and the associated particle flux (Anderson *et al.*, 1983). μ is an arbitrary parameter aimed to produce an exponential increase of the particle concentration in the deep waters. μ operates as if (1) increasing turbulence towards the seafloor and increases the particle concentration by formation of ne- pheloids and/or (2) a diffusive flux of dissolved Manganese (Mn) from the sediment which allows precipitation of Mn oxides (that scavenges Pa and Th) towards the sea floor. Assuming a steady state, we obtain:

$$\frac{dm^m}{dz} = \frac{k_m}{S^m}\left(m^i - m^m\right) + \frac{\mu}{S^m} \times m^m \quad (8)$$

$$\frac{dm^i}{dz} = \frac{k_i}{S^i}\left(m^m - m^i\right) \quad (9)$$

Bulk dissolution of particles was not considered. The observed increasing particulate $^{230}$Th fraction with depth points to an addition of particles with depth rather than a significant

dissolution with depth, which would induce a concave shaped $^{230}$Th profile (Roy-Barman *et al.*, 1996). Moreover, there is no direct constraint on the particle dissolution in the present study.

### 4.2.3. Transport of $^{230}Th_{xs}$ and $^{231}Pa_{xs}$

In each box, $^{230}$Th and $^{231}$Pa re produced by in-situ decay of U at a constant rate *P*. The produced $^{230}Th_{xs}$ and $^{231}Pa_{xs}$ are then transported towards the seafloor by reversible scavenging onto sinking particles and transported horizontally by the flow of water (Fig. 6). Considering the long half-life of $^{230}$Th (75,000 y) and $^{231}$Pa (32,700 y), the radioactive decay of the two isotopes was neglected. Dissolved and particulate concentrations are noted as $C_d^m$ and $C^m$ for the margin and $C^i$ and $C^i$ for the ocean interior. The conservation equation of total $^{230}$Th is given by:

The ocean margin:

$$\frac{d(C_d^m+C_p^m)}{dt} = -S^m \frac{dC_p^m}{dz} + k_m\left(\left[C_d^i + C_p^i\right] - \left[C_d^m + C_p^m\right]\right) + P_{230} \quad (10)$$

The ocean interior:

$$\frac{d\left(C_d^i+C_p^i\right)}{dt} = -S^i \frac{dC_p^i}{dz} + k_i\left(\left[C_d^m + C_p^m\right] - \left[C_d^i + C_p^i\right]\right) + P_{230} \quad (11)$$

At the margin (eq. 10), the only source term is the in-situ production because the particles introduced in the water column of the margin do not contain $^{230}Th_{xs}$ (hypothesis 3). The relationship between $C_d$ and $C_p$ is obtained by assuming a reversible equilibrium between dissolved and particulate Th:

$$C_p^i = K \times m^i \times C_d^i \quad (12)$$

$$C_p^m = K \times m^m \times C_d^m \quad (13)$$

where *K* is the equilibrium coefficient of Th or Pa between the particulate fraction (mass of radionuclide carried by particles per l of seawater) and the dissolved fraction (mass of radionuclide in solution per l of seawater) (*K* = concentration in particles/concentration in the dissolved phase).

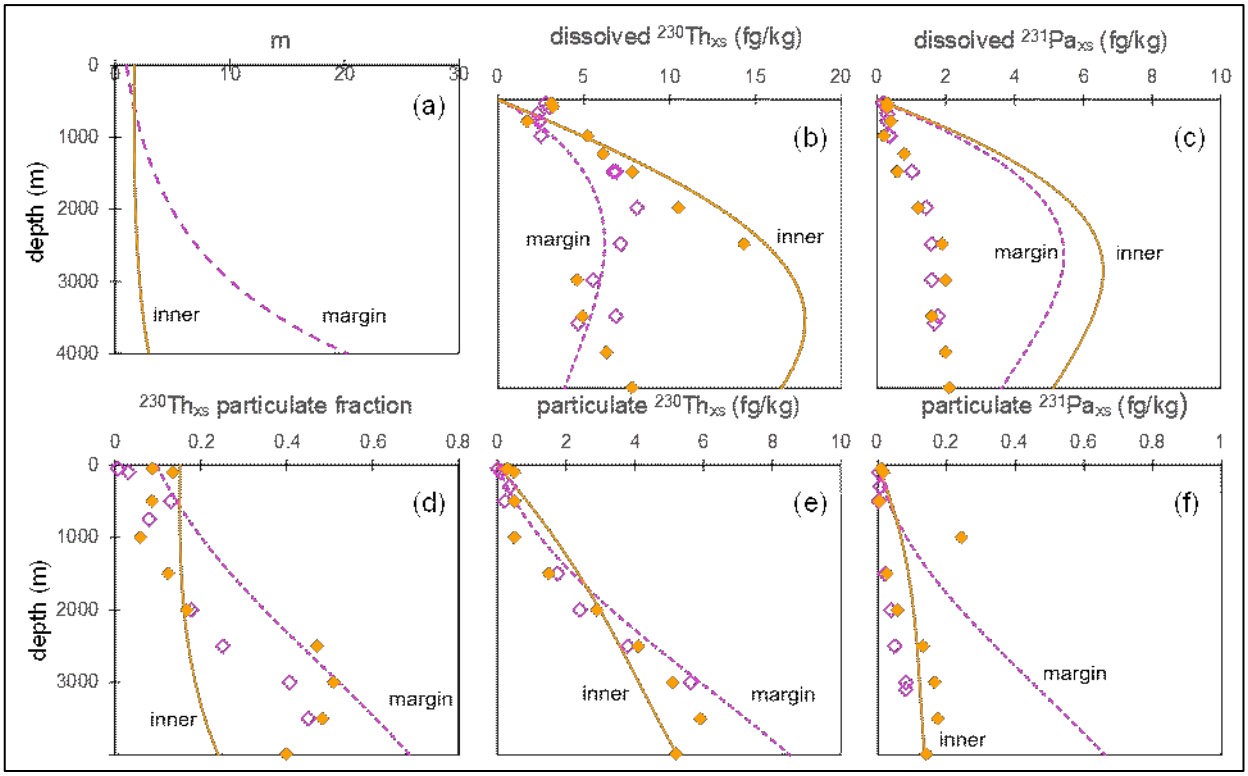


**Figure 7: Boundary scavenging model outputs. Modelled profiles of (a and d): particle abundance and the $^{230}$Th particulate fraction, (b and e): dissolved and particulate $^{230}Th_{xs}$ and c and f): dissolved and particulate $^{231}Pa_{xs}$ in comparison with measured data obtained at station 32 (margin) and 50 (interior). Pink open diamonds (st. 32) and orange diamonds (st. 50) represent measured data while the pink lines represent the margin model and orange lines represent the interior ocean model. (For interpretation of the references to colour in this figure legend, the reader is referred to the web version of this article.)**

*K* is assumed to be constant with depth and particle concentration. Assuming a steady state, we obtain:

$$\frac{d(m^m C_d^m)}{dz} = \frac{1}{S^m}\left\{k_m\left(\left(1+K\times m^i\right)C_d^i - \left(1+K\times m^m\right)C_d^m\right) + P_{230}\right\} \quad (14)$$

$$\frac{d\left(m^i C_d^i\right)}{dz} = \frac{1}{S^i}\left\{k_i\left(\left(1+K\times m^m\right)C_d^m - \left(1+K\times m^i\right)C_d^i\right) + P_{230}\right\} \quad (15)$$

Eqs. (10), (11), (14) and (15) are solved numerically. We use circulation parameters already obtained for modelling the boundary scavenging in the Arctic Ocean (Roy-Barman, 2009). The water residence time with respect to horizontal exchange is 10 y for the ocean margin and 50 y for the ocean interior (Table 1). All the other para- meter are adjusted by trial and error in order to obtain a reasonable agreement (Fig. 7) with the dissolved and particulate profiles of station 32 (Nansen margin) and station 50 (Nansen interior, above 2000 m to avoid the hydrothermal scavenging that is not represented in the model). Qualitatively equivalent results were obtained for station 32 and station 101 (not shown). The boundary conditions for the particle concentration are $m^m(0) = 1$ (by definition of m) and $m^i(0) = 1.5$ to obtain a reasonable fit between the model and the $^{230}$Th profile (see discussion below). This implies that there is an

input of particles in the surface waters at the margin and in the interior ocean. We use $\mu = 0.5$ $y^{-1}$. As the particle settling speed at the margin is set a 600 m/y, it corresponds to an increase of the particle concentration at the margin of a factor 2.71 every 1200 m of depth. By default, we choose the same value for $K$ (= 0.11), at the margin and in the inner ocean. If we want to reproduce the similar vertical $^{230}Th_p$ gradients observed at the margin and in the inner ocean (Fig. 3), the settling velocity of the particles must be higher at the margin (600 m/y) compared to the ocean interior (340 m/y. Indeed, if $\frac{dC_p^m}{dz} \approx \frac{dC_p^i}{dz}$, Eqs. (14) and (15) can be combined to yield:

$$\frac{S^i}{S^m} \approx \frac{P_{230} - k_i\left(C_{d+p}^i - C_{d+p}^m\right)}{P_{230} + k_m\left(C_{d+p}^i - C_{d+p}^m\right)} \quad (16)$$

As $C_{d+p}^i - C_{d+p}^m > 0$, it follows that $S^i < S^m$.

In other words, $S^i < S^m$ because at the margin, an excess of $^{230}$Th advected from the inner ocean must be removed by settling particles with the same vertical $^{230}Th_p$ gradient as in the inner ocean. Conversely, in the inner ocean, less $^{230}$Th must be removed by settling particles with the same vertical $^{230}Th_p$ gradient as at the margin. Note that $S^i = S^m$, only if $k_i = k_m = 0$. This corresponds to the 1D reversible scavenging model that would not account for the increasing $^{230}$Th particulate fraction with depth and for the non-linear dissolved $^{230}$Th profiles. Given the simplicity of the model, we do not expect a full agreement with the data despite some tuning of the parameters. For example, the hydrothermal scavenging of $^{230}Th_{xs}$ below 2000 m depth, possibly occurring at station 50 is not represented in the model. Nevertheless, we believe that the model captures some effects of particle accumulation and scavenging at depth. This is in line with 3D modelling results showing that dissolved Th and Pa profiles in the Atlantic Ocean are better simulated when a parametrization of boundary and bottom scavenging is introduced (Rempfer *et al.*, 2017). As observed in the data, the modelled dissolved $^{230}Th_{xs}$ concentration profiles increase with depth followed by a decrease in concentration approaching the seafloor (Fig. 7). The model also captures the linear increase of the particulate $^{230}Th_{xs}$ concentrations with depth, as observed in the data (Fig. 7). Despite the reversible scavenging equilibrium hypothesis, dissolved and particulate $^{230}Th_{xs}$ are not proportional because the mass of particles "*m*" increases with depth (eq. 1).

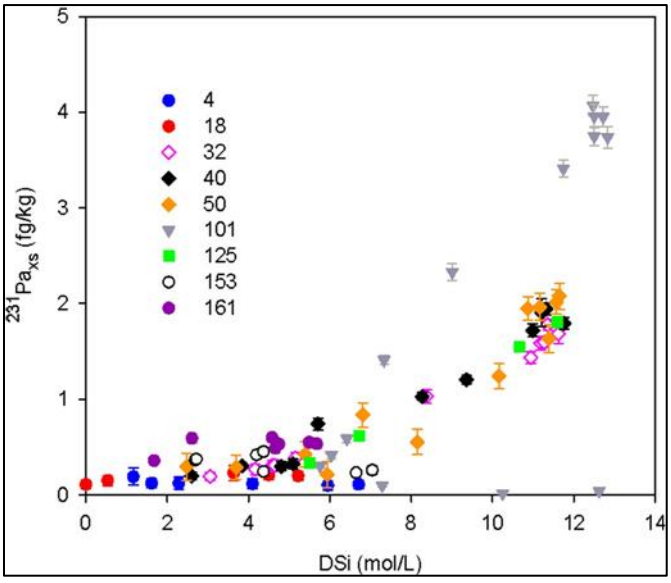


**Figure 8: Dissolved $^{231}Pa_{xs}$ versus DSi measured during PS94 (Van Ooijen *et al.*, 2016). Diamonds: Nansen Basin, squares: Amundsen basin, triangles: Makarov Basin and circles: shelf stations.**

Therefore, the linear particulate $^{230}Th_{xs}$ profiles result from the gross linear increase of the $^{230}Th_{xs}$ in-situ production with depth (it is not perfectly linear due to lateral transport). Despite this linear increase of the particulate $^{230}Th_{xs}$, the dissolved $^{230}Th_{xs}$ concentrations can de- crease with depth due to the increased particulate scavenging. As a consequence of the dissolved and particulate profile shapes, the particulate/total fraction of $^{230}Th_{xs}$ increases with depth as observed in the data (Figs. 5 and 7). The measured particulate $^{230}Th_{xs}$ concentrations are relatively similar at stations 32, 50 and 101 (Fig. 3). This is surprising and probably circumstantial: the high particle mass equilibrating with a low dissolved $^{230}Th_{xs}$ content at the margin balances the lower mass of particles equilibrating with a higher dissolved $^{230}Th_{xs}$ concentration at the interior ocean. A direct consequence of these similar particulate $^{230}Th_{xs}$ profiles is that the vertical flux of $^{230}Th_{xs}$ is increased at the margin where the particle settling velocity is higher compared to the ocean interior. Hence, boundary scavenging occurs.

### 4.3. $^{231}Pa_{xs}$ Profiles: Scavenging versus Circulation

$^{231}Pa_{xs}$ is less particle reactive compared to $^{230}Th_{xs}$, as indicated by the lower $^{231}Pa_{xs}$ particulate fraction compared to the $^{230}Th_{xs}$ particulate fraction (Fig. 5). As a consequence, $^{231}Pa_{xs}$ profiles generally deviate more strongly from the linear increase expected from reversible scavenging due to a significant transport by advection (e.g. Hayes *et al.*, 2015a, 2015b; Gdaniec *et al.*, 2017). In the Arctic, Moran *et al.* (2005) estimated that 39% of the $^{231}Pa_{xs}$ produced in the Arctic Ocean is expected to be exported to the Atlantic Ocean through the Fram Strait. However, in the Makarov Basin, ventilation cannot account for the non- linear $^{231}$Pa profile, as the residence time of the deep water is several hundreds of years (e.g. Rutgers van der Loeff *et al.*, 2018).

Therefore, this non-linear profile may be related to scavenging along the basin boundaries (Roy-Barman, 2009).

On the Barents Shelf (St. 153 and 161), representing the inflow of unmodified Atlantic waters, the dissolved $^{231}Pa_{xs}$ is in the same range as the concentrations ($^{231}Pa_{xs}$ = 0.33–0.68 fg/kg) measured in the north- eastern Atlantic (Hayes *et al.*, 2015a, 2015b). At stations 04 and 18, the dissolved $^{231}Pa_{xs}$ (0.19–0.36 fg/kg) becomes slightly lower, possibly reflecting scavenging of $^{231}Pa_{xs}$ on the Barents Shelf (Fig. 2). Pa scavenging over the Barents Self is not surprising because the area is known for its diatom blooms (Wassmann *et al.*, 1990). The dissolved $^{231}Pa_{xs}$ in shallow waters (< 500 m) over the slope (St. 32) and the Nansen Basin (stations 40 and 50) ($^{231}Pa_{xs}$ = 0.20–0.4 fg/kg) are intermediate between the Atlantic inflowing water (stations 153 and 161) and close to Svalbard (St. 4).

As for the $^{230}Th_{xs}$ (and $^{232}$Th) in bottom waters of station 153 and 161, depleted concentrations of dissolved $^{231}Pa_{xs}$ were accompanied with elevated particulate $^{231}Pa_{xs}$ concentrations (Figs. 2 and 3), indicating removal of $^{231}Pa_{xs}$ at the Barents shelf, close to the seafloor. The particulate fraction of $^{231}Pa_{xs}$ in deep waters of the interior Nansen was very small (0.2–0.9%) compared to $^{230}Th_{xs}$ (25–48%), which is expected due to the overall lower particle reactivity of $^{231}$Pa (compared to $^{230}$Th).Extremely low dissolved $^{231}Pa_{xs}$ concentrations (0.02 ± 0.005 fg/ kg) were observed in surface waters (10–100 m) of station 101 (Fig. 2). As the high $^{232}$Th content of these waters was attributed to advection by the transpolar drift (e.g. Rutgers van der Loeff *et al.*, 2018), it is likely that these waters were completely depleted of their $^{231}$Pa over the shelf and that during their transit to station 101 reversible scavenging has acted to build up a linear equilibrium profile. The sea-ice cover has prevented this equilibrium profile (> 100 m) from re-homogenization by wind-induced mixing. In the deep basins, deep/bottom scavenging also occurs, as suggested by the elevated particulate $^{231}Pa_{xs}$ concentrations below 2000 m depth observed at station 32 and 50 that indicate removal of $^{231}Pa_{xs}$ in deep waters of the Nansen Basin (Fig. 3). However, in contrast to $^{230}Th_{xs}$, higher $^{231}Pa_{xs}$ particulate fractions were observed at station 50 relative to station 32 (Fig. 5), suggesting the presence at station 50 of hydrothermal particles which are known to have a high affinity for Pa. Unlike dissolved $^{230}Th_{xs}$ profiles, the dissolved $^{231}Pa_{xs}$ profiles in the Nansen and Amundsen Basin have similar shapes probably due to the much longer scavenging residence time of Pa relative to Th. By contrast, $^{231}Pa_{xs}$ concentrations are higher in the intermediate/deep Makarov Basin (St. 101) than in the Eurasian Basin due to the long term isolation of these 2 basins by the Lomonosov ridge (Fig. 2). Interestingly, there are two distinct correlations between dissolved silica (DSi) and dis- solved

$^{231}Pa_{xs}$ in the deep waters of the Nansen and the Makarov Basins (Fig. 8). These positive correlations are likely due to the high affinity of $^{231}$Pa for biogenic silica (BSi) (e.g. Chase *et al.*, 2002). We propose that $^{231}$Pa is scavenged by BSi formed in surface waters. As these particles settle through the water column, BSi dissolves and releases $^{231}$Pa into solution again. The steeper slope of the dissolved $^{231}Pa_{xs}$ versus DSi correlation in the Makarov Basin compared to the Nansen Basin is likely due to accumulation of in-situ produced $^{231}$Pa (in addition to the BSi dissolution effect) during the longer aging of the deep Makarov/Canadian waters.

### 4.4. Applying the Boundary Scavenging Model to Pa

The boundary scavenging model developed for $^{230}$Th is now applied to $^{231}$Pa with the appropriate changes (Table 1). The production rate is changed (0.025 fg/kg/y) and the dissolved-particulate partition coefficient is divided by 12 because we have estimated that $F_{Th/Pa}$ ~12 (Fig. 4). Several similarities and differences arise between the model and measured data. The model reproduces the non-linear shape of the dissolved $^{231}Pa_{xs}$ profiles (particularly at St. 50) and the relatively linear particulate $^{231}Pa_{xs}$ profiles of station 32 and 50. However, the modelled dissolved $^{231}Pa_{xs}$ concentrations are overestimated by a factor 2 to 4 (Fig. 7). Modelled particulate $^{231}Pa_{xs}$ concentrations at the margin are also overestimated. The reason for the overestimated dissolved $^{231}Pa_{xs}$ concentrations is probably a mix of previously discussed processes and because of the possible underestimation of the particulate Pa con- centration revealed by intercomparison work at station 101 (higher particulate Pa concentration would result in a higher removal rate by scavenging on setting particles). Scavenging of $^{231}Pa_{xs}$ by hydrothermal plumes can severely deplete the concentrations of $^{231}Pa_{xs}$ in the deep Arctic Ocean (Valk *et al.*, 2018). Export of $^{231}$Pa through advection has been proposed to have a significant importance in several studies (e.g. Hoffmann *et al.*, 2013; Moran *et al.*, 2005). The dissolved $^{231}$Pa concentrations of the deep inflow through the Fram Strait Branch ($^{231}$Pa ~1–1.5 fg/kg) agrees well with the value ($^{231}$Pa = 1.5 fg/kg) used in Moran *et al.* (2005). The $^{231}$Pa concentrations reported here for the return in the Nansen Basin at station 50 ($^{231}$Pa ~ 1–1.5 fg/kg) is close to the Fram Strait Branch. By contrast, in the deep Makarov Basin, above the sill on the Lomonosov ridge is ($^{231}$Pa ~1.5–3.0 fg/kg) consistent with Moran *et al.* (2005) estimates. This $^{231}$Pa gradient between the inflow and outflow supports a net export of $^{231}$Pa into the Atlantic. Finally, boundary scavenging along the slopes of the Eurasian Basin can reduce the dissolved $^{231}$Pa in the deep Arctic Ocean. Probably, $^{231}$Pa/$^{230}$Th ratios of the suspended particles of the Nansen Basin were below the $^{231}$Pa/$^{230}$Th production ratio, but top-core sediments of the Nansen margin and slope have high $^{231}$Pa/$^{230}$Th-ratios, suggesting that the Nansen margin is in fact a large sink for $^{231}$Pa in the Arctic Ocean.

Roy-Barman (2009) proposed a balanced Arctic budget of $^{231}$Pa between the inner ocean and the margin without export of $^{231}$Pa through the Fram Strait. However, it was based on very low $F_{Th/Pa}$ values (~ 3–10) compared to the values reported in the present work.

### 4.5. Factors Controlling Pa-Th Fractionation

#### 4.5.1. The Th-Pa Fractionation Factor

$^{231}Pa_{xs}$ is generally less particle reactive than $^{230}Th_{xs}$, which results in $^{231}Pa_{xs}$ profiles that deviate more strongly from the linear increase expected from reversible scavenging due to transport by advection (e.g. Chase *et al.*, 2002; Hayes *et al.*, 2015a, 2015b; Gdaniec *et al.*, 2017). The particulate content of $^{231}Pa_{xs}$ relative to the total $^{231}Pa_{xs}$ concentrations was in the order of 0.6–1% in the deep stations (< 2000 m) and up to 15% on the shelf, while particulate/total ratios for $^{230}Th_{xs}$ ranged between 6% and 17% in the deep stations and up to 80% on the shelf (Fig. 5). This reflects the preferential scavenging of $^{230}Th_{xs}$ relative to $^{231}Pa_{xs}$, As a consequence, the $F_{Th/Pa}$ in the open ocean is typically around 20 (e.g. Hayes *et al.*, 2015b), mostly when carbonate, organic and lithogenic particles dominates. Notable exceptions are environments where particulate matter is dominated by diatoms ($F_{Th/Pa} < 5$, e.g. Scholten *et al.*, 2008; Venchiarutti *et al.*, 2011a; Venchiarutti *et al.*, 2011b) or Mn-Fe (oxy)hydroxides, such as in hydrothermal plumes ($F_{Th/Pa} = 6 \pm 3$ for $MnO_2$ and $F_{Th/Pa} = 11 \pm 6$ for $Fe(OH)_3$, Hayes *et al.*, 2015a, 2015b; Pavia *et al.*, 2018). As a con- sequence of these different drivers, 2 types of $F_{Th/Pa}$ depth profiles are generally observed:

1) In the North Atlantic $F_{Th/Pa}$ decreases with depth because the particulate matter composition evolves from lithogenic/carbonated in the surface water to strongly affected by Fe-Mn oxides due to hydrothermal particles above and around the Mid-Atlantic Ridge or to oxidation/precipitation of Fe-Mn released in the oxygen minimum zone off the Mauritanian coast.

2) In areas dominated by diatom production, $F_{Th/Pa}$ tends to increase with depth as a consequence of the biogenic silica dissolution (Scholten *et al.*, 2008; Venchiarutti *et al.*, 2011a, 2011b), because opal tends to dissolve during the settling through the water column (Nelson *et al.*, 1995). In the Arctic, this view is supported by the strong correlation observed between dissolved $^{231}$Pa and dissolved Si of the deep Makarov and Nansen Basins (Fig. 8).

The $F_{Th/Pa}$ profiles that we obtained on the Nansen margin (St. 32, 153 and 161) and in the Makarov Basin (St. 101) show a clear increase with depth (from $F_{Th/Pa} \approx 2–5$ in the shallow waters to $F_{Th/Pa} \approx 20$ in the deep waters) suggesting surface particles dominated by diatoms and

deeper particles with an increasing influence of lithogenic particles resuspended and advected from the margin. At station 50, the limited increase of $F_{Th/Pa}$ below 2000 m ($F_{Th/Pa} \approx 10$) supports that particles at this station still include some particles derived from the hydrothermal activity, even if at the time of sampling most of the plume itself had left the Gakkel Ridge and cannot be clearly detected with beam transmission data (Valk *et al.*, 2018).

### 4.5.2. Large Scale Pa-Th Fractionation

Early studies of Pa-Th in the Arctic Ocean have emphasized that despite of the large shelf areas, the large Pa-Th fractionation observed in the Pacific Ocean sediments between the ocean margin ($[^{231}Pa_{xs}/^{230}Th_{xs}] \approx 3$ * production ratio) and the ocean interior ($[^{231}Pa_{xs}/^{230}Th_{xs}] \approx 0.3$ * production ratio) was not present in Arctic Ocean sediments. Instead, most Arctic sediments have $[^{231}Pa_{xs}/^{230}Th_{xs}]$ activity ratios significantly lower than the production ratio (Edmonds *et al.*, 2004; Moran *et al.*, 2005). Recently, a few sediment samples collected on the Siberian shelf margins were reported to have $^{231}Pa_{xs}/^{230}Th_{xs}$ ratios that slightly exceed the production ratio (Luo and Lippold, 2015). Moreover, Hoffmann *et al.* (2013) observed decreasing Arctic sedimentary $^{231}Pa/^{230}Th$ ratios with water depth, over the last 30 kyr. This general deficit in $^{231}Pa_{xs}$ was attributed to the export of a significant fraction of the Arctic $^{231}Pa_{xs}$ into the Atlantic Ocean through the Fram Strait and to the hypothetical possibility that some of the $^{231}Pa_{xs}$ was lost by boundary scavenging in a location not identified at that time. The data obtained in this work on the suspended particles of the Nansen margin (St. 32, 158 and 161) show particulate $[^{231}Pa_{xs}/^{230}Th_{xs}]$ activity ratios below the production ratio except in the surface waters, but the calculation of the particulate $^{231}Pa_{xs}$ is affected by large un- certainties (Table ES2). However, Top-core sediments from the Nansen margin (St. 161 and 32) have distinctly high $[^{231}Pa_{xs}/^{230}Th_{xs}]$ activity ratios: $[^{231}Pa_{xs}/^{230}Th_{xs}] = 0.40$ at station 161 and 0.18 at station 32 (Table S3). Hence, the $[^{231}Pa_{xs}/^{230}Th_{xs}]$ activity ratios of these two surface sediment samples are much higher than the corresponding ratio in the suspended particles. These ratios at station 161 and 32 are well above the values reported by Moran *et al.* (2005). So boundary scavenging along the Nansen margin could contribute to the $^{231}Pa$ depletion in the Arctic Ocean. Scavenging by the hydrothermal plume turns out to be an alternative sink. Moreover, the discrepancies between the sediment and particulate $^{231}Pa/^{230}Th$ ratios might be related to the different timescales of these data records. Still, particulate samples in the deep part of the station 50 have $^{231}Pa_{xs}/^{230}Th_{xs}$ ratios below the production ratio despite the relatively low $F_{Th/Pa}$ (Table ES2). Whether these particles are still dominated by hydrothermal particles or not remains ambiguous (Valk *et al.*, 2018).

## 5. Conclusions

The distribution of $^{231}Pa_{xs}$ and $^{230}Th_{xs}$ in the Arctic Ocean deviates from the linear increase expected from reversible scavenging in absence of lateral advection. While the role of hydrothermal scavenging of $^{230}$Th recently has been highlighted in the Nansen Basin (Valk *et al.*, 2018), we show here that boundary scavenging also removes significant amounts of $^{230}$Th at the Nansen margin. Scavenging on particles derived from hydrothermal activity is associated with a relatively low $F_{Th/Pa}$ fractionation factor (≈10), while higher $F_{Th/Pa}$ (≈20) were observed for deep and bottom waters both of the Eurasian and Makarov Basin. The modified boundary scavenging model developed here for the Nansen Basin, successfully modelled the increasing $^{230}Th_{xs}$ particulate fraction with depth and the decrease of dissolved Pa-Th contents approaching the seafloor observed on various margins. Modelled dis- solved $^{231}$Pa distributions were largely overestimated. These results suggest that advection of dissolved $^{231}$Pa out the Atlantic is an important sink for the Arctic $^{231}$Pa budget. However, the high sedimentary $^{231}Pa_{xs}/^{230}Th_{xs}$ ratios observed at the Barents Sea shelf and Nansen margin indicate that the Arctic margins could indeed act as a major sink for the missing Arctic $^{231}$Pa. More data focused on shelves and slopes of the Arctic Ocean are required to better constrain this effect and the chemical nature of the particles and their physical mode of resuspension have to be addressed more precisely.

Supplementary data to this article can be found online at https://doi.org/10.1016/j.chemgeo.2019.119380

### Declaration of Competing Interest

The authors declare that they have no known competing financial interests or personal relationships that could have appeared to influ- ence the work reported in this paper.

### Acknowledgements

This work was conducted in the framework of the GEOTRACES program and was supported by the Swedish Research Council (VR 349- 202-6287). The authors are pleased to thank the captains and the crew of the research vessel R/V Polarstern. Ronja Paffrath is thanked for the sampling of seawater. Karin Wallner is acknowledged for their critical roles in the laboratory work. Aridane G. González is acknowledged for melting ice rafted sediments samples. Lise Missiaen was supported by an ERC funding to the ACCLIMATE project. The constructive comments of 2 anonymous reviewers greatly improved the present manuscript.

## References

Aagaard, K., Britain, G., Aagaard, K., Carmack, E., 1981. On the halocline of the Arctic Ocean. Deep. Res. 28, 529–545.

Anderson, R.F., Bacon, M.P., Brewer, P.G., 1983. Removal of $^{230}$Th and $^{231}$Pa at ocean margins. Earth Planet. Sci. Lett. 66, 73–90. https://doi.org/10.1016/0012-821X(83) 90127-9.

Bacon, M.P., Anderson, R.F., 1982. Distribution of Thorium isotopes between dissolved and particulate forms in the deep sea. J. Geophys. Res. 87, 2045–2056. https://doi.org/10.1029/JC087iC03p02045.

Bacon, M.P., Huh, C.A., Moore, R.M., 1989. Vertical profiles of some natural radio- nuclides over the Alpha Ridge, Arctic Ocean. Earth Planet. Sci. Lett. 95, 15–22. https://doi.org/10.1016/0012-821X(89)90164-7.

Björk, G., Jakobsson, M., Rudels, B., Swift, J.H., Anderson, L., Darby, D.A., Backman, J., Coakley, B., Winsor, P., Polyak, L., Edwards, M., 2007. Bathymetry and deep-water exchange across the central Lomonosov Ridge at 88-89°N. Deep. Res. Part I Oceanogr. Res. Pap. 54, 1197–1208. https://doi.org/10.1016/j.dsr.2007.05.010.

Björk, G., Anderson, L.G., Jakobsson, M., Antony, D., Eriksson, P.B., Hell, B., Hjalmarsson, S., Janzen, T., Jutterstr, S., Marcussen, C., Olsson, K.A., Rudels, B., Linders, J., Ludvig, L., Sølvsten, M., Selle, E., 2010. Deep-Sea Research I Flow of Canadian Basin Deep Water in the Western Eurasian Basin of the Arctic Ocean. 57. pp. 577–586. https://doi.org/10.1016/j.dsr.2010.01.006.

Bourne-Worster, Mark, Thomas, Alex, Macniocaill, Conall, Henderson, Gideon, 2012. Improved determination of marine sedimentation rates using $^{230}Th_{xs}$. Geochemistry Geophysics Geosystems 13, Q09017. https://doi.org/10.1029/2012GC004295.

Burckel, P., 2014. Reconstructing last glacial changes in Atlantic meridional overturning rate using marine sediment ($^{231}$Pa/$^{230}$Th. Oceanography Université de Versailles- Saint Quentin en Yvelines English. ffNNT: 2014VERS0051ff.fftel-01235193.

Brewer, P.G., Nozaki, Y., Spencer, D.W., Fleer, A.P., 1980. A sediment trap experiment in the deep sub-tropical Atlantic: Isotopic and elemental fluxes. J. Mar. Res. 38, 703–728.

Chase, Z., Anderson, R.F., Fleisher, M.Q., Kubik, P.W., 2002. The influence of particle composition and particle flux on scavenging of Th, Pa and Be in the ocean. Earth Planet. Sci. Lett. 204, 215–229. https://doi.org/10.1016/S0012-821X(02)00984-6.

Cheng, H., Edwards, R.L., Murrell, M.T., Benjamin, T.M., 1998. Uranium-thorium-protactinium dating systematics. Geochim. Cosmochim. Acta 62, 3437–3452. https://doi.org/10.1016/S0016-7037(98)00255-5.

Cochran, J.K., Hirschberg, D.J., Livingston, H.D., Buesseler, K.O., Key, R.M., 1995. Natural and anthropogenic radionuclide distributions in the Nansen Basin, Artic Ocean: scavenging rates and circulation timescales. Deep. Res. Part II 42, 1495–1517. https://doi.org/10.1016/0967-0645(95)00051-8.

Condon, D.J., McLean, N., Noble, S.R., Bowring, S.A., 2010. Isotopic composition ($^{238}$U/$^{235}$U) of some commonly used uranium reference materials. Geochim. Cosmochim. Acta 74, 7127–7143. https://doi.org/10.1016/j.gca.2010.09.019.

Edmonds, H.N., 1998. Protactinium-231 and thorium-230 abundances and high scavenging rates in the Western Arctic Ocean. Science (80-.) 280, 405–407. https://doi.org/10.1126/science.280.5362.405.

Edmonds, H.N., Moran, S.B., Cheng, H., Edwards, R.L., 2004. $^{230}$Th and $^{231}$Pa in the Arctic Ocean: implications for particle fluxes and basin-scale Th/Pa fractionation. Earth Planet. Sci. Lett. 227, 155–167. https://doi.org/10.1016/j.epsl.2004.08.008.

Gdaniec, S., Roy-Barman, M., Foliot, L., Thil, F., Dapoigny, A., Burckel, P., Garcia- Orellana, J., Masqué, P., Mörth, C.-M., Andersson, P.S., 2017. Thorium and pro- tactinium isotopes as tracers of marine particle fluxes and deep water circulation in the Mediterranean Sea. Mar. Chem. 199, 12–23. https://doi.org/10.1016/j.marchem. 2017.12.002.

Guihou, A., Pichat, S., Nave, S., Govin, A., Labeyrie, L., Michel, E., Waelbroeck, C., 2010. Late slowdown of the Atlantic meridional overturning circulation during the last glacial inception: new constraints from sedimentary ($^{231}$Pa/$^{230}$Th). Earth Planet. Sci. Lett. 289, 520–529. https://doi.org/10.1016/j.epsl.2009.11.045.

Hayes, C.T., Anderson, R.F., Fleisher, M.Q., Huang, K.F., Robinson, L.F., Lu, Y., Cheng, H., Edwards, R.L., Moran, S.B., 2015a. $^{230}$Th and $^{231}$Pa on GEOTRACES GA03, the U.S. GEOTRACES North Atlantic transect, and implications for modern and paleoceano- graphic chemical fluxes. Deep. Res. Part II Top. Stud. Oceanogr. 116, 29–41. https://doi.org/10.1016/j.dsr2.2014.07.007.

Hayes, C.T., Anderson, R.F., Fleisher, M.Q., Vivancos, S.M., Lam, P.J., Ohnemus, D.C.,

Huang, K.F., Robinson, L.F., Lu, Y., Cheng, H., Edwards, R.L., Moran, S.B., 2015b. Intensity of Th and Pa scavenging partitioned by particle chemistry in the North Atlantic Ocean. Mar. Chem. 170, 49–60. https://doi.org/10.1016/j.marchem.2015.01.006.

Hillaire-Marcel, C., McManus, J., Ghaleb, B., Vernal, A. de, Maccali, J., Cuny, K., Jacobel, A., Le Duc, C., 2017. A New Chronology of Late Quaternary Sequences from the Central Arctic Ocean Based on '"Extinction Ages"' of their Excesses in $^{231}$Pa and $^{230}$Th 4573–4585. https://doi.org/10.1002/2017GC007050.

Hoffmann, S.S., McManus, J.F., Curry, W.B., Susan Brown-Leger, L., 2013. Persistent export of $^{231}$Pa from the deep central Arctic Ocean over the past 35,000 years. Nature 497, 603–606. https://doi.org/10.1038/nature12145.

Huh, C.A., Pisias, N.G., Kelley, J.M., Maiti, T.C., Grantz, A., 1997. Natural radionuclides and plutonium in sediments from the western Arctic Ocean: sedimentation rates and pathways of radionuclides. Deep. Res. Part II Top. Stud. Oceanogr. 44, 1725–1743. https://doi.org/10.1016/S0967-0645(97)00040-4.

Ivanova, E.V., Murdmaa, I.O., Duplessy, J., Paterne, M., 2002. Late Weichselian to Holocene paleoenvironments in the Barents Sea. Glob. Planet. Change 34, 209–218.

Jakobsson, M., 2002. Hypsometry and volume of the Arctic Ocean and its constituent seas. Geochemistry, Geophys. Geosystems 3, 1–18. https://doi.org/10.1029/ 2004GC000694.

Klunder, M., Bauch, Dorothea, Laan, Patrick, de Baar, Hein, van Heuven, Steven, Ober, S., 2012. Dissolved iron in the Arctic shelf seas and surface waters of the central Arctic Ocean: Impact of Arctic river water and ice-melt. Journal of Geophysical Research (Oceans) 117, 1027. https://doi.org/10.1029/2011JC007133.

Lukashin, V.N., Shcherbinin, A.D., 2007. Hydrological properties, suspended matter, and particulate fluxes in the water column of the Bear Island Trough. Mar. Geol. 47, 68–79. https://doi.org/10.1134/S0001437007010109.

Luo, Y., Lippold, J., 2015. Controls on $^{231}$Pa and $^{230}$Th in the Arctic Ocean. Geophys. Res. Lett. https://doi.org/10.1002/2015GL064671. n/a-n/a.

Moran, S.B., Hoff, J.A., Buesseler, K.O., Edwards, R.L., 1995. High precision $^{230}$Th and $^{232}$Th in the Norwegian Sea and Denmark by thermal ionization mass spectrometry. Geophys. Res. Lett. 22, 2589–2592.

Moran, S.B., Shen, C.C., Weinstein, S.E., Hettinger, L.H., Hoff, J.H., Edmonds, H.N., Edwards, R.L., 2001. Constraints on deep water age and particle flux in the Equatorial and South Atlantic Ocean based on seawater $^{231}$Pa and $^{230}$Th data. Geophys. Res. Lett. 28, 3437–3440. https://doi.org/10.1029/2001GL013339.

Moran, S.B., Shen, C.C., Edmonds, H.N., Weinstein, S.E., Smith, J.N., Edwards, R.L., 2002. Dissolved and particulate $^{231}$Pa and $^{230}$Th in the Atlantic Ocean: constraints on intermediate/deep water age, boundary scavenging, and $^{231}$Pa/$^{230}$Th fractionation. Earth Planet. Sci. Lett. 203, 999–1014. https://doi.org/10.1016/S0012-821X(02)00928-7.

Moran, S.B., Shen, C.C., Edwards, R.L., Edmonds, H.N., Scholten, J.C., Smith, J.N., Ku, T.L., 2005. $^{231}$Pa and $^{230}$Th in surface sediments of the Arctic Ocean: implications for $^{231}$Pa/$^{230}$Th fractionation, boundary scavenging, and advective export. Earth Planet. Sci. Lett. 234, 235–248. https://doi.org/10.1016/j.epsl.2005.02.016.

Nelson, D.M., Tréguer, P., Brzezinski, M.A., Leynaert, A., Quéguiner, B., 1995. Production and dissolution of biogenic silica in the ocean: revised global estimates, comparison with regional data and relationship to biogenic sedimentation. Glob. Biogeochem. Cycles 9, 359–372. https://doi.org/10.1029/95GB01070.

Not, C., Brown, K., Ghaleb, B., Hillaire-Marcel, C., 2012. Conservative behavior of uranium vs. salinity in Arctic Sea ice and brine. Mar. Chem. 130–131, 33–39. https://doi.org/10.1016/j.marchem.2011.12.005.

Nowaczyk, N.R., Frederichs, T.W., Kassens, H., Norgaard-pedersen, N., Spielhagen, R.F., Stein, R., Weiel, D., 2001. Sedimentation rates in the Makarov Basin, central Arctic Ocean: a paleomagnetic and rock magnetic approach. Paleoceanography 16, 368–389.

Okubo, A., Takeda, S., Obata, H., 2013. Atmospheric deposition of trace metals to the western North Pacific Ocean observed at coastal station in Japan. Atmos. Res. 129–130, 20–32. https://doi.org/10.1016/j.atmosres.2013.03.014.

Owens, S.A., Buesseler, K.O., Sims, K.W.W., 2011. Re-evaluating the $^{238}$U-salinity relationship in seawater: Implications for the $^{238}$U-$^{234}$Th disequilibrium method. Mar. Chem. 127, 31–39. https://doi.org/10.1016/j.marchem.2011.07.005.

Pavia, F., Anderson, R., Vivancos, S., Fleisher, M., Lam, P., Lu, Y., Cheng, H., Zhang, P., Lawrence Edwards, R., 2018. Intense hydrothermal scavenging of $^{230}$Th and $^{231}$Pa in the deep Southeast Pacific. Mar. Chem. 201, 212–228. https://doi.org/10.1016/j.marchem.2017.08.003.

Pfirman, S., Thiede, J., 1987. Lithogenic sediment on Arctic pack ice: potential aeolian flux and contribution to deep sea sediments. In: Paleoclimatology and Paleometeorology: Modern and Past Patterns of Global Atmospheric Transport, pp. 463–493.

Rabe, B., Schauer, U., Ober, S., Horn, M., Hoppmann, M., Korhonen, M., Pisarev, S., Hampe, H., 2016. Physical oceanography during POLARSTERN cruise PS94 (ARK- XXIX/3). Alfred Wegener Institute, Helmholtz Centre for Polar and Marine Research, Bremerhaven, PANGAEA. https://doi.org/10.1594/PANGAEA.859558.

Rempfer, Johannes, Stocker, Thomas F., Joos, Fortunat, Lippold, Jörg, Jaccard, Samuel L., 2017. New insights into cycling of $^{231}$Pa and $^{230}$Th in the Atlantic Ocean. Earth and Planetary Science Letters 468, 27–37. https://doi.org/10.1016/j.epsl.2017.03.027.

Rijkenberg, M.J.A., Slagter, H.A., Rutgers van der Loeff, M., van Ooijen, J., Gerringa, L.J.A., 2018. Dissolved Fe in the deep and upper Arctic Ocean with a focus on Fe limitation in the Nansen Basin. Front. Mar. Sci. 5, 1–14. https://doi.org/10.3389/fmars.2018.00088.

Roy-Barman, M., Chen, J.H., Wasserburg, G.J., 1996. The sources and the fates of thorium. Earth Planet. Sci. Lett 139, 351–363.

Roy-Barman, M., 2009. Modelling the effect of boundary scavenging on Thorium and Protactinium profiles in the ocean. Biogeosciences 6, 7853–7896. https://doi.org/10.5194/bgd-6-7853-2009.

Rudels, B., 2012. Arctic Ocean circulation and variability – advection and external forcing encounter constraints and local processes. Ocean Sci. 8, 261–286. https://doi.org/10.5194/os-8-261-2012.

Rudels, B., Jones, E.P, Erson, L.G, Kattner, G., 1994. On the intermediate depth waters of the Arctic ocean. AGU Geophysical Monograph 85, 33–46.

Rudels, B., Korhonen, M., Schauer, U., Pisarev, S., Rabe, B., Wisotzki, A., 2015. Circulation and transformation of Atlantic water in the Eurasian Basin and the contribution of the Fram Strait inflow branch to the Arctic Ocean heat budget. Progress in Oceanography 132, 128–152. https://doi.org/10.1016/j.pocean.2014.04.003.

Rudels, B., 2009. Arctic Ocean Circulation, in: Steele, J., Thorpe, S., Turekian, K. (Eds.), Encyclopedia of Ocean Sciences. Academic Press, pp. 211-225

Rutgers van der Loeff, M.M., Berger, G.W., 1993. Scavenging of $^{230}$Th and $^{231}$Pa near the antarctic polar front in the South Atlantic. Deep. Res. Part I 40, 339–357. https://doi.org/10.1016/0967-0637(93)90007-P.

Rutgers van der Loeff, M.M., Boudreau, B.P., 1997. The effect of resuspension on chemical exchanges at the sediment-water interface in the deep sea: a modelling and natural radiotracer approach. J. Mar. Syst. 11, 305–342.

Rutgers van der Loeff, M., Kipp, L., Charette, M.A., Moore, W.S., Black, E., Stimac, I., Charkin, A., Bauch, D., Valk, O., Karcher, M., Krumpen, T., Casacuberta, N., Smethie, W., Rember, R., 2018. Radium Isotopes across the Arctic Ocean show Time Scales of Water Mass Ventilation and Increasing Shelf Inputs. Journal of Geophysical Research: Oceans 123, 4853-4873.

Schlosser, P., Kromer, B., Ekwurzel, B., Bönisch, G., McNichol, A., Schneider, R., von Reden, K., Östlund, H.G., Swift, J.H., 1997. The first trans-Arctic $^{14}$C section: comparison of the mean ages of the deep waters in the Eurasian and Canadian basins of the Arctic Ocean. Nucl. Instruments Methods Phys. Res. Sect. B Beam Interact. with Mater. Atoms 123, 431–437. https://doi.org/10.1016/S0168-583X(96)00677-5.

Scholten, J.C., Rutgers van der Loeff, M.M., Michel, A., 1995. Distribution of $^{230}$Th and $^{231}$Pa in the water column in relation to the ventilation of the deep Arctic basins. Deep. Res. Part II 42, 1519–1531. https://doi.org/10.1016/0967-0645(95)00052-6.

Scholten, J.C., Fietzke, J., Mangini, A., Garbe-Schönberg, C.D., Eisenhauer, A., Schneider, R., Stoffers, P., 2008. Advection and scavenging: effects on $^{230}$Th and $^{231}$Pa dis- tribution off Southwest Africa. Earth Planet. Sci. Lett. 271, 159–169. https://doi.org/ 10.1016/j.epsl.2008.03.060.

Smith, J.N., Moran, S.B., Macdonald, R.W., 2003. Shelf-basin interactions in the Arctic Ocean based on $^{210}$Pb and Ra isotope tracer distributions. Deep. Res. Part I Oceanogr. Res. Pap. 50, 397–416. https://doi.org/10.1016/S0967-0637(02)00166-8.

Tanhua, T., Jones, E.P., Jeansson, E., Jutterstro, S., Jr, W.M.S., Wallace, D.W.R., Anderson, L.G., 2009. Ventilation of the Arctic Ocean: mean ages and inventories of anthropogenic $CO_2$ and CFC-11. J. Geophys. Res. 114, 1–11. https://doi.org/10.1029/2008JC004868.

Valk, O., Rutgers van der Loeff, M.M., Geibert, W., Gdaniec, S., Rijkenberg, M.J.A., Moran, S.B., Lepore, K., Edwards, R.L., Lu, Y., Puigcorbé, V., 2018. Importance of hydrothermal vents in scavenging removal of $^{230}$Th in the Nansen Basin. Geophys. Res. Lett. 1–10. https://doi.org/10.1029/2018GL079829.

van Ooijen, Jan C., Rijkenberg, Micha J.A, Gerringa, Loes J.A., Rabe, Benjamin, Rutgers van der Loeff, Michiel, M., 2016. Inorganic nutrients measured on water bottle samples during POLARSTERN cruise PS94 (ARK-XXIX/3). Royal Netherlands Institute for Sea Research, Texel, PANGAEA. https://doi.org/10.1594/PANGAEA.868396.

Venchiarutti, C., Roy-Barman, M., Freydier, R., Van Beek, P., Souhaut, M., Jeandel, C., 2011a. Influence of intense scavenging on Pa-Th fractionation in the wake of Kerguelen Island (Southern Ocean). Biogeosciences 8, 3187–3201. https://doi.org/10.5194/bg-8-3187-2011.

Venchiarutti, C., van der Loeff, M.R., Stimac, I., 2011b. Scavenging of $^{231}$Pa and thorium isotopes based on dissolved and size-fractionated particulate distributions at Drake Passage (ANTXXIV-3). Deep. Res. Part II Top. Stud. Oceanogr. 58, 2767–2784. https://doi.org/10.1016/j.dsr2.2010.10.040.

Wassmann, P., Vernet, M., Mitchell, B., Rey, F., 1990. Mass sedimentation of Phaeocystis pouchetii in the Barents Sea. Mar. Ecol. Prog. Ser. 66, 183–195. https://doi.org/10. 3354/meps066183.

# CHAPTER 6: Changes in Circulation and Particle Scavenging in the Amerasian Basin of the Arctic Ocean over the Last Three Decades Inferred from the Water Column Distribution of Geochemical Tracers

**Melanie Grenier[1], Roger François[1], Maureen Soon[1], Michiel M. Rutgers van der Loeff[2], Xiaoxin Yu[1], Ole Valk[2], Christelle Not[3], S. Bradley Moran[4], R. Lawrence Edwards[5], Yanbin Lu[5], Kate Lepore[6] and Susan E. Allen[1]**

[1]Department of Earth, Ocean and Atmospheric Sciences, University of British Columbia, 2207 Main Mall, Vancouver, BC V6T 1Z4, Canada

[2]Alfred-Wegener-Institute, Helmholtz Centre for Polar and Marine Research, Am Handelshafen 12, 27570 Bremerhaven, Germany.

[3]Department of Earth Sciences, The University of Hong Kong, Hong Kong SAR.

[4]College of Fisheries and Ocean Sciences, University of Alaska Fairbanks, Fairbanks, AK 99775, USA.

[5]Department of Earth Sciences, University of Minnesota, 310 Pillsbury Dr SE, Minneapolis, MN 55455, USA.

[6]Mount Holyoke College, South Hadley, MA 01075, USA.

**Key Points:**

• Concentration decreases of $^{230}Th_d$ and $^{231}Pa_d$ suggest an enhancement of particulate scavenging since the 2000s in the Amerasian Basin

• Particulate scavenging results from higher productivity and sediment resuspension from the shelves

• Post-2000s changes in intermediate and deep layers suggest enhanced lateral mixing between the margins and central areas of the basins

Manuscript published in *Journal of Geophysical Research: Oceans,* 124, 9338– 9363.
https://doi.org/10.1029/2019JC015265

Received: 8 May 2019
Accepted: 15 November 2019
Accepted article online: 21 November 2019
Published online: 18 December 2019

**Abstract**

Since the 1980-90s, international research efforts have augmented our knowledge of the physical and chemical properties of the Arctic Ocean water masses and recent studies have documented changes. Understanding the processes responsible for these changes is necessary to be able to forecast the local and global consequences of these property evolutions on climate. The present work investigates the distributions of geochemical tracers of particle fluxes and circulation in the Amerasian Basin and their temporal evolution over the last three decades (from stations visited between 1983 and 2015). Profiles of 230-thorium ($^{230}$Th) and 231-protactinium ($^{231}$Pa) concentration and neodymium isotopes (expressed as $\varepsilon_{Nd}$) measured in the Amerasian Basin prior to 2000 are compared to a new, post-2000s dataset. The comparison shows a large scale decrease in dissolved $^{230}$Th and $^{231}$Pa concentrations, suggesting intensification of scavenging by particle flux, especially in coastal areas. Higher productivity and sediment resuspension from the shelves appear responsible for the concentration decrease along the margins. In the basin interior, increased lateral exchanges with the boundary circulation also contribute to the decrease in concentration. This study illustrates how dissolved $^{230}$Th and $^{231}$Pa, with $\varepsilon_{Nd}$ support, can provide unique insights not only into changes in particle flux but also into the evolution of ocean circulation and mixing.

**Plain Language Summary**

The Arctic Ocean is one of the oceanic regions most affected by climate change. The increasing summer retreat of sea ice allows greater atmosphere-ocean exchanges and light penetration, while land-ocean exchanges are expected to increase, due to enhanced continental erosion (notably through permafrost thawing and increased river flow). These changes are driven by climate and in turn, impact the climate. This study aims at assessing possible shifts in oceanic circulation and particle fluxes resulting from these climate-driven changes in the Amerasian Basin of the Arctic Ocean, during the last few decades. To achieve this goal, we measured geochemical tracers of circulation and particle fluxes in seawater samples collected in this area between 2005 and 2015, which we compared to published data from samples collected between 1983 and 2000. The primary geochemical tracers studied here are $^{230}$Th and $^{231}$Pa. These radioisotopes are uniformly produced in seawater, from uranium decay, and are strongly reactive with particles. Therefore, their oceanic distribution depends on particle fluxes and circulation. The evolution of their distribution in the Amerasian Basin over space and time documents enhancement of particle flux and lateral mixing in the Amerasian basin of the Arctic Ocean over the last three decades.

## 1: Introduction

The pathways that waters follow in the ocean and the physico-chemical changes they undergo along these pathways dictate the redistribution of key parameters such as heat, salt, energy, nutrients, and pollutants. It is of particular interest to examine the pathways and fate of waters in the Arctic Ocean because some of these waters eventually exit to enter the Atlantic Ocean and impact North Atlantic deep water formation and the global overturning circulation (Aagaard *et al.*, 1985; Hansen and Østerhus, 2000). Arctic Ocean waters are made of Pacific and Atlantic Ocean waters that enter the Amerasian Basin through the shallow Bering Strait, and the Eurasian Basin through the shallow Barents Sea and deep Fram Strait. They eventually return to the Atlantic Ocean through Fram Strait and the relatively shallow Canadian Arctic Archipelago as upper or intermediate waters (Aagaard and Greisman, 1975). During their transit in the Arctic Ocean, these waters are transported by the upper wind-driven circulation and the intermediate cyclonic topographical-steered circulation (Figure 1; Rudels, 2001; Rudels *et al.*, 2013).

Investigating the pathways and fate of waters in the Arctic Ocean is all the more important as the Arctic Ocean represents one of the most rapidly changing regions of the world's oceans (Pörtner *et al.*, 2015). With a reduction in seasonal sea ice coverage, changes in hydrography and water mass circulation have been observed, not only at the surface but also at depth (e.g. Polyakov *et al.*, 2013). Particle concentrations are also projected to increase in the rapidly changing Arctic Ocean, as a result of increased continental runoff and biological production, impacting the chemical properties of Arctic waters and downstream (e.g. Carmack *et al.*, 2006).

The first observed changes in temperature - abnormally warm Atlantic water (hereafter, awAW) - occurred in 1990 in Fram Strait (Quadfasel *et al.*, 1991). This awAW propagated through the whole Arctic, first into the Eurasian Basin, then beyond the Lomonosov Ridge, and into the Amerasian Basin. This temperature anomaly was observed in the southern Makarov Basin (MB) and Mendeleyev Ridge in 1993 (E. Carmack *et al.*, 1995), in the central MB in 2000 (Kikuchi *et al.*, 2005), at the northern tip of the Northwind Ridge in 2003 (Woodgate *et al.*, 2007), and within most of the Canada Basin (CB) in 2007 (McLaughlin *et al.*, 2009; see Figure 1 for the basin and ridge locations). However, these studies did not reveal significant changes in circulation related to the awAW propagation in the Arctic. Likewise, no significant changes in particle distribution were reported from limited measurements in the CB conducted between 2003 and 2008 (Jackson *et al.*, 2010). However, the latter study documented a sharp contrast between low particle concentrations of the central basin and much higher concentrations near the CB continental margin.

Because of their affinity for particles and residence times similar to the time scale of regional changes occurring in the Arctic, geochemical tracers such as $^{230}$Th and $^{231}$Pa are powerful tools to quantify the recent evolution of particle flux and circulation in the Arctic Ocean. $^{230}$Th and $^{231}$Pa are produced in the ocean by radioactive α-decay of uranium-234 ($^{234}$U) and uranium-235 ($^{235}$U), respectively; uranium input to the ocean occurs through continental weathering. Uranium is soluble in seawater and has a long residence time in the ocean (~400 000 yr; Brewer, 1975; Chen *et al.*, 1986), such that its concentration and the rate of production of $^{230}$Th and $^{231}$Pa are uniform and well known (Ku *et al.*, 1977; Turekian and Chan, 1971). Unlike parent U, Th and Pa –especially Th– are highly insoluble in seawater and effectively removed to the sediment by adsorption onto sinking particles (Anderson *et al.*, 1983), a process referred to as particulate scavenging. As a result, $^{230}$Th residence times in seawater range from a few years in shallow water to a few decades in deep water; for $^{231}$Pa, residence times range from a few decades in shallow water to a few centuries in deep water (Henderson and Anderson, 2003). If transport of $^{230}$Th and $^{231}$Pa by advection and turbulent diffusion can be neglected, the oceanic distribution of these radionuclides is largely controlled by reversible scavenging: dissolved radionuclides ($R_d$; unit: concentration) are produced continuously at fixed rates (α; unit: concentration per time) and adsorbed reversibly onto sinking particles ($k_a$ and $k_d$ are adsorption and desorption coefficients; unit: per time) to produce sinking particulate radionuclides ($R_p$; unit: concentration), removed at a sinking rate S (unit: length per time) to the underlying sediment (Bacon and Anderson, 1982; Nozaki *et al.*, 1981). Thus, neglecting advection and diffusion, the conservation equations for the radionuclide dissolved and particulate concentrations ([$R_d$] and [$R_p$], respectively) are given by:

$$\frac{\partial [\mathbf{R}]_d}{\partial \mathbf{t}} = \alpha + \boldsymbol{k_d} \cdot [\mathbf{R}]_p - \boldsymbol{k_a} \cdot [\mathbf{R}]_d \quad \textbf{(1)}$$

$$\frac{\partial [\mathbf{R}]_p}{\partial \mathbf{t}} = \boldsymbol{k_a} \cdot [\mathbf{R}]_d - \boldsymbol{k_d} \cdot [\mathbf{R}]_p - \mathbf{S} \cdot \frac{\partial [\mathbf{R}]_p}{\partial \mathbf{z}} \quad \textbf{(2)}$$

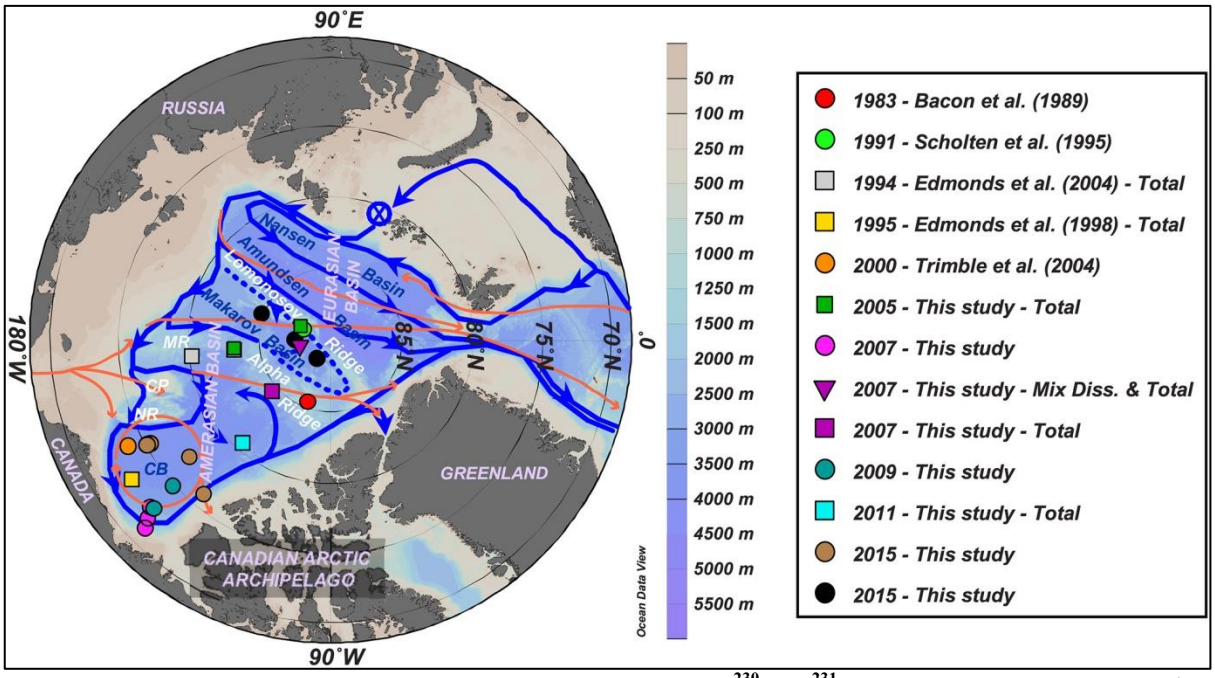


**Figure1: Location of the deep stations (>500mdepth) where $^{230}$Th, $^{231}$Pa, or εNd were measured in the Amerasian Basin of the Arctic so far. This study adds nine new stations in the Canada Basin (CB; 2007: pink dots; 2009: blue-green dots; 2011: cyan square; 2015: brown dots), one new on the Mendeleev Ridge (MR; 2005: green square), five in the Makarov Basin (2005: green square; 2007: purple inverted triangle; 2015: black dots), and one on the Alpha Ridge (2007: purple square). The red arrows show the circulation schematics of the upper layers; the blue ⊗ and arrows show the formation area and circulation schematics of the Atlantic layer, respectively (after Bluhm *et al.*, 2015; Rudels *et al.*, 2013). CP = Chukchi Plateau; NR = Northwind Ridge. This map and the following were created with the software Ocean Data View (Schlitzer, 2015), using the IBCAO bathymetry (version 3; Jakobsson *et al.*, 2012).**

where z is depth, increasing downward. The sinking flux is the last term in equation (2). Under assumptions of steady state and constant S, $k_a$ and $k_d$, equations (1) and (2) predict a linear increase of $^{230}$Th and $^{231}$Pa concentrations with depth, with a slope inversely proportional to the sinking rate of particles:

$$[\mathbf{R}]_d = \frac{\alpha}{k_a} + \frac{k_d \cdot \alpha}{k_a \cdot \mathbf{S}} \cdot z \qquad (3)$$

$$[\mathbf{R}]_p = \frac{\alpha}{\mathbf{S}} \cdot z \qquad (4)$$

Based on observations of a strong positive correlation between $k_a$ and the concentration of suspended matter (Bacon and Anderson, 1982), we expect to find lower concentrations and a reduced downward increase of dissolved concentrations in areas of high particle concentrations and flux. For example, this scenario is expected for the seasonally ice-free CB continental margin (Figure 2a), compared to higher concentrations and a faster downward increase in areas of low particle concentrations and flux, such as the permanently ice-covered central basin (Figure 2c).

These simplified schematics actually reproduce quite well the $^{230}$Th and $^{231}$Pa oceanic distributions of the Amerasian Basin reported from the first observations, in the 1980-1990s. Low and linear vertical profiles were observed in 1995 in the southern CB, reflecting the integrated impact of particle scavenging in the boundary currents (Edmonds *et al.*, 1998). In contrast, higher concentrations were found over the Alpha Ridge in 1983 and in the northern MB in 1991 (Bacon *et al.*, 1989; Scholten *et al.*, 1995; see Figure 1 for station locations). Such high concentrations of $^{230}$Th and $^{231}$Pa in seawater not only suggest that particle concentrations and fluxes were locally very low, but also that these waters had been isolated for a few decades from the dynamic boundary circulation, allowing for in-growth of $^{230}$Th and $^{231}$Pa. A subsequent increase in particle flux should lead to a decrease in dissolved $^{230}$Th and $^{231}$Pa concentrations. Furthermore, as the affinity of $^{230}$Th and $^{231}$Pa changes with their particle composition (e.g. Chase *et al.*, 2002), differences in the evolution of the distribution of $^{230}$Th relative to $^{231}$Pa (i.e. decoupling) could also occur depending on particle composition (e.g. biogenic silica vs. lithogenic particles).

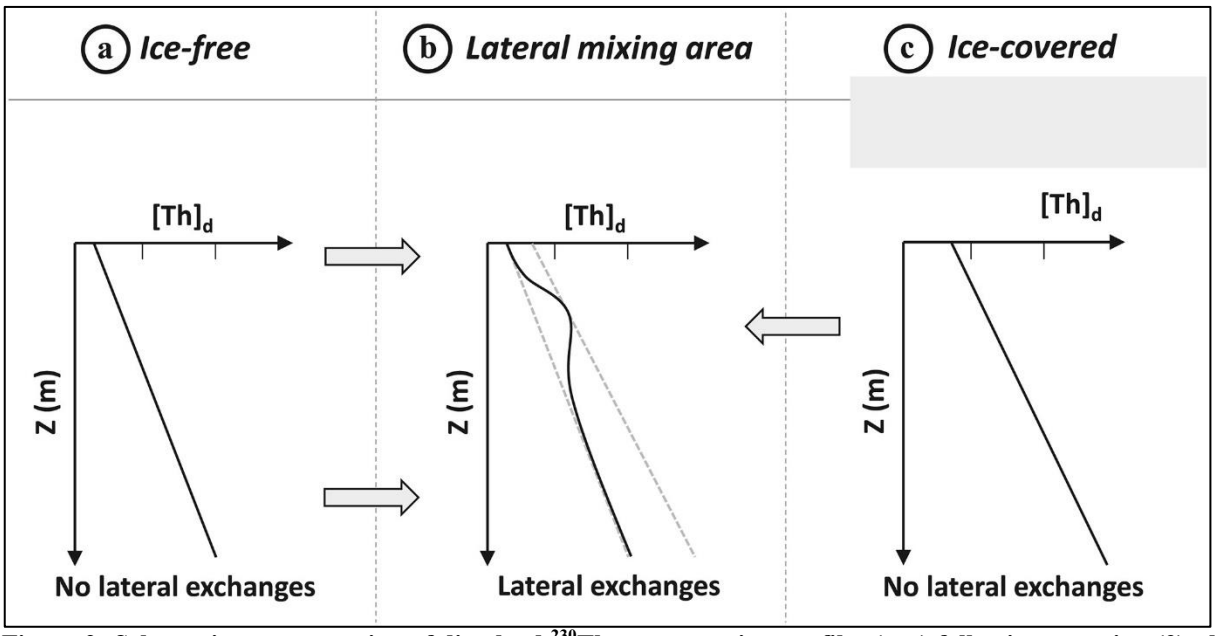


**Figure 2: Schematic representation of dissolved $^{230}$Th concentration profiles (a, c) following equation (3), that is, neglecting advection and turbulent diffusion and assuming steady state, in (a) a seasonally ice-free area, where the surface value is lower and the increase with depth is weaker due to higher scavenging and particulate sinking rates than in (c) a permanently ice-covered area. Profiles with deviations from linearity are expected in (b) areas where lateral advection of $^{230}$Th from (a) (low grey dotted line) and (c) (high grey dotted line) occurs (grey arrows).**

In addition, changes in horizontal mixing or advection rates between the basin interior and the margins could decrease the contrast in $^{230}$Th and $^{231}$Pa concentration between the two regions or even produce subsurface maxima in the concentration profiles (see Figure 2b). Note that the assumption of constant S and $k_a$ relies on a constant vertical flux of particulate $^{230}$Th, which is a

good approximation as organic matter decomposition does not release significant amounts of $^{230}$Th -or $^{231}$Pa- to seawater because of the high particle reactivity of these radionuclides.

The present work aims to investigate changes in particle scavenging and circulation over the last three decades in the Amerasian Basin by comparing $^{230}$Th and $^{231}$Pa concentration profiles collected in the 1980s and 1990s to 13 water-column profiles collected between 2005 and 2015. A companion paper (Yu *et al.*, submitted) further exploits these data by introducing $^{230}$Th scavenging into a three-dimensional model hindcasting Arctic circulation and particle scavenging between 2002 and 2015.

We also report three dissolved profiles of neodymium isotopic compositions from 2015 that are compared to early-2000s data (Porcelli *et al.*, 2009), and which support the interpretation of the $^{230}$Th-$^{231}$Pa profiles. Neodymium (Nd) is a rare earth element (REE) that is supplied to the ocean via continental weathering. As the neodymium isotopic composition (expressed as $\varepsilon_{Nd}$) of rocks varies with age and lithology, the $\varepsilon_{Nd}$ of outcropping rocks is heterogeneous (Jeandel *et al.*, 2007). Thus, the $\varepsilon_{Nd}$ signal of the water masses is set by the continental Nd they receive along their circulation pathways (through direct input or through mixing with a water mass of different $\varepsilon_{Nd}$; e.g. Frank, 2002; Goldstein and Hemming, 2003; Grenier *et al.*, 2013; Piepgras *et al.*, 1979; Tachikawa *et al.*, 2003). Pacific waters in the Bering Strait have $\varepsilon_{Nd}$ values of ~-5 (Dahlqvist *et al.*, 2007), while Atlantic waters have values of ~-11 (Andersson *et al.*, 2008). These distinct signatures allowed Porcelli *et al.* (2009) to trace distinct water masses and follow the evolution of their $\varepsilon_{Nd}$ during their transit in the Arctic in the early-2000s.

## 2. Water Masses of the Amerasian Basin

The water column in the Amerasian Basin can be separated vertically into three layers, recognizable in Figures 3, 4 and S1: i) the low-salinity Polar Surface Water (PSW) including the Polar Mixed Layer (PML) and the halocline; ii) the warm Atlantic water, identified as a subsurface layer with a temperature maximum bounded above and below by the 0°C isotherm, and the underlying intermediate water; iii) colder and more saline deep and bottom waters. The θ-S profiles presented in Figure S1 are subdivided following these 3 layers.

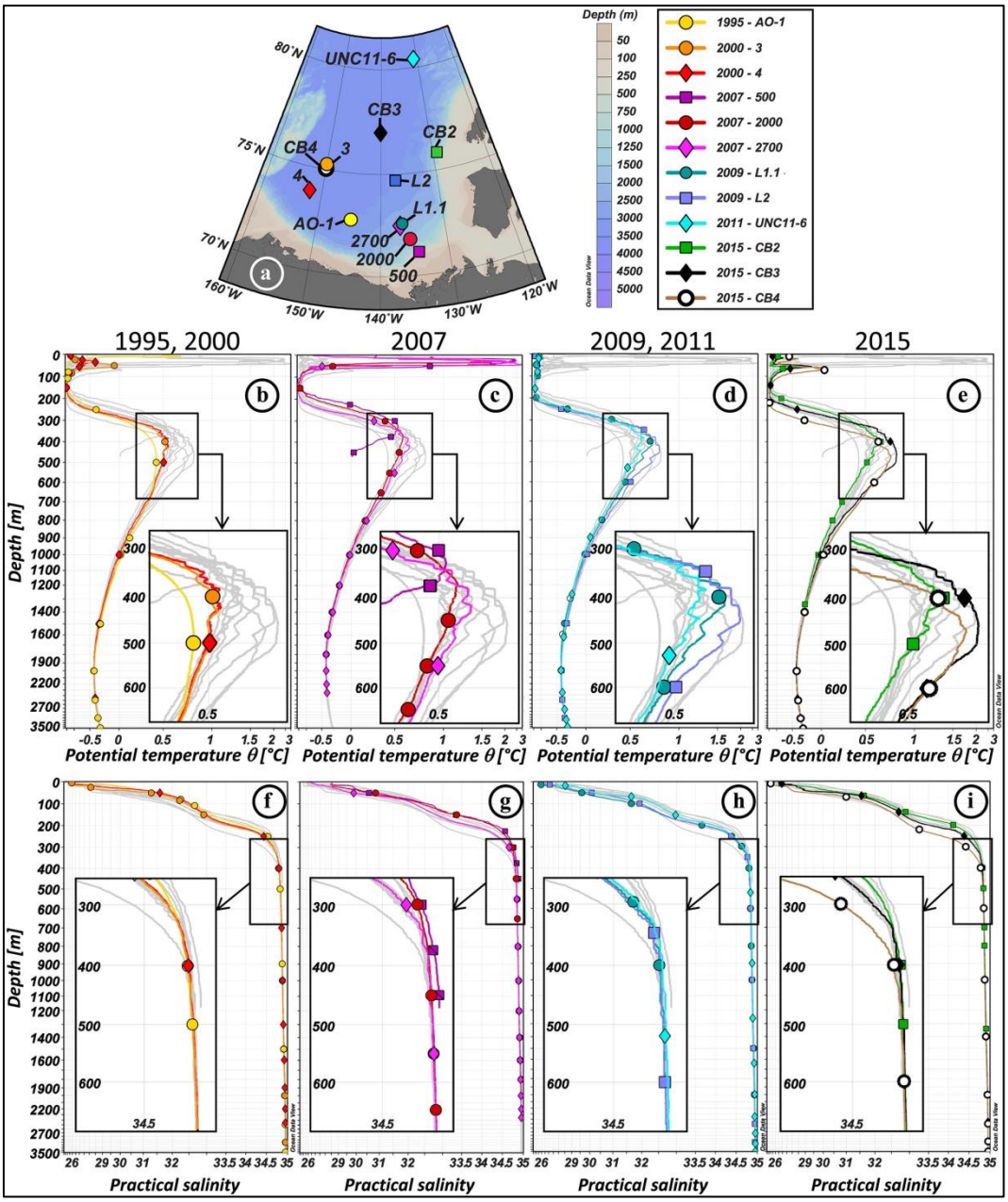


**Figure 3: Vertical profiles of hydrological parameters of the Canada Basin stations. (a) Location of the stations. Vertical profiles of potential temperature (°C; b–e) and practical salinity (f–i) of the 12 stations, in grey, superimposed by the colored profiles of stations sampled in 1995 and 2000 (b, f), 2007 (c, g), 2009 and 2011 (d, h), and 2015 (e, i). Hydrological references: Carmack *et al.* (1996) (1995: AO-1); Porcelli *et al.* (2009) (2000: 3, 4); McLaughlin *et al.* (2009) (2007: 500, 2000, 2700); Rail *et al.* (2011) (2009: L1.1, L2); Mosher (2012) (2011: UNC11-6); Amundsen Science Data Collection (2016) (2015: CB2, CB3, CB4). Symbols on the colored profiles represent the samples collected at each station. For the sake of clarity, horizontal and vertical axes are stretched in order to better visualize the properties of the Atlantic layer, and a zoom on this layer, defined by the black square, is shown in an inset for each plot.**

The PML is the homogenized surface layer undergoing brine rejection and haline convection in winter and receiving fresh water from sea ice melt in summer. The underlying halocline water originates from the Pacific Ocean and includes the fresher and warmer Alaskan Coastal Water (ACW) overlying the saltier and colder Bering Sea Water (BSW; Coachman and Barnes, 1961; Steele *et al.*, 2004; Timmermans *et al.*, 2014). The ACW is characterized by a subsurface temperature maximum in the salinity range [29-32.2], usually found between 50 and 100 m depth. The BSW has a summer and winter component. The Bering Sea Winter Water (BSWW) is more easily distinguished than the Bering Sea Summer Water (BSSW) and more widely spread. The denser BSWW is identified by a temperature minimum (~ -1.6 °C) at S ~ 33 while the BSSW can be found in the salinity range [32.2-33] and is characterized, like the overlying ACW, by a temperature maximum.

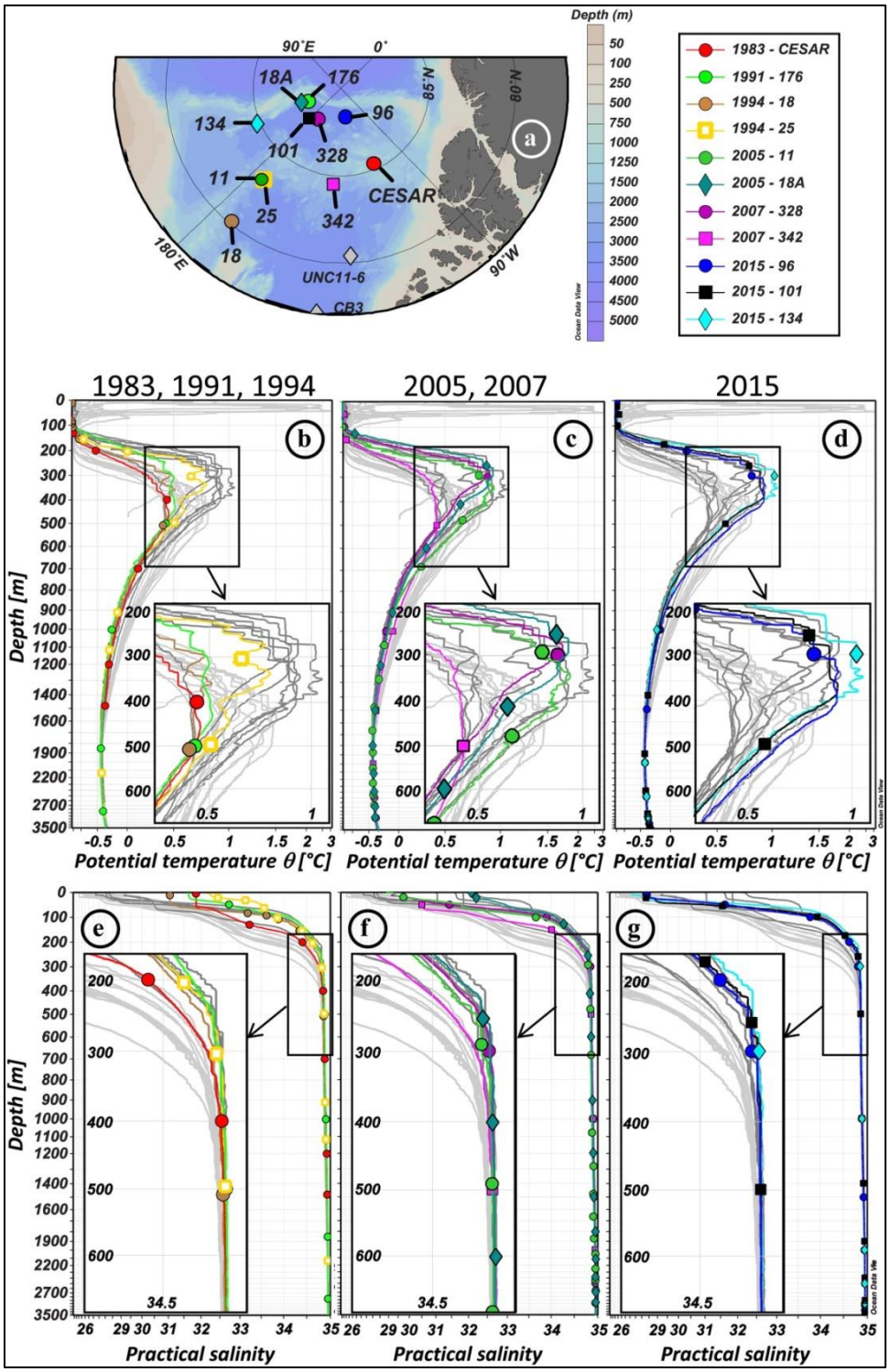


**Figure 4: Vertical profiles of hydrological parameters of the Makarov Basin and ridges stations. (a) Location of the stations. Vertical profiles of potential temperature (°C; b–d) and practical salinity (e–g) of the 11 stations, in dark grey, superimposed by the colored profiles of stations sampled in 1983, 1991, and 1994 (b, e), 2005 and 2007 (c, f), and 2015 (d, g). Canada Basin light grey profiles are also reported in the background, for comparison. Hydrological references: Jones and Anderson (1986) (1983: CESAR); Anderson *et al.* (1994) (1991: 176); Swift *et al.* (1997) (1994: 18, 25); Darby *et al.* (2006) (2005: 11, 18A); Schauer (2008) (2007: 328, 342); Rabe *et al.* (2016) (2015: 96, 101, 134). Symbols on the colored profiles represent the samples collected at each station. For the sake of clarity, horizontal and vertical axes are stretched in order to better visualize the properties of the Atlantic layer, and a zoom on this layer, defined by the black square, is shown in an inset for each plot.**

The halocline extends to gradually shallower depths from the CB (200-250 m), to the Alpha Ridge (150-200 m), and to the MB (100-150 m). Below lies the Atlantic layer, marked by a prominent temperature maximum. This water is mostly derived from the Barents Sea branch (Rudels *et al.*, 2013) and found between 250 and 1000 m depth in the CB, between 250 and 800/900 m depth on the Alpha Ridge and between 200 and 800 m depth in the MB. Deeper, bounded by the 0 °C temperature above and by the deep temperature minimum at about 2400 m depth is the upper Polar Deep Water (uPDW; Rudels, 2009). Finally, below the 2400 m temperature minimum, which marks the depth of lateral exchange between the Canada and Makarov Basins (E. Carmack *et al.*, 2012), are the Canada Basin Deep Water (CBDW) and the Makarov Basin Deep Water (MBDW). The higher salinity of the CBDW and the MBDW compared to the Eurasian Basin bottom water could be explained by their relative isolation and the formation of dense water by brine rejection on the shelves (Aagaard *et al.*, 1985; Jones *et al.*, 1995; Mauritzen *et al.*, 2013). CBDW temperature is also slightly higher, suggesting geothermal heating and mixing (E. Carmack *et al.*, 2012), while MBDW gradually cools toward the bottom. There may be some exchange of deep water with the Eurasian Basin where the Lomonosov Ridge deepens to 1800 m (close to the North Pole, around 175°E; Cochran *et al.*, 2006), but the flow appears to be mostly from the MB to the Amundsen Basin (Rudels, 2009). While surface and halocline water circulation is anticyclonic in the CB and driven by the Transpolar Drift above the Lomonosov Ridge, the Atlantic layer below mainly follows topographically-steered cyclonic gyres (circulation schematics in Figure 1). The circulation of bottom water remains virtually unknown. The different water masses described here have been sampled at most of the stations reported in this study (samples are identified by markers in Figures 3, 4 and S1).

## 3. Methods

New $^{230}$Th, $^{231}$Pa and $\varepsilon_{Nd}$ data presented in this study (Tables 1 and 2) are from ~15 L seawater samples collected during seven different cruises (Figure 1). Four cruises were conducted in the CB: 1) in September 2007, on the CCGS Sir Wilfrid Laurier; 2) in September 2009, on the CCGS Amundsen (GEOTRACES section IPY14); 3) in September 2011, on the CCGS Louis St-Laurent; 4) in September 2015, on the CCGS Amundsen (GEOTRACES section GN03). The 5$^{th}$ cruise, a Trans Arctic Expedition (HOTRAX), occurred in Aug-Sep 2005, aboard the USCG Healy. The 6$^{th}$ and 7$^{th}$ cruises were mostly conducted in the Eurasian Basin, on-board the R/V Polarstern, in 2007 (GEOTRACES section IPY11) and 2015 (GEOTRACES section GN04; Schauer, 2016), respectively. In our study, we only report five stations from these last two cruises: two collected in the MB and Alpha Ridge area in September 2007, and three in the MB

in September 2015. Eurasian Basin $^{230}$Th profiles from these two cruises are reported in Valk *et al.* (2018).

### 3.1. $^{230}$Th and $^{231}$Pa Concentrations

$^{230}$Th and $^{231}$Pa concentrations were determined by isotopic dilution, after element separation and purification by chromatography. The analytical methodology followed for the samples collected in 2007 and 2015 in the MB and Alpha Ridge area is detailed in Valk *et al.* (2018). For the samples collected in 2005 in the MB and Mendeleev Ridge area and in 2007, 2009, 2011 and 2015 in the CB, $^{230}$Th and $^{231}$Pa were determined following the method described by Choi *et al.* (2001). For the 2015 samples the method was slightly modified as follows: 1) environmental grade acids were used to clean the sampling material and for the chemistry, to limit contamination for the determination of $\varepsilon_{Nd}$ on the same samples. 2) The filtration was done through a single-use 0.45 µm pore size filter cartridge (AquaPrep®; the 2011 samples remained unfiltered). 3) Before analysis, the purified fractions of Th and Pa were both treated with 4 mL of concentrated perchloric acid to eliminate any organic component, then treated with concentrated $HNO_3$ to remove the perchloric acid. The CB samples were measured at the University of British Columbia (Vancouver, Canada) on an inductively coupled plasma mass spectrometer (Element2, Thermo Scientific) coupled to a desolvating nebulizer system (Aridus II™, Teledyne CETAC) to increase the sensitivity. $^{230}$Th procedural blank contribution, mainly coming from the $^{229}$Th spike, was on average 14% for the 2009-2011 samples (10.21 ± 0.87 fg) and 2% for the 2015 samples (0.99 ± 0.09 fg). The Th recovery of the two chromatographic columns was estimated for the 2015 samples and found to be 77% in average. Isotope fractionation during ICPMS analysis was estimated at 0.6% per amu.

**Table 1: Dissolved $^{230}$Th and $^{231}$Pa concentrations (in fg kg$^{-1}$), and neodymium isotopic compositions (expressed as $\varepsilon_{Nd}$, unitless) of the Canada Basin stations collected in 2015, with their associated standard errors and hydrological properties (potential temperature, in °C; salinity, unitless; potential density, in kg m$^{-3}$).**

| Depth (m) | θ (°C) | Salinity | $\sigma_\theta$ (kg m$^{-3}$) | $^{230}$Th (fg kg$^{-1}$) | SE (95%) | $^{231}$Pa (fg kg$^{-1}$) | SE (95%) | $\varepsilon_{Nd}$ | SE (95%) |
|---|---|---|---|---|---|---|---|---|---|
| *Canada Basin* | | | | | | | | | |
| *CB2 (September 9, 2015; -129.234°E, 75.806°N; depth: 1350 m)* | | | | | | | | | |
| 10 | -0.677 | 27.058 | 21.716 | 1.89 | 0.07 | 0.05 | 0.07 | -8 | 0.1 |
| 65 | -0.773 | 31.661 | 25.441 | 2.03 | 0.07 | 0.29 | 0.19 | -5.8 | 0.1 |
| 140 | -1.399 | 32.895 | 26.459 | 1.33 | 0.04 | 0.17 | 0.07 | -5.8 | 0.1 |
| 200 | -0.819 | 34.112 | 27.426 | 2.05 | 0.2 | 0.17 | 0.09 | -8.1 | 0.1 |
| 400 | 0.598 | 34.821 | 27.926 | 4.2 | 0.11 | 0.54 | 0.05 | -9.9 | 0.2 |
| 400 | 0.598 | 34.821 | 27.926 | - | - | 0.54 | 0.06 | -10.3 | 0.2 |
| 500 | 0.465 | 34.842 | 27.951 | 3.54 | 0.1 | 0.9 | 0.09 | -9.7 | 0.2 |
| 700 | 0.205 | 34.863 | 27.983 | 2.98 | 0.1 | 0.54 | 0.07 | -9.3 | 0.2 |
| 800 | 0.1 | 34.87 | 27.994 | 2.97 | 0.09 | 0.58 | 0.07 | -9.3 | 0.2 |
| 1000 | -0.083 | 34.882 | 28.013 | 3.22 | 0.09 | 0.46 | 0.07 | -9.4 | 0.1 |
| 1338 | - | - | - | 1.98 | 0.07 | 0.44 | 0.07 | -9.4 | 0.1 |
| *CB3 (September 12, 2015; -140.053°E, 76.975°N; depth: 3730 m)* | | | | | | | | | |
| 10 | -1.284 | 26.539 | 21.303 | 1.75 | 0.05 | 0.18 | 0.05 | -8.2 | 0.2 |
| 65 | -0.399 | 31.443 | 25.251 | 1.97 | 0.06 | <DL | - | -7.1 | 0.1 |
| 140 | -1.375 | 32.679 | 26.283 | 1.15 | 0.06 | <DL | - | -6.3 | 0.1 |
| 250 | -0.455 | 34.348 | 27.602 | 2.92 | 0.07 | - | - | -8.4 | 0.1 |
| 400 | 0.693 | 34.795 | 27.899 | 5.66 | 0.11 | 0.66 | 0.04 | -10.4 | 0.1 |
| 600 | 0.539 | 34.848 | 27.951 | 6.57 | 0.12 | 0.68 | 0.06 | -9.9 | 0.3 |
| 1001 | -0.05 | 34.874 | 28.005 | 8.66 | 0.13 | 0.96 | 0.07 | -10.3 | 0.2 |
| 1400 | -0.318 | 34.908 | 28.049 | 11.15 | 0.24 | 1.34 | 0.11 | -10.1 | 0.2 |
| 1400 | -0.318 | 34.908 | 28.049 | 10.93 | 0.37 | 1.42 | 0.09 | -10.5 | 0.3 |
| 2001 | -0.509 | 34.942 | 28.085 | 10.46 | 0.23 | 2.11 | 0.11 | -9.9 | 0.2 |
| 2459 | -0.519 | 34.953 | 28.094 | 12.31 | 0.23 | 3.11 | 0.12 | -9.8 | 0.2 |
| 3000 | -0.508 | 34.957 | 28.097 | 11.92 | 0.26 | 2.33 | 0.16 | -9.7 | 0.1 |
| 3496 | -0.507 | 34.957 | 28.097 | 12.65 | 0.32 | 2.36 | 0.11 | -9.9 | 0.2 |
| *CB4 (September 15, 2015; -150.001°E, 75.002 °N; depth: 3830 m)* | | | | | | | | | |
| 10 | -0.479 | 25.27 | 20.268 | 2.22 | 0.05 | 0.29 | 0.04 | -8.2 | 0.1 |
| 71 | 0.047 | 31.014 | 24.887 | 2.39 | 0.07 | 0.05 | 0.06 | -9 | 0.2 |
| 220 | -1.476 | 33.248 | 26.748 | 1.81 | 0.06 | <DL | - | -6.3 | 0.1 |
| 300 | -0.265 | 34.424 | 27.654 | 2.56 | 0.09 | 0.06 | 0.06 | -8.1 | 0.1 |
| 400 | 0.609 | 34.775 | 27.889 | 4.3 | 0.11 | 0.82 | 0.06 | -10.4 | 0.3 |
| 600 | 0.564 | 34.843 | 27.945 | 2.34 | 0.08 | 0.8 | 0.06 | -8.9 | 0.2 |
| 1000 | -0.025 | 34.87 | 28 | 3.49 | 0.09 | 0.98 | 0.08 | -10.1 | 0.1 |
| 1400 | -0.32 | 34.902 | 28.044 | 6.32 | 0.15 | 1.27 | 0.05 | -10.3 | 0.1 |
| 1400 | -0.32 | 34.902 | 28.044 | 6.56 | 0.21 | 1.34 | 0.09 | -10.4 | 0.2 |
| 2000 | -0.504 | 34.94 | 28.084 | 10.21 | 0.22 | 1.87 | 0.06 | -9.5 | 0.1 |
| 3000 | -0.507 | 34.957 | 28.097 | 11.57 | 0.24 | 3.13 | 0.11 | -9.6 | 0.1 |
| 3500 | -0.507 | 34.957 | 28.097 | 11.62 | 0.26 | 2.29 | 0.09 | -10.2 | 0.5 |

As the U/Th chromatographic separation of the 2009 samples was done 8 years after the sample collection, measured $^{230}Th_d$ concentrations were corrected from a substantial $^{230}Th$ ingrowth. $^{231}Pa$ procedural blank contribution, mainly coming from the $^{233}Pa$ spike, was on average 56% for the 2009-2011 samples (46.5 ± 1.9 fg) and 70% for the 2015 samples (26.7 ± 1.6 fg). This large contribution resulted from over-spiking but was well monitored by the set of chemical blanks and accurately corrected. The Pa recovery of the two chromatographic columns was estimated for the 2015 samples and found to be 80% in average.

### 3.2. Nd Isotopic Composition

The REE measurements came from the same initial natural samples used for Pa and Th. They were eluted with the Th fraction during the first chromatographic column and separated from Th on the second column in the 24 mL of 8 N $HNO_3$. This fraction was dried and dissolved in 1.5 mL of HCl 1 N and was processed as described in Grenier *et al.* (2013). After the chemical extraction and purification of Nd, samples were dissolved in 2 µL of 2 N HCl, loaded on a rhenium filament and analysed by thermal ionization mass spectrometry (TIMS) in static mode (Thermo Fisher Scientific mass spectrometer Triton, *Observatoire Midi-Pyrénées, Toulouse*). 13 analyses of Rennes standard and 7 of La Jolla standard were performed to monitor instrumental drift and gave 0.511955 ± 0.000005 and 0.511854 ± 0.000009, respectively. All measurements were corrected for a machine bias of -0.000005, based on the accepted value being 0.511961 ± 0.000013 for Rennes (Chauvel and Blichert-Toft, 2001) and 0.511858 ± 0.000007 for La Jolla (Lugmair *et al.*, 1983).

**Table 2: Dissolved (or total, in italic) $^{230}$Th and $^{231}$Pa concentrations (in fg kg$^{-1}$) of the Mendeleev Ridge, Makarov Basin, and Alpha Ridge stations, collected in 2005, 2007 and 2015, with their associated standard errors and hydrological properties (potential temperature, in °C; salinity, unitless; potential density, in kg m$^{-3}$).**

| Depth (m) | θ (°C) | Salinity | $\sigma_0$ (kg m$^{-3}$) | $^{230}$Th (fg kg$^{-1}$) | SE (0.95) | $^{231}$Pa (fg kg$^{-1}$) | SE (0.95) |
|---|---|---|---|---|---|---|---|
| *500 (October 1, 2007; -134.364°E, 71.077°N; depth: 500 m)* | | | | | | | |
| 50 | 0.798 | 30.55 | 24.484 | 0.71 | 0.08 | 0.33 | 0.07 |
| 150 | -1.377 | 33.345 | 26.832 | 0.87 | 0.09 | 0.11 | 0.09 |
| 225 | -0.03 | 34.559 | 27.756 | 0.79 | 0.12 | 0.05 | 0.07 |
| 300 | 0.488 | 34.766 | 27.893 | 0.44 | 0.06 | 0.2 | 0.05 |
| 375 | 0.445 | 34.841 | 27.957 | 0.63 | 0.11 | 0.2 | 0.04 |
| 375 | 0.444 | 34.841 | 27.957 | 0.74 | 0.08 | 0.2 | 0.07 |
| 450 | 0.021 | 34.881 | 28.013 | 1.01 | 0.1 | 0.37 | 0.1 |
| 450 | 0.02 | 34.881 | 28.013 | 1.19 | 0.11 | 0.37 | 0.07 |
| *2000 (September 30, 2007; -135.497°E, 71.732°N; depth: 2000 m)* | | | | | | | |
| 50 | -0.073 | 30.816 | 24.738 | 1.2 | 0.14 | - | - |
| 150 | -1.399 | 33.357 | 26.842 | 1.06 | 0.1 | - | - |
| 300 | 0.389 | 34.737 | 27.876 | 1.77 | 0.15 | 0.19 | 0.07 |
| 450 | 0.526 | 34.829 | 27.942 | 1.47 | 0.09 | 0.1 | 0.07 |
| 550 | 0.424 | 34.847 | 27.962 | 1.73 | 0.12 | 0.41 | 0.07 |
| 650 | 0.327 | 34.859 | 27.977 | 1.83 | 0.12 | 0.31 | 0.07 |
| 800 | 0.141 | 34.871 | 27.998 | 1.95 | 0.13 | 0.35 | 0.06 |
| 1000 | -0.063 | 34.886 | 28.02 | 2.49 | 0.13 | 0.35 | 0.11 |
| 1200 | -0.221 | 34.899 | 28.04 | 3.27 | 0.2 | 0.46 | 0.08 |
| 1400 | -0.356 | 34.914 | 28.059 | 2.32 | 0.16 | 0.45 | 0.07 |
| 1600 | -0.448 | 34.928 | 28.075 | 2.47 | 0.17 | 1.19 | 0.12 |
| 1800 | -0.491 | 34.942 | 28.089 | 2.31 | 0.17 | 1.17 | 0.09 |
| *2700 (September 29, 2007; -136.936°E, 72.415°N; depth:2700m)* | | | | | | | |
| 50 | -0.365 | 29.831 | 23.954 | 2.01 | 0.31 | 0.13 | 0.18 |
| 300 | 0.269 | 34.661 | 27.822 | 4.44 | 0.22 | 0.19 | 0.17 |
| 550 | 0.473 | 34.845 | 27.958 | 6.34 | 0.39 | 0.34 | 0.16 |
| 800 | 0.161 | 34.87 | 27.996 | 6.32 | 0.34 | 0.5 | 0.11 |
| 1000 | -0.056 | 34.885 | 28.019 | 5.65 | 0.29 | 1.07 | 0.17 |
| 1200 | -0.218 | 34.898 | 28.038 | 4.98 | 0.26 | 0.61 | 0.13 |
| 1400 | -0.343 | 34.911 | 28.056 | 3.81 | 0.21 | 1.21 | 0.17 |
| 1600 | -0.438 | 34.924 | 28.072 | 2.82 | 0.23 | 0.89 | 0.12 |
| 1800 | -0.489 | 34.937 | 28.084 | 3.73 | 0.14 | 2.07 | 0.23 |
| 2000 | -0.505 | 34.945 | 28.091 | 4.45 | 0.28 | 2.37 | 0.32 |
| 2200 | -0.511 | 34.95 | 28.096 | 4.3 | 0.22 | 2.43 | 0.15 |
| 2349 | -0.51 | 34.953 | 28.099 | 5.47 | 0.34 | 2.99 | 0.24 |
| *L1.1 (September 9, 2009; -136.599°E, 72.514°N; depth: 2530 m)* | | | | | | | |
| 9 | -1.14 | 26.155 | 20.991 | 0.79 | 0.24 | 0.5 | 0.08 |
| 50 | -1.321 | 29.65 | 23.825 | 1.79 | 0.29 | 1.05 | 0.08 |
| 100 | -1.214 | 31.762 | 25.535 | 1.7 | 0.24 | 0.85 | 0.11 |
| 200 | -1.294 | 33.697 | 27.107 | 2.9 | 0.22 | 0.74 | 0.09 |

| Depth (m) | θ (°C) | Salinity | $\sigma_0$ (kg m$^{-3}$) | $^{230}$Th (fg kg$^{-1}$) | SE (0.95) | $^{231}$Pa (fg kg$^{-1}$) | SE (0.95) |
|---|---|---|---|---|---|---|---|
| 250 | -0.294 | 34.39 | 27.628 | 3.53 | 0.23 | 0.7 | 0.1 |
| 300 | 0.292 | 34.639 | 27.798 | 4.7 | 0.42 | 0.87 | 0.1 |
| 400 | 0.683 | 34.802 | 27.906 | 5.44 | 0.26 | 0.88 | 0.07 |
| 600 | 0.422 | 34.841 | 27.953 | 4 | 0.26 | 1.13 | 0.09 |
| 800 | 0.16 | 34.858 | 27.981 | 4.26 | 0.38 | 1.37 | 0.16 |
| 1000 | -0.059 | 34.873 | 28.005 | 3.68 | 0.32 | 1.03 | 0.06 |
| 1500 | -0.406 | 34.907 | 28.048 | 2.95 | 1.28 | 0.79 | 0.06 |
| 2000 | -0.506 | 34.934 | 28.074 | 3.97 | 0.26 | 1.63 | 0.11 |
| *L2 (September 4, 2009; -137.383°E, 74.653°N; depth: 3600 m)* | | | | | | | |
| 10 | -1.392 | 26.576 | 21.334 | 0.21 | 0.19 | 0.32 | 0.03 |
| 50 | -1.214 | 30.1 | 24.188 | 0.78 | 0.2 | 0.04 | 0.05 |
| 100 | -1.173 | 31.974 | 25.706 | 1.06 | 0.22 | 0.54 | 0.05 |
| 250 | -0.409 | 34.375 | 27.621 | 3.47 | 0.24 | - | - |
| 350 | 0.645 | 34.768 | 27.881 | 4.59 | 0.21 | 0.8 | 0.07 |
| 600 | 0.474 | 34.84 | 27.949 | 6.99 | 0.24 | 0.9 | 0.07 |
| 1000 | -0.029 | 34.873 | 28.003 | 9.98 | 0.27 | 1.25 | 0.07 |
| 1500 | -0.368 | 34.906 | 28.046 | 9.82 | 0.29 | 0.94 | 0.09 |
| 2000 | -0.511 | 34.93 | 28.071 | 8.97 | 0.44 | 3.13 | 0.13 |
| 2500 | -0.52 | 34.941 | 28.078 | 8.45 | 0.29 | 1.06 | 0.07 |
| 3000 | -0.509 | 34.945 | 28.079 | 9.66 | 0.58 | 2.54 | 0.15 |
| *UNC11-6 (September 18, 2011; -130.745°E, 80.37°N; depth: 3480 m)* | | | | | | | |
| 20* | -1.16 | 29.135 | 23.406 | 1.36 | 0.19 | - | - |
| 70* | -1.151 | 31.724 | 25.503 | 1.74 | 0.22 | - | - |
| 160* | -1.501 | 33.063 | 26.598 | 1.46 | 0.2 | 0.21 | 0.08 |
| 525* | 0.453 | 34.845 | 27.955 | 9.69 | 0.26 | 0.71 | 0.05 |
| 900* | 0.015 | 34.879 | 28.008 | 12.29 | 0.27 | 0.86 | 0.05 |
| 1265* | -0.271 | 34.905 | 28.043 | 13.1 | 0.29 | 1.14 | 0.09 |
| 1630* | -0.443 | 34.927 | 28.069 | 15.1 | 0.74 | 1.71 | 0.12 |
| 2000* | -0.512 | 34.943 | 28.086 | 15.23 | 0.29 | 2.02 | 0.07 |
| 2365* | -0.52 | 34.951 | 28.093 | 15.81 | 0.29 | 1.87 | 0.09 |
| 2735* | -0.51 | 34.955 | 28.096 | 18.02 | 0.29 | 2.48 | 0.08 |
| 3100* | -0.508 | 34.956 | 28.096 | 17.59 | 0.39 | 2.05 | 0.12 |
| 3470* | -0.508 | 34.956 | 28.096 | 17.78 | 0.46 | 2 | 0.13 |
| *Mendeleev Ridge* | | | | | | | |
| *11 (August 25, 2005; -174.92°E, 83.11°N; depth: 2700 m)* | | | | | | | |
| 20* | -1.551 | 29.845 | 23.987 | 1.43 | 0.31 | - | - |
| 99* | -1.679 | 33.695 | 27.115 | 2.64 | 0.44 | - | - |
| 290* | 0.805 | 34.791 | 27.891 | 5.57 | 0.52 | - | - |
| 485* | 0.634 | 34.852 | 27.95 | 8.37 | 0.56 | - | - |
| 683* | 0.223 | 34.859 | 27.98 | 7.39 | 0.45 | - | - |
| 1078* | -0.24 | 34.883 | 28.024 | 9.42 | 0.72 | - | - |
| 1273* | -0.367 | 34.897 | 28.042 | 9.71 | 0.36 | - | - |
| 1470* | -0.429 | 34.914 | 28.059 | 13.06 | 0.83 | - | - |
| 1667* | -0.499 | 34.925 | 28.071 | 12.01 | 0.53 | - | - |

| Depth (m) | θ (°C) | Salinity | $\sigma_0$ (kg $m^{-3}$) | $^{230}$Th (fg $kg^{-1}$) | SE (0.95) | $^{231}$Pa (fg $kg^{-1}$) | SE (0.95) |
|---|---|---|---|---|---|---|---|
| 1862* | -0.498 | 34.939 | 28.083 | 14.44 | 0.79 | - | - |
| 2059* | -0.505 | 34.946 | 28.088 | 15.68 | 0.54 | - | - |
| 2254* | -0.506 | 34.949 | 28.091 | 17.47 | 0.75 | - | - |
| 2439* | -0.506 | 34.951 | 28.093 | 18.14 | 0.92 | - | - |
| 2646* | -0.505 | 34.954 | 28.095 | 23.42 | 0.94 | - | - |
| *Alpha Ridge* | | | | | | | |
| *342 (September 7, 2007; -138.413°E, 84.500°N; depth: 2275 m)* | | | | | | | |
| 50* | -1.581 | 30.5079 | 24.526 | 1.57 | 0.03 | 0.05 | 0.01 |
| 150* | -1.376 | 34.0082 | 27.362 | 5.14 | 0.06 | 0.08 | 0.01 |
| 500* | 0.396 | 34.8605 | 27.971 | 15.11 | 0.14 | 1.23 | 0.04 |
| 1000* | -0.126 | 34.9013 | 28.033 | 14.34 | 0.13 | 1.39 | 0.04 |
| 1001* | -0.127 | 34.9013 | 28.033 | 14.48 | 0.13 | 1.47 | 0.04 |
| 1500* | -0.416 | 34.9282 | 28.07 | 14.75 | 0.13 | 1.73 | 0.06 |
| 2200* | -0.503 | 34.952 | 28.093 | 11.7 | 0.11 | 2.42 | 0.05 |
| *Makarov Basin* | | | | | | | |
| *18A (September 6, 2005; 156.216°E, 87.628°N; depth: 4000 m)* | | | | | | | |
| 2* | -1.737 | 32.069 | 25.796 | 1.6 | 0.31 | - | - |
| 21* | -1.741 | 32.137 | 25.852 | 1.9 | 0.43 | - | - |
| 126* | -0.858 | 34.263 | 27.551 | 5.24 | 0.36 | - | - |
| 255* | 0.894 | 34.81 | 27.9 | 12.86 | 0.73 | - | - |
| 404* | 0.66 | 34.855 | 27.951 | 9.64 | 0.55 | - | - |
| 603* | 0.29 | 34.868 | 27.984 | 10.59 | 0.42 | - | - |
| 902* | -0.124 | 34.884 | 28.02 | 12.72 | 0.68 | - | - |
| 1201* | -0.324 | 34.907 | 28.048 | 16.84 | 0.7 | - | - |
| 1501* | -0.438 | 34.928 | 28.07 | 20.78 | 0.9 | - | - |
| 1802* | -0.489 | 34.942 | 28.084 | 24.3 | 0.97 | - | - |
| 2105* | -0.509 | 34.948 | 28.09 | 27.72 | 1.25 | - | - |
| 2401* | -0.516 | 34.951 | 28.093 | 27.09 | 0.9 | - | - |
| 2705* | -0.523 | 34.952 | 28.094 | 27.61 | 0.9 | - | - |
| 3008* | -0.53 | 34.952 | 28.094 | 30.67 | 0.9 | - | - |
| 3649* | -0.534 | 34.952 | 28.095 | 34.23 | 1 | - | - |
| 3948* | -0.534 | 34.952 | 28.095 | 34.46 | 1.14 | - | - |
| *328 (September 2, 2007; -170.407°E, 87.827°N; depth: 3990 m)* | | | | | | | |
| 50 | -1.628 | 31.445 | 25.288 | 2.5 | 0.06 | - | - |
| 100* | -1.545 | 33.899 | 27.279 | 3.36 | 0.06 | 0.2 | 0.01 |
| 300 | 0.865 | 34.841 | 27.927 | 6.85 | 0.07 | 0.78 | 0.02 |
| 1000 | -0.218 | 34.896 | 28.034 | 12.4 | 0.12 | 1.31 | 0.02 |
| 1001 | -0.218 | 34.896 | 28.034 | 12.46 | 0.12 | 1.36 | 0.02 |
| 2500* | -0.523 | 34.955 | 28.096 | 29.08 | 0.2 | 3.62 | 0.04 |
| 3000 | -0.534 | 34.955 | 28.097 | 23.06 | 0.17 | 3.48 | 0.04 |
| 3750 | -0.538 | 34.955 | 28.097 | 19.46 | 0.16 | 3.34 | 0.04 |
| *96 (September 11, 2015; -125.094°E, 88.3598°N; depth: 3612 m)* | | | | | | | |
| 10 | -1.505 | 28.344 | 22.769 | 2.6 | 0.14 | 0.24 | 0.13 |
| 50 | -1.62 | 31.632 | 25.439 | 2.14 | 0.15 | 0.11 | 0.13 |

| Depth (m) | θ (°C) | Salinity | $\sigma_0$ (kg m$^{-3}$) | $^{230}$Th (fg kg$^{-1}$) | SE (0.95) | $^{231}$Pa (fg kg$^{-1}$) | SE (0.95) |
|---|---|---|---|---|---|---|---|
| 100 | -1.453 | 33.776 | 27.177 | 2.54 | 0.15 | 0.13 | 0.13 |
| 200 | 0.189 | 34.623 | 27.792 | 4.61 | 0.18 | 0.35 | 0.13 |
| 300 | 0.801 | 34.812 | 27.907 | 6.91 | 0.17 | 0.25 | 0.13 |
| 1000 | -0.189 | 34.887 | 28.025 | 14.12 | 0.32 | 0.92 | 0.13 |
| 1500 | -0.437 | 34.926 | 28.069 | 16.32 | 0.24 | 2.03 | 0.13 |

## 4. Results

### 4.1. Hydrographic Change in the Atlantic and Bottom Water

Comparing temperature profiles taken in the same area at different time clearly shows that the Atlantic water has generally warmed in the Amerasian Basin between the ~1990s and 2010s. This warming was mainly observed in the upper part of the Atlantic water, around 300 m, for the MB and Mendeleev Ridge area, with a warming of ~0.4°C between 1991 (station 176) and 2005 (station 18A) in the western MB and of ~0.1°C between 1994 (station 25) and 2005 (station 11) on the Mendeleev Ridge (Figure 4a-c). In contrast, on Alpha Ridge, the warming between 1983 (station CESAR) and 2007 (station 342) was not observed in the core of the Atlantic Water layer (~ 450 m) but mainly between 500 and 1500 m, in the lower part of the Atlantic layer and in the underlying uPDW. In the CB, the warming was centered in the upper part of the Atlantic Water (Figure 3a-e). An increase of temperature of ~0.1°C was observed between 2007 (station 2700) and 2009 (station L1.1) between 300-500 m in the southern CB (Figure 5c). In the western CB, a deeper warming of ~0.25°C was observed to a depth of 800 m between 2000 (station 3) and 2015 (station CB4). The warm Atlantic water observed over the Mendeleev Ridge in 1994, in the MB in 2005, and in the CB in 2007 and, to a greater extent, in 2009 documents the propagation of the awAW. The deep and bottom waters of the CB were fresher and lighter in 2009, compared to the other years sampled (stations L1.1 and L2; Figure 5d and Tables 1 and 2). In the MB, the deep waters were warmer, fresher and lighter in the mid-2000s than in 1991, and even slightly lighter in 2015, while the bottom MBDW were getting slightly saltier, warmer, and denser (Figure 5h and Table 2).

### 4.2. Geochemical Tracer Results

$^{230}$Th, $^{231}$Pa and $\varepsilon_{Nd}$ data from the new stations collected in the Amerasian Basin between 2005 and 2015are compared to previously published samples collected between 1983 and 2000 (Figures 6 and 7). Most of the data refer to the dissolved fraction, from filtered samples, but some represent the total fraction, from unfiltered samples. We distinguished data referring to the

total fraction by reporting them in *italic* in Table 2. To facilitate the comparison between unfiltered and filtered profiles, dissolved profiles of $^{230}$Th and $^{231}$Pa were estimated at stations where samples were unfiltered, by multiplying the measured total concentrations by 0.8 for $^{230}$Th and by 0.95 for $^{231}$Pa (from the average dissolved/total ratios of the $^{230}$Th and $^{231}$Pa water column database http://climotope.earth.ox.ac.uk/data_compilations, by considering only Arctic stations, i.e. for station latitudes greater or equal to 75 °N). These estimated dissolved profiles are represented by dashed lines in Figures 6 and 7. In order to track fractionation between $^{230}$Th and $^{231}$Pa, dissolved $^{231}$Pa/$^{230}$Th activity ratios are also shown, for each area, in Figure 8.

The geochemical tracer results reported from the different areas of the Amerasian Basin compare well with the published data (Figures 6 and 7). Concentrations of $^{230}$Th and $^{231}$Pa are consistently higher in the MB and over ridges than in the CB. Profiles from the deep central CB and MB show smaller increase with depth in the bottom layer, reflecting particulate scavenging by sediment resuspension (Anderson *et al.*, 1983; Rempfer *et al.*, 2017; Scholten *et al.*, 1995). $^{230}$Th exhibit a greater spatial heterogeneity than $^{231}$Pa, also consistent with the previously published profiles. Lower $^{230}$Th concentrations are found in the sampling sites close to the boundary circulation, while higher concentrations characterize the central basins, consistent with the gradient described in Figure 2. New 2015 $\varepsilon_{Nd}$ profiles fall well within the range defined by the profiles collected in the western CB in 2000 (Porcelli *et al.*, 2009).

## 5. Discussion

### 5.1. Spatial and Temporal Variability in $^{230}$Th and $^{231}$Pa Concentrations and Seawater εNd

Overall, none of the $^{230}$Th profiles collected after 2000 exceeds the concentration levels of the published, pre-2000s, deep profiles; they are equally high or significantly lower. This observation suggests that the intensity of particulate scavenging in the Amerasian Basin has, in the last two decades, been maintained or increased depending on the area, preventing $^{230}$Th concentrations from building up due to uranium (U) decay.

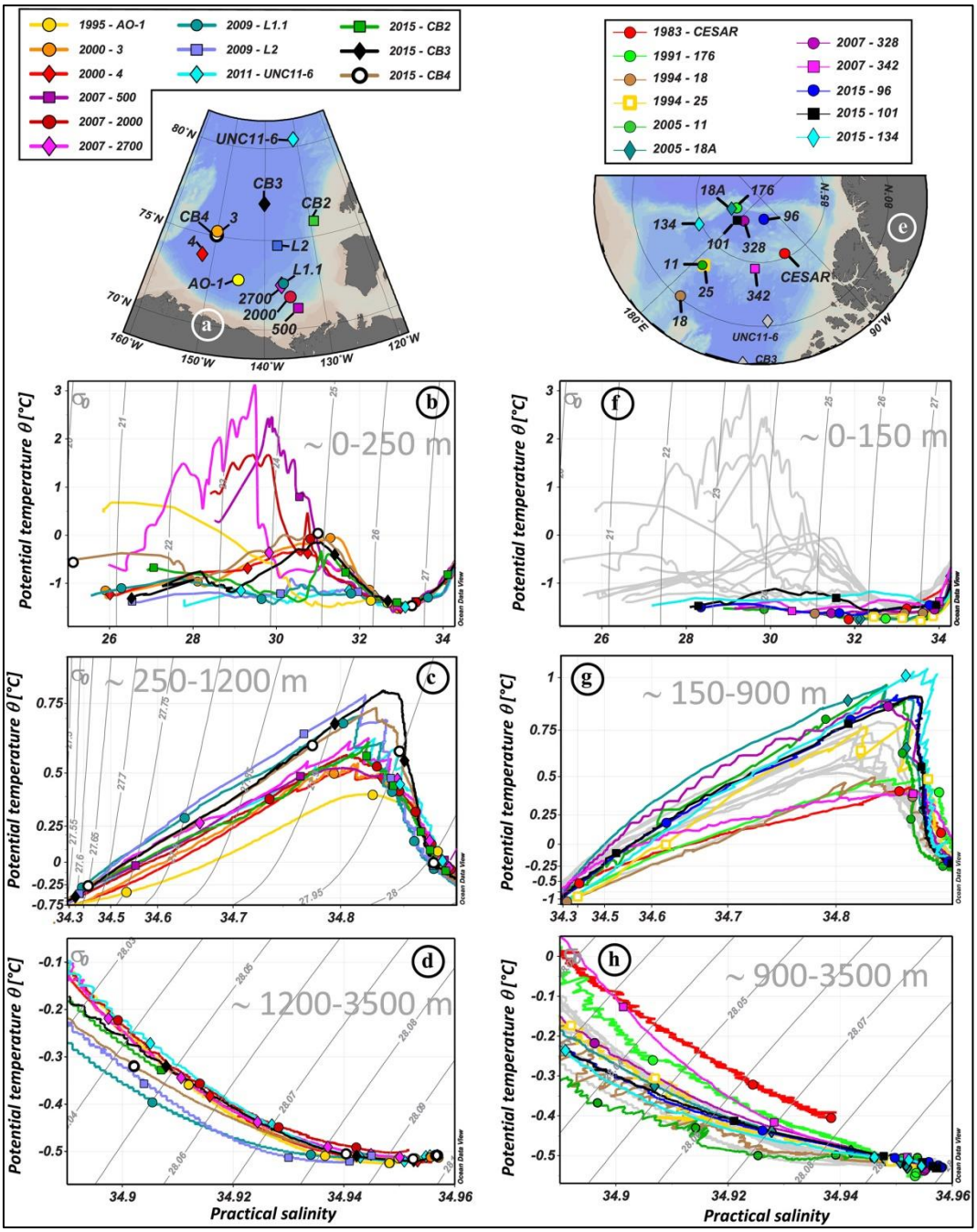


**Figure 5: Potential temperature (in °C)—practical salinity (θ-S) profiles of the Canada Basin stations (a–d) and of the Makarov Basin and Mendeleev/Alpha Ridge stations (e–h), showing the hydrological evolution of the shallow (b, f), intermediate (c, g), and deep and bottom (d, h) water masses between the ~1990s and ~2010s. Hydrological references are given in Figures 3 and 4. The symbols on the profiles represent the samples. Potential density contours σ0 are shown in solid grey. Canada Basin profiles are reported in light grey in the background of the Makarov Basin and ridges plots (e–h) to facilitate comparison.**

### 5.1.1. Variability of $^{230}$Th and $^{231}$Pa in the CB

In the interior of CB, the $^{230}$Th profiles measured at stations 3 (orange circles) sampled in 2000 (Trimble *et al.*, 2004), UNC11-6 (cyan diamonds) sampled in 2011, and CB3 (black diamonds) sampled in 2015 (Figure 6a) are very similar (Figure 6b), suggesting that the balance between $^{230}$Th removal by particle scavenging and production from U decay was maintained over that time period. By contrast, at the southern CB coastal stations 2000 (dark red circles) and 500 (purple squares) sampled in 2007, $^{230}$Th concentrations are significantly lower compared to the 1995 profile measured at AO-1 in 1995 (yellow circles; Edmonds *et al.*, 1998).

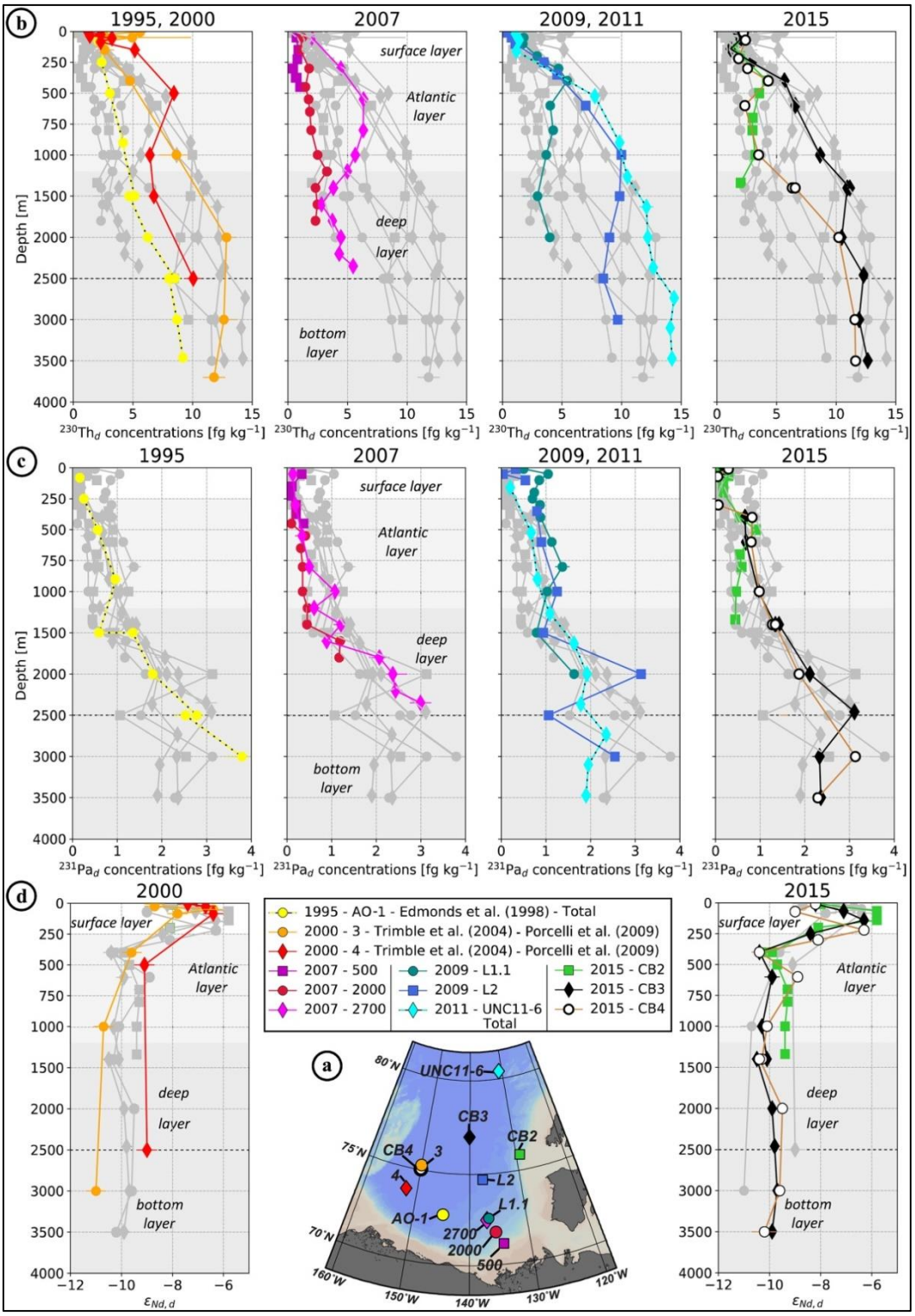


**Figure 6: Vertical distribution of (b) $^{230}Th_d$ concentrations (in fg kg$^{-1}$), (c) $^{231}Pa_d$ concentrations (in fg kg$^{-1}$) and (d) εNd of the Canada Basin stations (shown in a). The white, light grey, and dark grey backgrounds refer to the surface, intermediate Atlantic, deep uPDW and bottom CBDW layers, respectively, as subdivided in Figures 5b, 5c, and 5d. To facilitate the comparison between unfiltered and filtered profiles, dissolved profiles of $^{230}Th$ and $^{231}Pa$ were estimated at stations where samples were unfiltered, by multiplying the measured total concentrations by 0.8 for $^{230}Th$ and by 0.95 for $^{231}Pa$ (from the average dissolved/total ratios of the $^{230}Th$ and $^{231}Pa$ water column database http://climotope.earth.ox.ac.uk/data_compilations, by considering only Arctic stations, i.e., for station latitudes greater or equal to 75°N). These estimated dissolved profiles are represented by dashed lines.**

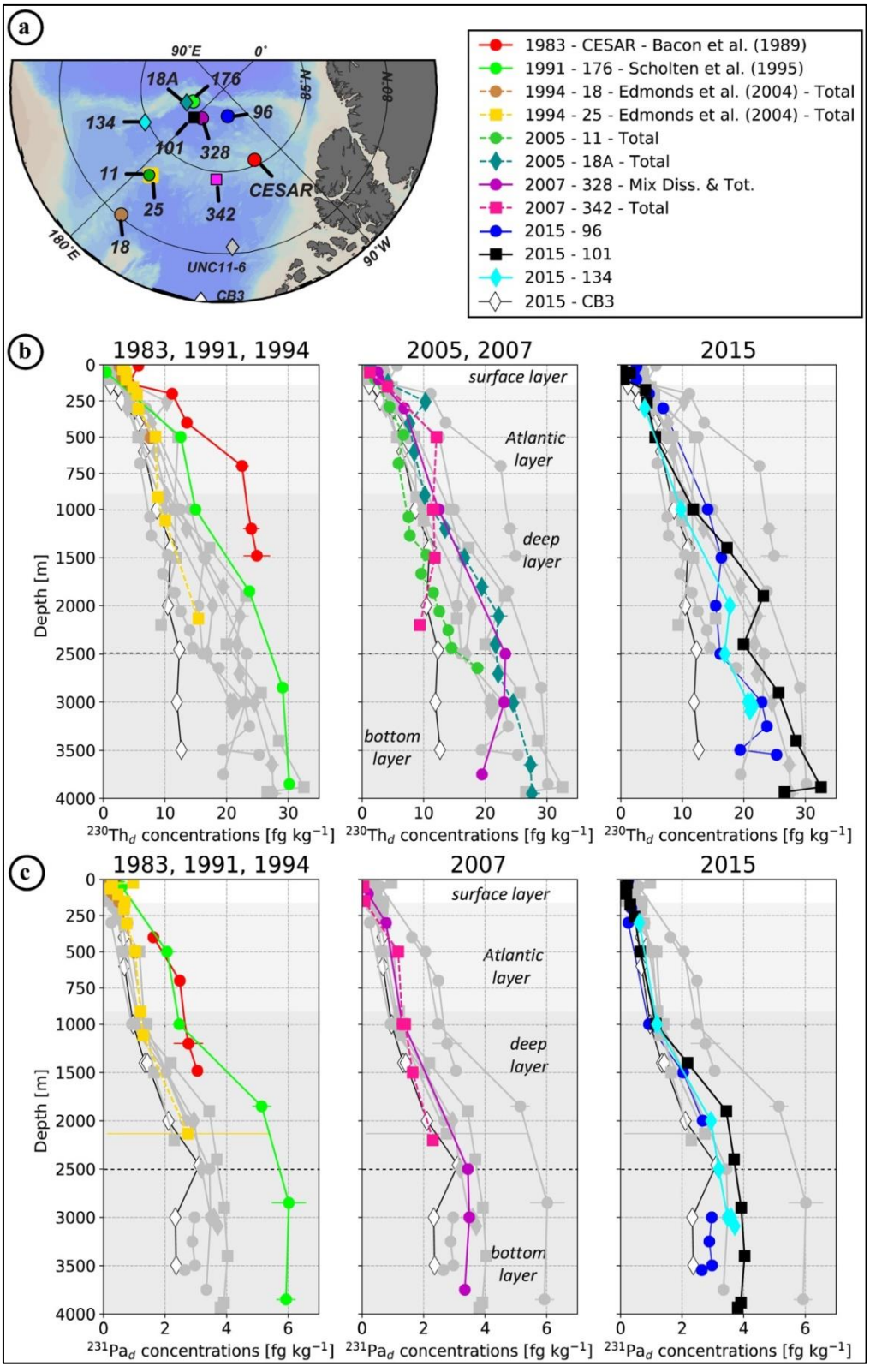


**Figure 7: Vertical distribution of (b) $^{230}Th_d$ concentrations (in fg kg$^{-1}$) and (c) $^{231}Pa_d$ concentrations (in fg kg$^{-1}$) of the Makarov Basin and Mendeleev/Alpha Ridges stations (shown in a). The white, light grey, and dark grey backgrounds refer to the shallow, intermediate, and deep and bottom layers, respectively, as subdivided in Figures 5f, 5g, and 5h. As in Figure 6, dissolved profiles of $^{230}Th$ and $^{231}Pa$ were estimated at stations where samples were unfiltered to facilitate the comparison between unfiltered and filtered profiles, by multiplying the measured total concentrations by 0.8 for $^{230}Th$ and by 0.95 for $^{231}Pa$. These estimated dissolved profiles are represented by dashed lines.**

A similar change is observed for $^{231}$Pa between station 2000 (dark red circles) and AO-1 (yellow circles; Figure 6c). These observations indicate increasing particle scavenging in the southern coastal region of the CB between 1995 and 2007. In the transition zone between the southern margin and the interior zone discussed above, station 4 (red diamonds) sampled in 2000 (Trimble *et al.*, 2004), 2700 (pink diamonds) sampled in 2007, and L2 (blue square) sampled in 2009 exhibit a pronounced $^{230}$Th maximum in the Atlantic layer, suggesting a lateral exchange signature, as schematized in Figure 2b. Particularly remarkable is the sharp difference in the profiles measured in 2007 at stations 2000 and 2700 (Figure 6b), as these two stations are only 51 nautical miles apart and were sampled within a few days (see sampling dates and locations in Table 2).

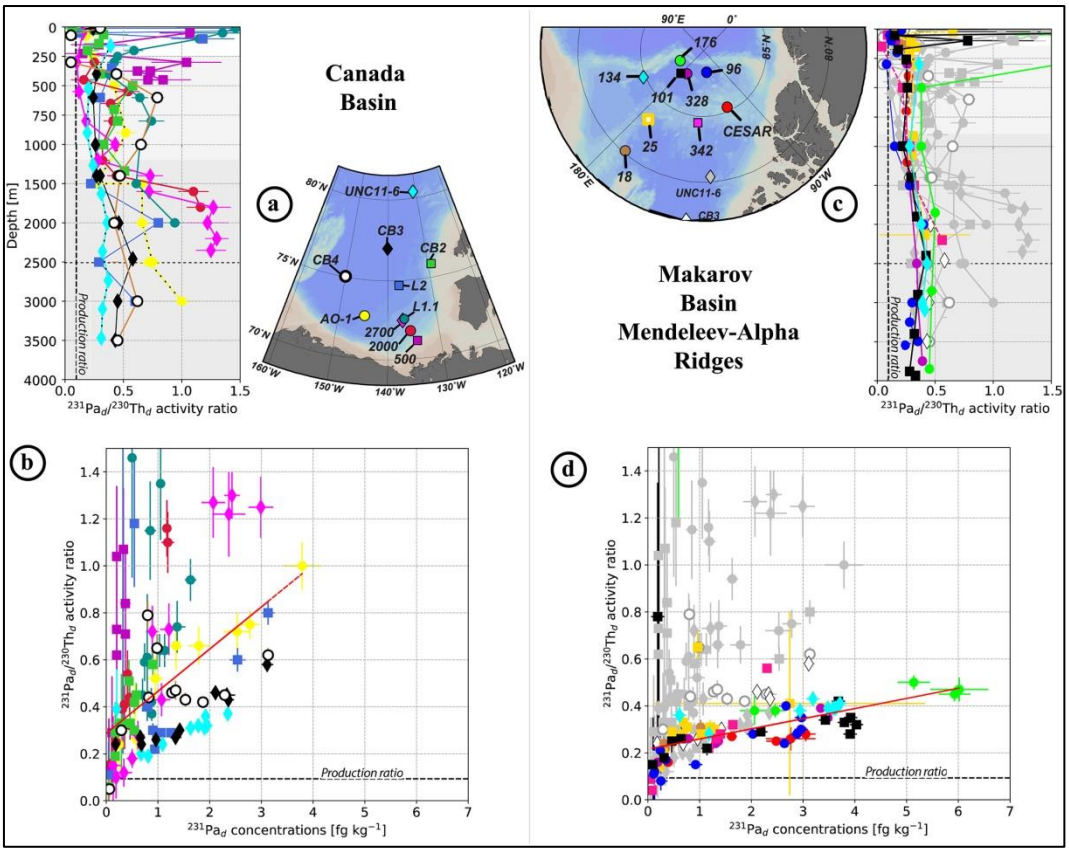


**Figure 8: $^{231}$Pa/$^{230}$Th activity ratio as a function of depth (top) and of Pa concentrations (bottom; in fg kg$^{-1}$) at the Canada Basin stations (a, b) and at the Makarov Basin and Mendeleev-Alpha Ridge stations (c, d), in color, superimposed on the Canada Basin ones, in grey, for comparison. The dotted black line represents the production rate ratio ($^{231}$Pa/$^{230}$Th = 0.093; Anderson *et al.*, 1983). The red line in (b) and (d) is the linear regression of the colored dots (excluding samples shallower than 50 m). In a steady state system, the slope of this red line reflects differences in the relative adsorption of Pa and Th. Steeper slopes reflect more intense scavenging of Th (higher $k_a$) than for Pa. This is discussed further in the text.**

### 5.1.2. Variability of $\varepsilon_{Nd}$ in the CB

Differences between coastal and interior regions of the CB are also observed in $\varepsilon_{Nd}$ profiles (Figure 6d). Stations sampled in 2000 (Porcelli *et al.*, 2009) exhibited significant differences in $\varepsilon_{Nd}$, with station 4 (red diamonds), identified as a transition zone station from its $^{230}$Th profile (Figure 6b), having significantly more radiogenic values than station 3 (interior basin). This observation suggests that in 2000, these two locations were in areas of distinct circulation, with little lateral exchange between them. The southern, more radiogenic 2000 profile resembles the one observed at CB2 in 2015, on the eastern CB margin (red diamond and green square in Figure 6d): they are likely representative of the water masses associated with the boundary circulation. The northern, less radiogenic 2000 profile (station 3, orange circles) resembles those observed at the deep stations in 2015 (black diamond and white circle profiles): these are likely representative of the central basin water masses. The more pronounced horizontal $\varepsilon_{Nd}$ gradient between the boundary vs. central CB in 2000 compared to 2015 reflects increasing lateral exchanges between these two areas between 2000 and 2015.

### 5.1.3. Contrasting $^{230}$Th, $^{231}$Pa and $\varepsilon_{Nd}$ Variability in the 2015 CB

The two 2015 deep stations (CB3 and CB4; Figure 6a) exhibit very similar profiles in $\varepsilon_{Nd}$ (Figure 6d) and $^{231}$Pa (Figure 6c), but not in $^{230}$Th (Figure 6b). For the latter, the Atlantic layer at CB4 (white circles) exhibits much lower concentrations than at CB3 (black diamonds), resulting in higher $^{231}$Pa/$^{230}$Th ratios (Figure 8a-b). These differences reveal on-going processes for which $^{230}$Th is more sensitive than $^{231}$Pa and $\varepsilon_{Nd}$, most likely an increase in particle fluxes that removes $^{230}$Th faster than the two other geochemical tracers, which are less susceptible to scavenging. CB4 is in closer vicinity to the boundary circulation and exhibits $^{230}$Th concentrations in the Atlantic water similar to those found at the 2015 coastal station CB2 (green squares). However, unlike CB4, CB3 also has lower $^{231}$Pa concentrations and more radiogenic $\varepsilon_{Nd}$. These results suggest that in 2015, the coastal region of the CB is impacted by higher fluxes of particles, which started to affect CB4. It seems to also be the case in 2009 at station L1.1 (blue circles), which is very close to station 2700 sampled in 2007 (pink diamonds). The $^{230}$Th profile at station L1.1 resembles more that at CB2 than at 2700, while $^{231}$Pa profiles measured in 2009 at L1.1 are closer to 2700 measured in 2009 than CB2 measured in 2015.

To summarize, in the CB, the comparison of published and new geochemical profiles suggests: 1) enhanced fluxes of particles along the radiogenic boundary circulation pathway after 2000, evidenced by lower $^{230}$Th and $^{231}$Pa concentrations and $^{230}$Th-$^{231}$Pa fractionation; 2) a transition

zone between the margin and the CB interior where lateral exchanges of water was between the margin and the basin interior was captured in 2000, 2007 and 2009 by non-linear $^{230}$Th profiles, showing a concentration maximum in the Atlantic layer; 3) an area north of 75°N in the central basin subject to low exchanges with the boundary circulation, with more negative $\varepsilon_{Nd}$ and a particle flux maintained at relatively low level.

### 5.1.4 Variability of $^{230}$Th and $^{231}$Pa in the MB

In the Makarov Basin and adjacent ridges area (hereafter MBAR), the highest dissolved $^{230}$Th and $^{231}$Pa concentrations were measured over Alpha Ridge in 1983 (red circles; Bacon *et al.* 1989) and the northern MB in 1991 (green circles; Scholten *et al.*, 1995; Figure 7). Building up such high concentration requires a residence time exceeding several decades in a region subjected to a very low particle flux region, as would be expected under permanent sea ice cover, to allow ingrowth of the two nuclides from their parent U isotopes. Dissolved $^{231}$Pa/$^{230}$Th ratios at these two stations are not as high as generally observed in the CB (Figure 8c-d), which is also consistent with a multidecadal residence time under permanent sea ice. As a water mass enters a region subjected to a lower particle flux, its $^{230}$Th concentration build up faster than $^{231}$Pa concentrations because of the differences in production rate and residence time with respect to scavenging between the two radionuclides, resulting in a gradually decreasing dissolved $^{231}$Pa/$^{230}$Th ratio with time. However, the MB profile comparison highlights 1) a significant decrease of $^{231}$Pa in the post-2000 profiles, not as marked in $^{230}$Th (Figure 7c), 2) an inflexion in $^{230}$Th profiles with a minimum around 2500 m for all the 2015 profiles (blue and black profiles in Figure 7a). The comparison of the two Alpha Ridge profiles shows significantly lower concentrations of $^{231}$Pa at the 2007 station, even more pronounced for $^{230}$Th, surprisingly tending toward CB concentrations with depth (pink square profile in Figure 7). In the following, we further develop the hypothesis presented above for the CB and hypotheses to explain the MBAR features.

## 5.2. Increased Particle Flux in the Margin Area

In the CB, the low $^{230}$Th and $^{231}$Pa profiles of the two 2007 coastal stations compared to the coastal 1995 profile reveal the impact of an enhanced vertical particle flux. The 2007 stations were located on the margin close to the Mackenzie River mouth, an area more and more seasonally free of ice (Figure S1): particulate riverine material and biological productivity could both explain an enhanced vertical particle flux at these coastal stations. The deeper 2007 coastal stations (stations 2000 and 2700) exhibit lower dissolved oxygen concentrations than measured

in 1995 at station AO-1, supporting an increasing flux of biogenic particles (Figure 9a-b). Ice rafted particles may also be released during the seasonal ice melt and possibly reinforce the particle flux and scavenging rate in this margin area (Baskaran *et al.*, 2003; Trimble *et al.*, 2004). In addition to enhanced vertical fluxes of particles in the margin area by increased biological productivity, our 2015 results also suggest lateral fluxes of continental particles.

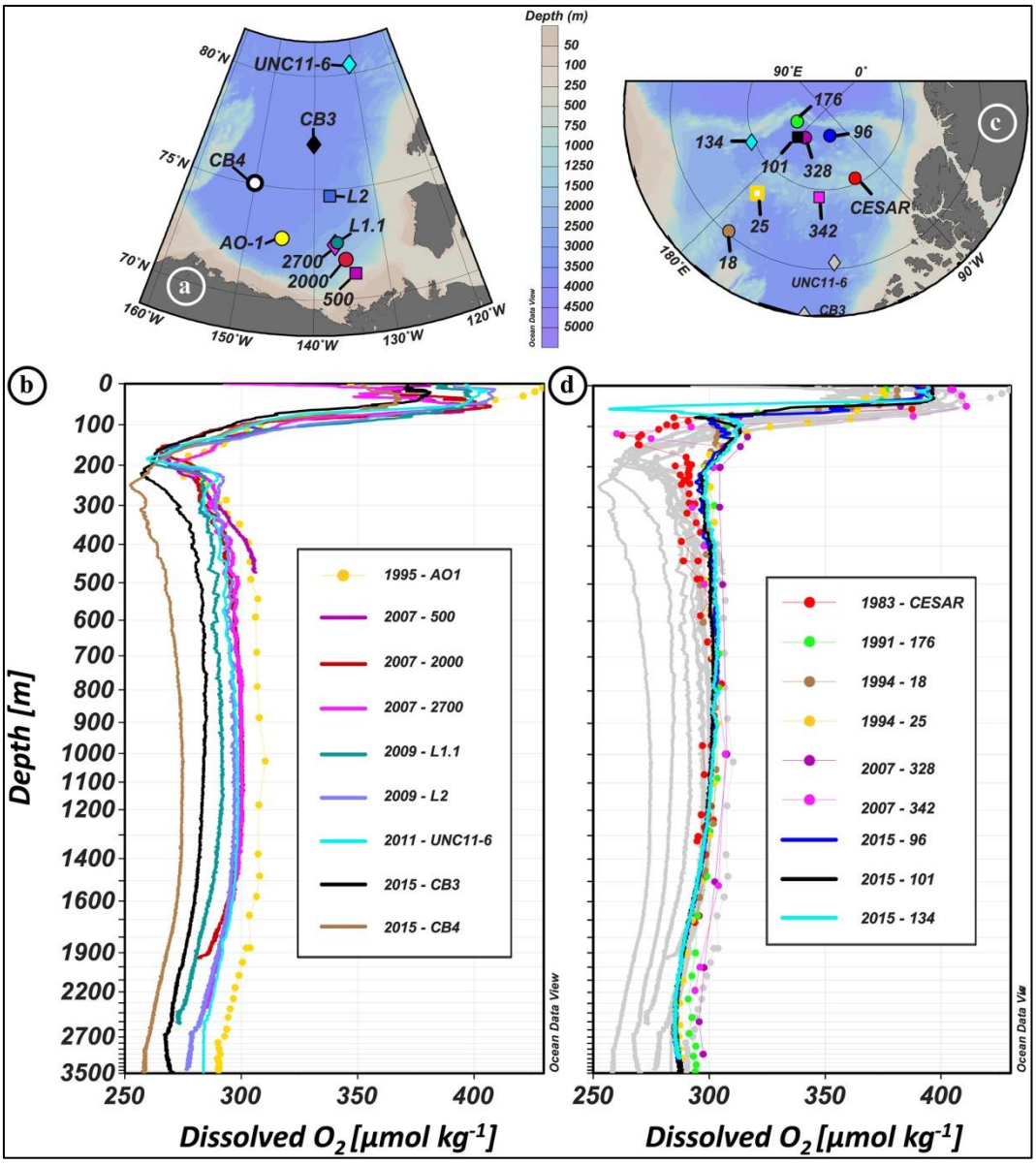


**Figure 9: Dissolved oxygen concentrations (in µmol kg$^{-1}$) measured at the different stations shown in (a) and (c), for (b) the Canada Basin and for (d) the Makarov Basin and Mendeleev-Alpha Ridges, in color, superimposed on the Canada Basin ones, in grey, for comparison. References are given in Figures 3 and 4.**

As noted above, the 2015 profiles measured at the two deep stations CB3 and CB4 have similar $\varepsilon_{Nd}$ (Figure 6d) and $^{231}$Pa (Figure 6c) concentrations in the Atlantic layer, but lower $^{230}$Th concentration at CB4 (Fig. 6b), while at the coastal station (CB2), $\varepsilon_{Nd}$ was more radiogenic and both $^{230}$Th and $^{231}$Pa concentrations were lower than at CB3. Comparing the $^{230}$Th profiles to

particulate iron (pFe) measured at the same stations (Figure 10; Li, 2017) reveals that the $^{230}$Th minimum observed in the Atlantic layer at CB4 coincides with a maximum of pFe, both of which are not observed at CB3 (Figure 10b-c). These observations suggest scavenging by lithogenic particle at CB4, possibly coming from the margin or the Northwind Ridge (this ridge rises to ~520 m below the surface, 250 km west of CB4; see Figure 3a). Moreover, the Atlantic layer at the coastal station CB2 exhibits much higher pFe and much lower $^{230}$Th concentrations than at the deep stations (Figure 10a), suggesting higher flux of coastal particles that scavenges both $^{230}$Th and $^{231}$Pa. The more radiogenic $\varepsilon_{Nd}$ below 500 m at CB2 compared to CB3 and CB4 (Figure 6d) further suggests that this signature is imparted from margin sediments, which is consistent with the $\varepsilon_{Nd}$ of the acetic acid leachates of surface sediments measured in the area (Haley and Polyak, 2013). The suggested impact of coastal particles on $^{230}$Th, $^{231}$Pa and $\varepsilon_{Nd}$ data at CB4 cannot only be the result of coastal processes transmitted offshore by advection. Instead coastal particles must be advected from the margin to CB4 to explain the pFe data. The transport of dissolved and particulate lithogenic signature from nepheloid layers formed by sediment resuspension along the CB margin across the area of boundary circulation could explain the distribution of all these 4 tracers. The occurrence of nepheloid layers has indeed been reported in the CB margin area (e.g. Ehn *et al.*, 2019; O'Brien *et al.*, 2006, 2013). Coastal water and particles could also be transported through eddies generated in the southern CB boundary current (Watanabe, 2011; Zhao *et al.*, 2014), whose number has intensified over the last two decades (Zhao *et al.*, 2016).

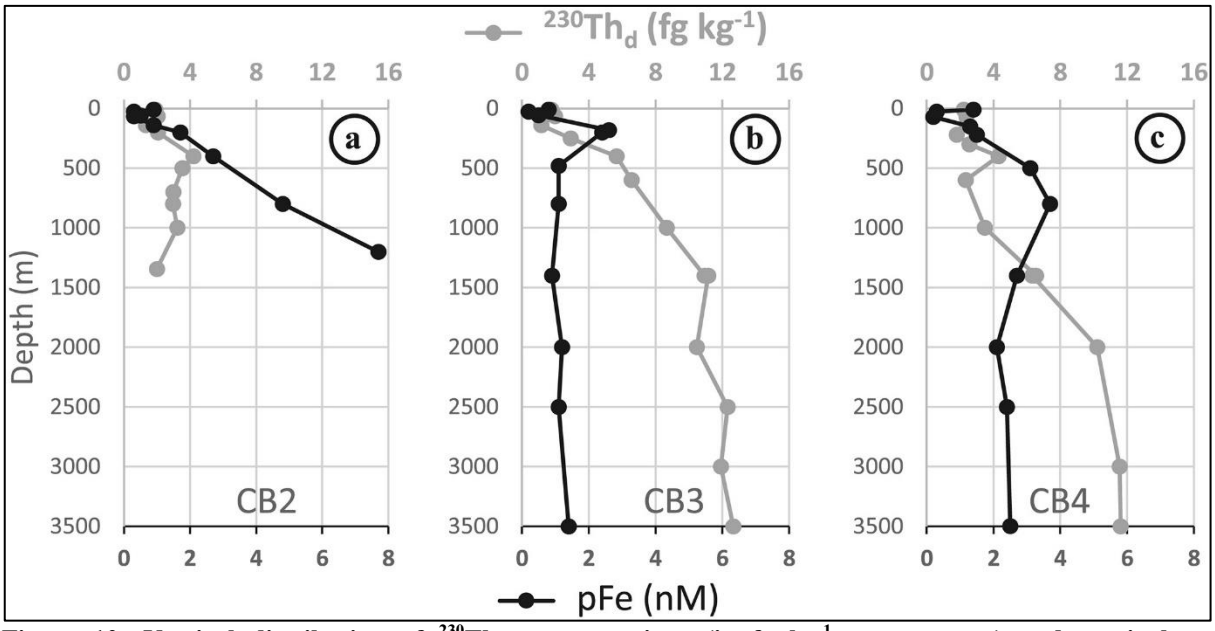


**Figure 10: Vertical distribution of $^{230}Th_d$ concentrations (in fg $kg^{-1}$; grey curves) and particulate Fe concentrations (pFe, in nM; black lines, from Li, 2017) in the Canada Basin in 2015, at (a) station CB2 (eastern CB), (b) station CB3 (northern CB), and (c) station CB4 (western CB). $^{230}$Th and pFe ranges are kept the same for the three stations to highlight differences.**

The high dissolved $^{231}$Pa/$^{230}$Th activity ratios in the Atlantic layer of most CB coastal stations collected after 2000 (Figure 8a-b) is consistent with the preferential scavenging of $^{230}$Th by lithogenic particles (Chase *et al.*, 2002). Such high $^{231}$Pa/$^{230}$Th activity ratios are not observed in the MBAR area (Figure 8c-d) where dissolved oxygen concentration profiles are not decreasing with time as in the CB (Figure 9c-d), suggesting that fluxes of lithogenic and biogenic particles are lower and more constant in time in the MBAR area. This difference is consistent with the evolution of sea ice coverage, more persistent in the MBAR area than in the CB (Figure S1), limiting biological productivity and ice rafted debris release.

### 5.3. Spatial Characterization of an Area of Lateral Exchanges Between the Boundary Circulation and Northern Central CB

The non-linear profiles observed in 2000 (station 4), 2007 (station 2700) and 2009 (station L2; Figure 6b) document the presence of an area where coastal low-$^{230}$Th and offshore high-$^{230}$Th waters influence the $^{230}$Th profiles to different extents at different depths. At these three stations, the relatively high concentrations measured at intermediate depths reflect advection or mixing of water originating from the northern CB. The southern limit of this mixing area in 2007 is fairly well captured by the sharp difference in $^{230}$Th concentrations and potential temperature within the Atlantic layer between the most offshore station 2700) and the more inshore station 2000 located 51 nautical miles south. At station 2700, the Atlantic Water has higher $^{230}$Th concentrations (Figure 6b), a higher temperature maximum (Figure 3c; inset), and a temperature

profile showing zigzags indicating weak turbulence and double-diffusive intrusions (Woodgate *et al.*, 2007) – consistent with an offshore northern CB origin (McLaughlin *et al.*, 2009). In contrast, the low $^{230}$Th concentration and smooth θ-S profile in the Atlantic layer of station 2000 is consistent with a boundary origin (Figures 5c and 6b). These two profiles are likely located across the front separating the cyclonic boundary current from the central anticyclonic flow (McLaughlin *et al.*, 2009). The 1995 $^{230}$Th profile did not exhibit such deviations from linearity and was therefore likely located south of this front.

Interestingly, it seems that the location of this front has moved further north between 2007 and 2009. Station L1.1, sampled in 2009 (blue circles) is almost at the same location as station 2700 sampled in 2007 (most offshore station; pink vs green profiles in Figure 11a).

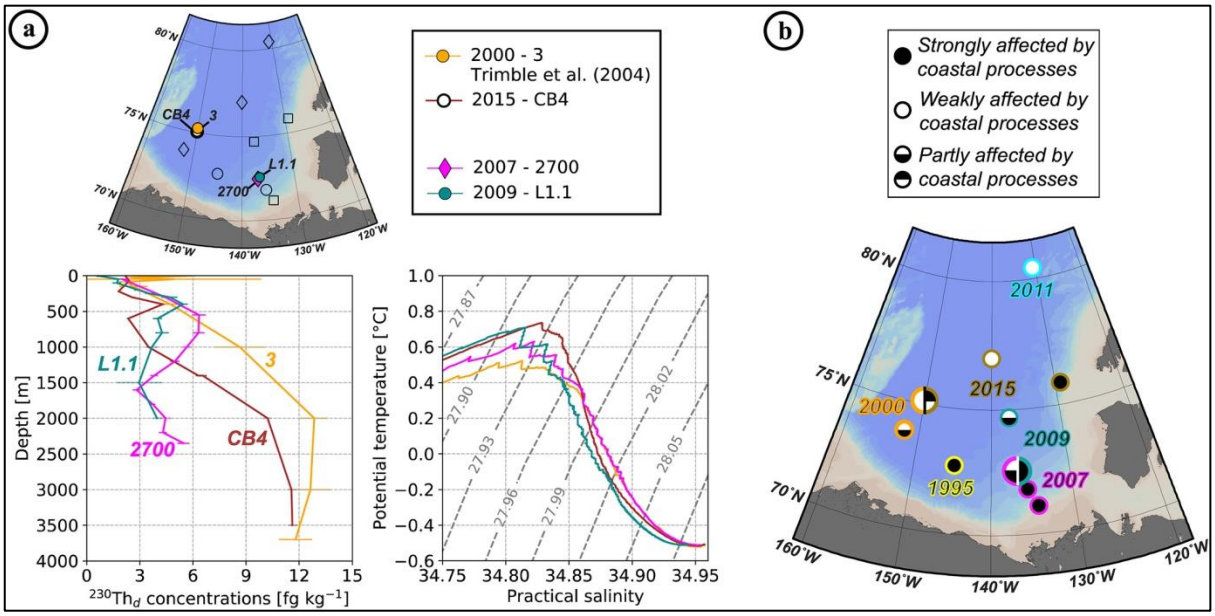


**Figure 11: Comparison of $^{230}$Th$_d$ concentrations (in fg kg$^{-1}$) and θ-S profiles (with superimposed isopycnal σ0) at stations of very close location but of different sampling year. (b) Schematic representation of the Canada Basin (CB) areas as defined from the $^{230}$Th profile features. Each station location is characterized following its degree of impact by coastal processes: weak, strong, or intermediate (white, black, and black/white filled circles, respectively), closely related to the extension of the boundary, northern, and mixed water areas. Color contours refer to the year of station sampling (same color code as in Figure 1). Larger circles, cut in two halves, represent temporal variability of the spatial extension of boundary processes from the stations visited twice (a).**

It is difficult to explain the sharp decrease observed in $^{230}$Th concentrations within the Atlantic layer between 2007 and 2009 only as a result of increased particle flux and scavenging, considering the residence time of Th at these depths. Instead, it most likely reflects a greater relative proportion of "margin" vs "offshore" water at this location in 2009. The smoother θ-S within the Atlantic layer and more radiogenic, $^{230}$Th-depleted signal found at 1000 m at the 2015 station CB4 (white circles, Figure 6), compared to the nearby 2000 station 3 (orange circles;

Figure 6) sampled 15 years before may also reflect the northward displacement of this front and increase lateral exchanges between the margin area and the central CB during the last two decades (orange vs brown profiles in Figure 11a and Figure 6d). Figure 11b summarizes, through the characteristics of the $^{230}$Th vertical profiles, the spatial distribution and temporal variability of the impact of coastal processes and lateral exchanges.

The lateral exchange variability suggested in the CB may be related to the propagation in the Arctic of the awAW: associated with a larger volume of inflowing Atlantic Water (Karcher *et al.*, 2003; Schauer *et al.*, 2004), this awAW propagated as a stronger intermediate flow, which presumably reinforced the two circulation schemes of the CB (anticyclonic circulation in the deep basin; Coachman and Barnes, 1963; Newton and Coachman, 1974; boundary cyclonic circulation) and enhanced the lateral mixing between the cyclonic boundary circulation and the anticyclonic central circulation. This is supported by the coexistence of the temporal increase of vertical variability within the $^{230}$Th profiles with the temporal increase of temperature of the upper Atlantic layer (Figure 11a). The eddy activity and its intensification over the last decades (Timmermans *et al.*, 2008; Watanabe, 2011; Zhao *et al.*, 2016) could also be partly responsible for the lateral exchange variability suggested by our profiles.

### 5.4. Lateral Exchanges in Other Areas of the Amerasian Basin

#### 5.4.1. Lateral Exchange in the Atlantic/Deep Layer Between the Northern CB and the Southern Alpha Ridge

Unlike at the stations in the CB, MB and Mendeleev Ridge areas, waters sampled in the Alpha Ridge (AR) area (station CESAR and 342) before and after 2000 do not exhibit significant hydrological changes (Figures 12b). The awAW propagation, seen in other regions, was not identifiable at station 342 in 2007, while it was evident at station 328 sampled the same year in the MB (Figure 12). This suggests the relative isolation of the water column in AR area from the MB and CB circulation. In addition, the high $^{230}Th_d$ and $^{231}Pa_d$ concentrations measured in 1983 in the northern AR (station CESAR) reveal the long isolation of the water column in this area under low flux of particles, allowing ingrowth of the two radionuclides (see Figure 2c; Bacon *et al.*, 1989). In 1996, Smethie *et al.* (2000) consistently found low CFC-11 concentrations and $^{3}$H-$^{3}$He ages of 25 years on average below 300 m in this area.

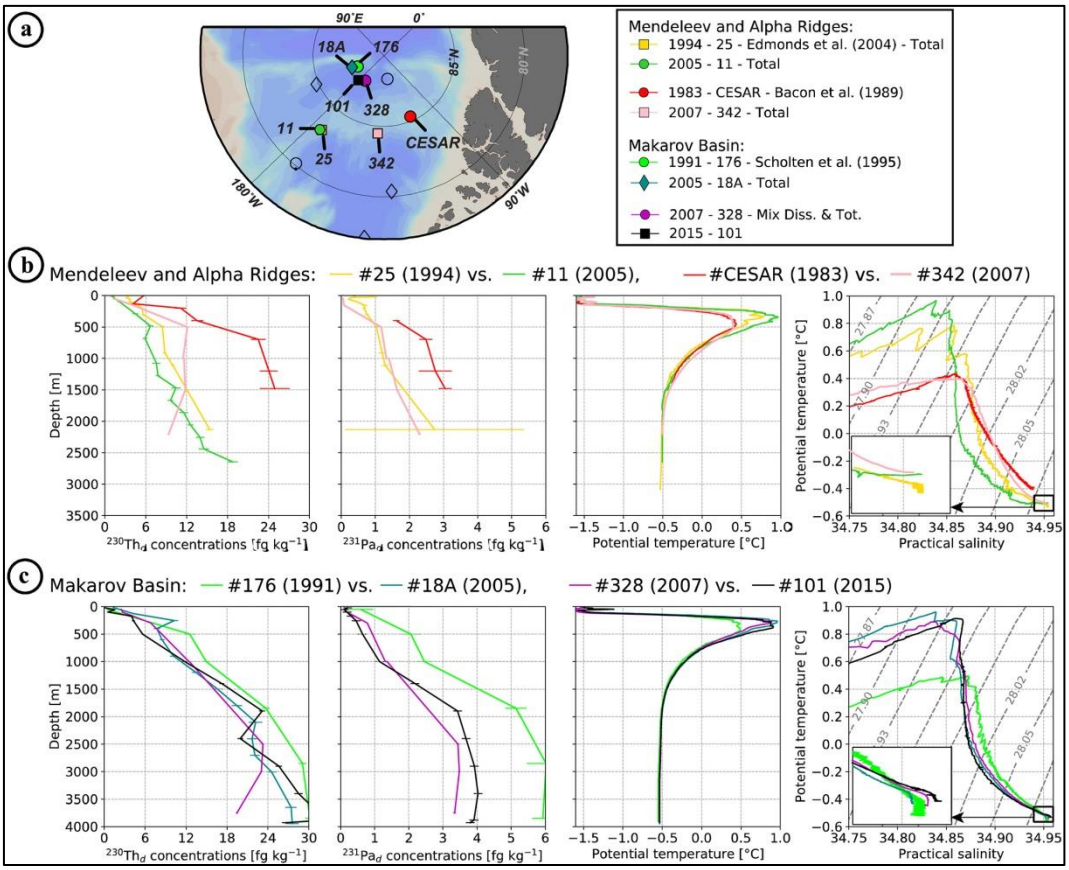


**Figure 12: Comparison of geochemical ($^{230}Th_d$ and $^{231}Pa_d$ concentrations, as shown in Figures 5 and 6, in fg $kg^{-1}$) and hydrological (potential temperature θ vertical profiles, in °C, and θ-S profiles with superimposed isopycnal σ0) properties at stations of very close location but of different sampling year (also referred in the text as "twice visited," except for the Alpha Ridge stations that are too far apart to be considered as such). Concerned stations are identified in the map shown in (a) and properties are shown in (b) for the Mendeleev and Alpha Ridge stations and in (c) for the Makarov Basin ones. The θ-S plot insets show a zoom on the θ-S bottom water characteristics delimited by the black squares.**

Yet, much lower $^{230}Th_d$ and $^{231}Pa_d$ concentrations were measured at station 342 in 2007, with a surprising decrease in $^{230}Th_d$ with depth (Figure 12b). Such differences between the 1983 and the 2007 profiles imply the presence of intermediate/deep waters at the 2007 station distinct from the water mass sampled in 1983. From the comparison of the hydrological profiles at these two AR stations to those of the whole station set reported here (Figures 3-5 and 9), AR waters appear to be dominantly derived from CB waters, and more particularly, from colder, saltier, denser waters predating the awAW propagation in the CB. The largest hydrological differences observed between the AR stations collected in 1983 and 2007 are actually not in the AW core (ca. 500 m) but in the lower halocline and lower AW, where the 2007 station is warmer (Figure 12b). These geochemical and hydrological features of the two AR stations are consistent with the lower AW and uPDW in 2007 being relatively recently renewed by CB waters. The $^{230}Th_d$ and $^{231}Pa_d$ profiles are consistent with this hypothesis, as well as the dissolved oxygen (Figures 7 and 9d). The water renewal had to occur about 10 years before the sampling of the 2007 station,

i.e. predating the awAW arrival in the CB (i.e. 2003; Woodgate *et al.*, 2007) but postdating the low CFC, $^{3}H$ and $^{3}He$ observed in the area in 1996 (Smethie *et al.*, 2000). It is possible that the $^{230}Th_d$ content of the uPDW in this area was additionally impacted by scavenging. Indeed, the 2007 station was collected on the deep southwestern flank of the AR, in contrast to the 1983 station which was situated over the top of the AR (Figures 12a). Sediment resuspension from the Alpha Ridge slope that rises to 1600 m, 60 km further north (84.9°N, 134.3°W; www.gmrt.org) and to 1300 m, 140 km further northeast of the 2007 station (85°N, 126°W) could impact the area sampled in 2007.

### 5.4.2. Lateral Exchanges Between the Deep Northern CB and the Deep MB

Intrusions of CB waters into the MB above the deeper sill between the Mendeleev and Alpha Ridges (~2400 m) could explain the $^{230}Th_d$ concentration minimum observed within the Deep Transitional Layer (DTL, 2000-2500 m; Timmermans *et al.*, 2003) in 2015 in the MB (stations 96, 101, 134; Figures 7 and 12c). Indeed, the deep and bottom layers of the CB are characterized by significantly lower concentrations of $^{230}Th$ than the MB; the uniformity in the $^{231}Pa$ concentrations of the MB and northern CB at this depth also support such exchanges. In addition, the MB $^{231}Pa/^{230}Th$ activity ratios show a consistent deviation around this depth toward slightly higher, CB-like, values (Figure 8c). The fact that this $^{230}Th$ minimum is clearly observed in the eastern MB (station 96) further suggests that this CB signature spreads through the entire Basin (i.e. east of 180°). Hydrological features such as the θ-S convexity and $O_2$ minimum observed within the DTL at the MB stations also support exchanges of CB deep waters toward the MB (Figures 4, 5h and 9d). Although the direction of exchanges we suggest here conflicts with former hydrological study conclusions that invoked a dominant flux of DTL water above the Mendeleev/Alpha Ridge from the MB toward the CB (e.g. Carmack *et al.*, 2012; Rudels, 2009), Swift *et al.* (1997) also invoked a flow from the CB toward the MB above the Mendeleev Ridge to explain the local silicate maximum observed in the MB around 2400 m depth.

Intrusions of CB deep waters into the MB could also explain the warmer and saltier water observed in the bottom waters at the MB and Mendeleev Ridge stations after 2000 (insets in the θ-S plots in Figure 12b-c). Nonetheless, considering the gradual decrease of tracer –especially $^{231}Pa_d$– concentrations with depth below 3000 m, coupled to a gradual increase of dissolved $O_2$ (Figure 9b and 12c), we agree with Middag *et al.*, (2009) and Roeske *et al.* (2012) that MB bottom water is also made of some colder and fresher Amundsen Basin Deep Water (ABDW)

that likely came over the Lomonosov Ridge (between 2000 and 2500 m) and sank due to its higher density than the local bottom waters (Timmermans *et al.*, 2005).

### 5.4.3. Lateral Exchanges Between the Eurasian Basin and the Central Makarov Basin

As previously mentioned, the data reported in this work suggest that fluxes of lithogenic and biogenic particles have been weaker and more constant in time in the MBAR area than in the CB (see section 5.2). Yet, significant differences are observed between the $^{230}Th_d$ and $^{231}Pa_d$ profiles in the MB before 2000 (Station 176; Scholten *et al.*, 1995) and those at the stations visited after 2000 (Figure 12c): post-2000s profiles exhibit lower radionuclide concentrations, especially pronounced in $^{231}Pa_d$, compared to the 1991 profile. The high $^{230}Th_d$ and $^{231}Pa_d$ concentrations measured in 1991 in the northern MB reflect, as for the 1983 station collected over the AR, a long isolation of the area from the dynamic boundary circulation of the MB and a low flux of particles (Scholten *et al.*, 1995). The difference of $^{231}Pa_d$ concentration between this 1991 station and those visited after 2000 increases with depth. It is difficult to explain the pre- vs post-2000s radionuclide differences observed in the MB as a stronger flux of particles, as a change in particle flux strong enough to explain the $^{231}Pa$ changes in depth should have also led to a much larger $^{230}Th$ depletion than those observed (Figure 12c). Not to mention that, despite the evolution of sea ice coverage since the 1990s, most of the MB has remained permanently covered by sea ice over these years (Figure S1), limiting an enhancement of productivity.

Therefore, our geochemical results suggest that waters with lower $^{230}Th$ concentrations and lower $^{231}Pa/^{230}Th$ activity ratios (due to lower concentrations of $^{231}Pa$ relatively to $^{230}Th$) propagated into the MB after 1991. CB waters are characterized by too high $^{231}Pa/^{230}Th$ activity ratios and too low oxygen concentrations to represent a valid candidate. In contrast, consistent lower $^{230}Th$ concentrations and lower $^{231}Pa/^{230}Th$ activity ratios have been documented in the Eurasian waters (Edmonds *et al.*, 2004), as well as similar oxygen concentrations (Schauer *et al.*, 2002). The presence of the awAW at the stations visited in the MB after 2000 supports the occurrence of exchanges between this previously isolated area and the topographically-steered intermediate circulation (Figure 12c).

## 6. Conclusion

This work presents a compilation of published and new depth profiles of $^{230}Th$, $^{231}Pa$, and $\varepsilon_{Nd}$ collected between 1983 and 2015 in the Amerasian Basin of the Arctic Ocean; in particular in the Canada and Makarov basins and over the Mendeleev and Alpha ridges. The distribution of these geochemical tracers allow an assessment of the spatial and temporal variability in particle

flux and water mass circulation and mixing in these different areas. A representation of intermediate-to-bottom layer circulation, including pathways likely dominant in the past but suggested to be more minor recently (section 5.4) as well as the circulation from the main conclusions (summarized below) is outlined in Figure 13.

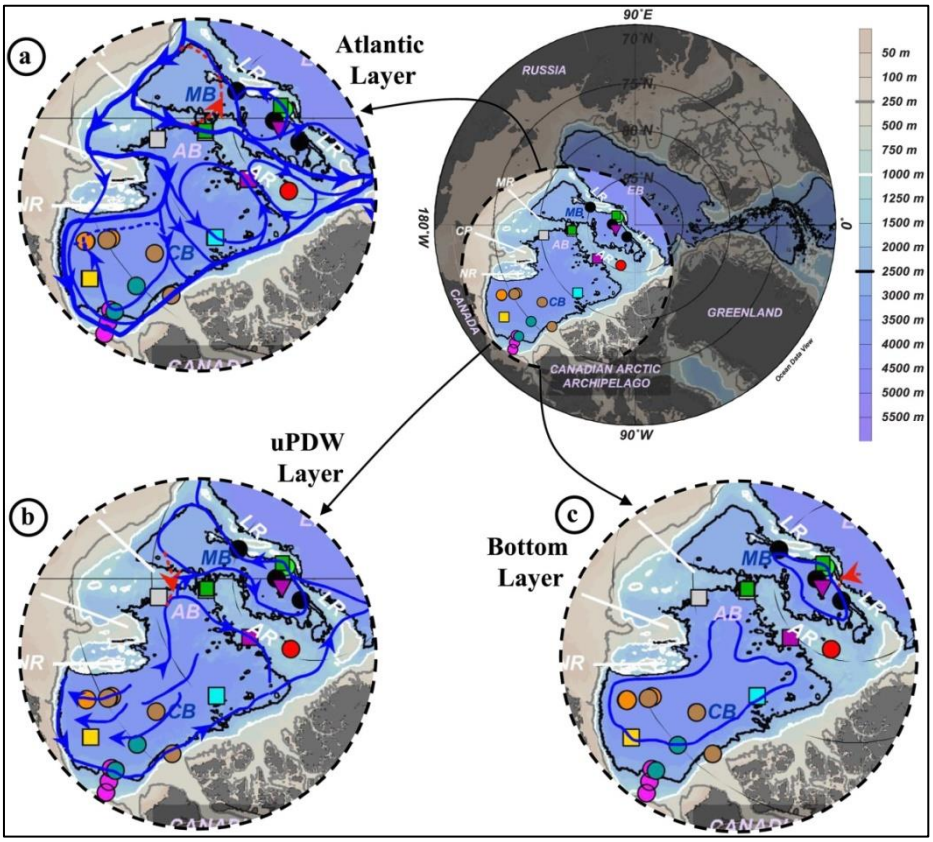


**Figure 13: Schematic representations of Amerasian Basin circulation layers: (a) Atlantic water layer (~250–1,000 m); (b) uPDW layer (~1,000–2,500 m); (c) bottom layer (~2,500 m bottom; flow direction not given, due to uncertainties). The 250, 1,000, and 2,500 m isobaths are represented by grey, white, and black lines, respectively. EB = Eurasian Basin; AB = Amerasian Basin; MB = Makarov Basin; CB = Canada Basin; LR = Lomonosov Ridge; AR = Alpha Ridge; MR = Mendeleev Ridge; NR = Northwind Ridge; CP = Chukchi Plateau. Dotted red pathways—within the MB in (a), over the MR toward the CB in (b), and over the LR toward the MB in (c)—are paths that were likely dominant in the past but are likely minor nowadays.**

A temporal decrease in concentrations of the particle-reactive tracers $^{230}$Th and $^{231}$Pa is observed in the whole Amerasian Basin and results from particle scavenging, and mixing and circulation variability. Particularly in the Canada Basin, the intensification of lithogenic and biologic particle fluxes likely results from margin sediment transport and enhanced biological production, respectively, in relation to sea ice retreat. Imprints of increased lateral exchange are also reported in several areas of the Amerasian Basin. In the Canada Basin, they are represented by the coexistence of high $^{230}$Th Atlantic water of northern origin overlying low $^{230}$Th waters that have their origin in the boundary; the spatial extent of this area of lateral exchange seems to vary in time. The geochemical and hydrological characteristics at the southern flank of the Alpha Ridge

in 2007 reflect the occurrence of lateral exchange in the Atlantic layer and uPDW with Canada Basin waters in the early 2000s, in contrast with the isolated character of this area reported in the 80-90s. Similarly, the geochemical and hydrological characteristics reported in the MB suggest that lateral exchange has connected the previously isolated northern MB with the main circulation (the pre-2000s Makarov Basin circulation was likely restricted to the red arrow shown in Figure 13a; blue arrows show the connection of the offshore Makarov Basin with the boundary circulation suggested from the post-2000s profiles). The results reported in this study also suggest increased intrusion of Canada Basin deep waters over the Mendeleev-Alpha Ridge sill into the Makarov Basin, impacting the Deep Transitional Layer (2000-2500 m) waters of the Makarov Basin (while a dominant overflow from the Makarov Basin toward the Canada Basin was previously suggested, as represented by the red arrow in Figure 13b). Canada Basin deep water intrusion also seems to mix with deeper waters of the Makarov Basin and decrease the Amundsen Basin Deep Water (ABDW) signature of the Makarov Basin Bottom Water (ABDW overflow represented by the red arrow in Figure 13c).

These conclusions are based on sparse samples, in space and time. Additional sampling is needed to refine the hypotheses proposed in this study. There is a need to better document the coastal Makarov Basin, from the Lomonosov Ridge to the Mendeleev Ridge, and the northern Canada Basin, from the Chukchi Plateau to the northeast Canadian Arctic Archipelago (CAA). It would be of interest to sample the Alpha Ridge again over the southern and northern flanks to determine whether this area is isolated, or if changes in the Arctic circulation have led to exchange of waters between this area and the Canada Basin. Finally, with the circulation changes suggested in the Makarov Basin, it would also be interesting to monitor the water circulation in the vicinity of the western Lomonosov Ridge, by sampling the Greenland side of the Makarov Basin, Alpha Ridge and Amundsen Basin, to better document the composition of waters flowing through Nares Strait (between the CAA and Greenland) and those returning to Fram Strait. The circulation and particle distribution of the Amerasian Basin are sufficiently heterogeneous to make these geochemical tracers a useful tool to study the Arctic Ocean state and evolution, though the utility of these tracers may be challenged if mixing and particle concentration dramatically increase and eventually erases the current gradients.

**Acknowledgments**

We wish to acknowledge the assistance of the officers and crew of the USCG *Healy*, the CCGS *Sir Wilfrid Laurier*, *Amundsen*, *Louis St-Laurent*, and the R/V *Polarstern* during the research expeditions. Jay Cullen, Philippe Tortell and Kristina Brown are also acknowledged for their implication in the scientific managing of the 2015 cruise. We are grateful to Pascal Guillot, Thomas Linkowski and Cris Seaton (Quebec-Ocean and ArcticNet) for their technical support at sea. We thank Cheng Kuang for her great help during the cruise preparation and on-board and Isabelle Baconnais for sampling at sea. We also acknowledge, on the one hand, Vivian Lai and Dominique Weis (Pacific Centre for Isotopic and Geochemical Research, EOAS) and, on the other hand, Stephanie Mounic and Mathieu Benoit (Centre National de la Recherche Scientifique, GET), for their technical support on the ICP-MS and on the TIMS, respectively. Finally, we thank the two anonymous reviewers whose insightful comments and suggestions helped to improve the manuscript.

The Canadian Arctic GEOTRACES project was funded by the Canadian research program NSERC CCAR. M. Grenier was supported by a European Union's Horizon 2020 research and innovation programme (Marie Skłodowska-Curie action, grant agreement #657853). Christelle Not was supported by Natural Sciences and Engineering Research Council of Canada research funds awarded to Claude Hillaire-Marcel and the Fonds Québécois de la Recherche sur la Nature et les Technologies from GEOTOP. The data set reported in the tables is available on the GEOTRACES International Data Assembly Centre (www.bodc.ac.uk/geotraces/data/).

**References**

Aagaard, K. and Greisman, P. (1975). Toward new mass and heat budgets for the Arctic Ocean. Journal of Geophysical Research, 80(27), 3821–3827. https://doi.org/10.1029/jc080i027p03821

Aagaard, K., Swift, J. H. and Carmack, E. C. (1985). Thermohaline circulation in the Arctic Mediterranean Seas. Journal of Geophysical Research, 90(C3), 4833. https://doi.org/10.1029/JC090iC03p04833

Amundsen Science Data Collection. (2016). CTD data collected by the CCGS Amundsen in the Canadian Arctic. [2015]. Processed data. 1502_int_R3, 1503_int_R1. Accessed on [01 November 2016]. Archived at www.polardata.ca. https://doi.org/10.5884/12713

Anderson, L. G., Björk, G., Holby, O., Jones, E. P., Kattner, G., Koltermann, K. P., *et al.* (1994). Results from the Oden 91 expedition, 99, 3273–3283.

Anderson, R. F., Bacon, M. P. and Brewer, P. G. (1983). Removal of $^{230}$Th and $^{231}$Pa from the open ocean. Earth and Planetary Science Letters, 62, 7–23.

Andersson, P. S., Porcelli, D., Frank, M., Björk, G., Dahlqvist, R. and Gustafsson, Ö. (2008). Neodymium isotopes in seawater from the Barents Sea and Fram Strait Arctic-Atlantic gateways. Geochimica et Cosmochimica Acta, 72(12), 2854–2867. https://doi.org/10.1016/j.gca.2008.04.008

Bacon, M. P. and Anderson, R. F. (1982). Distribution of Thorium Isotopes Between Dissolved and Particulate Forms in The Deep Sea. Journal of Geophysical Research, 87(1), 2045–2056. https://doi.org/10.1029/JC087iC03p02045

Bacon, M. P., Huh, C.-A. and Moore, R. M. (1989). Vertical Profiles of Some Natural Radionuclides Over the Alpha-Ridge, Arctic Ocean. Earth and Planetary Science Letters, 95(1–2), 15–22.

Baskaran, M., Swarzenski, P. W. and Porcelli, D. (2003). Role of colloidal material in the removal of $^{234}$Th in the Canada basin of the Arctic Ocean. Deep Sea Research Part I: Oceanographic Research Papers, 50(10–11), 1353–1373. https://doi.org/10.1016/S0967-0637(03)00140-7

Bluhm, B. A., Kosobokova, K. N., and Carmack, E. C. (2015). A tale of two basins: An integrated physical and biological perspective of the deep Arctic Ocean. Progress in Oceanography, 139(August), 89–121. https://doi.org/10.1016/j.pocean.2015.07.011

Brewer, P. G. (1975). Minor elements in seawater. In J. P. Riley and G. Skirrow (Eds.), Chemical Oceanography (2nd ed.). New York: Academic Press.

Carmack, E., Macdonald, R. W., Perkin, R. G., Mclaughlin, F. A. and Pearson, R. J. (1995). Evidence for warming of Atlantic water in the southern Canadian Basin of the Arctic Ocean: Results from the Larsen-93 expedition. Geophysical Research Letters, 22(9), 1061–1064.

Carmack, E., Macdonald, R. W., O'Brien, M., Pearson, R., Timmermans, M.-L., Sieberg, D., *et al.* (1996). Physical and chemical data collected in the Beaufort Sea and Canadian Archipelago August - September 1995. Can. Data Rept. Hydrogr. Ocean. Sci., 147, 281.

Carmack, E., Williams, W. J., Zimmermann, S. L. and McLaughlin, F. A. (2012). The Arctic Ocean warms from below. Geophysical Research Letters, 39(7), 1–6. https://doi.org/10.1029/2012GL050890

Carmack, E. C., Barber, D., Christensen, J., Macdonald, R., Rudels, B. and Sakshaug, E. (2006). Climate variability and physical forcing of the food webs and the carbon budget on panarctic shelves. Progress in Oceanography, 71(2–4), 145–181. https://doi.org/10.1016/j.pocean.2006.10.005

Chase, Z., Anderson, R. F., Fleisher, M. Q. and Kubik, P. W. (2002). The Influence of Particle Composition on Scavenging of Th, Pa and Be in the Ocean. Earth and Planetary Science Letters, 204, 215–229.

Chauvel, C. and Blichert-Toft, J. (2001). A hafnium isotope and trace element perspective on melting of the depleted mantle. Earth and Planetary Science Letters, 190(3–4), 137–151. https://doi.org/10.1016/S0012-821X(01)00379-X

Chen, J. H., Edwards, R. L. and Wasserburg, G. J. (1986). $^{238}$U, $^{234}$U and $^{232}$Th in seawater. Earth and Planetary Science Letters, 80(3–4), 241–251. https://doi.org/10.1016/0012-821X(86)90108-1

Choi, M. S., Francois, R., Sims, K., Bacon, M. P., Brown-Leger, S., Fleer, A. P., *et al.* (2001). Rapid determination of $^{230}$Th and $^{231}$Pa in seawater by desolvated micro-nebulization Inductively Coupled Plasma magnetic sector mass spectrometry. Marine Chemistry, 76(1–2), 99–112. https://doi.org/10.1016/S0304-4203(01)00050-0

Coachman, L. K. and Barnes, C. A. (1961). The Contribution of Bering Sea Water to the Arctic Ocean. Arctic, 14, 147–161. https://doi.org/10.14430/arctic3670

Coachman, L. K. and Barnes, C. A. (1963). The Movement of Atlantic Water in the Arctic Ocean. Arctic, 16(1), 8. https://doi.org/10.14430/arctic3517

Cochran, J. R., Edwards, M. H. and Coakley, B. J. (2006). Morphology and structure of the Lomonosov Ridge, Arctic Ocean. Geochemistry, Geophysics, Geosystems, 7(5). https://doi.org/10.1029/2005GC001114

Dahlqvist, R., Andersson, P. S. and Porcelli, D. (2007). Nd isotopes in Bering Strait and Chukchi Sea water. Goldschmidt Conf. Abstr., A196. Retrieved from http://goldschmidt.info/2007/abstracts_Abs_Vol/4877.pdf

Darby, D., Polyak, L., Jakobsson, M., Berger, G., Lövlie, R., Perovich, D., *et al.* (2006). HLY0503 Cruise Report, UNOLS, USCG, and NSF, 51pp.

Edmonds, H. N., Moran, S. B., Hoff, J. A., Smith, J. N., and Edwards, R. L. (1998). Protactinium-231 and thorium-230 abundances and high scavenging rates in the Western Arctic Ocean. Science, 280(5362), 405–407. https://doi.org/10.1126/science.280.5362.405

Edmonds, H. N., Moran, S. B., Cheng, H., and Edwards, R. L. (2004). $^{230}$Th and $^{231}$Pa in the Arctic Ocean: Implications for particle fluxes and basin-scale Th/Pa fractionation. Earth and Planetary Science Letters, 227(1–2), 155–167. https://doi.org/10.1016/j.epsl.2004.08.008

Ehn, J. K., Reynolds, R. A., Stramski, D., Doxaran, D., Lansard, B., and Babin, M. (2019). Patterns of suspended particulate matter across the continental margin in the Canadian Beaufort Sea during summer. Biogeosciences, 16(7), 1583–1605. https://doi.org/10.5194/bg-16-1583-2019

Frank, M. (2002). Radiogenic isotopes: Tracers of past ocean circulation and erosional input. Reviews of Geophysics, 40(1). https://doi.org/10.1029/2000RG000094

Goldstein, S. L., and Hemming, S. R. (2003). Long-lived Isotopic Tracers in Oceanography, Paleoceanography, and Ice-sheet Dynamics. Treatise on Geochemistry: Second Edition, 8, 453–483. https://doi.org/10.1016/B978-0-08-095975-7.00617-3

Grenier, M., Jeandel, C., Lacan, F., Vance, D., Venchiarutti, C., Cros, A., and Cravatte, S. (2013). From the subtropics to the central equatorial Pacific Ocean: Neodymium isotopic composition and rare earth element concentration variations. Journal of Geophysical Research: Oceans, 118(2), 592–618. https://doi.org/10.1029/2012JC008239

Haley, B. A., and Polyak, L. (2013). Pre-modern Arctic Ocean circulation from surface sediment neodymium isotopes. Geophysical Research Letters, 40(5), 893–897. https://doi.org/10.1002/grl.50188

Hansen, B., and Østerhus, S. (2000). North Atlantic-Nordic Seas exchanges. Progress in Oceanography, 45(2), 109–208. https://doi.org/10.1016/S0079-6611(99)00052-X

Henderson, G. M., and Anderson, R. F. (2003). The U-series toolbox for paleoceanography. Uranium-Series Geochemistry, 52, 493–531.

Jackson, J. M., Allen, S. E., Carmack, E. C., and McLaughlin, F. A. (2010). Suspended particles in the Canada Basin from optical and bottle data, 2003-2008. Ocean Science, 6(3), 799–813. https://doi.org/10.5194/os-6-799-2010

Jakobsson, M., Mayer, L., Coakley, B., Dowdeswell, J. A., Forbes, S., Fridman, B., *et al.* (2012). The International Bathymetric Chart of the Arctic Ocean (IBCAO) Version 3.0. Geophysical Research Letters, 39(12). https://doi.org/10.1029/2012GL052219

Jeandel, C., Arsouze, T., Lacan, F., Téchiné, P., and Dutay, J. C. (2007). Isotopic Nd compositions and concentrations of the lithogenic inputs into the ocean: A compilation, with an emphasis on the margins. Chemical Geology, 239(1–2), 156–164. https://doi.org/10.1016/j.chemgeo.2006.11.013

Jones, E. P., and Anderson, L. G. (1986). On the origin of the chemical properties of the Arctic Ocean halocline. Journal of Geophysical Research, 91(6), 10759. https://doi.org/10.1029/JC091iC09p10759

Jones, E. P., Rudels, B., and Anderson, L. G. (1995). Deep waters of the Arctic Ocean: origins and circulation. Deep-Sea Research Part I, 42(5), 737–760. https://doi.org/10.1016/0967-0637(95)00013-V

Karcher, M. J., Gerdes, R., Kauker, F., and Köberle, C. (2003). Arctic warming: Evolution and spreading of the 1990s warm event in the Nordic seas and the Arctic Ocean. Journal of Geophysical Research, 108, 3034. https://doi.org/10.1029/2001JC001265

Kikuchi, T., Inoue, J., and Morison, J. H. (2005). Temperature difference across the Lomonosov Ridge: Implications for the Atlantic water circulation in the Arctic Ocean. Geophysical Research Letters, 32(20), 1–4. https://doi.org/10.1029/2005GL023982

Ku, T. L., Knauss, K. G., and Mathieu, G. G. (1977). Uranium in open ocean: concentration and isotopic composition. Deep-Sea Research, 24(11), 1005–1017. https://doi.org/10.1016/0146-6291(77)90571-9

Li, J. (2017). Particulate trace metals and iron availability to phytoplankton in a changing Arctic Ocean (Master Thesis), (April). https://doi.org/10.14288/1.0348666

Lugmair, G. W., Shimamura, T., Lewis, R. S., and Anders, E. (1983). Samarium-146 in the early solar system: Evidence from neodymium in the allende meteorite. Science, 222(4627), 1015–1018. https://doi.org/10.1126/science.222.4627.1015

Mauritzen, C., Rudels, B., and Toole, J. (2013). The Arctic and Subarctic Oceans/Seas. International Geophysics, 103, 443–470. https://doi.org/10.1016/B978-0-12-391851-2.00017-9

McLaughlin, F. A., Carmack, E. C., Williams, W. J., Zimmermann, S., Shimada, K., and Itoh, M. (2009). Joint effects of boundary currents and thermohaline intrusions on the warming of Atlantic water in the Canada Basin, 1993-2007. Journal of Geophysical Research: Oceans, 114(7), 1993–2007. https://doi.org/10.1029/2008JC005001

Middag, R., de Baar, H. J. W., Laan, P., and Bakker, K. (2009). Dissolved aluminium and the silicon cycle in the Arctic Ocean. Marine Chemistry, 115(3–4), 176–195. https://doi.org/10.1016/j.marchem.2009.08.002

Mosher, D. C. (2012). 2011 Canadian High Arctic Seismic Expedition: CCGS Louis S. St-Laurent expedition report. https://doi.org/10.4095/290241

Newton, J. L., and Coachman, L. K. (1974). Atlantic Water Circulation in the Canada Basin. Arctic, 27(4). https://doi.org/10.14430/arctic2886

Nozaki, Y., Horibe, Y., and Tsubota, H. (1981). The water column distributions of thorium isotopes in the western North Pacific. Earth and Planetary Science Letters, 54(2), 203–216. https://doi.org/10.1016/0012-821X(81)90004-2

O'Brien, M. C., Macdonald, R. W., Melling, H., and Iseki, K. (2006). Particle fluxes and geochemistry on the Canadian Beaufort Shelf: Implications for sediment transport and deposition. Continental Shelf Research, 26(1), 41–81. https://doi.org/10.1016/j.csr.2005.09.007

O'Brien, M. C., Melling, H., Pedersen, T. F., and Macdonald, R. W. (2013). The role of eddies on particle flux in the Canada Basin of the Arctic Ocean. Deep-Sea Research Part I: Oceanographic Research Papers, 71, 1–20. https://doi.org/10.1016/j.dsr.2012.10.004

Piepgras, D. J., Wasserburg, G. J., and Dasch, E. J. (1979). The isotopic composition of Nd in different ocean masses. Earth and Planetary Science Letters, 45, 223–236.

Polyakov, I. V., Pnyushkov, A. V., Rember, R., Padman, L., Carmack, E. C., and Jackson, J. M. (2013). Winter Convection Transports Atlantic Water Heat to the Surface Layer in the Eastern Arctic Ocean*. Journal of Physical Oceanography, 43(10), 2142–2155. https://doi.org/10.1175/JPO-D-12-0169.1

Porcelli, D., Andersson, P. S., Baskaran, M., Frank, M., Björk, G., and Semiletov, I. (2009). The distribution of neodymium isotopes in Arctic Ocean basins. Geochimica et Cosmochimica Acta, 73(9), 2645–2659. https://doi.org/10.1016/j.gca.2008.11.046

Pörtner, H. O., Karl, D. M., Boyd, P. W., Cheung, W. W. L., Lluch-Cota, S. E., Nojiri, Y., *et al.* (2015). Ocean systems. Climate Change 2014 Impacts, Adaptation and Vulnerability: Part A: Global and Sectoral Aspects. https://doi.org/10.1017/CBO9781107415379.011

Quadfasel, D., Sy, A., Wells, D., and Tunik, A. (1991). Warming in the Arctic. Nature, 350(6317), 385. https://doi.org/10.1038/350385a0

Rabe, B., Schauer, U., Ober, S., Horn, M., Hoppmann, M., Korhonen, M., *et al.* (2016). Physical oceanography measured on water bottle samples during POLARSTERN cruise PS94 (ARK-XXIX/3). Bremerhaven, PANGAEA. https://doi.org/10.1594/PANGAEA.859559

Rail, M.-E., Gratton, Y., and Prieur, L. (2011). DISTRIBUTION OF TEMPERATURE AND SALINITY IN THE CANADIAN ARCTIC ARCHIPELAGO DURING THE 2009 ARCTICNET SAMPLING EXPEDITION. https://doi.org/10.1107/S090904959801677X S090904959801677X [pii]

Rempfer, J., Stocker, T. F., Joos, F., Lippold, J., and Jaccard, S. L. (2017). New insights into cycling of $^{231}$Pa and $^{230}$Th in the Atlantic Ocean. Earth and Planetary Science Letters, 468, 27–37. https://doi.org/10.1016/j.epsl.2017.03.027

Roeske, T., Loeff, R. vd M., Middag, R., and Bakker, K. (2012). Deep water circulation and composition in the Arctic Ocean by dissolved barium, aluminium and silicate. Marine Chemistry, 132–133, 56–67. https://doi.org/10.1016/j.marchem.2012.02.001

Rudels, B. (2001). Arctic basin circulation. In J. Steele, K. K. Turekian, and S. A. Thorpe (Eds.), Encyclopedia of Ocean Sciences (pp. 177–187). San Diego: Academic Press. https://doi.org/10.1016/rwos.2001.0372

Rudels, B. (2009). Arctic Ocean Circulation. Encyclopedia of Ocean Sciences, 211–225. https://doi.org/10.1016/B978-012374473-9.00601-9

Rudels, B., Schauer, U., Björk, G., Korhonen, M., Pisarev, S., Rabe, B., and Wisotzki, A. (2013). Observations of water masses and circulation with focus on the Eurasian Basin of the Arctic Ocean from the 1990s to the late 2000s. Ocean Science, 9(1), 147–169. https://doi.org/10.5194/os-9-147-2013

Schauer, U. (2008). ARKTIS-XXII/2, The Expedition 2007, of the Research Vessel "Polarstern" in. Reports on Polar and Marine Research.

Schauer, U. (2016). The Expedition PS94 of the Research Vessel POLARSTERN to the central Arctic Ocean in 2015. Reports on Polar and Marine Research (Vol. 703). Bremerhaven. https://doi.org/10.2312/BzPM_0703_2016

Schauer, U., Rudels, B., Jones, E. P., Anderson, L. G., Muench, R. D., Björk, G., *et al.* (2002). Confluence and redistribution of Atlantic water in the Nansen, Amundsen and Makarov basins. Annales Geophysicae, 20(2), 257–273. https://doi.org/10.5194/angeo-20-257-2002

Schauer, U., Fahrbach, E., Osterhus, S., and Rohardt, G. (2004). Arctic warming through the Fram Strait: Oceanic heat transport from 3 years of measurements. Journal of Geophysical Research C: Oceans, 109(6), 1–14. https://doi.org/10.1029/2003JC001823

Schlitzer, R. (2015). Ocean Data View. Retrieved from http://odv.awi.de.

Scholten, J. C., Rutgers van der Loeff, M. M., and Michel, A. (1995). Distribution of $^{230}$Th and $^{231}$Pa in the water column in relation to the ventilation of the deep Arctic basins. Deep-Sea Research Part II, 42(6), 1519–1531. https://doi.org/10.1016/0967-0645(95)00052-6

Smethie, W. M., Schlosser, P., Bönisch, G., and Hopkins, T. S. (2000). Renewal and circulation of intermediate waters in the Canadian Basin observed on the SCICEX 96 cruise. Journal of Geophysical Research: Oceans, 105(C1), 1105–1121.

Steele, M., Morison, J., Ermold, W., Rigor, I., Ortmeyer, M., and Shimada, K. (2004). Circulation of summer Pacific halocline water in the Arctic Ocean. Journal of Geophysical Research, 109(C2), C02027. https://doi.org/10.1029/2003JC002009

Swift, J. H., Jones, E. P., Aagaard, K., Carmack, E. C., Hingston, M., Macdonald, R. W., *et al.* (1997). Waters of the Makarov and Canada basins. Deep-Sea Research Part II: Topical Studies in Oceanography, 44(8), 1503–1529. https://doi.org/10.1016/S0967-0645(97)00055-6

Tachikawa, K., Athias, V., and Jeandel, C. (2003). Neodymium budget in the modern ocean and paleo-oceanographic implications. Journal of Geophysical Research, 108(C8), 3254. https://doi.org/10.1029/1999JC000285

Timmermans, M.-L., Garrett, C., and Carmack, E. (2003). The thermohaline structure and evolution of the deep waters in the Canada Basin, Arctic Ocean. Deep-Sea Research Part I: Oceanographic Research Papers, 50(10–11), 1305–1321. https://doi.org/10.1016/S0967-0637(03)00125-0

Timmermans, M.-L., Winsor, P., and Whitehead, J. A. (2005). Deep-Water Flow over the Lomonosov Ridge in the Arctic Ocean. Journal of Physical Oceanography, 35(8), 1489–1493. https://doi.org/10.1175/JPO2765.1

Timmermans, M.-L., Toole, J., Proshutinsky, A., Krishfield, R., and Plueddemann, A. (2008). Eddies in the Canada Basin, Arctic Ocean, Observed from Ice-Tethered Profilers. Journal of Physical Oceanography, 38(1), 133–145. https://doi.org/10.1175/2007JPO3782.1

Timmermans, M.-L., Proshutinsky, A., Golubeva, E., Jackson, J. M., Krishfield, R., McCall, M., *et al.* (2014). Mechanisms of Pacific Summer Water variability in the Arctic's Central Canada Basin. Journal of Geophysical Research: Oceans, 119(11), 7523–7548. https://doi.org/10.1002/2014JC010273

Trimble, S. M., Baskaran, M., and Porcelli, D. (2004). Scavenging of thorium isotopes in the Canada Basin of the Arctic Ocean. Earth and Planetary Science Letters, 222(3–4), 915–932. https://doi.org/10.1016/j.epsl.2004.03.027

Turekian, K. K., and Chan, L. H. (1971). The marine geochemistry of the uranium isotopes, $^{230}$Th and $^{231}$Pa. In A. O. Brunfelt and E. Steinnes (Eds.), Activation Analysis in Geochemistry and Cosmochemistry (Universite, pp. 311–320). Oslo.

Valk, O., Rutgers van der Loeff, M. M., Geibert, W., Gdaniec, S., Rijkenberg, M. J. A., Moran, S. B., *et al.* (2018). Importance of hydrothermal vents in scavenging removal of $^{230}$Th in the Nansen Basin. Geophysical Research Letters, 1–10. https://doi.org/10.1029/2018GL079829

Watanabe, E. (2011). Beaufort shelf break eddies and shelf-basin exchange of Pacific summer water in the western Arctic Ocean detected by satellite and modeling analyses. Journal of Geophysical Research: Oceans, 116(8), 1–16. https://doi.org/10.1029/2010JC006259

Woodgate, R. A., Aagaard, K., Swift, J. H., Smethie, W. M., and Falkner, K. K. (2007). Atlantic water circulation over the Mendeleev Ridge and Chukchi Borderland from thermohaline intrusions and water mass properties. Journal of Geophysical Research: Oceans, 112(2), 1–20. https://doi.org/10.1029/2005JC003416

Yu, X., Allen, S.E., François, R., Grenier, M., Myers, P.G., Hu, X., 2020. Modelling Dissolved and Particulate Th in the Canada Basin: Implications for Recent Changes in Particle Flux and Intermediate Circulation. Journal of Geophysical Research: Oceans 125 (2), e2019JC015640.

Zhao, M., Timmermans, M.-L., Cole, S., Krishfield, R., Proshutinsky, A., and Toole, J. (2014). Characterizing the eddy field in the Arctic Ocean halocline. Journal of Geophysical Research: Oceans, 119(12), 8800–8817. https://doi.org/10.1002/2014JC010488

Zhao, M., Timmermans, M., Cole, S., Krishfield, R., and Toole, J. (2016). Evolution of the eddy field in the Arctic Ocean's Canada Basin , 2005 – 2015. Geophical Research Letters, 43(May), 8106–8114. https://doi.org/10.1002/2016GL069671

# CHAPTER 7: Conclusions and Perspectives

## Main Conclusions

The main aim of this thesis was to identify removal processes of $^{230}$Th and $^{231}$Pa in order to determine effects of environmental changes on scavenging behaviour and export of particle reactive trace elements. In order to achieve this, a time series of dissolved $^{230}$Th and $^{231}$Pa from 1991 over 2007 to 2015 was established, allowing to determine changes over time and to interpret their implications in relation to changing environmental conditions. The main aims of this thesis were broken down to the following questions:

**I)** What are the natural background processes affecting $^{231}$Pa and $^{230}$Th in the Arctic Ocean?

- Hydrothermal plumes emitted from major submarine volcanic eruptions at the Gakkel Ridge caused a drastic reduction of dissolved $^{230}$Th below 2000 m in the central Nansen Basin in only eight years. This scavenging event took place between 2007 and 2015. It shows the importance of scavenging removal of trace elements during or after phases of hydrothermal or volcanic activity in the Nansen Basin. These eruptions might present not only a source to but also an important removal process of trace elements in the deep Nansen Basin.
- Dissolved $^{230}$Th concentrations decreased by 50% in the central Amundsen Basin above 1500 m and by 30% below 1500 m between 2007 and 2015. This depletion is ascribed to increased scavenging removal of $^{230}$Th from inflowing Atlantic waters over the Barents Sea shelf and along the margins of the Nansen Basin.
- Increased scavenging removal of $^{230}$Th at the margins of the Eurasian Basin leads to reduced export of $^{230}$Th out of the Arctic Ocean, potentially influencing sediment inventories in the GIN Seas over time.
- Boundary scavenging removes significant amounts of $^{230}$Th at the Nansen Basin margin.

**II)** Do ongoing environmental changes in the Arctic Ocean already result in measurable changes in $^{230}$Th and $^{231}$Pa concentrations and distributions and what are the implications?

- $^{230}$Th and $^{231}$Pa concentrations decreased over time from the 1980s to 2015 in the entire Amerasian Basin due to increased scavenging removal and variations in circulation and water mass mixing. Particularly the Canada Basin experiences an

increase of lithogenic and biological particle fluxes, due to sea ice retreat and intensified lateral input of margin sediments. Hence climate change causes changes on $^{230}$Th and $^{231}$Pa concentrations in the entire Amerasian Basin.

**III)** To which extent can the budgets of $^{231}$Pa and $^{230}$Th in the Arctic Ocean be used to trace important environmental processes in time?

- Water column inventories of dissolved $^{230}$Th and $^{231}$Pa are variable in the central Arctic Ocean. Especially inventories of dissolved $^{230}$Th can change rather quickly in the central Arctic Ocean. Dissolved $^{230}$Th decreased by up to 50% from 2007 to 2015.
- $^{230}$Th and $^{231}$Pa budgets and box model calculations, based on water column time series, indicate that the Eurasian Basin margins become a sink for $^{230}$Th, and possibly $^{231}$Pa. Export of $^{231}$Pa out of the Arctic Ocean may be less important than previously thought.

An important finding of the research conducted in the framework of this thesis is the high variability of dissolved $^{230}$Th and $^{231}$Pa inventories in the Arctic Ocean. Their water column concentrations and distributions can change significantly over the course of only eight years. In addition to the temporal variability there are also spatial differences in $^{230}$Th and $^{231}$Pa concentrations and depth distributions within one basin, indicating the importance of local features, such as hydrothermal vents. Furthermore the quite high temporal variability of $^{230}$Th and $^{231}$Pa concentrations and distributions highlights the importance of repetitive sampling campaigns. On a broader scale this finding implies that it is important to take samples at several stations per basin and choose their location in a way that allows comparison with previous expeditions, but that also covers areas that can be expected to be under the influence of different processes.

Valk *et al.* (2018), Grenier *et al.* (2019) and Valk *et al.* (2020) have shown that it is valuable to have repeated sampling campaigns, allowing the creation of time series of naturally occurring radionuclides. It is also good to have data from different locations distributed over potential inflow passages of Atlantic waters. Their findings, based on the dissolved $^{230}$Th and $^{231}$Pa time series, show that it is important to cross features, like a transect from the shelves to the central basins, as shown by Gdaniec *et al.* (2020), but also choose stations along a feature, e.g. following circulation pathways.

The high variability of $^{230}$Th and $^{231}$Pa concentrations and distributions in the Arctic Ocean is expressed by a reduction or an increase of $^{230}$Th and $^{231}$Pa in certain basins and depth ranges of the Eurasian and Amerasian Basin over the past 26 years, but especially after 2007. Different processes are responsible for the temporal developments of $^{230}$Th and $^{231}$Pa in the Arctic Ocean. Some of these processes are caused by climate change, such as increased particle fluxes at the margins of the Nansen and Canada Basins (Dalpadado *et al.*, 2020; Günther *et al.*, 2013; Jensen *et al.*, 2020), but others are caused by seismic events, like the volcanic eruptions at the Gakkel Ridge (Sohn *et al.*, 2008). None of the studies on $^{230}$Th developments in the Eurasian Basin, presented in this thesis, give evidence for increased particle fluxes from the surface within the central Eurasian Basin. Hence particles from increasing particle input from the shelves, surrounding continents, slopes and sea ice retreat do not yet reach the central basins or not yet in full strength, but the signals of such processes can be observed in the central basins.

The finding, that scavenging removal of $^{230}$Th increases, especially at the margins of the Arctic Ocean, shows the importance of basin-margin exchange and interaction. Time series of dissolved $^{230}$Th and water column profiles of 2015 particulate and dissolved $^{230}$Th, $^{232}$Th and partly $^{231}$Pa indicate increasing scavenging removal of $^{230}$Th along the Nansen Basin margin and in the Barents Sea. This increase in scavenging intensity makes the margins of the Eurasian Basin a sink for $^{230}$Th. This could indicate that these areas are or become also sinks for other trace elements, such as Fe. If trace elements, including micro nutrients, whose inputs to the Arctic Ocean increase (Klunder *et al.*, 2012; Peterson *et al.*, 2002; Rijkenberg *et al.*, 2018), are removed directly or soon after entering the central Arctic Ocean by scavenging removal, it would decrease the availability of nutrients for central Arctic Ocean ecosystems. This is reflected by $^{230}$Th scavenging removal from inflowing Atlantic waters as they flow along the margin of the Nansen Basin and through the Barents Sea. When entering the Amundsen Basin those waters have undergone significant scavenging removal of $^{230}$Th and have lost a major amount of their dissolved $^{230}$Th content. Therefore those $^{230}$Th depleted waters decrease the $^{230}$Th inventory in the upper Amundsen Basin by reducing the lateral $^{230}$Th supply. This process also has influence on the deep waters below 1500 m, where dissolved $^{230}$Th also decreased after 2007. This decrease is due to reversible scavenging transporting the depletion signal from above 1500 m downwards. This highlights the importance of shelf-basin interactions, as well as the connection of horizontal transport by advection and vertical fluxes by (reversible) scavenging removal. If this process also affects other trace elements it would result in a significantly reduced input of those to the central Arctic Ocean and eventually to the GIN Seas. Hence increased

scavenging at Eurasian Basin margins has impact on Arctic Ocean and Atlantic Ocean ecosystems. Decreased export of $^{230}$Th through the Fram Strait also is important for the interpretation of $^{230}$Th accumulation in sediments from the GIN Seas. Such influences could impact the future development of $^{230}$Th sediment accumulation and the $^{231}$Pa/$^{230}$Th ratio in GIN Sea sediments, as well as the interpretation of existing sediment records. Both would only be measurable if the underlying conditions, driving the removal process, persist long enough to exceed the threshold set by sedimentation rates and bioturbation depths. Hence there might be periods of similar export situations from past climate transitions showing similar $^{230}$Th and $^{231}$Pa export patterns, as set by the current climate changes, preserved in sediments, albeit probably hidden under background sedimentation situation patterns. Combined with the hypothesis that $^{231}$Pa advective export out of the Arctic Ocean is less important than previously assumed and that $^{231}$Pa scavenging removal plays a more important role, the interpretation of the sedimentary $^{231}$Pa/$^{230}$Th ratio might need to be adapted.

Increased particle fluxes at the Nansen Basin margins cause more intense scavenging of particle reactive elements, such as $^{230}$Th. In combination with potentially increased exchange between the central Eurasian Basin and its margins, due to changing surface currents, increased upwelling or re-circulation and lateral eddy transport, it could lead to the establishment or the intensification of boundary scavenging in the Eurasian Basin. This would decrease the input to the central Arctic Ocean of trace elements and nutrients from several sources. Externally derived trace elements from the Atlantic Ocean, such as Th, will be removed by scavenging removal at the inflow passages. Trace elements and particle reactive (micro) nutrients from sources within the Arctic, such as Fe from riverine discharge for example, will be removed during the transport from their sources through the Barents Sea and subsequently during their transit in the Boundary Current along the Nansen Basin margin. Furthermore, if there will be a fully developed boundary scavenging situation, the exchange flux between the margin and the central basin, at least parts of it, would also contribute to a reduction of TPD transported dissolved trace elements in the central basins. Those trace elements would otherwise be excluded from margin scavenging, due to their relatively fast transport out of the Arctic Ocean, but might become subject of boundary scavenging by recirculation.

In addition to climate change, seismic activity, controlling hydrothermal venting as well as volcanic eruptions, is important in terms of $^{230}$Th scavenging removal over time. Eruptions following a major earthquake swarm in 2001 (Riedel and Schlindwein, 2010; Schlindwein *et al.*, 2005) released huge amounts of hydrothermal fluids and particles, which were travelling in the

deep Nansen Basin as a hydrothermal plume. Due to its buoyancy this plume did not influence waters above 2000 m (Baker *et al.*, 2004). In the deep Nansen Basin below 2000 m particles, probably iron Fe oxy-hydroxide particles or dissolved Fe that reacted with particles there, caused a significant scavenging removal of $^{230}$Th by 2015. This scavenging removal can be translated to the removal of other particle reactive elements. It shows the importance of major explosive submarine volcanic eruptions for inventories and budgets of scavenging prone trace elements in the deep Nansen Basin by adding an effective sink. Furthermore, those scavenging events can bias the annual sediment accumulation of $^{230}$Th in the deep Nansen Basin, and probably, due to deep water circulation, as well at its slopes. Both the hydrothermal plume in 2007, represented by dissolved Fe (Klunder *et al.*, 2012), and its consequences on dissolved $^{230}$Th by 2015, based on $^{230}$Th and dissolved Fe reduction (Klunder *et al.*, 2012; Rijkenberg *et al.*, 2018; Valk *et al.*, 2018), were observed in the Nansen Basin and only to a much smaller degree, if at all, in the Amundsen Basin. This underpins the theory of distinct deep water (re)circulation within the Nansen Basin, minimizing deep waters from exchange with the Amundsen Basin over the Gakkel Ridge, as proposed by Valk *et al.* (2018).

Summarizing the major findings of the research presented in this thesis, climate change caused notable changes in $^{230}$Th and $^{231}$Pa concentrations and distributions over the past 26 years, especially after 2007. This implies that climate change also affects other particle reactive trace elements. Whether these changes result in measurable changes in concentration and distribution depends on the particle reactivity of specific elements and their isotopes, defined by their scavenging residence times, as well as on other element-specific removal mechanisms, like biological consumption. Finally one can conclude that climate change caused or intensified removal processes of $^{230}$Th will have an impact on sedimentary $^{230}$Th accumulation and therefore also on the sedimentary $^{231}$Pa/$^{230}$Th activity ratios in the Arctic Ocean and the GIN Seas. The measurability of these consequences depends on the duration of these conditions, with respect to sedimentation rates and bioturbation depths in the areas of deposition.

**Perspectives**

While the temporal development of $^{230}$Th in the Eurasian Basin is rather well described and understood (Valk *et al.*, 2020; Valk *et al.*, 2018), the temporal development of $^{231}$Pa is much less clear and still leaves questions open.

It would be interesting to investigate if dissolved $^{231}$Pa reacts to the processes that control the $^{230}$Th removal in recent years with a temporal delay, set by the lower particle reactivity of $^{231}$Pa. The eight years between 2007 and 2015 seem to be too short for $^{231}$Pa to fully adapt to

environmental changes and possible changing (boundary) scavenging conditions at the margins of the Eurasian Basin, as well as in the deep Nansen Basin.

Although there are indications for increasing $^{231}$Pa scavenging at the margins, there is no evident decrease in dissolved $^{231}$Pa inventories between 2007 and 2015, as reported for dissolved $^{230}$Th. Answering this question would allow determining effects of changing climate conditions on the Arctic export $^{231}$Pa/$^{230}$Th ratio and subsequent sedimentation in the GIN Seas. In order to identify the reason for the lack of $^{231}$Pa in Arctic sediments it would be helpful to collect and analyse sediment cores from the margins of the Eurasian Basin and from the Barents Sea.

The importance of hydrothermal vents for scavenging removal of $^{230}$Th after submarine volcanic eruptions at the Gakkel Ridge shows the importance of a combination of geochemistry and geophysical research. It would be interesting to investigate the development of particulate and dissolved $^{230}$Th and $^{231}$Pa in a high resolution time series after earthquake triggered explosive eruptions, in order to evaluate the theory of hydrothermal scavenging presented in (Valk *et al.*, 2018). Investigating $^{230}$Th and $^{231}$Pa developments after submarine volcanic eruptions has the potential to increase knowledge about removal processes of various trace elements over time. Hence it seems to be interesting to compare the findings from the Arctic Ocean with other ocean basins, where seismic active ridges are present. Especially other ultra-slow spreading ridges might be comparable, like the Southwest Indian Ridge (Schmid *et al.*, 2017), or probably better suited, although having much faster spreading ridges, the Eastern Mediterranean Sea, due to its enclosed nature, which is comparable to the Eurasian Basin, in terms of retaining a hydrothermal plume over time.

In order to understand $^{230}$Th and $^{231}$Pa developments on an entire Arctic Ocean scale, it would be promising to create a circulation-scavenging model for the Eurasian Basin and the entire Arctic Ocean as Yu *et al.* (2020) did for the Amerasian Basin.

Finally analysing and interpreting samples obtained from the Fram Strait during GEOTRACES section GN05 (*RV Polarstern* (PS100), 2016) would be a crucial step in identifying exchange of trace elements between the Arctic Ocean and the Atlantic Ocean. These data are also key in answering the question where the missing $^{231}$Pa in the Arctic Ocean is deposited.

**References**

Baker, E.T., Edmonds, H.N., Michael, P.J., Bach, W., Dick, H.J.B., Snow, J.E., Walker, S.L., Banerjee, N.R., Langmuir, C.H., 2004. Hydrothermal venting in magma deserts: The ultraslow-spreading Gakkel and Southwest Indian Ridges. Geochemistry, Geophysics, Geosystems 5 (8).

Dalpadado, P., Arrigo, K.R., van Dijken, G.L., Skjoldal, H.R., Bagøien, E., Dolgov, A.V., Prokopchuk, I.P., Sperfeld, E., 2020. Climate effects on temporal and spatial dynamics of phytoplankton and zooplankton in the Barents Sea. Progress in Oceanography 185, 102320.

Gdaniec, S., Roy-Barman, M., Levier, M., Valk, O., van der Loeff, M.R., Foliot, L., Dapoigny, A., Missiaen, L., Mörth, C.-M., Andersson, P.S., 2020. $^{231}$Pa and $^{230}$Th in the Arctic Ocean: Implications for boundary scavenging and $^{231}$Pa-$^{230}$Th fractionation in the Eurasian Basin. Chemical Geology 532, 119380.

Grenier, M., François, R., Soon, M., Rutgers van der Loeff, M., Yu, X., Valk, O., Not, C., Moran, S.B., Edwards, R.L., Lu, Y., Lepore, K., Allen, S.E., 2019. Changes in Circulation and Particle Scavenging in the Amerasian Basin of the Arctic Ocean over the Last Three Decades Inferred from the Water Column Distribution of Geochemical Tracers. Journal of Geophysical Research: Oceans 124 (12), 9338-9363.

Günther, F., Overduin, P.P., Sandakov, A.V., Grosse, G., Grigoriev, M.N., 2013. Short- and long-term thermo-erosion of ice-rich permafrost coasts in the Laptev Sea region. Biogeosciences 10 (6), 4297-4318.

Jensen, L.T., Morton, P., Twining, B.S., Heller, M.I., Hatta, M., Measures, C.I., John, S., Zhang, R., Pinedo-Gonzalez, P., Sherrell, R.M., Fitzsimmons, J.N., 2020. A comparison of marine Fe and Mn cycling: U.S. GEOTRACES GN01 Western Arctic case study. Geochimica et Cosmochimica Acta.

Klunder, M.B., Laan, P., Middag, R., de Baar, H.J.W., Bakker, K., 2012. Dissolved iron in the Arctic Ocean: Important role of hydrothermal sources, shelf input and scavenging removal. Journal of Geophysical Research-Oceans 117 (C4).

Peterson, B.J., Holmes, R.M., McClelland, J.W., Vörösmarty, C.J., Lammers, R.B., Shiklomanov, A.I., Shiklomanov, I.A., Rahmstorf, S., 2002. Increasing River Discharge to the Arctic Ocean. Science 298 (5601), 2171-2173.

Riedel, C., Schlindwein, V., 2010. Did the 1999 earthquake swarm on Gakkel Ridge open a volcanic conduit? A detailed teleseismic data analysis. Journal of Seismology 14 (3), 505-522.

Rijkenberg, M.J.A., Slagter, H.A., Rutgers van der Loeff, M., van Ooijen, J., Gerringa, L.J.A., 2018. Dissolved Fe in the Deep and Upper Arctic Ocean With a Focus on Fe Limitation in the Nansen Basin. Frontiers in Marine Science 5 (88).

Schlindwein, V., Müller, C., Jokat, W., 2005. Seismoacoustic evidence for volcanic activity on the ultraslow-spreading Gakkel Ridge, Arctic Ocean. Geophysical Research Letters 32 (18), n/a-n/a.

Schmid, F., Schlindwein, V., Koulakov, I., Plötz, A., Scholz, J.-R., 2017. Magma plumbing system and seismicity of an active mid-ocean ridge volcano. 7, 42949.

Sohn, R.A., Willis, C., Humphris, S., Shank, T.M., Singh, H., Edmonds, H.N., Kunz, C., Hedman, U., Helmke, E., Jakuba, M., Liljebladh, B., Linder, J., Murphy, C., Nakamura, K.-i., Sato, T., Schlindwein, V., Stranne, C., Tausenfreund, M., Upchurch, L., Winsor, P., Jakobsson, M., Soule, A., 2008. Explosive volcanism on the ultraslow-spreading Gakkel ridge, Arctic Ocean. Nature 453 (7199), 1236-1238.

Valk, O., Rutgers van der Loeff, M.M., Geibert, W., Gdaniec, S., Moran, S.B., Lepore, K., Edwards, R.L., Lu, Y., Puigcorbé, V., Casacuberta, N., Paffrath, R., Smethie, W., Roy-Barman, M., 2020. Decrease in $^{230}$Th in the Amundsen Basin since 2007: far-field effect of increased scavenging on the shelf? Ocean Sci. 16 (1), 221-234.

Valk, O., Rutgers van der Loeff, M.M., Geibert, W., Gdaniec, S., Rijkenberg, M.J.A., Moran, S.B., Lepore, K., Edwards, R.L., Lu, Y., Puigcorbé, V., 2018. Importance of Hydrothermal Vents in Scavenging Removal of $^{230}$Th in the Nansen Basin. Geophysical Research Letters 0 (0).

Yu, X., Allen, S.E., François, R., Grenier, M., Myers, P.G., Hu, X., 2020. Modeling Dissolved and Particulate Th in the Canada Basin: Implications for Recent Changes in Particle Flux and Intermediate Circulation. Journal of Geophysical Research: Oceans 125 (2), e2019JC015640.

# APPENDIX

**Table A1: Dissolved $^{230}$Th, $^{231}$Pa and $^{232}$Th from 2007 and 2015.**

| Year | Cruise | Station-Cast | Lat. | Long. | depth | $^{230}$Th | err | $^{231}$Pa | err | $^{232}$Th | err |
|---|---|---|---|---|---|---|---|---|---|---|---|
| | | | | | [m] | [uBq/kg] | [uBq/kg] | [uBq/kg] | [uBq/kg] | [pmol/kg] | [pmol/kg] |
| 2015 | PS94 | 50-4 | 84.399 | 30.715 | 50 | 2.522 | 0.130 | 0.525 | 0.175 | 0.174 | 0.003 |
| 2015 | PS94 | 50-4 | 84.399 | 30.715 | 100 | 2.598 | 0.138 | 0.525 | 0.175 | 0.205 | 0.004 |
| 2015 | PS94 | 50-4 | 84.399 | 30.715 | 300 | 1.406 | 0.107 | 0.700 | 0.175 | 0.153 | 0.002 |
| 2015 | PS94 | 50-4 | 84.399 | 30.715 | 500 | 4.142 | 0.130 | 0.350 | 0.175 | 0.257 | 0.003 |
| 2015 | PS94 | 50-4 | 84.399 | 30.715 | 750 | 4.845 | 0.138 | 1.399 | 0.175 | 0.242 | 0.002 |
| 2015 | PS94 | 50-4 | 84.399 | 30.715 | 1000 | 6.053 | 0.145 | 1.050 | 0.175 | 0.172 | 0.002 |
| 2015 | PS94 | 50-4 | 84.399 | 30.715 | 1500 | 8.154 | 0.145 | 2.099 | 0.175 | 0.151 | 0.001 |
| 2015 | PS94 | 50-4 | 84.399 | 30.715 | 2000 | 11.043 | 0.267 | 3.324 | 0.175 | 0.168 | 0.003 |
| 2015 | PS94 | 50-4 | 84.399 | 30.715 | 2500 | 3.531 | 0.122 | 3.498 | 0.175 | 0.050 | 0.001 |
| 2015 | PS94 | 50-4 | 84.399 | 30.715 | 3000 | 3.783 | 0.138 | 2.799 | 0.175 | 0.065 | 0.001 |
| 2015 | PS94 | 50-4 | 84.399 | 30.715 | 3500 | 4.853 | 0.145 | 3.498 | 0.175 | 0.048 | 0.001 |
| 2015 | PS94 | 50-4 | 84.399 | 30.715 | 3990 | 6.015 | 0.130 | 3.673 | 0.175 | 0.058 | 0.000 |
| 2015 | PS94 | 58-3 | 85.297 | 59.935 | 50 | 0.023 | 0.084 | 1.132 | 0.228 | 0.044 | 0.001 |
| 2015 | PS94 | 58-3 | 85.297 | 59.935 | 100 | 1.536 | 0.122 | 1.904 | 0.229 | 0.015 | 0.000 |
| 2015 | PS94 | 58-3 | 85.297 | 59.935 | 200 | 3.691 | 0.153 | 1.622 | 0.229 | 0.157 | 0.003 |
| 2015 | PS94 | 58-3 | 85.297 | 59.935 | 200 | 3.821 | 0.191 | 1.684 | 0.229 | 0.415 | 0.011 |
| 2015 | PS94 | 58-3 | 85.297 | 59.935 | 300 | 2.896 | 0.138 | 2.398 | 0.229 | 0.143 | 0.002 |
| 2015 | PS94 | 58-3 | 85.297 | 59.935 | 500 | 2.018 | 0.153 | 2.421 | 0.229 | 0.153 | 0.005 |
| 2015 | PS94 | 58-3 | 85.297 | 59.935 | 1000 | 2.835 | 0.130 | 2.573 | 0.229 | 0.019 | 0.000 |
| 2015 | PS94 | 58-3 | 85.297 | 59.935 | 1500 | 4.692 | 0.183 | 3.036 | 0.229 | 0.460 | 0.009 |
| 2015 | PS94 | 58-3 | 85.297 | 59.935 | 2000 | 8.338 | 0.267 | 3.276 | 0.229 | 0.119 | 0.003 |
| 2015 | PS94 | 58-3 | 85.297 | 59.935 | 2500 | 6.725 | 0.145 | 3.509 | 0.229 | 0.446 | 0.004 |
| 2015 | PS94 | 58-3 | 85.297 | 59.935 | 3000 | 4.838 | 0.138 | 3.189 | 0.229 | 0.024 | 0.000 |
| 2015 | PS94 | 58-3 | 85.297 | 59.935 | 3500 | 5.036 | 0.199 | 3.407 | 0.229 | 0.122 | 0.003 |
| 2015 | PS94 | 58-3 | 85.297 | 59.935 | 3860 | 5.403 | 0.183 | 4.733 | 0.229 | 0.034 | 0.001 |
| 2015 | PS94 | 68-1 | 86.997 | 58.615 | 50 | 2.522 | 0.130 | 0.320 | 0.228 | 0.339 | 0.006 |
| 2015 | PS94 | 68-1 | 86.997 | 58.615 | 100 | 3.523 | 0.138 | 0.413 | 0.228 | 0.259 | 0.004 |
| 2015 | PS94 | 68-1 | 86.997 | 58.615 | 200 | 4.417 | 0.138 | 0.768 | 0.228 | 0.224 | 0.003 |
| 2015 | PS94 | 68-1 | 86.997 | 58.615 | 300 | 5.319 | 0.153 | 1.451 | 0.229 | 0.228 | 0.003 |
| 2015 | PS94 | 68-1 | 86.997 | 58.615 | 500 | 5.632 | 0.153 | 1.582 | 0.229 | 0.200 | 0.002 |
| 2015 | PS94 | 68-1 | 86.997 | 58.615 | 1000 | 5.487 | 0.130 | 1.663 | 0.229 | 0.222 | 0.002 |
| 2015 | PS94 | 68-1 | 86.997 | 58.615 | 1500 | 7.085 | 0.176 | 2.773 | 0.229 | 0.134 | 0.002 |
| 2015 | PS94 | 68-1 | 86.997 | 58.615 | 2000 | 3.890 | 0.138 | 1.844 | 0.229 | 0.054 | 0.001 |
| 2015 | PS94 | 68-1 | 86.997 | 58.615 | 2600 | 4.945 | 0.138 | 3.155 | 0.229 | 0.064 | 0.001 |
| 2015 | PS94 | 68-1 | 86.997 | 58.615 | 3000 | 4.937 | 0.130 | 3.250 | 0.229 | 0.042 | 0.000 |
| 2015 | PS94 | 68-1 | 86.997 | 58.615 | 3500 | 5.632 | 0.153 | 3.454 | 0.229 | 0.041 | 0.000 |
| 2015 | PS94 | 68-1 | 86.997 | 58.615 | 4000 | 6.450 | 0.160 | 3.585 | 0.229 | 0.072 | 0.001 |

| Year | Cruise | Station-Cast | Lat. | Long. | depth | $^{230}$Th | err | $^{231}$Pa | err | $^{232}$Th | err |
|---|---|---|---|---|---|---|---|---|---|---|---|
| | | | | | [m] | [uBq/kg] | [uBq/kg] | [uBq/kg] | [uBq/kg] | [pmol/kg] | [pmol/kg] |
| 2015 | PS94 | 68-1 | 86.997 | 58.615 | 4850 | 7.299 | 0.168 | 3.648 | 0.229 | 0.066 | 0.001 |
| 2015 | PS94 | 81-5 | 88.992 | 61.155 | 50 | 2.377 | 0.122 | 0.153 | 0.228 | 0.492 | 0.007 |
| 2015 | PS94 | 81-5 | 88.992 | 61.155 | 100 | 3.156 | 0.115 | 0.538 | 0.228 | 0.219 | 0.002 |
| 2015 | PS94 | 81-5 | 88.992 | 61.155 | 200 | 2.484 | 0.122 | 0.270 | 0.228 | 0.316 | 0.005 |
| 2015 | PS94 | 81-5 | 88.992 | 61.155 | 300 | 3.378 | 0.176 | 1.157 | 0.229 | 0.229 | 0.006 |
| 2015 | PS94 | 81-5 | 88.992 | 61.155 | 500 | 3.966 | 0.153 | 1.186 | 0.229 | 0.201 | 0.003 |
| 2015 | PS94 | 81-5 | 88.992 | 61.155 | 1000 | 2.759 | 0.115 | 2.369 | 0.229 | 0.136 | 0.002 |
| 2015 | PS94 | 81-5 | 88.992 | 61.155 | 1500 | 3.928 | 0.237 | 2.101 | 0.229 | 0.135 | 0.005 |
| 2015 | PS94 | 81-5 | 88.992 | 61.155 | 2000 | 4.242 | 0.138 | 1.911 | 0.229 | 0.132 | 0.002 |
| 2015 | PS94 | 81-5 | 88.992 | 61.155 | 2000 | 4.417 | 0.145 | 2.529 | 0.229 | 0.233 | 0.003 |
| 2015 | PS94 | 81-5 | 88.992 | 61.155 | 2500 | 5.426 | 0.176 | 2.615 | 0.229 | 0.134 | 0.002 |
| 2015 | PS94 | 81-5 | 88.992 | 61.155 | 2500 | 5.319 | 0.160 | 2.940 | 0.229 | 0.150 | 0.002 |
| 2015 | PS94 | 81-5 | 88.992 | 61.155 | 3000 | 5.839 | 0.214 | 3.131 | 0.229 | 0.136 | 0.003 |
| 2015 | PS94 | 81-5 | 88.992 | 61.155 | 3500 | 7.742 | 0.199 | 4.033 | 0.229 | 0.205 | 0.003 |
| 2015 | PS94 | 81-5 | 88.992 | 61.155 | 4000 | 7.902 | 0.352 | 3.955 | 0.229 | 0.128 | 0.004 |
| 2015 | PS94 | 81-5 | 88.992 | 61.155 | 4335 | 8.330 | 0.160 | 15.758 | 0.239 | 0.189 | 0.002 |
| 2015 | PS94 | 96-2 | 88.338 | 124.328 | 10 | 1.987 | 0.107 | 0.420 | 0.227 | 1.031 | 0.012 |
| 2015 | PS94 | 96-2 | 88.338 | 124.328 | 50 | 1.635 | 0.115 | 0.192 | 0.227 | 0.492 | 0.007 |
| 2015 | PS94 | 96-2 | 88.338 | 124.328 | 100 | 1.941 | 0.115 | 0.227 | 0.227 | 0.335 | 0.005 |
| 2015 | PS94 | 96-2 | 88.338 | 124.328 | 200 | 3.523 | 0.138 | 0.612 | 0.227 | 0.269 | 0.004 |
| 2015 | PS94 | 96-2 | 88.338 | 124.328 | 300 | 5.281 | 0.130 | 0.437 | 0.227 | 0.508 | 0.004 |
| 2015 | PS94 | 96-2 | 88.338 | 124.328 | 1000 | 10.791 | 0.245 | 1.609 | 0.227 | 0.696 | 0.010 |
| 2015 | PS94 | 96-2 | 88.338 | 124.328 | 1500 | 12.472 | 0.183 | 3.551 | 0.227 | 0.149 | 0.001 |
| 2015 | PS94 | 96-2 | 88.338 | 124.328 | 2000 | 11.777 | 0.237 | 4.670 | 0.227 | 0.671 | 0.008 |
| 2015 | PS94 | 96-2 | 88.338 | 124.328 | 2500 | 12.335 | 0.191 | | | 0.092 | 0.001 |
| 2015 | PS94 | 96-2 | 88.338 | 124.328 | 3000 | 17.493 | 0.352 | 5.178 | 0.227 | 0.102 | 0.002 |
| 2015 | PS94 | 96-2 | 88.338 | 124.328 | 3250 | 18.120 | 0.321 | 5.038 | 0.227 | 0.080 | 0.001 |
| 2015 | PS94 | 96-2 | 88.338 | 124.328 | 3495 | 14.819 | 0.306 | 5.195 | 0.227 | 0.157 | 0.002 |
| 2015 | PS94 | 96-2 | 88.338 | 124.328 | 3545 | 19.328 | 0.504 | 4.618 | 0.227 | 0.245 | 0.003 |
| 2015 | PS94 | 101-5 | 87.500 | 179.807 | 23 | 0.138 | 0.099 | 0.367 | 0.227 | 0.569 | 0.009 |
| 2015 | PS94 | 101-5 | 87.500 | 179.807 | 55 | 1.146 | 0.130 | 0.175 | 0.227 | 0.797 | 0.013 |
| 2015 | PS94 | 101-5 | 87.500 | 179.807 | 99 | 0.436 | 0.107 | 0.332 | 0.227 | 0.349 | 0.005 |
| 2015 | PS94 | 101-5 | 87.500 | 179.807 | 174 | 3.088 | 0.206 | 0.542 | 0.227 | 0.286 | 0.004 |
| 2015 | PS94 | 101-5 | 87.500 | 179.807 | 259 | 3.263 | 0.145 | 0.805 | 0.227 | 0.292 | 0.004 |
| 2015 | PS94 | 101-5 | 87.500 | 179.807 | 499 | 4.287 | 0.153 | 1.120 | 0.227 | 0.230 | 0.004 |
| 2015 | PS94 | 101-5 | 87.500 | 179.807 | 999 | 9.010 | 0.237 | 1.994 | 0.227 | 0.171 | 0.002 |
| 2015 | PS94 | 101-5 | 87.500 | 179.807 | 1399 | 13.176 | 0.267 | 3.813 | 0.227 | 0.074 | 0.001 |
| 2015 | PS94 | 101-5 | 87.500 | 179.807 | 1899 | 17.700 | 0.352 | 6.000 | 0.227 | 0.138 | 0.002 |
| 2015 | PS94 | 101-5 | 87.500 | 179.807 | 2399 | 15.254 | 0.329 | 6.437 | 0.227 | 0.051 | 0.001 |
| 2015 | PS94 | 101-5 | 87.500 | 179.807 | 2899 | 19.565 | 0.359 | 6.857 | 0.227 | 0.617 | 0.010 |

| Year | Cruise | Station-Cast | Lat. | Long. | depth | $^{230}$Th | err | $^{231}$Pa | err | $^{232}$Th | err |
|---|---|---|---|---|---|---|---|---|---|---|---|
| | | | | | [m] | [uBq/kg] | [uBq/kg] | [uBq/kg] | [uBq/kg] | [pmol/kg] | [pmol/kg] |
| 2015 | PS94 | 101-5 | 87.500 | 179.807 | 3399 | 21.758 | 0.481 | 7.049 | 0.227 | 0.108 | 0.002 |
| 2015 | PS94 | 101-5 | 87.500 | 179.807 | 3881 | 24.861 | 0.527 | 6.839 | 0.227 | 0.125 | 0.002 |
| 2015 | PS94 | 101-5 | 87.500 | 179.807 | 3932 | 20.314 | 0.413 | 6.647 | 0.227 | 0.109 | 0.002 |
| 2015 | PS94 | 115-1 | 84.272 | 110.688 | 1900 | 6.435 | 0.214 | 1.874 | 0.229 | 0.075 | 0.002 |
| 2015 | PS94 | 115-1 | 84.272 | 110.688 | 3000 | 6.221 | 0.229 | 3.282 | 0.229 | 0.109 | 0.003 |
| 2015 | PS94 | 115-1 | 84.272 | 110.688 | 3249 | 5.571 | 0.176 | 2.678 | 0.229 | 0.300 | 0.005 |
| 2015 | PS94 | 115-1 | 84.272 | 110.688 | 3600 | 5.923 | 0.168 | 2.138 | 0.229 | 0.017 | 0.000 |
| 2015 | PS94 | 115-1 | 84.272 | 110.688 | 3687 | 5.640 | 0.183 | 2.490 | 0.229 | 0.021 | 0.000 |
| 2015 | PS94 | 115-1 | 84.272 | 110.688 | 3870 | 6.641 | 0.260 | 2.306 | 0.229 | 0.064 | 0.002 |
| 2015 | PS94 | 117-4 | 84.560 | 115.996 | 10 | 0.695 | 0.099 | 0.082 | 0.228 | 0.428 | 0.007 |
| 2015 | PS94 | 117-4 | 84.560 | 115.996 | 50 | 1.735 | 0.115 | 0.123 | 0.228 | 0.568 | 0.009 |
| 2015 | PS94 | 117-4 | 84.560 | 115.996 | 100 | 1.987 | 0.115 | 0.309 | 0.228 | 0.273 | 0.004 |
| 2015 | PS94 | 117-4 | 84.560 | 115.996 | 200 | 2.369 | 0.122 | 0.619 | 0.228 | 0.231 | 0.003 |
| 2015 | PS94 | 117-4 | 84.560 | 115.996 | 300 | 3.133 | 0.130 | 0.628 | 0.228 | 0.293 | 0.004 |
| 2015 | PS94 | 117-4 | 84.560 | 115.996 | 500 | 4.142 | 0.153 | 0.791 | 0.228 | 0.282 | 0.004 |
| 2015 | PS94 | 117-4 | 84.560 | 115.996 | 1000 | 3.485 | 0.130 | 1.004 | 0.229 | 0.151 | 0.002 |
| 2015 | PS94 | 117-4 | 84.560 | 115.996 | 1500 | 4.822 | 0.176 | 1.345 | 0.229 | 0.201 | 0.004 |
| 2015 | PS94 | 117-4 | 84.560 | 115.996 | 2000 | 6.297 | 0.191 | 1.757 | 0.229 | 0.244 | 0.004 |
| 2015 | PS94 | 117-4 | 84.560 | 115.996 | 2500 | 6.802 | 0.206 | 1.737 | 0.229 | 0.144 | 0.003 |
| 2015 | PS94 | 117-4 | 84.560 | 115.996 | 3000 | 6.733 | 0.199 | 1.965 | 0.229 | 0.094 | 0.002 |
| 2015 | PS94 | 117-4 | 84.560 | 115.996 | 3500 | 6.443 | 0.191 | 2.029 | 0.229 | 0.093 | 0.002 |
| 2015 | PS94 | 117-4 | 84.560 | 115.996 | 4000 | 7.665 | 0.199 | 2.141 | 0.229 | 0.123 | 0.002 |
| 2015 | PS94 | 117-4 | 84.560 | 115.996 | 4303 | 7.979 | 0.214 | 2.280 | 0.229 | 0.196 | 0.003 |
| 2015 | PS94 | 117-4 | 84.560 | 115.996 | 4353 | 7.696 | 0.191 | 2.214 | 0.229 | 0.150 | 0.002 |
| 2015 | PS94 | 125-2 | 85.098 | 139.625 | 10 | 2.124 | 0.134 | 0.002 | 0.228 | 0.896 | 0.020 |
| 2015 | PS94 | 125-2 | 85.098 | 139.625 | 50 | NA | NA | 0.668 | 0.228 | NA | NA |
| 2015 | PS94 | 125-2 | 85.098 | 139.625 | 100 | 1.525 | 0.120 | 0.161 | 0.228 | 0.306 | 0.007 |
| 2015 | PS94 | 125-2 | 85.098 | 139.625 | 200 | 1.799 | 0.122 | 0.414 | 0.228 | 0.248 | 0.005 |
| 2015 | PS94 | 125-2 | 85.098 | 139.625 | 300 | 2.168 | 0.128 | 0.961 | 0.228 | 0.221 | 0.004 |
| 2015 | PS94 | 125-2 | 85.098 | 139.625 | 500 | 1.946 | 0.126 | 1.160 | 0.228 | 0.178 | 0.004 |
| 2015 | PS94 | 125-2 | 85.098 | 139.625 | 1000 | 1.783 | 0.104 | 1.371 | 0.228 | 0.114 | 0.001 |
| 2015 | PS94 | 125-2 | 85.098 | 139.625 | 1500 | NA | NA | 1.774 | 0.229 | NA | NA |
| 2015 | PS94 | 125-2 | 85.098 | 139.625 | 2000 | 5.193 | 0.171 | 2.399 | 0.229 | 0.127 | 0.002 |
| 2015 | PS94 | 125-2 | 85.098 | 139.625 | 2500 | 4.893 | 0.282 | 2.412 | 0.229 | 0.124 | 0.005 |
| 2015 | PS94 | 125-2 | 85.098 | 139.625 | 3000 | 4.701 | 0.159 | 2.983 | 0.229 | 0.115 | 0.002 |
| 2015 | PS94 | 125-2 | 85.098 | 139.625 | 3500 | 5.507 | 0.135 | 3.331 | 0.229 | 0.121 | 0.001 |
| 2015 | PS94 | 125-2 | 85.098 | 139.625 | 3788.1 | 6.273 | 0.175 | 3.448 | 0.229 | 0.108 | 0.002 |
| 2015 | PS94 | 125-2 | 85.098 | 139.625 | 3838 | 6.288 | 0.134 | 3.437 | 0.229 | 0.106 | 0.001 |
| 2015 | PS94 | 134-1 | 84.844 | 159.035 | 300 | 2.981 | 0.130 | 1.067 | 0.227 | 0.273 | 0.004 |
| 2015 | PS94 | 134-1 | 84.844 | 159.035 | 1000 | 7.482 | 0.206 | 2.064 | 0.227 | 0.175 | 0.003 |

| Year | Cruise | Station-Cast | Lat. | Long. | depth | $^{230}$Th | err | $^{231}$Pa | err | $^{232}$Th | err |
|---|---|---|---|---|---|---|---|---|---|---|---|
| | | | | | [m] | [uBq/kg] | [uBq/kg] | [uBq/kg] | [uBq/kg] | [pmol/kg] | [pmol/kg] |
| 2015 | PS94 | 134-1 | 84.844 | 159.035 | 2000 | 13.558 | 0.245 | 5.143 | 0.227 | 0.200 | 0.002 |
| 2015 | PS94 | 134-1 | 84.844 | 159.035 | 2500 | 12.908 | 0.359 | 5.580 | 0.227 | 0.135 | 0.003 |
| 2015 | PS94 | 134-1 | 84.844 | 159.035 | 3000 | 15.774 | 0.466 | 6.087 | 0.227 | 0.110 | 0.003 |
| 2015 | PS94 | 134-1 | 84.844 | 159.035 | 3000 | 16.187 | 0.374 | 6.280 | 0.227 | 0.160 | 0.003 |
| 2015 | PS94 | 134-1 | 84.844 | 159.035 | 3040 | 16.431 | 0.413 | 6.350 | 0.227 | 0.275 | 0.007 |
| 2015 | PS94 | 134-1 | 84.844 | 159.035 | 3090 | 16.034 | 0.374 | 6.490 | 0.227 | 0.356 | 0.007 |
| 2007 | PS70 | 260-3 | 84.489 | 36.139 | 50 | 4.515 | 0.038 | 0.001 | 0.003 | 0.288 | 0.001 |
| 2007 | PS70 | 260-3 | 84.489 | 36.139 | 300 | 6.030 | 0.071 | 0.001 | 0.004 | 0.218 | 0.001 |
| 2007 | PS70 | 260-3 | 84.489 | 36.139 | 1000 | 7.211 | 0.108 | 0.002 | 0.004 | 0.145 | 0.001 |
| 2007 | PS70 | 260-3 | 84.489 | 36.139 | 2000 | 9.209 | 0.162 | 0.003 | 0.004 | 0.116 | 0.000 |
| 2007 | PS70 | 260-3 | 84.489 | 36.139 | 3000 | 8.210 | 0.189 | 0.003 | 0.004 | 0.096 | 0.000 |
| 2007 | PS70 | 260-3 | 84.489 | 36.139 | 4000 | 8.431 | 0.171 | 0.003 | 0.004 | 0.104 | 0.000 |
| 2007 | PS70 | 309-2 | 87.046 | 104.787 | 50 | 4.447 | 0.005 | 0.000 | 0.004 | 0.562 | 0.002 |
| 2007 | PS70 | 309-2 | 87.046 | 104.787 | 200 | 5.228 | 0.058 | 0.001 | 0.003 | 0.242 | 0.001 |
| 2007 | PS70 | 309-2 | 87.046 | 104.787 | 1000 | 6.665 | 0.075 | 0.002 | 0.004 | 0.139 | 0.000 |
| 2007 | PS70 | 309-2 | 87.046 | 104.787 | 2000 | 8.895 | 0.167 | 0.003 | 0.004 | 0.140 | 0.000 |
| 2007 | PS70 | 309-2 | 87.046 | 104.787 | 2000 | 9.016 | 0.168 | 0.003 | 0.004 | 0.143 | 0.000 |
| 2007 | PS70 | 309-2 | 87.046 | 104.787 | 2750 | 8.263 | 0.184 | 0.003 | 0.004 | 0.093 | 0.000 |
| 2007 | PS70 | 309-2 | 87.046 | 104.787 | 4500 | 11.392 | 0.205 | 0.003 | 0.004 | 0.177 | 0.001 |
| 2007 | PS70 | 328-2 | 87.830 | 170.568 | 50 | 4.407 | 0.000 | 0.000 | 0.005 | 1.061 | 0.004 |
| 2007 | PS70 | 328-2 | 87.830 | 170.568 | 300 | 8.095 | 0.083 | 0.002 | 0.004 | 0.248 | 0.001 |
| 2007 | PS70 | 328-2 | 87.830 | 170.568 | 1000 | 12.445 | 0.140 | 0.003 | 0.005 | 0.167 | 0.001 |
| 2007 | PS70 | 328-2 | 87.830 | 170.568 | 1000 | 12.492 | 0.146 | 0.003 | 0.005 | 0.169 | 0.000 |
| 2007 | PS70 | 328-2 | 87.830 | 170.568 | 3000 | 20.805 | 0.374 | 0.004 | 0.005 | 0.095 | 0.000 |
| 2007 | PS70 | 328-2 | 87.830 | 170.568 | 3750 | 17.981 | 0.358 | 0.004 | 0.006 | 0.118 | 0.000 |
| 2007 | PS70 | 400-2 | 77.368 | 123.418 | 50 | 3.040 | 0.005 | 0.000 | 0.003 | 0.132 | 0.001 |
| 2007 | PS70 | 400-2 | 77.368 | 123.418 | 100 | 3.588 | 0.013 | 0.001 | 0.006 | 0.170 | 0.001 |
| 2007 | PS70 | 400-2 | 77.368 | 123.418 | 300 | 4.236 | 0.050 | 0.002 | 0.002 | 0.172 | 0.001 |
| 2007 | PS70 | 400-2 | 77.368 | 123.418 | 500 | 4.364 | 0.044 | 0.002 | 0.003 | 0.125 | 0.000 |
| 2007 | PS70 | 400-2 | 77.368 | 123.418 | 1150 | 4.203 | 0.043 | 0.001 | 0.003 | 0.117 | 0.001 |

**Table A2: Particulate $^{230}$Th and $^{232}$Th from 2015.**

| Year | Cruise | Station-Cast | Lat. | Long. | depth | $^{230}$Th | err | $^{232}$Th | err |
|---|---|---|---|---|---|---|---|---|---|
| | | | | | [m] | [uBq/kg] | [uBq/kg] | [pmol/kg] | [pmol/kg] |
| 2015 | PS94 | 50-6 | 84.399 | 30.715 | 50 | 0.220 | 0.201 | 0.028 | 0.001 |
| 2015 | PS94 | 50-6 | 84.399 | 30.715 | 100 | 0.400 | 0.219 | 0.052 | 0.001 |
| 2015 | PS94 | 50-6 | 84.399 | 30.715 | 300 | 0.423 | 0.221 | 0.009 | 0.001 |
| 2015 | PS94 | 50-6 | 84.399 | 30.715 | 500 | 0.444 | 0.201 | 0.113 | 0.005 |
| 2015 | PS94 | 50-6 | 84.399 | 30.715 | 750 | 1.266 | 0.206 | 0.104 | 0.004 |
| 2015 | PS94 | 50-6 | 84.399 | 30.715 | 1000 | 2.396 | 0.228 | 0.151 | 0.006 |
| 2015 | PS94 | 50-6 | 84.399 | 30.715 | 1500 | 3.285 | 0.228 | 0.138 | 0.006 |
| 2015 | PS94 | 50-6 | 84.399 | 30.715 | 2000 | 4.219 | 0.272 | 0.116 | 0.008 |
| 2015 | PS94 | 50-6 | 84.399 | 30.715 | 2500 | 4.083 | 0.248 | 0.099 | 0.006 |
| 2015 | PS94 | 50-6 | 84.399 | 30.715 | 3000 | 5.162 | 0.267 | 0.109 | 0.006 |
| 2015 | PS94 | 50-6 | 84.399 | 30.715 | 3500 | 4.682 | 0.577 | 0.100 | 0.035 |
| 2015 | PS94 | 50-6 | 84.399 | 30.715 | 3990 | 4.189 | 0.282 | 0.129 | 0.011 |

**Table A3: Percent of particulate $^{234}$Th from total $^{234}$Th, calculated from $^{238}$U activities, assuming equilibrium of $^{234}$Th with total $^{238}$U in deep water (Owens *et al.*, 2011).**

| Year | Cruise | Station-Cast | Lat. | Long. | depth | $^{234}Th_p$ |
|---|---|---|---|---|---|---|
| | | | | | [m] | % from tot. |
| 2015 | PS94 | 50-6 | 84.399 | 30.715 | 500 | 3.14 |
| 2015 | PS94 | 50-6 | 84.399 | 30.715 | 1500 | 1.49 |
| 2015 | PS94 | 50-6 | 84.399 | 30.715 | 2000 | 2.65 |
| 2015 | PS94 | 50-6 | 84.399 | 30.715 | 2500 | 1.18 |
| 2015 | PS94 | 50-6 | 84.399 | 30.715 | 2750 | 8.48 |
| 2015 | PS94 | 50-6 | 84.399 | 30.715 | 3000 | 7.32 |
| 2015 | PS94 | 50-6 | 84.399 | 30.715 | 3250 | 9.86 |
| 2015 | PS94 | 50-6 | 84.399 | 30.715 | 3500 | 5.97 |
| 2015 | PS94 | 50-6 | 84.399 | 30.715 | 3990 | 3.57 |
| 2015 | PS94 | 81-9 | 88.992 | 61.155 | 50 | 1.93 |
| 2015 | PS94 | 81-9 | 88.992 | 61.155 | 100 | 2.76 |
| 2015 | PS94 | 81-9 | 88.992 | 61.155 | 500 | 1.49 |
| 2015 | PS94 | 81-9 | 88.992 | 61.155 | 1000 | 2.66 |
| 2015 | PS94 | 81-9 | 88.992 | 61.155 | 1500 | 4.12 |
| 2015 | PS94 | 81-9 | 88.992 | 61.155 | 2000 | 1.36 |
| 2015 | PS94 | 81-9 | 88.992 | 61.155 | 2500 | 3.29 |
| 2015 | PS94 | 81-9 | 88.992 | 61.155 | 3000 | 3.02 |
| 2015 | PS94 | 81-9 | 88.992 | 61.155 | 3500 | 3.46 |
| 2015 | PS94 | 81-9 | 88.992 | 61.155 | 4000 | 5.89 |
| 2015 | PS94 | 81-9 | 88.992 | 61.155 | 4165 | 4.51 |
| 2015 | PS94 | 117-7 | 84.560 | 115.996 | 50 | 12.74 |
| 2015 | PS94 | 117-7 | 84.560 | 115.996 | 300 | 5.17 |
| 2015 | PS94 | 117-7 | 84.560 | 115.996 | 500 | 3.88 |

| Year | Cruise | Station-Cast | Lat. | Long. | depth | $^{234}Th_p$ |
|---|---|---|---|---|---|---|
| | | | | | [m] | % from tot. |
| 2015 | PS94 | 117-7 | 84.560 | 115.996 | 1000 | 3.12 |
| 2015 | PS94 | 117-7 | 84.560 | 115.996 | 1500 | 3.44 |
| 2015 | PS94 | 117-7 | 84.560 | 115.996 | 2000 | 2.65 |
| 2015 | PS94 | 117-7 | 84.560 | 115.996 | 2500 | 3.22 |
| 2015 | PS94 | 117-7 | 84.560 | 115.996 | 3000 | 4.89 |
| 2015 | PS94 | 117-7 | 84.560 | 115.996 | 3500 | 4.37 |
| 2015 | PS94 | 117-7 | 84.560 | 115.996 | 3750 | 2.85 |
| 2015 | PS94 | 117-7 | 84.560 | 115.996 | 4140 | 3.62 |
| 2015 | PS94 | 125-8 | 85.098 | 139.625 | 50 | 10.57 |
| 2015 | PS94 | 125-8 | 85.098 | 139.625 | 100 | 6.25 |
| 2015 | PS94 | 125-8 | 85.098 | 139.625 | 300 | 7.23 |
| 2015 | PS94 | 125-8 | 85.098 | 139.625 | 500 | 2.58 |
| 2015 | PS94 | 125-8 | 85.098 | 139.625 | 1500 | 6.42 |
| 2015 | PS94 | 125-8 | 85.098 | 139.625 | 2000 | 4.36 |
| 2015 | PS94 | 125-8 | 85.098 | 139.625 | 2500 | 6.29 |
| 2015 | PS94 | 125-8 | 85.098 | 139.625 | 3000 | 5.84 |
| 2015 | PS94 | 125-8 | 85.098 | 139.625 | 3500 | 5.51 |
| 2015 | PS94 | 125-8 | 85.098 | 139.625 | 3750 | 6.83 |
| 2015 | PS94 | 125-8 | 85.098 | 139.625 | 3765 | 3.36 |

## ACKNOWLEDGEMENT

First of all, I want to thank Michiel M. Rutgers van der Loeff for trusting me and providing the opportunity to conduct this Thesis. I am grateful for all the support and help on scientific and personal levels Michiel provided, even after his retirement. His thorough and critical comments on manuscripts were always helpful and improved all manuscripts and the pace of getting feedback was always beyond belief. I am deeply grateful for having the chance to work together and learn a lot about scientific work and maybe at the same degree about live from him. I highly appreciate that Michiel introduced me to a lot of colleagues, helping making contacts e.g. at conferences and generally included me in everything. I will never forget our joint polar-expeditions and the conversation we had.

I thank Walter Geibert for constructive critic and support, especially in difficult times. I am grateful that the "transition" in terms of a daily contact person from Walter to Michiel went so smooth. Walters's invaluable help, while preparing manuscripts or presentations, were crucial for publishing research articles and conference contributions. I highly esteem the freedom my supervisors gave me and allowed me to work independently and let me follow and develop my own ideas, while being available for help and supervision at all times. This provided the possibility to work independently but never being alone when help was needed.

Sabine Kasten is thanked for providing support and help whenever it was needed and for enabling traveling to conferences and summer schools. Sabine always had an open ear for problems and helped immediately. I am extremely grateful that I always got help when needed and my working place and everything I needed.

I thank Ingrid Stimac for helping me during times of intensive lab work and teaching me how to conduct the natural occurring radionuclide analyses and measurements in the clean lab facilities, showing a lot of patience, even in late afternoon hours. Without Ingrid I would probably not have gained a single data point from all the samples. Ingrid Dohrmann is thanked for our smoking breaks and always being supportive and having an open ear.

My colleagues and friends Sandra Gdaniec and Ronja Paffrath are thanked for constructive discussions on results and ideas and mutual help throughout the years, as well as for great collaboration on board *RV Polarstern*. Additionally, I want to thank all participants of RV Polarstern cruises PS94 and PS100 for making these expeditions a unforgettable experiences.

I am grateful and proud to have been part of the Marine Geochemistry Section of the Alfred-Wegener-Institute. Therefore, I thank especially my great and always helpful my co-PhD-

students Jessica Volz, Anne-Christin Melcher, Male Köster and Eva Kirschenmann for talks during coffee breaks and providing a nice and comfortable working atmosphere, as well as always having an open ear for any kind of problems. I am grateful to have shared the office with my friend Josefa Verdugo, for our conversations and sport sessions, contributing a lot to a successful outcome of the Thesis. I thank my AWI friends Josephine Rapp, Andreas, Christopher Danek and Rafael Gonçalves Araujo for being around and providing distraction and delight.

Katharina Pahnke is thanked for being part of my PhD-thesis-Committee, providing helpful comments during the regular committee meetings.
I thank the Alfred-Wegener-Institute in general for providing excellent research opportunities and facilities, and especially Claudia Sprengel, Claudia Hanfland, Dörte Rosenbaum and Jelle Bijma for help and support provided via the graduate school POLMAR.

Sabine Prader, my dearly beloved girlfriend, is thanked for always supporting me, despite all adversities that emerged in dark times in recent years. I am deeply grateful for her love and looking forward to a common future. I am exceptionally grateful for the support my parents Regina and Rüdiger and my siblings Anne and Jakob provided throughout the years, especially in difficult times. My friend Leo Bitter is thanked for always being there for me and our friendship in general.

S. Bradley Moran, Kate Lepore, Richard Lawrence Edwards and Yanbin Lu are thanked for providing radionuclide data from 2007. I thank Dennis Koehler for tremendous help maintaining and preparing the in-situ-pumps, as well as sampling, during *RV Polarstern* cruise PS100, particularly during the first hectic weeks. Lars-Eric Heimbürger-Boavida and Matthieuh Roy-Barman are thanked for providing 5 in-situ-pumps in 2015 and 2016, respectively. Finally, I want to thank the Captain and Crews of *RV Polarstern* cruises PS94 and PS100, as well as the chief scientist Ursula Schauer and Thorsten Kanzow.

# ERKLÄRUNG/*AFFIRMATION*

---

Name / *Name*: ..... Date / *Date*:.....

Anschrift / *Address:* .....

**Erklärung / *Affirmation***

---

Ich versichere, dass / *I affirm that*

1. die Dissertation ohne unerlaubte fremde Hilfe angefertigt wurde /
   *I wrote the present thesis independently and without illicit assistance from third parties,*

2. keine anderen als die von mir angegebenen Quellen und Hilfsmittel benutzt wurden und /
   *I used no sources other than those indicated nor aids other than those permissible,*

3. die den benutzten Werken wörtlich oder inhaltlich entnommenen Stellen als solche kenntlich gemacht wurden. /
   *I appropriately referenced any text or content from other sources*

_____, den / *on this day*_____

_____

(Unterschrift / *Signature*)

# VERSICHERUNG AN EIDES STATT/*AFFIRMATION IN LIEU OF AN OATH*

**gem. § 5 Abs. 5 der Promotionsordnung vom 18.06.2018 /**
***according to § 5 (5) of the Doctoral Degree Rules and Regulations of 18 June, 2018***

Ich / I, _____
(Vorname / *First Name*, Name / *Name*, Anschrift / *Address*, ggf. Matr.-Nr. / *student ID no., if applicable)*

versichere an Eides Statt durch meine Unterschrift, dass ich die vorliegende Dissertation selbständig und ohne fremde Hilfe angefertigt und alle Stellen, die ich wörtlich dem Sinne nach aus Veröffentlichungen entnommen habe, als solche kenntlich gemacht habe, mich auch keiner anderen als der angegebenen Literatur oder sonstiger Hilfsmittel bedient habe und die zu Prüfungszwecken beigelegte elektronische Version (PDF) der Dissertation mit der abgegebenen gedruckten Version identisch ist. / *With my signature I affirm in lieu of an oath that I prepared the submitted dissertation independently and without illicit assistance from third parties, that I appropriately referenced any text or content from other sources, that I used only literature and resources listed in the dissertation, and that the electronic (PDF) and printed versions of the dissertation are identical.*

Ich versichere an Eides Statt, dass ich die vorgenannten Angaben nach bestem Wissen und Gewissen gemacht habe und dass die Angaben der Wahrheit entsprechen und ich nichts verschwiegen habe. / *I affirm in lieu of an oath that the information provided herein to the best of my knowledge is true and complete*.

Die Strafbarkeit einer falschen eidesstattlichen Versicherung ist mir bekannt, namentlich die Strafandrohung gemäß § 156 StGB bis zu drei Jahren Freiheitsstrafe oder Geldstrafe bei vorsätzlicher Begehung der Tat bzw. gemäß § 161 Abs. 1 StGB bis zu einem Jahr Freiheitsstrafe oder Geldstrafe bei fahrlässiger Begehung. / *I am aware that a false affidavit is a criminal offence which is punishable by law in accordance with § 156 of the German Criminal Code (StGB) with up to three years imprisonment or a fine in case of intention, or in accordance with § 161 (1) of the German Criminal Code with up to one year imprisonment or a fine in case of negligence.*

_____ _____

Ort / *Place*, Datum / *Date* Unterschrift / *Signature*